High-frequency flux measurements of reactive nitrogen as validation tool for dry deposition modeling: Technical improvements and application over different land-use types

Dissertation

Zur Erlangung des akademischen Grades

Doktor der Naturwissenschaften

am Fachbereich Geowissenschaften

der Freien Universität Berlin

Vorlegt von

Pascal Wintjen

Berlin November 2022

Gutachter

Erstgutachter: Prof. Dr. Martijn Schaap

Zweitgutachter: Prof. Dr. Arjan Hensen

Tag der Disputation: 03.02.2023

Zusammenfassung

Reaktive Stickstoffverbindungen (N_r) wie Ammoniak (NH_3), Stickstoffmonoxid (NO), Stickstoffdioxid, Salpetersäure, salpetrige Säure sowie partikelförmige Stickstoffverbindungen sind wichtige Nährstoffe für die Produktivität von Ökosystemen. Die Summe dieser reaktiven Verbindungen wird als reaktiver Gesamtstickstoff ΣN_r bezeichnet. Seit Beginn des 20. Jahrhunderts haben die Konzentrationen von N_r Verbindungen in der Atmosphäre durch industrielle und landwirtschaftliche Emissionen stark zugenommen, was eine erhöhte Deposition von N_r sowohl in natürliche als auch in bewirtschaftete Ökosysteme zur Folge hat. Jedoch kann eine kontinuierlich hohe Stickstoffdeposition negative Auswirkungen auf natürliche Ökosysteme haben. Je nach Art des Stickstoffüberschusses sind u.a. Versauerung oder Eutrophierung beobachtet worden, was vielerorts die Aufnahmefähigkeit des Pflanzenbestandes von Kohlenstoffdioxid beeinflussen kann. Daher ist eine genaue Abschätzung des Stickstoffaustausches zwischen Biosphäre und Atmosphäre essenziell, um potenziell gefährdete Ökosysteme zu identifizieren und die Effizienz von Umweltschutzmaßnahmen zu bewerten. Sogenannte Critical Loads (CL) geben die Belastungsgrenze von Ökosystemen gegenüber dem Eintrag von Luftschadstoffen an und haben sich als geeignetes Konzept erwiesen, um Regionen zu bestimmen, die durch langanhaltende und überhöhte Stickstoffdeposition gefährdet sind.

Um den Stickstoffeintrag in Ökosysteme zu beobachten, haben sich mikrometeorologische Methoden wie die Eddy-Kovarianz (EC) Methode bewährt, um den zeitlichen Verlauf und jährliche Budgets von Spurengasen, insbesondere nicht-reaktiven Treibhausgasen zu ermitteln. Der Austausch von Stoffen zwischen Erdoberfläche und Atmosphäre wird als Fluss bezeichnet. EC Flussmessungen für alle der zuvor genannten N_r Verbindungen sind aufgrund technischer Entwicklungen im Bereich der Laserspektroskopie erst seit wenigen Jahren möglich. Folglich gibt es noch große Unsicherheiten in der Flussberechnung und kaum mikrometeorologisch durchgeführte Langzeitflussmessungen, die jedoch für eine robuste Abschätzung der atmosphärischen Stickstoffdeposition nötig sind.

Daher ist ein wesentliches Ziel dieser Promotionsarbeit eine Verbesserung von Methoden, die im Zuge der EC Flussberechnung von N_r Verbindungen verwendet werden. Zudem werden Langzeitflussmessungen genutzt, um die Konzentrations- und Flussdynamiken von ΣN_r unter der Verwendung neuartiger Messgeräte an einem abgelegenen Mischwaldstandort zu untersuchen. Zuletzt werden die an dem Standort gemessenen Flüsse mit Depositionsmodellen verglichen. ΣN_r Flüsse wurden mittels eines Systems bestehend aus einem eigens gebauten Konverter, dem Total Reactive Atmospheric Nitrogen Converter (TRANC), und einem hieran angeschlossenen Chemilumineszenzdetektor (CLD) gemessen. Mit dem TRANC werden die o.g. N_r Verbindungen in NO umgewandelt. Die Konzentration von NO in der Probenluft wird von einem CLD gemessen und entspricht der Konzentration der umgewandelten Verbindungen.

Flüsse, die mit der EC Methode berechnet werden, müssen nachträglich korrigiert werden. EC Flüsse erfahren nieder- und hochfrequente Verluste, die vom experimentellen Messaufaufbau und von der gemessenen chemischen Verbindung abhängig sind. Die hochfrequenten Verluste sind jedoch ausschlaggebend für die exakte Angabe der Höhe des Flusses. Häufig sind verwendete Hochfrequenzkorrekturmethoden allerdings für nicht-reaktive (inerte) Verbindungen optimiert worden. In der ersten Studie wurden verschiedene theoretische und empirische Hochfrequenzkorrekturmethoden anhand von ΣN_r EC Flüssen miteinander verglichen. Die theoretischen Methoden verwenden modellierte sogenannte Cospektren, die empirischen Methoden nutzen gemessene Cospektren oder sogenannte Powerspektren. So wurde herausgefunden, dass theoretische und empirische Methoden, die für inerte Gase entwickelt worden sind und auf modellierten Cospektren oder Powerspektren basieren, die Verluste von Flüssen im hochfrequenten Bereich unterschätzen. Neu entwickelte Methoden, die gemessene Cospektren und Ogiven (kumulierte Cospektren) nutzen, lieferten für ΣN_r Flussverluste zwischen 16 % und 22 % für den Waldstandort.

Trotz jüngsten Fortschritten in der Messtechnik von N_r Verbindungen sind langfristige EC Flussmessungen von N_r rar, jedoch nötig um den Anteil des trocken deponierten Stickstoffs am gesamt (nass+trocken) deponierten Stickstoff möglichst genau zu bestimmen. Während der Aufwand zur Messung der nassen Deposition überschaubar ist, ist das simultane Messen der einzelnen N_r Verbindungen mittels mikrometeorologischer Methoden zur Bestimmung der Trockendeposition aufgrund eines immens hohen Kosten- und Arbeitsaufwands kaum praktizierbar sowie eine störungsfreie Umsetzung des Messaufbaus quasi unmöglich. In der zweiten Studie wurde das TRANC/CLD-System genutzt, um die ΣN_r Austauschdynamik zu untersuchen und die jährliche ΣN_r Trockendeposition an einem abgelegenen Waldstandort abzuschätzen. Über die gesamte Dauer der Messkampagne (2,5 Jahre) wurden zumeist Depositionsflüsse beobachtet. Die ΣN_r Deposition war im Falle von trockenen Blattoberflächen, hoher Lufttemperatur und geringer relativer Luftfeuchtigkeit erhöht. Saisonale Änderungen in den Konzentrationen von N_r Verbindungen und mikrometeorologische Parameter schienen die ΣN_r Trockendeposition am meisten zu beeinflussen. Für die beiden Messjahre Juni 2016 bis Mai 2017 und Juni 2017 bis Mai 2018 ergaben sich Trockendepositionen für ΣN_r von 3,8 und 4,0 kg N ha^{-1} a^{-1}. Die Berücksichtigung der nassen Deposition führte zu Gesamtdepositionen von 12,2 und 10,9 kg N ha^{-1} a^{-1}. Diese Werte lagen im Bereich der CL von Mischwäldern.

Um die gesamte Stickstoffdeposition für größere Regionen zu bestimmen und damit die Effizienz von Stickstoffminderungsmaßnahmen zu bewerten, werden chemische Transportmodelle zur Bestimmung der nassen und trockenen Deposition verwendet. Aufgrund fehlender Vergleichsmöglichkeiten zu Flussmessungen, sind diese jedoch mit erheblichen Unsicherheiten behaftet. In der dritten Studie wurde ein Vergleich verschiedener Methoden zur Bestimmung der Stickstofftrockendeposition durchgeführt. Trockendepositionsbudgets vom TRANC wurden mit einer Simulation des chemischen Transportmodells LOTOS-EUROS (LOng Term Ozone Simulation – EURopean Operational Smog), das das bidirektionale Austauschmodell DEPAC (Deposition of Acidifying Compounds) nutzt, verglichen. Des Weiteren wurden Depositionsflüsse mit einer in-situ Anwendung von DEPAC (hier als DEPAC-1D bezeichnet) berechnet. Zudem wurden Stickstofftrockendepositionen mit dem gängigen Kronenraumbilanzverfahren (CBT) abgeschätzt. Jährliche Trockenstickstoffdepositionen lagen im Bereich von 3,9 bis 7,0 kg N ha^{-1} a^{-1}, was zeigt, dass alle Methoden sinnvolle Abschätzungen boten. Die Gesamtdeposition war unterhalb der CL. Zudem zeigte die lokale Vegetation keine Anzeichen für ein Überschreiten der CL. Jedoch wurden bedeutsame Differenzen zwischen den modellierten und gemessen Flüssen festgestellt. So war die ΣN_r Deposition von DEPAC-1D bei niedrigen Lufttemperaturen, hoher relativer Luftfeuchtigkeit und nassen Blattoberflächen im Sommer erhöht, was im Widerspruch zu TRANC Messungen steht. Eine erhebliche Überschätzung der NH_3Konzentrationen durch LOTOS-EUROS wurde im Frühjahr und Herbst beobachtet, was hauptursächlich für die Differenz zu TRANC Flüssen war.

In dieser Dissertationsschrift wurde erstmalig eine umfangreiche Studie der hochfrequenten Verluste von ΣN_r durchgeführt, was für eine präzise Bestimmung des Flusses notwendig ist. Korrekturmethoden, die für gewöhnlich im Bereich der EC Flussmessungen genutzt werden, waren neu entwickelten Methoden unterlegen. Durch das erfolgreiche Einrichten eines Messsystems für ΣN_r, konnte erstmals eine langfristige Studie von ΣN_r Flussmessungen basierend auf der EC Methode durchgeführt werden, was Einblicke in das natürliche Austauschmuster von ΣN_r und eine Abschätzung der jährlichen Trockenstickstoffdeposition für ein abgelegenes Waldökosystem ermöglichte. Dieser robuste Flussdatensatz bot die einmalige Gelegenheit einen Vergleich mit Depositionsmodellen durchzuführen, was für eine Modellvalidierung entscheidend ist.

Im Zuge der Promotion wurde das bestehende Messystem aus TRANC und CLD weiterentwickelt und ermöglicht nun eine Messung der oxidierten Stickstoffverbindungen und des reaktiven Gesamtstickstoffs. Mit dem neuen System lässt sich der Austausch des reduzierten Stickstoffs, NH_3 und Ammoniumpartikel, abschätzen. Somit kann eine Validierung der modellierten NH_3 Flüsse an Standorten geringer Partikelkonzentrationen oder hoher NH_3 Konzentrationen durchgeführt werden. Mit der Separierung der Stickstoffverbindungen in oxidierte und reduzierte Verbindungen lassen sich

im Fall von Depositionsflüssen Rückschlüsse über die Herkunft des deponierten Stickstoffs treffen. So haben oxidierte Stickstoffverbindungen ihren Ursprung in der Industrie und dem Verkehr. Reduzierte Stickstoffverbindungen sind hauptsächlich landwirtschaftlichen Ursprungs. Ein folgerichtiger Schritt der Quellenseparierung wäre eine Partitionierung der N_r Flüsse, sodass sich aus den EC-Nettoflüssen die Bruttoemission und Bruttodeposition ableiten lassen. Eine entsprechende Partitionierungsmethode ist für N_r Verbindungen noch nicht vorhanden, wird aber zu einem besseren Verständnis des Austausches von N_r Verbindungen führen.

Abstract

Reactive forms of nitrogen (N_r) like ammonia (NH_3), nitric oxide (NO), nitrogen dioxide, nitric acid, nitrous acid, and particulate nitrogen compounds are essential nutrients for the productivity of ecosystems. The sum of these reactive compounds is called total reactive nitrogen (ΣN_r). Since the beginning of the 20th century, atmospheric concentrations of N_r compounds have strongly increased due to industrial and agricultural emissions leading to enhanced N_r deposition in natural and managed ecosystems. A continuously high nitrogen deposition can have adverse effects on natural ecosystems. Depending on the form of nitrogen, soil acidification or eutrophication have been observed, which can affect the carbon dioxide uptake capacity of the vegetation. Thus, an accurate estimation of the nitrogen exchange between biosphere and atmosphere is needed in order to identify endangered ecosystems and evaluate the efficiency of environmental protection guidelines. So-called Critical loads (CL) indicate the load limit of ecosystems with regard to the input of air pollutants and have proven to be a suitable concept for identifying regions, which are endangered by long-term excessive atmospheric nitrogen deposition.

To observe the nitrogen deposition to ecosystems, micrometeorological methods like the eddy-covariance (EC) method have emerged as an approved tool to investigate the temporal patterns and determine annual budgets for trace gases, in particular non-reactive greenhouse gases. The exchange of substances between the earth's surface and atmosphere is referred to as flux. Only for a few years, EC flux measurements are possible for all of the above mentioned N_r species due to technical developments in laser spectroscopy. There are still considerable uncertainties in the flux calculation and hardly any long-term measurements based on micrometeorological methods, which, however, are needed for a robust estimation of the atmospheric nitrogen deposition.

Thus, one main objective of this thesis is to improve methods, which are required in the EC flux calculation for N_r compounds. In addition, long-term flux measurements are used to investigate temporal concentration and flux dynamics of ΣN_r based on novel measurement devices at a remote mixed forest site. At last, a comparison of these flux measurements against deposition models is carried out. ΣN_r fluxes were measured with a system using a custom-built converter, the Total Reactive Atmospheric Nitrogen Converter (TRANC), coupled to a chemiluminescence detector (CLD). The TRANC performs the conversion of the above mentioned N_r compounds to NO. The concentration of NO in the sample air is measured by a CLD and corresponds to the concentration of all converted N_r compounds.

After flux calculation, EC fluxes must be corrected for low and high-frequency losses. These flux losses depend on the experimental setup and the measured chemical compound. High-frequency flux losses are more important for determining the exact flux value. Commonly used high-frequency flux correction methods are usually optimized for non-reactive (inert) gases. In the first study, we applied different high-frequency flux loss correction methods of theoretical and empirical nature to EC fluxes of ΣN_r. Theoretical methods use so-called modeled cospectra, empirical methods need measured cospectra or so-called power spectra. Theoretical and empirical methods, which have been developed for inert gases and take modeled cospectra or power spectra into account, were found to underestimate flux losses. Newly developed empirical methods provided ΣN_r flux losses ranging from 16 % to 22 % for the forest site.

Besides recent developments in flux measurement techniques of N_r, long-term flux measurements of N_r using micrometeorological measurement techniques are scarce but needed to determine the contribution of nitrogen dry deposition to total (wet+dry) nitrogen deposition with highest possible accuracy. While the effort for measuring wet deposition of N_r is manageable, establishing a setup with micrometeorological flux measurements for each N_r compound to estimate dry deposition is hardly

possible due to high costs and a non-practicable implementation of the measurement setup. In the second study, the TRANC/CLD system was used to examine the ΣN_r exchange dynamics and to estimate annual ΣN_r dry deposition based on measured fluxes at a remote mixed forest in southeast Germany. During the 2.5-year campaign, mostly deposition fluxes were observed. ΣN_r deposition was enhanced in the presence of dry leaf surfaces, high air temperature, and low relative humidity. Seasonal changes in the concentrations of N_r species and micrometeorological parameters appeared to influence ΣN_r dry deposition at most. For the two measurement years, June 2016 to May 2017 and June 2017 to May 2018, dry deposition estimates were approx. 3.8 and 4.0 kg N ha^{-1} a^{-1}, respectively. Adding the results from wet deposition measurements led to annual total N depositions of 12.2 and 10.9 kg N ha^{-1} a^{-1}, respectively, which were within the CL ranges proposed for mixed forests.

To determine total nitrogen deposition over larger regions and to evaluate the efficiency of nitrogen mitigation strategies, chemical transport models are used for determining wet and dry deposition. However, models are affected by considerable uncertainties due to the lack of comparison opportunities to flux measurements. In the third study, a comparison of different methods for estimating N dry deposition was made. Dry deposition budgets of the TRANC were compared to a simulation of the chemical transport model LOTOS-EUROS (LOng Term Ozone Simulation – EURopean Operational Smog), which uses the bidirectional flux model DEPAC. A site-based application of DEPAC (Deposition of Acidifying Compounds), here called DEPAC-1D, was applied to determine deposition fluxes. Furthermore, nitrogen dry deposition was estimated with the Canopy Budget technique (CBT). Annual dry deposition budgets ranged from 3.9 to 7.0 kg N ha^{-1} a^{-1} showing that all methods provided reasonable estimates. Total deposition was below critical loads. In addition, local vegetation examinations showed no indications of critical load exceedances. However, substantial differences between modeled and measured fluxes were found. During summer, ΣN_r deposition of DEPAC-1D was enhanced at lower air temperatures, high relative humidity, and wet leaf surfaces, which is in contrast to TRANC measurements. A substantial overestimation of NH_3 concentration by LOTOS-EUROS was found to be most responsible for the disagreement to TRANC fluxes in spring and autumn.

In this thesis, the first comprehensive study analyzing the high-frequency flux loss of ΣN_r, which is necessary for a precise flux determination, was made. Flux correction methods usually used in the field of EC flux measurements were found to be inferior to newly developed methods. With the successful installation of a ΣN_r measurement system, the first long-term study of ΣN_r flux measurements based on the EC method was carried out providing insights into the natural exchange pattern of ΣN_r and enabling the estimation of the annual nitrogen dry deposition to a remote forest ecosystem. This robust flux dataset enabled the unique opportunity to perform a comparison against deposition models, which is essential for model validation.

During my PhD, the TRANC/CLD system was developed further and currently performs measurements of oxidized N_r compounds and ΣN_r. With the new system, an estimation of the reduced N_r exchange, NH_3 and ammonium aerosols, is possible, and a validation of modeled NH_3 fluxes can be made at sites with low particle or high NH_3 concentrations. Separating N_r compounds into oxidized and reduced N_r compounds, conclusions about the origin of N_r can be made in case of deposition fluxes. Oxidized nitrogen compounds are caused by emissions from industry and traffic, and reduced nitrogen compounds can be related to emissions from agriculture. Due to source separation a logical step would be the partitioning of the net N_r EC fluxes into gross emission and gross deposition fluxes. A corresponding partitioning method for N_r compounds is not available yet, but it will result in a better understanding of the N_r exchange.

1. Introduction

Nitrogen containing compounds impact the earth's environment in many different ways, causing a range of negative impacts on human heath, biodiversity, and climate change. The nitrogen compounds travel through the Earth system, in which the atmosphere plays as an important role. This thesis is focused on obtaining a better understanding of the exchange of reactive nitrogen compounds between atmosphere and biosphere using state-of-the-art observation techniques. In this introduction, I provide a background and motivation of the main research topics addressed in this thesis.

1.1 The world of reactive nitrogen

1.1.1 Human induced emissions of reactive nitrogen

On Earth, most elemental nitrogen is available in its molecular, inert form called dinitrogen (N_2). In this form, nitrogen cannot be consumed by living organisms like plants, fungi, and bacteria. They need nitrogen converted into reactive compounds like nitrogen oxides (NO_x), known as nitric oxide (NO) and nitrogen dioxide (NO_2), or ammonia (NH_3) usually described as reactive nitrogen (N_r). From biological nitrogen fixation (Vitousek et al., 2002), the supply of N_r to living organisms is limited since the conversion of N_2 to NH_3 by nitrogenase enzymes available in soil-living microorganisms is energy intensive. Decay of dead organic material, wildlife, and volcanic eruptions are of further natural source of NH_3 (Galloway et al., 2003). Nitrogen oxides are naturally formed in small quantities by soil bacteria, lighting, and burning processes.

Since natural availability of N_r is limited, farmers before the 20th century had only a few possibilities to increase the crop production of their fields like using organic waste (compost, manure) or consider cultivating N fixating plants (leguminous). With the invention of the Haber-Bosch-Process in 1908 (Haber, 1908), a synthetic and commercially viable way of producing NH_3 became available. The ammonia was synthesized by the reaction of N_2 with H_2 under high temperature and pressure using a catalyst made of iron (Smil, 2001).

With the industrial production of nitrogen based fertilizers, food security of the ever growing world population in particular after the first half of the 20th century was ensured. Synthetic nitrogen fertilizers take a key role in feeding world population (Fig. 1.1). It is assumed that more than half of the consumed agricultural food products rely on the availability of synthetic fertilizers (Erisman et al., 2008).

The second large scale development that altered availability of N_r worldwide was the industrial and transport revolution. Mankind relies on the combustion of fossil fuels for energy production. At high temperatures, combustion of fuels leads to splitting of atmospheric N_2 and O_2 into atoms, which may recombine to NO (EPA, 1999). NO_x emissions, mainly in the form of NO, originate from biomass burning, traffic, and energy production by gas, oil, or coal burning. Once emitted, NO is converted rapidly to NO_2 by reacting with ozone (O_3) (e.g., Jacob, 1999). Emissions from vehicle, shipping, and air transport contribute most to total NO_x emissions (Granrier et al., 2011; Vestreng et al., 2009), whereas natural NO_x emissions as described above play only a minor role (Fowler et al., 2013). As visualized by Fig. 1.1, NO_x emission have been increased by a factor of three since the beginning of the 20th century (Erisman et al., 2015).

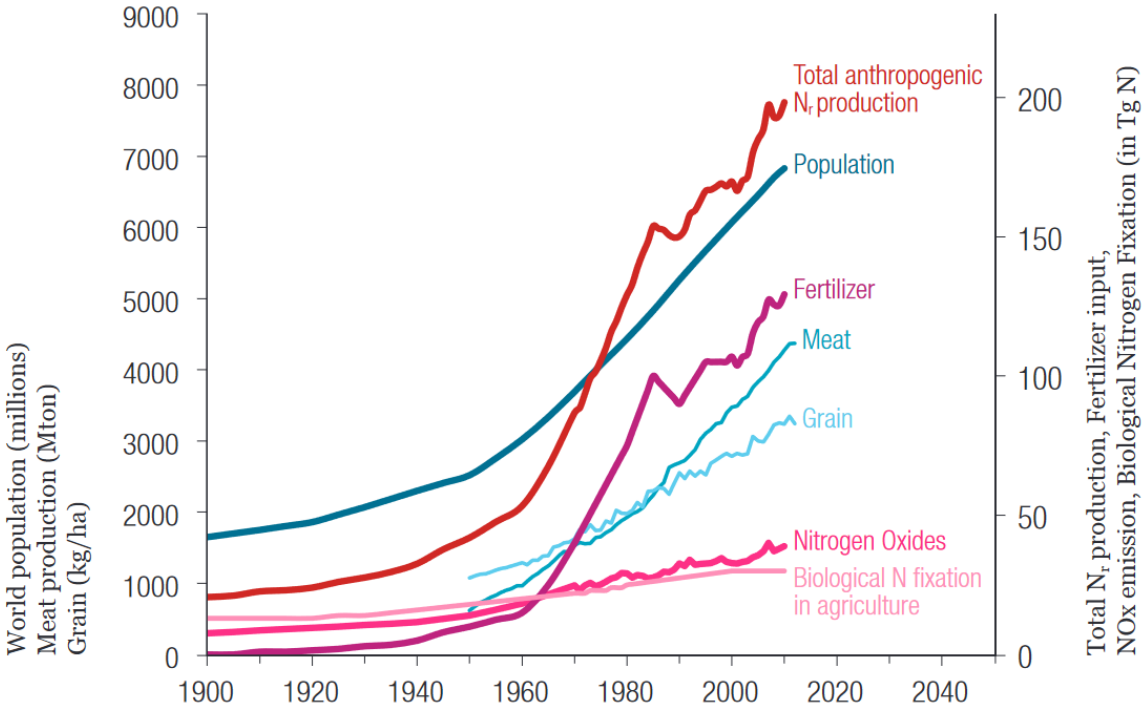

Figure 1.1: Global trends in human population and total anthropogenic N_r emissions from 1900 to 2012 (adapted from Erisman et al. (2015))

NH_3 has the largest contribution to global N_r emissions. Approximately, half of global N_r emissions refer to NH_3 (Reis et al., 2009) with emissions ranging from 46–85 Tg N yr^{-1} (Sutton et al., 2013). Most of those emissions can be related to the agricultural sector (Sutton et al., 2013) including livestock housing and grazing and the volatilization of applied organic and mineral fertilizer on crop or grass fields. Volatilization of fertilizer caused about 40 % of global NH_3 emissions (Sutton et al., 2013). Thus, human activities, the production of fertilizer, and fossil fuel combustion have substantially increased the release of N_r to the atmosphere.

Despite the large benefits, these developments brought to human welfare worldwide, the losses of N_r into the environment largely imbalanced the natural nitrogen cycle (Galloway et al., 2003; Rockström et al., 2009; Sutton et al., 2013). The additional nitrogen inputs lead to several adverse impacts on aquatic and terrestrial ecosystems (Sala et al., 2000; Dise et al., 2011) and on human health (Erisman et al., 2013) since N_r compounds cannot be effectively removed anymore by denitrifying bacteria. After compounds like NO_x or NH_3 are emitted through combustion processes or agricultural activities, they are converted into different forms of N_r compounds. The most import atmospheric N_r species besides NH_3 and NO_x are nitric acid (HNO_3), nitrous acid (HNO_2), particulate ammonium (pNH_4^+), and particulate nitrate (pNO_3^-). These compounds are currently causing various adverse impacts on health, ecosystems, and climate before being converted back to N_2. These processes are described by the so-called nitrogen cascade (Fig. 1.2) (Galloway et al., 2003; Sutton et al., 2013). The term cascade is used as a single molecule of reactive nitrogen may contribute to several of these environmental effects while cycling through the Earth system.

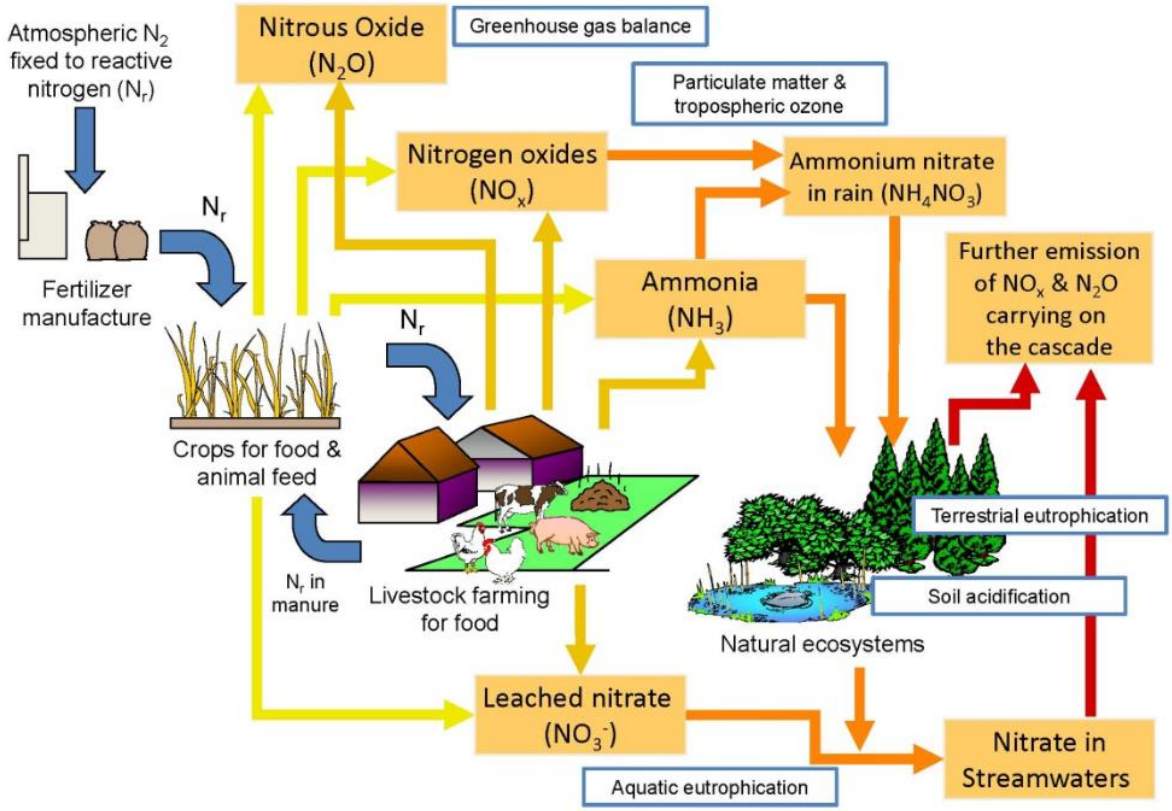

Figure 1.2: Simplified illustration of the nitrogen cascade showing the synthetic production of N_r compounds from atmospheric N_2 and their impacts on the environment before being converted back to N_2. Environmental concerns are shown in blue boxes, different pollutant forms of N_r are highlighted in the orange boxes. Apart from the blue arrows representing intended flows, all other flows are unintended. Figure is adapted from Sutton et al. (2011).

1.1.2. Negative environmental effects of reactive nitrogen

Nitrate and ammonium ions not taken up by plants or retained by the soil can lead to N_r enrichments in ground and surface water and trigger excessive algae blooms in water bodies. This phenomenon is called (aquatic) eutrophication (Sutton et al., 2011). Due excessive algae growth, light penetration into deeper water layers is inhibited resulting in a loss of subaquatic vegetation (Smith and Schindler, 2009). For depleting died plant material and other organisms, oxygen is consumed (aerobic decomposition) leading to a significant reduction in oxygen concentration in water bodies (Selman et al., 2008) and even to hypoxic waters. Consequently, species diversity is greatly reduced in aquatic ecosystems due to eutrophication (Selman et al., 2008; Sutton et al., 2011). In addition, drink water contaminated with nitrate is harmful for human health, e.g., it increases the risk for cancer (van Grinsven et al., 2010).

NO_x emissions play an important role in air pollution. NO_2 itself was found to be responsible for respiratory disorders (Erisman et al., 2013). Furthermore, NO_x plays a central role in the formation of tropospheric O_3 in the presence of volatile organic compounds and carbon monoxide. O_3 is a highly oxidative gas associated with adverse health impacts and damage to plants (De Vries, 2021; Soares and Silva, 2022). The damage from O_3 not only relates to the natural ecosystems as significant crop yield reductions are associated with O_3 exposure (van Dingenen et al., 2009; Averny et al., 2011).

NO_x and NH_3 influence the formation of particulate nitrogen compounds such as ammonium nitrate (NH_4NO_3) and ammonium sulfate ($(NH_4)_2SO_4$) in the atmosphere, which contribute mainly to fine particulate matter (with aerodynamic diameters of less than 2.5 μm ($PM_{2.5}$)). A large fraction of the ambient NO_x and SO_2 is converted into nitric acid (HNO_3) and sulfuric acid (H_2SO_4), which react with

NH_3 to form ammonium aerosols or are directly deposited on land or water surfaces thereby leading to an acidification of ecosystems. Especially in agricultural regions, enhanced concentration levels of fine particulate matter are observed due to the abundance of atmospheric NH_3 (Erisman and Schaap, 2004, Wu et al., 2016). Exposure to $PM_{2.5}$ causes respiratory diseases and impairs cardiovascular functionality (Pope et al., 2009; Sutton et al., 2011; Lelieveld et al., 2015; Giannakis et al., 2019).

Deposition of acidic N and S compounds to soils by atmospheric deposition or ammonium based fertilizer lowers the soils pH value. Due to the buffer capacity of soils, the reduction in pH does not happen initially. If the buffering substance is depleted, the acidification of soils continues. The consumption of the buffering substance by protons (Driscoll et al., 2003) leads to a release of soil nutrients like calcium and magnesium ions and toxic metals like aluminum (Al) and iron (Fe) ions (Meng et al., 2019) and subsequently to a leaching into rivers and lakes. High Al and Fe concentrations in combination with a low pH are toxic for plants resulting in a dieback of roots and reduced microbial activity (e.g., Poschenrieder et al., 2008; de Vries, 2021).

For water organisms, high concentrations of Fe and Al in combination with a low pH value are toxic, too. Compared to soils, the buffering capacity of water bodies is relatively low resulting in a faster reduction in pH. Nowadays, occurrences of fish kills due to acid deposition are greatly reduced due to absence acidic S compounds (de Vries, 2021).

N_r also alters the Earth's radiation balance by triggering the release of the greenhouse gas N_2O, which is preliminary emitted by the production of fertilizers and microbial processes in nitrogen enriched soils after application of manure or synthetic fertilizer or in water bodies due to leaching of nitrates (Davidson, 2009, Myhre et al., 2013; Pilegaard, 2013). The impact of tropospheric O_3, another greenhouse gas, on the global warming is influenced by NO_x as outlined before (Erisman et al., 2011). A net cooling effect is achieved by the formation of nitrogen aerosols, which scatter shortwave incoming radiation (Butterbach-Bahl et al., 2011; Erisman et al., 2011; Myhre et al., 2013). Hence, emissions of reactive nitrogen have direct impacts on the climate system (IPCC, 2013).

Indirectly, N_r deposition to terrestrial ecosystems influences their methane (CH_4) and carbon dioxide (CO_2) exchange. High O_3 concentrations due to substantial NO_x and VOC emissions are toxic to plants like agricultural crops and plants in natural ecosystems, which lowers their CO_2 uptake capacity. N deposition to natural wetlands appears to increase their CH_4 emissions (Aert et al., 1999). In case of rice paddies, N deposition decreases CH_4 emission due to high CO_2 concentrations (Bodelier and Steenbergh, 2014; Luan et al., 2019). Differences in soil properties, plant and microbial response, and type of applied fertilizer are possible reasons for the wide range in CH_4 fluxes (Bodelier and Steenbergh, 2014).

On the other hand, N deposition can enhance plant growth of various ecosystems, mainly forests (Pan et al., 2011) and thus increases the terrestrial CO_2 uptake capacity (Butterbach-Bahl et al., 2011; de Vries et al., 2014) to a certain extent. The increased carbon sequestration results in a net cooling effect (Erisman et al., 2011), but the magnitude of this additional sink is uncertain (Flechard et al., 2020). In total, the net effect of nitrogen deposition on global warming is assumed to be negative but still highly uncertain (Erisman et al., 2011; Erisman et al., 2015).

If ecosystems are exposed to high N_r deposition on a long-term scale, the ecosystem's integrity is impaired and its natural CO_2 response is distorted (Bobbink et al., 2010). Ecosystems such as peat and heathlands are assigned with low soil nutrient concentrations and therefore are sensitive to long-term nitrogen deposition. As shown by Sutton et al. (2008b), Damgaard et al. (2011), and Paulissen et al. (2016), a shift in plant diversity has been observed for sensitive habitats due to continuous atmospheric nitrogen deposition. Atmospheric deposition of N_r and excessive fertilizer application to terrestrial ecosystems lead to the formation of nitrate and ammonium ions (nitrification) and increase soil acidity as written above. Plant species adapted to low soil acidity and high nutrient concentrations drive out native species, which prefer low nutrient concentrations. This phenomenon is described as terrestrial

eutrophication. Disappearances of species may have consequences for species, which dependent directly or indirectly on their existence (Erisman et al., 2013; WallisDeVries, 2014). Atmospheric deposition of NH_3 can also cause direct damage to plants such as lichens (Sheppard et al., 2011; Carter et al., 2017).

Critical loads for eutrophication indicate at which level long-term nitrogen deposition may impair the health status of an ecosystem. Thus, assessing the nitrogen deposition in comparison to these thresholds is useful to determine the area of threatened ecosystems and to evaluate the effect of nitrogen mitigation strategies. According to recent calculations, about 70 % of ecosystems in Germany exceed their respective critical load limit by eutrophication (Schaap et al., 2018) as shown in Fig. 1.3.

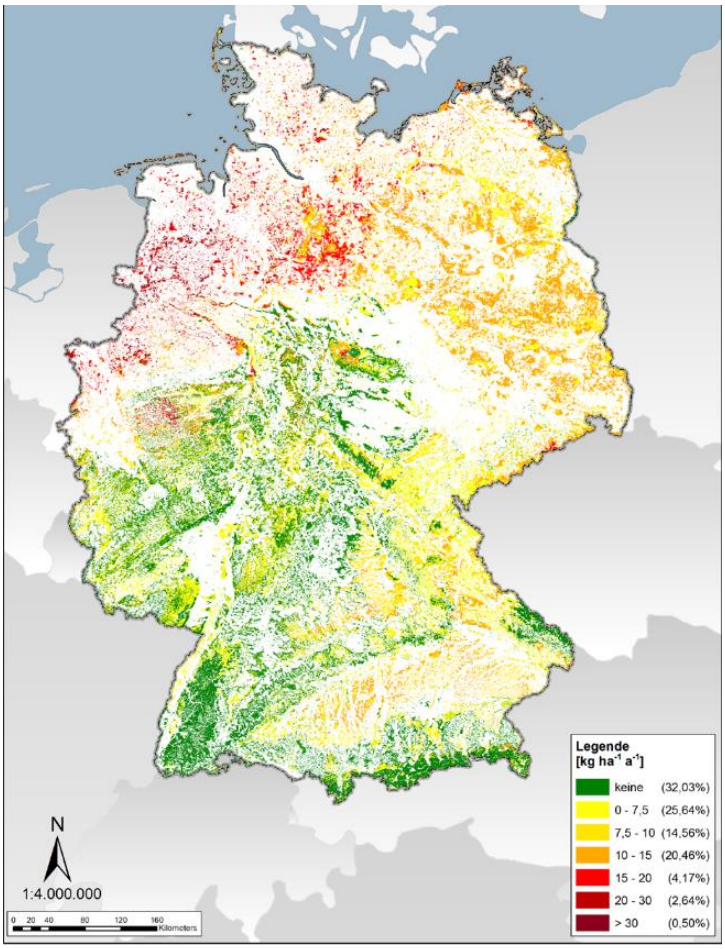

Figure 1.3: Exceedances of critical loads by eutrophication due to nitrogen deposition for Germany in 2015 (adapted from Schaap et al., 2018)

As visualized by Fig. 1.3, there is a dire need to reduce nitrogen deposition and thus emissions across Germany. Exceedances of critical loads are found in northwest Germany and in the southeast and east of the country. Although NO_x emissions have continuously been declining (Geupel et al., 2021), current air pollution reduction policies haven't been led to substantial lowering in NH_3 emissions (Schaap et al., 2018; Giannakis et al., 2019). This has to change in the near future as for both NO_x and NH_3 emission reductions relative to 2005 are set in the National Emission Ceilings (NEC) directive (https://eur-lex.europa.eu/eli/dir/2016/2284/oj, last access: 2 November 2022). Compared to 2005, Germany has to reduce NH_3 emission by 29 % and NO_x by 65 % until 2030. Attaining these targets is thought to lower the percentage of critical load exceedances to about 50% in 2030 (Schaap et al., 2018). Hence, the issue of eutrophication will stay relevant as nitrogen deposition needs to go down further to protect the majority of the German habitats. It is therefore important to understand how to reduce the emissions such that the deposition is lowered towards the critical level. Establishing the nitrogen deposition, however, is a challenging endeavor as the system is complex and the deposition fluxes are hard to quantify experimentally.

1.1.3 From emission to deposition

After release of NH_3 and NO_x into the atmosphere, a number of processes are relevant. At first, near source dispersion dilutes the plume downwind of the source. The concentrations are mixed into the planetary boundary layer and concentrations decline fast with distance to the source. Further transport is governed by the advection along the wind. During transport, N_r compounds are subject to chemistry and removal by wet and dry deposition.

After emission, NO is converted rapidly into NO_2 by reacting with O_3. The NO_2 is mostly oxidated further to nitric acid (HNO_3) though reaction with free hydroxyl radicals during daytime and through a reaction chain involving dinitrogen pentoxide (N_2O_5) during nighttime (Hertel et al., 2012). Both reactions occur relatively fast, and the atmospheric lifetime of NO_x ranges from a few hours to days (Seinfeld and Pandis, 2006; Kenagy et al., 2018). Additional reaction pathways include the formation of reservoir species (Peroxyacetylnitrate (PAN) and HONO) which react back to NO_x. Hence, the nitrogen oxide chemistry is relatively complex. In contrast, the chemistry of NH_3 is quite simple.

NH_3 only reacts to with acids to form particulate matter. Besides the mentioned HNO_3, H_2SO_4 plays an important role. The conversion to $(NH_4)_2SO_4$ occurs relatively fast (Seinfeld and Pandis, 2006), whereas the reaction of NH_3 with HNO_3 to NH_4NO_3 is in an equilibrium and depends on temperature and relative humidity (Behera et al., 2013). At warmer and low humid conditions, the equilibrium shifts towards the gas phase, whereas in winter NH_4NO_3 is formed efficiently (Wyers and Duyzer, 1997; Van Oss et al., 1998). Due to chemical conversions, the fates of NH_3, NO_x, and sulfur compounds are connected. Moreover, they form compounds that are more or less likely to be removed from the atmosphere, thereby affecting their transport distance.

At a certain point, all N_r compounds are removed from the atmosphere through deposition. Nitrogen compounds are removed from the atmosphere mainly by wet and dry deposition. Wet deposition refers to the uptake of the compounds in cloud water or rain droplets, which remove them from the atmosphere when the rain droplets reach the surface. Water soluble gases like NH_3, HNO_3, and particles, which favor water nucleation on their surface, can be efficiently removed by the process of wet deposition (Hertel et al., 2012) but water insoluble gases like NO_x not. Note that there is also a wet process called occult deposition, which usually occurs during dawn due to fog or dew (Fowler et al., 1989). It is less important compared to rain out but probably more relevant in the mountains (Hertel et al., 2011; Lovett et al., 1982).

The second main removal process is dry deposition. Dry deposition describes the direct removal of N_r compounds by plants, soil, or water surfaces (Farquhar et al., 1980; Flechard et al., 2013; Nemitz et al., 2001). Describing the process of dry deposition for N_r compounds is challenging since the direction of the biosphere-atmosphere exchange differs for each N_r compound. In general, the dry deposition velocity, which describes the speed of dry deposition, is large for water soluble, reactive gases, whereas that of insoluble gases and small particles is slow. In case of NH_3, exchange is bidirectional, i.e., it can be taken up by the surface or re-emitted (e.g., Nemitz et al., 2001; van Zanten et al., 2010; Wichink Kruit et al., 2010; Zhang et al., 2010). The concentration, at which the net exchange is balanced, is called (total) compensation point (Farquhar et al., 1980; Sutton et al., 1998) that is influenced by exchange pathways with the stomata, leaves, and soil surfaces with each of them having a compensation point (e.g., Farquhar et al., 1980; Neirynck and Ceulemans, (2008); Nemitz et al., 2000,2001; Schrader et al., 2016: Wichnik Kruit et al., 2010,2017). Emission of NH_3 from the surface occurs if NH_3 concentration, which is stored in plants or the soil, is higher than the ambient concentration. For HNO_3 (Pryor and Klemm, 2004; Horii et al., 2006), NO_2, and particulate nitrogen compounds (Wolff et al., 2010b), exchange is usually unidirectional, i.e., uptake by the surface, although a compensation point for NO_2

is still under discussion (Chaparro-Suarez et al., 2011; Breuninger et al., 2013). Deposition of NO is rarely observed (Meixner, 1994).

Due to its high water-solubility and reactivity, NH_3 has a short atmospheric lifetime (e.g., Dammers et al., 2019) and thus its transport range is limited. About half of the NH_3 is deposited within 100 km from its source. In forms of ammonium aerosols, nitrogen can typically remain in the atmosphere for a week before it is rained out (e.g., Pye et al., 2009; Liakakou et al., 2022), and can therefore affect regions far away from their emission sources. As stated above NO and NO_2 have an atmospheric lifetime from an hour to days and are mainly oxidized to nitric acid as their deposition is rather ineffective. Due to its high reactivity and water solubility, HNO_3 has a short atmospheric lifetime and it is easily deposited or converted into particulate matter. The latter extends the transport range of the oxidized nitrogen significantly.

In short, the transport, chemical transformation, and wet and dry deposition all take place continuously causing a highly variable system of N_r compounds driven by weather conditions. The location and size of emission sources and the interplay of these weather dependent processes determine where the nitrogen compounds are deposited. Current modelling efforts indicate that, on average, the dry deposition contributes almost half (46 %) to total N deposition in Germany (Schaap et al., 2018), which highlights the need of an accurate quantification of N dry deposition to provide reasonable total nitrogen deposition estimates.

1.1.4 Measurement techniques for establishing nitrogen deposition

To evaluate the efficiency of nitrogen mitigation strategies and identify exceedances of critical loads, accurate measurements of nitrogen deposition are necessary. Wet deposition is usually measured by collecting precipitation (Fowler et al., 1990; Erisman and Draaijers, 1995) using bulk or wet-only samplers (Staelens et al., 2005). Especially measuring the N dry deposition is challenging since dry deposition of N_r compounds depend on several parameters like atmospheric turbulence, meteorology, surface properties, surface concentration, and their different chemical and physical properties as outlined above.

First attempts in measuring boundary layer concentrations of particulate and water-soluble N_r compounds were made by using wet chemical samplers like KAPS denuders (Kananaskis Atmospheric Pollutant Sampler, Peake, 1985; Peake and Legge, 1987) and passive samplers (Ferm, 1991). Using dry deposition models (Grünhage and Haenel, 1997, 2008) and measurements of local turbulence, dry deposition fluxes of N_r compounds can be estimated (Dämmgen et al., 2010; Hurkuck et al., 2014). However, samplers need a long exposure duration of weeks or a month for collecting a sufficient amount on coated surfaces. In addition, using long-term concentration averages instead of high-resolution data in modeling applications can lead to significant deviations in deposition estimates (Schrader et al., 2018).

For measuring the exchange of N_r compounds the most direct approach is the eddy-covariance (EC) method (Dabbert et al., 1993) but most gas analyzers commercially available during that time did not meet the requirements for EC flux measurements. Analyzers were not able to sample with a high frequency (> 5 Hz) and their response time was higher than 1 sec (Ammann et al., 2012). In case of NO and NO_2, first direct flux measurements using the EC method have been reported since end of 20th century (e.g., Civerolo and Dickerson, 1998; Delany et al., 1986; Eugster and Hesterberg, 1996; Farmer et al., 2006; Horii et al., 2004; Li et al., 1997). Designing instruments measuring N_r species like NH_3 or HNO_3 was challenging due to their high reactivity and water solubility. Thus, two different flux calculation methods, the aerodynamic gradient method (AGM) (Businger et al., 1971,1986; Dyer and Hicks, 1970) and the relaxed eddy accumulation method (REA) (Hicks and McMillen, 1984; Businger

and Oncley, 1990), were developed. These methods are suitable for instruments with a lower sampling resolution (> minutes). Both methods were successfully applied in past field studies of NH_3 (e.g., Hansen et al., 2015; Hensen et al., 2009; Loubet et al., 2009; Milford et al., 2009; Myles et al., 2007; Nemitz et al., 2004; Wolff et al., 2010; Wyers and Erisman, 1998), HNO_3 (e.g., Meyers et al., 1998; Sievering et al., 2001; Pryor et al., 2002; Pryor and Klemm, 2004), and even for NO and NO_2 (e.g., Muller et al., 2009; Watt et al., 2004; Stella et al., 2012) due to high acquisition costs of fast-response instruments. For a detailed overview of applied flux calculation techniques please see Table 1 of Walker et al. (2020).

With technological advances in laser spectroscopy and progress in the instrument's inlet design (Ellis et al., 2010), flux measurements of NH_3 using the EC method were successfully made with closed-path instruments (e.g., Ferrara et al., 2012; Zoell et al., 2016; Moravek et al., 2019) and quite recently with open-path instruments (Wang et al., 2021, 2022; Swart et al., 2022). However, for long-term monitoring of total reactive nitrogen deposition several individual instruments measuring each compound individually are needed, which is not affordable due to high acquisition cost and maintenance of the instruments. Only a few EC flux measurements were made on NO_y (Munger et al., 1996,1998; Horii et al., 2006), the sum of all oxidized nitrogen species, but no high-resolution flux measurements of reduced nitrogen NH_x were made by the authors.

The total reactive atmospheric nitrogen converter, hereafter called TRANC, designed by Marx et al. (2012) closed the gap. The TRANC converts the most important N_r compounds including NO_2, NH_3, HNO_3, HONO, pNH_4^+, and pNO_3^- to NO efficiently as shown by Marx et al. (2012). Coupling the TRANC to a fast-response CLD, the setup performs high-frequency concentration measurements of NO, which corresponds to the total reactive nitrogen concentration, hereafter abbreviated as ΣN_r. In combination with a sonic anemometer, this setup performs high-resolution flux measurements of ΣN_r using the EC method, and thereby allows the estimation of the ΣN_r dry deposition to various ecosystems with a single instrument. In a recent review of measurement techniques by Cowan et al. (2022), the TRANC/CLD flux system was highlighted as "*the most cost-effective eddy covariance approach for the direct measurements of N_r fluxes by avoiding the need for multiple instruments.*"

Field studies by Ammann et al. (2012), Brümmer et al. (2013), and Zoell et al. (2019) have shown that the TRANC/CLD system is suitable for investigating the ΣN_r exchange. Measuring fluxes of N_r compounds with the EC method is still challenging. Originally, the EC technique was designed for calculating turbulent, energy, and greenhouse gas fluxes (Aubinet et al., 1999; Baldocchi et al., 2003) and is nowadays the standardized flux calculation procedure in greenhouse gas flux observation networks (FLUXNET Baldocchi et al., 2001, ICOS Heiskanen et al., 2022). Consequently, developed pre and post-processing routines for flux calculation are not directly applicable to N_r compounds. Thus, there is a dire need for new methods in particular for estimating high-frequency flux losses and filling gaps in flux time series in order to provide reasonable estimates of N_r deposition. As already mentioned, instruments integrated in EC setups have high acquisition costs and require continuous monitoring of their performance and extensive maintenance. Thus, only a few long-term observations on N_r compounds using micrometeorological methods have been made so far. Even no long-term, continuous measurements of ΣN_r have been conducted yet.

Generally, measurements of N_r compounds have only a limited spatial representativeness. Furthermore, common observation networks of N_r compounds are generally scare and mostly provide measured data with low temporal resolution. Due to limitations in measurements and the large variability in the exchange dynamics of N_r species, chemical transport models (CTMs) have been developed to predict N_r deposition of large regions allowing the evaluation nitrogen mitigation strategies. The CTM LOTOS-EUROS (LOng Term Ozone Simulation – EURopean Operational Smog) (Wichink Kruit et al., 2012; Manders et al., 2017; van der Graaf et al., 2020) is used to determine N dry deposition of NO, NO_2, NH_3, HNO_3, pNH_4^+, and pNO_3^- using the bidirectional exchange model DEPAC (van Zanten et al., 2010; Wichink Kruit et al., 2012) across Germany. As input variables meteorological data obtained from the

European Centre for Medium Range Weather Forecasts (ECMWF), information about the land use fractions of the grid cell based on the Corine Landcover classification (Büttner and Kosztra, 2011,2017) and an emission inventory are used to determine modeled input concentrations. However, there are still large uncertainties in modeled deposition budgets (Theobald et al., 2019). A comparison study to flux measurements of ΣN_r may provide important feedback on the representativeness of the input data and the bidirectional parameterization.

In thesis, novel EC measurements of ΣN_r using the TRANC were performed and interpreted. Therefore, I first provide a deeper introduction to the different flux calculation methods including the EC method below. Second, a description of the TRANC/CLD system and its integration in an EC setup is provided focusing on the design of the TRANC and the necessary steps for flux pre- and post-processing. The introductory section is closed with an overview about modeling N_r fluxes including information about DEPAC and LOTOS-EUROS. Finally, the aims of this thesis are written out based on the formulated research questions.

1.2 Measuring the net exchange using micrometeorological methods

For estimating the net exchange between biosphere and atmosphere, several methods were developed as outlined above, for example, the aerodynamic gradient, the relaxed eddy accumulation, and the eddy-covariance method. These methods are described in the following subsections.

1.2.1 The Aerodynamic Gradient Method (AGM)

The aerodynamic gradient method (AGM) relies in principle on Fick's first law and the Monin–Obukhov similarity theory (Foken, 2006). The flux is calculated by multiplying the diffusion coefficient in air (K), which depends on friction velocity (u_*), Obukhov-length (L), and aerodynamic measurement height (z-d), with the vertical concentration gradient (Businger et al., 1971,1986; Dyer and Hicks, 1970). Negative fluxes indicate exchange directed towards the surface. This sign convention is used throughout this thesis.

$$F = -K(u_*, z-d, L) \cdot \frac{\partial C}{\partial z} \tag{1.1}$$

By integrating Eq. (1.1) between the measurement heights z_1 and z_2, the resulting flux equation has the following form (e.g., Trebs et al., 2021):

$$F = -\frac{u_* \cdot \kappa}{\ln\left(\frac{z_2}{z_1}\right) - \psi_H\left(\frac{z_2}{L}\right) + \psi_H\left(\frac{z_1}{L}\right)} \cdot \Delta C \tag{1.2}$$

Here, κ is the von Karman constant and ψ_H is the integrated stability correction function for stable (Webb, 1970) and unstable stratification (Paulson, 1970; Businger et al., 1971). Mueller et al. (1993) describes the left term of the product as transfer velocity (v_{tr}). Its inverse is the resistance related to vertical turbulent transport between the measurement heights.

Using the AGM in field applications, does not require fast-response analyzers. Micrometeorological variables like u_* and sensible heat (H) are usually determined from sonic anemometer measurements using the EC approach as done by Kamp et al. (2020) for example. Still, the gas analyzer has to resolve vertical concentration differences accurately (Edwards et al., 2005; Wolff et al., 2010a), which may be challenging for sites with a generally low background concentration (Foken et al., 2016). Increasing the measurement height has to be thoroughly considered, since the footprint dimensions change and may not be representative for the ecosystem anymore. In addition, measured profiles of micrometeorological

variables can deviate from their theoretical entities, especially above high canopies, e.g., forests (Foken et al., 2016).

1.2.2 The Relaxed Eddy Accumulation (REA) method

Similar to AGM, the relaxed eddy accumulation (REA), which originates from the eddy accumulation method (Desjardins, 1972,1974) and written out by Hicks and McMillen (1984) and Businger and Oncley (1990), enables flux measurements using a slow-response gas analyzer (a few minutes to hours) combined with a fast-response sonic anemometer. The flux is determined by the difference of the mean concentrations of the upward ($\bar{c}_{\uparrow}$) and downward ($\bar{c}_{\downarrow}$) moving eddies.

$$F = \beta\, \sigma_{\mathrm{w}}\, (\bar{c}_{\uparrow} - \bar{c}_{\downarrow}) \tag{1.3}$$

For differentiating between those eddy motions, a switching valve reacting to instantaneous changes in the direction of the vertical wind is connected to the sampling inlets. The standard deviation of the vertical wind is given by σ_{w}. β is an empirical unitless value, which is usually determined from sensible heat or momentum flux measurements (Pattey et al., 1993; Ammann, 1999; Zemmelink et al., 2004) and is usually between 0.40 and 0.63 according to Milne et al. (1999).

$$\beta = \frac{\overline{w's'}}{\sigma_{\mathrm{w}}\, (\bar{s}_{\uparrow} - \bar{s}_{\downarrow})} \tag{1.4}$$

Here, *s* represents averages of a scalar quantity like temperature for the up and downward turbulent motions. In case of temperature, $\overline{w's'}$ represent the sensible heat flux. Since REA relies on vertical wind speeds different from zero, determining concentrations differences for *w* close to zero is challenging or even not possible. Therefore, a so-called deadband is introduced using a constant β (Hensen et al., 2009).

1.2.3 The Eddy-Covariance (EC) method

When using the eddy-covariance (EC) method, each eddy contributing to the flux during a certain time interval can be recorded if the response time of the gas analyzer is fast enough. Often, eddy covariance and eddy correlation are named in the same context, but both phrases refer to different methods (Foken et al., 2016). Nowadays, most analyzers for gases or aerosols have a response time less than 1 s (Ammann et al., 2012) and record concentrations with sampling frequencies larger than 5 Hz (Burba, 2013), which is necessary for EC flux measurements. Thus, the EC method is the most direct approach (Dabbert et al., 1993) for calculating the vertical flux as the covariance of the deviations of vertical wind and concentration ($\overline{w'c'}$) multiplied with the mean half-hourly air density (ρ_{a}). In case of time-displaced measurements of vertical wind and concentration, a time lag (t_{lag}) in concentration measurements must be considered (Foken et al., 2016).

$$F \approx \overline{\rho_{\mathrm{a}}} \cdot \overline{w'c'} = \overline{\rho_{\mathrm{a}}} \cdot \sum_{i=1}^{n} (w(t) - \bar{w}) \cdot (c(t + t_{\mathrm{lag}}) - \bar{c}) \tag{1.5}$$

Generally, the vertical flux to the surface is the mean product of the air density, the vertical wind, and the concentration. To extract the instantaneous variation from each variable, Reynolds' Decomposition is applied, which defines time-averages of fluctuations as zero.

(1.6)

$$F = \overline{\rho_a w c} = (\overline{\rho_a} \cdot \overline{w'c'} + \overline{\rho_a}\,\overline{w}\,\overline{c} + \overline{w} \cdot \overline{\rho_a' c'} + \bar{s} \cdot \overline{\rho_a' w'} + \overline{\rho_a' w' s'}) \approx \overline{\rho_a} \cdot \overline{w'c'}$$

For calculating fluxes following the EC approach, two important assumptions have to be made. Density fluctuations and the mean vertical flow are assumed to be negligible. The latter implies no flow convergences and divergences (Burba, 2013). These assumptions hold for a flat and horizontal homogenous surface (footprint). Analog to AGM and REA, it is assumed that measurements at a single point represent the upwind area and done in the "constant flux layer" (Sect. 1.2.4), and the footprint has to be chosen wisely so that most fluxes refer to the area of interest (Burba, 2013).

1.2.4 Limitations of flux measurements using micrometeorological methods

Equation (1.6) addresses the vertical turbulent exchange occurring at the top of a control volume and contributes to the generalized EC equation (Foken et al., 2016). The latter can be derived by integrating the continuity equation. For the full description of the net ecosystem flux, a storage term, which considers temporal variations in the concentrations between the ground and the measurement height, and horizontal and vertical advection terms have to be added. The advection terms are more likely non-negligible but quantifying their contribution to the total net flux is challenging due to missing possibilities of direct measurements and uncertainties in the advection calculation (Aubinet et al., 2010; Montagnani et al., 2010; Siebicke et al., 2012; Aubinet et al., 2012; Foken et al., 2016). Instead of correcting the determined fluxes for advections by doing flux measurements at different locations in the flux footprint, it is suggested to exclude flux measurements of insufficient turbulence mostly occurring during nighttime, prove if the mean vertical wind is close to zero, and check flux stationarity and turbulent conditions following the steady state test and integral turbulence characteristic test (Foken et al., 2016).

Quantifying the storage term sufficiently needs additional concentrations measurements below and above the EC measurement height. However, this requires additional analyzers or multiple inlets connected to a single analyzer (Montagnani et al., 2018). Both approaches for obtaining a vertical concentration profile have merits and drawbacks: One gas analyzer connected to different inlets results in a reduction in data coverage. Using more gas analyzers leads to a better data coverage but parameters affecting the instrument's performance like temperature or humidity have to be adjusted with care in order to acquire the same signal strength for all instruments. In addition, the increased spatial dimensions of the EC setup, which may affect local turbulence, acquisition costs, and maintenance effort should be considered. This significant investment in site equipment is usually not realizable

A one-point approach like assuming a constant trace gas concentration below the EC measurement height and a linear vertical profile, is a crucial assumption and associated with large uncertainties. In case of N_r compounds, only a few field studies concentrated on the impact of advection and storage fluxes on NH_3 using AGM (Loubet et al., 2009; Milford et al., 2009) and REA (Hensen et al., 2009). Storage flux calculations using EC were made for NO_x (Munger et al., 1996) and NO_y (Geddes and Murphy, 2014). In case of NH_3, storage and advection fluxes are generally small compared to vertical fluxes and thus close to the flux detection limit of the instrument (Loubet et al., 2009; Milford et al., 2009; Hensen et al., 2009). Storage terms are probably negligible since NH_3 is consumed or emitted relatively fast by the surface (Sutton et al., 1993). On longer time scales, the effects by advection are probably compensated.

Generally, these micrometeorological methods are established in measurement setups, which are installed in the lowest part of the planetary boundary layer (PBL), the surface layer (SL). The surface layer height is approximately 10 % of the PBL (Panofsky and Dutton, 1984). The height of the PBL depends on various parameters like wind speed, surface roughness, and thermal heating and cooling

inducing changes in the stratification of the PBL. During daytime, the typical PBL height ranges between 1 to 2 km, whereas 50 to 500 m are observed during the night (Oke, 1987). In the surface layer, variations of vertical fluxes are usually lower than 10 %, which are likely close the flux detection limit of the instruments (Ammann, 1999). Thus, fluxes in the SL are commonly treated as constant in the vertical leading to term constant flux layer. Since the surface has a certain roughness, the SL is divided into an inertial sublayer and a roughness layer. The roughness layer height is approximately 1.5-2 times the canopy height (Burba, 2013). So, strictly speaking the inertial sublayer, in which fluxes are assumed to be vertically and horizontally constant and surface fluxes are equal to the vertical fluxes at any height in that layer, refers to the term constant flux layer. The micrometeorological methods described above are based on this concept and limited to that layer.

1.2.5. Spectral description of the flux – Spectra and Cospectra

Considering the air flow in the constant flux layer, it is assumed that most of the transport is done by eddies, which have different sizes and rotating velocities. At surface level, small-scale faster rotating eddies prevail in the measured flux, whereas the contribution of large-scale slow rotating eddies to the flux is larger further away from the canopy. In the first case, air transport is done by high-frequency motion, in the second case by low-frequency motion (Burba, 2013). Thus, the air flow consists of eddies varying in spatial and temporal scale. Due to Taylor's frozen turbulence hypothesis (Taylor, 1938) assuming that eddies do not change in size significantly when carried by the mean wind and finally recorded by the instrument, the flux calculation following Eq. (1.5) and a subsequent spectral analysis of turbulent motion can actually be made. A (co)spectrum shows the distribution of small and large-scale eddies to the measured (co)variance and further shows the ability of the instrument to detect certain eddies.

Spectra and Cospectra are determined by applying the Fast-Fourier-Transformation (FFT) to high-resolution raw data. The measured time series is decomposed in a linear combination of harmonic cosine and sine functions multiplied with their respective Fourier components A_x and B_x, respectively. FFT processing is done until the Nyquist frequency (n_f) is reached. Thus, eddies only occurring below half of sampling frequency can be resolved. According to Parseval's theorem, the variance spectrum, also called power spectrum (Ps), can be expressed by the variances of the Fourier components. The total variance is determined by the sum of all frequencies contributing to the power spectrum until n_f. Here, *n* is a dimensionless variable defined as the product of the frequency *f* multiplied with the corresponding time averaging interval T_a.

$$\mathrm{Ps_x}(n) = \frac{1}{2}\left(A_\mathrm{x}^2(n) + B_\mathrm{x}^2(n)\right) \text{ with } \sigma_x^2 = \sum_{n=1}^{n_\mathrm{f}} \mathrm{Ps_x}(n) \tag{1.7}$$

The cospectrum (Co) can be derived from the covariance of the Fourier components of the measured raw time series, and the sum of all frequencies of the cospectrum is the total covariance – the measured flux. The cumulative of all cospectral frequencies is called ogive.

$$\mathrm{Co_{xy}}(n) = \frac{1}{2}\left(A_\mathrm{x}(n)A_\mathrm{y}(n) + B_\mathrm{x}(n)B_\mathrm{y}(n)\right) \text{ with } \mathrm{cov}(x,y) = \overline{xy} = \sum_{n=1}^{n_\mathrm{f}} \mathrm{Co_{xy}}(n) \tag{1.8}$$

It is convenient to multiply the obtained power spectrum and cospectrum with the frequency and normalize them by their total (co)variance. Thus, the area under the curve is normalized to one and insufficient spectral responses of different instruments can be directly identified by comparing them to an ideal (co)spectrum. For an optimized visualization, the normalized (co)spectrum is plotted against logarithmic scaled frequencies since most frequencies are at the end of the available frequency range and averaged into evenly logarithmic spaced bins. Details to the derivation of the power and cospectrum are given in Ammann (1999).

Since the cospectrum is calculated by multiplying FFT coefficients of different raw time series, the raw time series have to be shifted against each other according to the measured time lag. Obviously, this mathematical operation is not required for power spectra, but they are affected by noise occurring in the high-frequency range. The noise can be removed by subtracting a linear regression, which is made on the affected high frequencies, from the measured power spectrum (Ibrom et al., 2007). The cospectrum is not influenced by noise since noise of the different time series is not or hardly correlated with each other. Depending on the measurement setup and the investigated compounds, power spectra or cospectra are useful for describing the contribution of small and large-scale eddies to the measured flux. For the spectral analysis of ΣN_r fluxes, cospectra were chosen since they are hardly affected by any noise. Power spectra of ΣN_r fluxes exhibited distinct uncorrelated noise, so-called white noise, making them unusable for the spectral analysis (see chapter 2).

The ability of the instruments to resolve large and small-scale eddies is characterized by comparing the power spectrum of concentration or the cospectrum of vertical gas or particle flux to an ideal, unattenuated spectrum (Aubinet et al., 2012; Burba, 2013). An "ideal" power spectrum is the spectrum of temperature, the corresponding cospectrum is the (sensible) heat flux cospectrum. Both spectra are derived from instantaneous sonic anemometer measurements. Using them as reference spectra is strictly speaking not correct since measurements of temperature and wind components are damped due to the path length of sonic transducers and electronic filters. However, these effects are negligible compared to the damping of the compound's flux.

Figure 1.4 shows a comparison of cospectra for the heat flux (Co(w,T)) and ΣN_r flux (Co(w, ΣN_r)). Here, common cospectra are shown calculated from EC flux measurements done at a semi-natural peatland site (BOG) and above a mixed forest site (FOR) using the TRANC/CLD system. Basically, the installed EC setup was the same besides tube length and measuring height. The EC setups were installed close to the ground (~2.5 m) and 30 m above the forest floor.

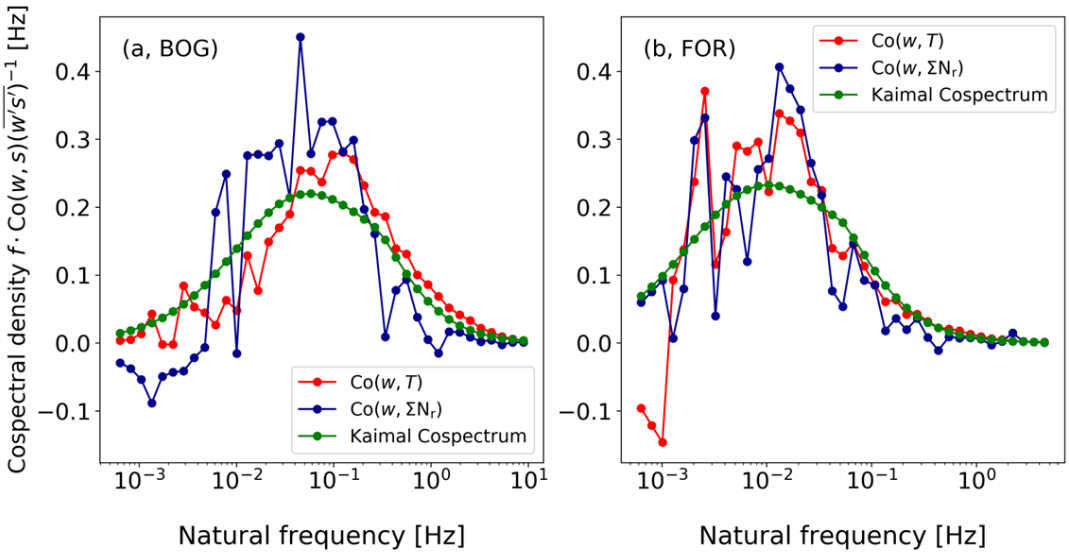

Figure 1.4: Comparison of observed normalized cospectra of the heat flux (Co(w,T)) (red) and ΣN_r flux (Co(w, ΣN_r)) (blue) with modified Kaimal cospectra (green) for similar wind speed and stability at the seminatural peatland site (BOG) and the forest site (FOR).

In the low-frequency range, sensible heat and gas flux cospectra showed no explicit differences. Thus, low-frequency contributions to the flux were captured by the gas analyzer. After the cospectral peak, which is around 0.2 Hz for BOG and around 0.02 Hz for FOR in the shown example, the contribution

of high-frequencies to Co(w, ΣN_r) decreased sharply, in particular at the BOG site. Also for the FOR site, a mismatch in the shape between the cospectra was identified, but the difference to Co(w,T) was smaller. However, small-scale eddies had not been fully resolved by the gas analyzer leading to a missing spectral response. The (co)spectral flux loss characterize the ability of the installed EC system to measure fluxes with high-temporal resolution. Generally, flux losses occurring in the low and high-frequency range of the cospectrum or power spectrum cannot be avoided, because a combination of site, instrument, and compound specific parameters influence the spectral response. However, different methods have been developed in order to determine the low and high-frequency flux losses. A description to these methods is given in Sect. 1.3.3 and chapter 2.

In addition, with increasing wind speed, the cospectral peak usually shifts towards higher frequencies leading to an increase in flux attenuation. During stable stratification, the cospectrum is mostly broader around its maximum with a significant contribution of high frequencies to the measured flux. At unstable conditions, the cospectum narrows around its maximum. Flux attenuation should be invariant to unstable stratification. The observations on wind speed, stability, and measurement height lead to the theoretical formulation of stable and unstable cospectra done by Kaimal et al. (1972) and further modified by Moncrieff et al. (1997). This theoretical cospectrum is shown Fig. 1.4 and depends only on variables determined by turbulence.

1.3 Implementing the EC method in field applications

1.3.1 Setting up the TRANC for ΣN_r flux measurements

For investigating the ΣN_r exchange of various ecosystems, a custom-built converter, the Total Reactive Atmospheric Nitrogen Converter called TRANC and designed after Marx et al. (2012), was coupled to a fast-response chemical luminescence detector (CLD 780 TR, ECO PHYSICS AG, Dürnten, Switzerland) recording NO concentrations in the sample air with a high sampling frequency of 10 or 20 Hz. CLD and TRANC were connected via an opaque PFTE tube preventing reactions of NO with oxygen (O_2) induced by sunlight. Air transport through the tubes was performed by a dry vacuum scroll pump (BOC Edwards XDS10, Sussex, UK) connected to the CLD. This system has response time of 0.3 s (Marx et al., 2012) thereby being fast enough for flux measurements using the EC method. To estimate the ΣN_r exchange, the TRANC-CLD setup was complemented by a 3-D ultrasonic anemometer (GILL-R3, Gill Instruments, Lymington, UK) measuring local turbulence including wind direction, wind speed, stability, and friction velocity. In addition, the EC setup was extended with meteorological instruments. Generally, fluxes were evaluated on half-hourly time intervals, which is a common agreement in the flux community. Choosing a larger or smaller window leads to an underestimation of small or large-scale eddies, respectively. Therefore, we made the ogive test (Aubinet et al., 2012). If the ogive of the half-hourly time interval approaches constant values at low frequencies, the interval is sufficient for measuring turbulent fluctuations. This criterium was fulfilled at the measurement sites.

Figure 1.5: TRANC installation at the measurement sites (**left**: semi-natural peatland with bog-heather, moor birches, and Scots pines; **right**: natural mixed forest with mainly spruce and approx. 20% beech trees in the flux footprint)

Basically, this setup was the same at both measurement sites, a temperate mixed forest located the Bavarian Forest National Park in southeast Germany and a semi-natural peat land in northwest Germany (Fig. 1.5). Site-specific vegetation and meteorology are described in chapters 2 and 3. Further details about the peatland site can be found in Hurkuck et al. (2014, 2016). For the forest site, studies by Beudert and Gietl (2015) and Zöll et al. (2019) are recommended. Due to the different vegetation types and height, the arrangement of the setup was different in tube length and sensor separation.

As written in Sect. 1.1.4, the TRANC converts the most important reactive nitrogen compounds to NO providing the possibility to determine ΣN_r concentrations. A schematic sketch of the TRANC is shown in Fig. 1.6.

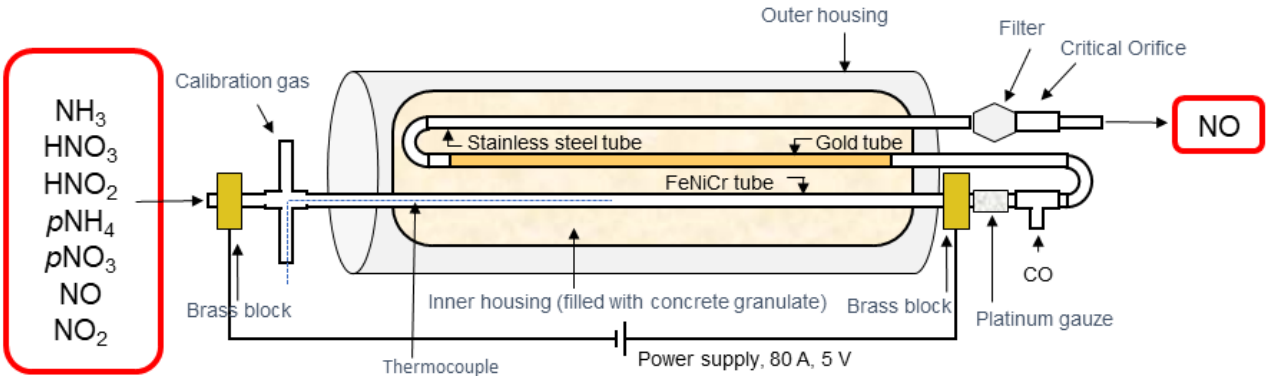

Figure 1.6: Schematic sketch of the total reactive atmospheric nitrogen converter (TRANC). Adapted from Marx et al. (2012)

The conversion of N_r compounds to NO is happening in two steps. A thermal conversion takes place in an iron-nickel-chrome (FeNiCr) tube. This tube is heated up to 870°C via an electric resistance heater. At this temperature, NH_4^+ and NO_3^- aerosols like NH_4NO_3, $(NH_4)_2SO_4$, sodium and calcium nitrate are separated into their subcomponents (Yuvarai et al., 2001). These aerosols are properly converted by the TRANC as shown by Marx et al. (2012). The authors found conversion efficiencies of 142 %, 78 %, and 91 % for NH_4NO_3, sodium nitrate, and $(NH_4)_2SO_4$, respectively. The high conversion efficiency of NH_4NO_3 is probably related to the fast volatilization of NH_4NO_3 into NH_3 and HNO_3. For N_r gases, the authors determined conversion efficiencies close to 100%, for example 95 % and 99 % in case of NH_3 and NO_2, respectively. The following thermal conversions occurs inside the FeNiCr tube:

$$\begin{aligned} NH_4NO_3 &\rightarrow NH_3 + HNO_3 \\ 2\,HNO_3 &\rightarrow 2\,NO_2 + H_2O + 1/2\,O_2 \\ HONO &\rightarrow NO + OH \\ 4\,NH_3 + 5\,O_2 &\rightarrow 4\,NO + 6\,H_2O \end{aligned} \qquad (1.9)$$

In that tube, NH_4NO_3, as an example, is thermally split up into NH_3 and HNO_3. Due to the high temperatures, HNO_3 dissociates into NO_2, H_2O, and O_2. After passing the FeNiCr tube, a platinum gauze is mounted enabling the oxidation of NH_3 with O_2. At this stage, all convertible N_r compounds were oxidized to NO_2 or NO. Before entering the gold tube, carbon monoxide (CO) is added to the air sample. Inside the gold tube, which is passively heated to 300°C, a chemical conversion of NO_2 to NO utilizing CO as reducing agent occurs.

$$NO_2 + CO \rightarrow NO + CO_2 \tag{1.10}$$

At the end of the TRANC a critical orifice was mounted. This ensures a low-pressure regime along the sample line assuring a turbulent flow regime inside the sample line.

The chemiluminescence principle is used to detect NO in the sample air. Therefore, the CLD has to be supplied with O_2, which is converted to O_3 by an integrated ozone generator, and the sample air is flushed into the analyzing cell. In the presence of O_3, the following reactions happen inside the analyzing cell.

$$\begin{aligned} NO + O_3 &\rightarrow NO_2 + O_2 \\ NO + O_3 &\rightarrow NO_2^* + O_2 \\ NO_2^* &\rightarrow NO_2 + h\nu \\ NO_2^* + M &\rightarrow NO_2 + M \end{aligned} \tag{1.11}$$

Excited NO_2^* molecules are formed from NO and O_3 in the sample air and leave the unstable energetic state by emitting a photon spontaneously. The light emission is recorded by a photomultiplier. Registered counts are proportional to NO concentration in the sample air. However, most of the NO_2^* molecules collide with other molecules and thereby returning into the ground state without emitting a photon. To reduce the impact of the so-called quantum mechanical quenching, pressure regime in the analyzing cell has to be kept between 10 and 20 mbar suggested by the manufacturer. Thus, CLD cell pressure, TRANC temperature, and flow rate were continuously monitored to keep luminous efficacy of the CLD and conversion efficiency of the TRANC at maximum.

Measured concentrations of the CLD and wind components were collected at the interface of the sonic anemometer, and the software package EddyMeas, included in EddySoft (Kolle and Rebmann, 2007) was used to record data with a sampling rate of at least 10 Hz.

1.3.2 From concentrations to fluxes – pre and post-processing steps in EC applications

Before fluxes could be determined from raw concentrations with the EC method, several pre-processing steps were applied to concentration and wind component measurements. Flux calculation and pre-processing steps were carried out by the flux calculation software EddyPro on half-hourly basis. EddyPro is an open-source flux calculation software (https://github.com/LI-COR/eddypro-engine, last access: 2 November 2022) provided by the company LI-COR Biosciences. In the following, necessary steps for flux calculation are described.

At first, concentrations were calibrated. Gas tanks providing different concentrations of NO were connected to the TRANC, and zero air was generated with a pure air generator. Calibrations of the system were repeated approximately each month.

Next, outliers were removed and replaced by a linear interpolation. Spike detection was done after Vickers and Mahrt (1997). Basically, values exceeding their average plus n times the standard deviation within a certain time window (one six of the flux averaging interval) are labelled as spikes. If more than

three consecutive values are labeled as outliers, values are not removed since it may hint on a physical trend. The value for n was set according to the standard settings of EddyPro.

Sonic temperature is averaged from estimates of the individual measurement paths of the sonic anemometer. A correction to each measurement path is applied due to the influence of the wind component perpendicular to each measurement path. For the chosen anemometer, the so-called cross-wind correction was done by the anemometer software. Since we used a Gill-R3 at the measurement sites, wind component measurements are inaccurate due to a distortion of the flow caused by the frame of the anemometer. Nakai et al. (2006) developed an algorithm in order to correct wind component measurements for the so-called angle of attack describing the deviation of the wind from the horizontal.

A further correction of the wind components is needed since they were measured in the coordinate system of the sonic anemometer. Thus, its coordinate system must be aligned to the local wind flow. A 2-D rotation of the anemometer's coordinate system results in nullifying the mean crosswind and mean vertical wind component. Therefore, rotation matrices determined by the rotation angle are multiplied with the wind vector (Wilczak et al., 2001). The first rotation is made around the z-axis minimizing crosswind component, the second rotation is made round the new y-axis minimizing the vertical wind component. A third rotation around the new x-axis nullifying the cross-stream stress ($\overline{v'_{\mathrm{rot}} w'_{rot}}$) was not applied since it may lead to biased wind speeds (Aubinet et al., 1999).

The last correction on raw time series involves a trend removal, for example, done by subtracting the average from the raw time series or applying a linear function (Gash and Gulf, 1996), a moving average (Moncrieff et al., 2004), or an exponentially weighted average (McMillen, 1988; Rannik and Vesala, 1999). Recorded half-hourly raw time series were detrended by subtracting their corresponding average. The described corrections have to be made before any time lag compensation and corresponding flux calculation can follow.

A time lag between measured concentrations and instantaneously measured wind components arises due to the separation distance between the sonic anemometer and the sample cell of the gas analyzer. The time lag of the installed setup is determined by the residence time of the sample air in the TRANC, the CLD, the tube connecting both devices, and the flow rate limited by the dry vacuum scroll pump and the critical orifice. For the installed setups, the peatland and the forest setup, we estimated time lags of 2.5 s and 20 s, respectively. Differences in time lags are related to the different tube lengths and dimensions of the critical orifice. In general, time lags are meaningful indicators showing the flux measuring performance of the setup. A non-existent time lag may be caused by instrumental issues like a blocked inlet, damaged tubes, pump failures, TRANC heating issues, empty CO and O_2 gas tanks, or by missing or non-detectable short-term concentration variability of the measured compound.

Basically, the time lag is estimated by shifting the time series of vertical wind and concentration against each other until their covariance is maximized. The maximum covariance represents the flux of the measured time interval after converting into common flux units. If additional micrometeorological measurements of temperature, pressure, and relative humidity are available, unit conversion and additional corrections of sonic temperature are done by using data of fast-response meteorological instruments.

Afterwards, fluxes assigned with a bad quality according to the Mauder and Foken (2006) criteria were filtered out. The quality test by Mauder and Foken (2006) involves a steady state test and an integral turbulence test. In order to remove half-hourly fluxes measured during insufficient turbulent conditions, a friction velocity threshold of 0.1 m s^{-1} was set. For N_r compounds, no automatic friction velocity threshold algorithms are currently available (Zöll et al., 2019). Absolute flux and concentrations limits were set based on visual data screening.

Water vapor quenching is a specific problem of the CLD technique. As described above, no photon is detected by the photomultiplier if NO_2^* collides with certain collision partners like O_2, N_2, CO_2, and

H_2O. For the latter, a sensitivity reduction of 0.19 % per 1 mmol mol^{-1} water vapor increase was found by Marx (2004) for the current CLD model. The effect was taken into account by adding the NO interference flux, which is proportional to the measured water vapor flux, to the determined flux value. H_2O fluxes were obtained from an open-path infrared gas analyzer, which was installed next to the TRANC/CLD setup. For further details to the correction, the publications of Ammann et al. (2012) and Brümmer et al. (2013) are recommended. The last step in flux post-processing is the correction of flux losses occurring in the high and low-frequency range of their spectrum (Sect 1.3.3).

Depending on the dimension of the flux footprint, an allocation of measured fluxes has to be considered. Based on the theoretical footprint model by Kljun et al. (2015), areas contributing to the measured flux can be identified and further excluded if fluxes originate from an aera, which is not of particular interest. As noted above, the EC method requires a uniform footprint. Thus, a footprint analysis emerges as a potential tool showing the representativeness of flux measurements and should be carried out before setting up the measurement site, if possible. At our sites, vegetation inside the flux footprints were not uniform, but flux footprints represent the typical peatland and forest structure at the sites. Thus, no wind direction or area filter was applied to measured fluxes.

After a successful flux correction, gap-filling methods are used for estimating emission or deposition budgets. For N_r compounds, common gap-filling methods designed for CO_2 like the marginal distribution sampling (Reichstein et al., 2005) are not applicable due to the low autocorrelation of N_r fluxes. Statistical methods like the Mean-Diurnal-Variation principle or interpolation techniques (Falge et al., 2001) are reasonable gap-filling methods, but the application on long-term gaps is not recommended. Progress has been made on artificial neural networks (Lucas-Moffat et al., 2022) and random forest approaches (Mahabbati et al al., 2021; Zhu et al., 2022) but experience on the performance of N_r species is still scarce.

1.3.3 Methods for estimating high-frequency flux losses of N_r compounds

As described in Sect. 1.2.5, measured fluxes show spectral losses in the high and low-frequency part of the (co)spectrum. Low-frequency attenuation is commonly related to the time averaging interval and the applied detrending method. Low-frequency flux losses are corrected by applying the method of Moncrieff et al. (2004) based on theoretical formulations of the Kaimal Cospectra for stable and unstable conditions (Moncrieff et al., 1997; Ammann, 1999) and an analytical spectral transfer function. Generally, a so-called spectral transfer function describes the flux attenuation for a specific frequency range. In the low frequency range, the shape of the transfer function is defined by the detrending method, which was applied to measured raw data. Transfer functions for different detrending methods are given in Rannik and Vesala (1999).

Spectral losses in the high-frequency range are commonly related to the dynamic frequency response of the instruments and possible mismatches in response characteristics between the instruments resulting in a phase-shift. Furthermore, physical characteristics of the setup like the design of the instruments, for example, the dimension of the analyzer cell and the path-length of the sonic anemometer, the separation distance between the analyzer's inlet and the sonic anemometer, and the prevailing flow regime inside tubes in case of enclosed-path instruments contribute to high-frequency flux losses. For each of these processes a spectral transfer function is defined. In order to determine the transfer function of the entire measurement setup, individual transfer functions are multiplied leading to the total transfer function (TF_{total}). In the following, the equations of commonly used transfer functions are described. A detailed description to the transfer functions are given in Moore (1986), Moncrieff et al. (1997), Ammann (1999), and Aubinet et al. (2012).

(1.12)

$$TF_{total} = TF_S \cdot \sqrt{TF_p} \cdot \sqrt{TF_w} \cdot \sqrt{TF_T} \cdot TF_R \cdot TF_{\Delta R}$$

The flux loss due to lateral sensor separation between the sonic anemometer and the cell of the open-path analyzer or the inlet of the closed-path analyzer is described by the transfer function TF_S.

(1.13)

$$TF_S(f) = \exp(-9.9(f\, d_s/u)^{1.5}) \text{ with } d_s = d_{sa}|\sin(\alpha_d)|$$

The frequency *f* is normalized by multiplying with the effective lateral separation distance d_s divided by the measured wind speed *u*. The measured lateral distance is represented by d_s, and α_d is the angle between an imaginary line connecting the sensors and the wind direction (Aubinet et al., 2012). The impact of longitudinal sensor separation on the measured flux is already corrected by the time lag adjustment (Ammann, 1999).

The transfer function TF_p, which describes the flux loss of scalar quantities like gas concentration and temperature due to spatial averaging along the sensor's path length (p_{sl}) , is defined as:

(1.14)

$$TF_p(f_p) = \frac{1}{2\pi f_p}\left(3 + \exp(-2\pi f_p) - 4\frac{1-\exp(-2\pi f_p)}{2\pi f_p}\right);\ f_p = \frac{f\, p_{sl}}{u_{ps}}$$

Here, u_{ps} is the flow speed in the sensor's path length. In case of open-path instruments, it is basically the averaged wind speed. The normalized frequency is represented by f_p. For the vertical measurement path of the sonic anemometer, a transfer function similar to TF_p is given (TF_w) but coefficients are slightly different. No generalized transfer functions are available for the other measurement paths. The sonic anemometer path length is given by p_{sw}, and the normalized frequency is f_w.

(1.15)

$$TF_w(f_w) = \frac{2}{\pi f_w}\left(1 + \frac{1}{2}\exp(-2\pi f_w) - 3\frac{1-\exp(-2\pi f_w)}{4\pi f_w}\right);\ f_w = \frac{f\, p_{sw}}{u}$$

Most measurement devices show a frequency response similar to a simple resistor capacitor (RC) filter. According to Moore (1986), the transfer function of a linear first-order filter has the following form:

(1.16)

$$TF_R(f) = \frac{1}{\sqrt{1 + (2\pi\tau_r f)^2}}$$

The response time of the measuring device (τ_r) indicates the time at which a recorded signal is reduced by 1/e after a step change. The cut-off frequency (f_0) is linked to τ_r and indicates the frequency at which the power spectrum is damped to 0.5 or the cospectrum to ca. 0.71.

Due to the different response times of the instruments, a phase-shift affects the flux measurements. Zeller et al. (1988) provided a generalized transfer function for the phase-shift mismatch. Since the sonic anemometer has a much faster response time than the instrument measuring the concentration, the response effect of the faster sensor is neglectable compared to the slower sensor. The resulting transfer function is only affected by the response time of the slower sensor, the measuring device.

(1.17)

$$TF_{\Delta R}(f) \approx \cos[\tan^{-1}(2\pi\tau_r f)]$$

In closed-path systems, sample air is transported through tubes before entering the analyzing cell. The flux attenuation through air transport is strongly related to the flow type (laminar or turbulent). In case

of compounds, which show no interactions with tube walls or other compounds, the tube transfer function (TF_T) is described by the laminar (TF_{lam}) or turbulent (TF_{turb}) transfer function which are defined as follows:

$$\mathrm{TF_{lam}}(f) = \exp\left(-\frac{\pi^3 r^4 f^2 L}{6DQ}\right) \text{ and } \mathrm{TF_{turb}}(f) = \exp\left(-160 \cdot \mathrm{Re}^{-0.125} \cdot \frac{\pi^2 r^5 f^2 L}{Q^2}\right) \tag{1.18}$$

Here, *D* represents the molecular diffusivity of the investigated compound. A list of molecular diffusivities is given by Massmann et al. (1998) for several gases. The radius and length of the tube are described by *r* and *L*, respectively. The variable *Q* corresponds to the flow rate. Re is the Reynolds number and determines the type of the flow. If Re is higher than 2300, the flow is classified as turbulent. The Reynolds number is calculated using the following equation with ν being the kinematic viscosity (Aubinet et al., 2012).

$$\mathrm{Re} = \frac{2\,Q}{\pi\, r_t\, \nu} \tag{1.19}$$

Recently, Massman and Ibrom (2008) proposed different formulations of the laminar and turbulent transfer functions for compounds, which can interact with tube walls. In chapter 2, the tube attenuation transfer function according to Eq. (1.18) was used in order to describe the theoretical flux damping, since NO is likely inert due to the absence of O_3 and NO_2 in the sampling line after the TRANC. Inside the TRANC, NO_2 and O_3 are effectively converted (Marx et al., 2012).

The high-frequency damping factor (α) is determined by calculating the ratio of the damped cospectrum to the ideal spectrum. Both cospectra are integrated above all frequencies. The inverse of α, corresponds to the flux correction factor CF.

$$\mathrm{CF} = \alpha^{-1} = \frac{\int_{f=0}^{\infty} \mathrm{TF_{total}}(f)\ \mathrm{Co}\ (f)\ \mathrm{d}f}{\int_{f=0}^{\infty} \mathrm{Co}\ (f)\ \mathrm{d}f} \tag{1.20}$$

Generally, all parameters needed for the determination of the individual transfer function can actually be measured without evaluating any measured covariances. Using theoretical cospectra, high-frequency flux losses can be determined without any flux measurements. This approach follows the correction method by Moncrieff et al. (1997). Using this method, implies that flux losses are assumed to be mostly related to physical characteristics of the setup. The theoretical transfer function of the TRANC system can be a combination of the individual transfer functions, e.g., the sensor separation, tube attenuation, the frequency response, and line-averaging. For an open-path setup, the total transfer function is different. Obviously, the tube dampening function is not needed. Thus, flux losses of a closed-path system are usually higher.

However, physical and chemical properties of the desired compound and its interactions with other chemical species or even with components of the setup like tube walls play an important role in the overall damping process of reactive compounds and may be not sufficiently captured by generalized transfer functions. H_2O and water-soluble species like NH_3 and HNO_3 show a different damping behavior than inert gases like CO_2. As seen in Fig. 1.4, a theoretical cospectrum represents the sensible heat cospectrum to a certain extent, but substantial deviations to the gas flux cospectrum of the TRANC were observed, in particular at high frequencies.

Using measured instead theoretical cospectra for estimating high-frequency flux losses, takes site, instrument, and compound related flux losses into account. The method by Ammann et al. (2006) based on measured ogives and does not rely on any transfer function. Ibrom et al. (2007) utilizes measured power spectra for estimating high-frequency flux losses. A method using measured cospectra in

combination with an empirical transfer function is introduced in chapter 2. Details to the performance of the different spectral correction methods are given in chapter 2 and in their original publications.

In previous publications of TRANC flux measurements (Ammann et al., 2012; Brümmer et al., 2013) and NH_3 EC flux measurements (Ferrara et al., 2012; Zoell et al., 2016), the ogive method by Ammann et al. (2006) was the method of choice for estimating high-frequency flux losses. However, performance studies of different high-frequency flux loss correction methods on N_r compounds are scarce and even not available in case of the TRANC. Previous studies of Ammann et al. (2012), Ferrara et al. (2012), Brümmer et al. (2013), Zöll et al. (2016), and Moravek et al. (2019) have shown that flux damping has a significant influence on measured fluxes of NH_3 and ΣN_r with flux losses between 10 % and 46 %, respectively.

Thus, **the first research question is how well do theoretical and empirical damping methods describe the flux damping of the TRANC at sites with contrasting nitrogen loads?**

1.3.4 Using the TRANC for measuring the ΣN_r exchange

As written in Sect. 1.1.4, flux measurements of N_r compounds are still scarce. In addition, most field campaigns were made on individual N_r species and limited to a few days or at least months making measurements of the annual N dry deposition impossible (e.g., see Table 1 of Walker et al. (2020)). In addition, multiple N_r compounds contribute to ΣN_r each with different chemical and physical properties, which would require a complex arrangement of highly specialized measurement devices for investigating the ΣN_r exchange. So far, no annual N dry deposition estimates using micrometeorological methods have been reported for (remote) forests. The effect of N_r deposition on carbon sequestration is still uncertain (Magnani et al., 2007; Högberg, 2007; Sutton et al., 2008a; Flechard et al., 2020). With the TRANC, the most relevant N_r species are converted, and a single instrument is sufficient for deriving N dry deposition. In addition, TRANC flux measurements provide insights in the exchange pattern of ΣN_r.

In total, two campaigns have shown the field applicability of the TRANC in an EC setup at sites exposed to high N concentrations (Ammann et al., 2012; Brümmer et al., 2013). However, this system has never been installed at sites with low N_r conditions. At sites with low short-term variability in ambient concentrations, commercially available analyzers designed to be used for micrometeorological flux measurements are not suitable as shown by Ferrara et al. (2021) for NH_3.

Thus, the pre-described TRANC/CLD system was installed above a temperate mixed forest and to monitor the ΣN_r exchange for 2.5 years. The ecosystem was characterized by low concentrations of NO_2 (1.9–4.4 ppb) and NH_3 (1.3 ppb) (Beudert and Breit, 2010). The EC setup was complemented with meteorological measurements and low-resolution wet-chemical samplers, passive samplers (Ferm, 1991) and a DELTA system (DEnuder for Long-Term Atmospheric sampling, e.g., Sutton et al., 2001; Tang et al., 2009), for measuring concentrations of different N_r species. This allows a discussion of the observed concentrations and fluxes with regard to different temporal scales. For example, the comparison to the total N_r concentration of low-resolution samplers shows if the TRANC provides reasonable concentrations, i.e., a check on the conversion efficiency of the TRANC. A flux analysis of micrometeorological influences on the ΣN_r exchange indicates possible parameters enhancing ΣN_r deposition. The estimation of the annual N deposition can be made by applying a gap-filling method to measured EC fluxes and adding complementary wet-deposition estimates from local samplers.

Thus, **the second research question is can we quantify the N deposition using the TRANC/CLD system in an EC setup at a remote mixed forest site in southeast Germany**.

1.4 Modeling nitrogen deposition fluxes

Since measurements of N_r compounds using fast-response instruments are still scarce due to high acquisition costs and maintenance effort, one often relies on modeling to establish nitrogen exchange fluxes. Commonly, dry deposition process descriptions are made by using bidirectional flux schemes in chemical transport models or as site-based (inferential) applications. In my thesis, the comparison of novel measurements to the modeling tools is carried out, which are used to assess the national scale N deposition with, i.e., DEPAC-1D and LOTOS-EUROS.

1.4.1 DEPAC – A bidirectional resistance model for NH_3

The Deposition of Acidifying Compounds (DEPAC) module (van Zanten et al., 2010; Wichink Kruit et al., 2012) determines the deposition flux as a product of deposition or exchange velocity (in case of gases exhibiting bidirectional exchange) with the concentration difference between the atmosphere (χ_a) and the total compensation point of the trace gas (χ_{tot}).

$$F = -v_d \cdot (\chi_a - \chi_{tot}) \tag{1.21}$$

From an electric analogy (Wesely, 1989; Erisman and Wyers, 1993), v_d can be described by three resistances in a series - the aerodynamic resistance (R_a), the quasi-laminar resistance (R_b), and the canopy resistance (R_c) (Fig. 1.7). R_a and R_b depend on micrometeorological parameters, surface roughness, and properties of individual N_r species (Paulson, 1970; Webb, 1970; Garland, 1977; Jensen and Hummelshøj, (1995, 1997)) and thus calculated externally. DEPAC determines R_c for NO, NO_2, HNO_3, and NH_3, which is principle the effective sum of different resistances, namely the stomatal (R_s) (Emberson et al., 2000a,b), cuticular (R_w) (Sutton and Fowler, 1993), in-canopy (R_{inc}) (van Pul and Jacobs, 1994), and soil resistance (R_{soil}) (Erisman et al., 1994), representing three parallel exchange pathways for these gases. These resistances are different for each N_r species, and further dependent on meteorological conditions like temperature, relative humidity, radiation, and plant specific parameters like the size of leaves, stems, and branches. Currently, χ_{tot} is determined only for NH_3 based on the works of Wichink Kruit et al. (2010, 2017) on the stomatal and cuticular compensation point χ_s and χ_w. In the current version of DEPAC, a soil compensation point is not implemented. Further details to the version of DEPAC are provided in the original publication of van Zanten et al. (2010) and in chapter 4.

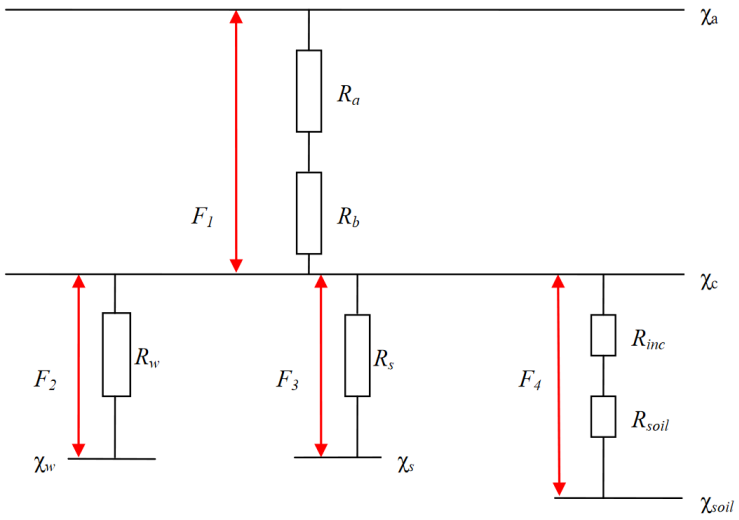

Figure 1.7: Overview of the resistance scheme for calculating dry deposition velocities (adapted from van Zanten et al. 2010).

1.4.2 An in-situ application of DEPAC - DEPAC-1D

As outlined above, a site-based or one-dimensional application of flux models like DEPAC is possible. Henceforth, this simulation is called DEPAC-1D. This concept has been proven successfully in various publications (Flechard et al., 2011, 2020; Hurkuck et al., 2014; Li et al., 2016; Schwede et al., 2011).

Doing so, dry deposition fluxes of N_r species can be modeled by using low-resolution data alone or in a combination with high-resolution measurements of different N_r species. In this PhD thesis, results from DELTA and passive sampler measurements providing concentration estimates for NH_3, HNO_3, NO_3^-, and NH_4^+, chemiluminescence measurement of NO and NO_2, and QCL measurements of NH_3 were used as concentration input data. Information about turbulence and meteorology were taken from a sonic anemometer and additional meteorological instruments. Dry deposition of particles is not included in DEPAC and therefore calculated using a size-resolved model for v_d.

In Sect. 1.3.2, difficulties in the gap-filling of N_r species were mentioned. At sites with (historically) prevailing N deposition like forest ecosystems, inferential models like DEPAC-1D may be a potential alternative for determining missing fluxes of N_r species. A description of DEPAC-1D and the evaluation of its performance as gap-filling tool are given in chapter 4.

1.4.3 Modeling nitrogen deposition on regional scale – LOTOS-EUROS

Having an inferential model and measured ΣN_r fluxes available, a comparison to chemical transport models like LOTOS-EUROS is valuable. LOTOS-EUROS provides nitrogen deposition based on HNO_3, pNO_3^-, pNH_4^+, NO, NO_2, and NH_3 for large spatial domains thereby using meteorological data from the European Centre for Medium Range Weather Forecasts (ECMWF), land-use data based on the CORINE-2012 land-use inventory, and modeled concentration of these compounds, which are determined from emission sources and chemical conversion processes. Also, LOTOS-EUROS uses DEPAC for predicting deposition velocities of gases and the same scheme for determining particle deposition as implemented in DEPAC-1D. Adding fluxes of all compounds weighted by land-use coverages results in the total N dry deposition. For further insights in the documentation of LOTOS-EUROS, publications of Wichink Kruit et al. (2012), Manders et al. (2017), and van der Graaf et al. (2020) are recommended.

Due to the limited availability of N_r flux measurements, modeled deposition fluxes remain uncertain. Recently, Theobald et al. (2019) made an intercomparison of different chemical transport models. Large differences in dry and wet deposition between the models were found, and the authors reported a substantial bias between modeled and measured wet deposition estimates. No comparison to measured N dry deposition estimates was possible due to lack of (continuous) observations.

TRANC flux measurements offer a unique opportunity for an evaluation of modeled dry deposition fluxes. Therefore, a multistage comparison scenario is carried out to investigate the performance of TRANC flux measurements, DEPAC-1D, and LOTOS-EUROS at a temperate mixed forest located exposed to low air pollution levels. Details to this investigation are provided in chapter 4.

Consequently, the third research question is **how well do modeled dry deposition fluxes of LOTOS-EUROS and DEPAC-1D agree with measured TRANC fluxes**.

1.5 Aims of this thesis

In case of N_r compounds, EC flux measurements are hardly available. These micrometeorological measurements of N_r compounds are technically challenging due to the nature of the involved compounds and the high requirements for the EC technique like a fast response time, high sampling rate, heated and/or special designed inlets, etc. The analysis of the results is also challenging as the required pre/post processing methods were optimized for greenhouse gases. It is questionable if currently developed high-frequency flux loss correction methods, as an example, are applicable to N_r compounds. This leads to the first research question:

RQ1: How well do theoretical and empirical damping methods describe the flux damping of the TRANC at sites with contrasting nitrogen loads?

With the coupling of the TRANC to a fast-response CLD in combination with a sonic anemometer, simultaneous flux measurements of the most important N_r gases and aerosols are realizable offering the possibility to determine total N dry deposition. Such long-term EC flux measurements of the ΣN_r dry deposition to an ecosystem have not been made so far at low concentrations of N_r species. This leads to the second research question:

RQ2: Can we quantify the N deposition using the TRANC/CLD system in an EC setup at a remote mixed forest site in southeast Germany?

These high-resolution flux measurements are a valuable data set for determining the accuracy of modeled N dry deposition since modeled deposition estimates are still affected by uncertainties regarding input data and implemented in dry deposition algorithms. This leads to the third research question:

RQ3: How well do modeled dry deposition fluxes of LOTOS-EUROS and DEPAC-1D agree with measured TRANC fluxes?

These objectives are addressed in the upcoming three chapters each consisting of one academic article, which have been published in peer-reviewed scientific journals. Currently, the third article is accepted for publication. In short, these articles are:

- Wintjen, P., Ammann, C., Schrader, F., and Brümmer, C.: Correcting high-frequency losses of reactive nitrogen flux measurements, Atmos. Meas. Tech., 13, 2923–2948, https://doi.org/10.5194/amt-13-2923-2020, 2020.
    - In this article, I compared the performance of theoretical and empirical high-frequency flux loss correction methods with regard to ΣN_r fluxes and finally provide recommendations on the spectral analysis of reactive nitrogen fluxes.

- Wintjen, P., Schrader, F., Schaap, M., Beudert, B., and Brümmer, C.: Forest–atmosphere exchange of reactive nitrogen in a remote region – Part I: Measuring temporal dynamics, Biogeosciences, 19, 389–413, https://doi.org/10.5194/bg-19-389-2022, 2022.
    - In this article, I analyzed EC flux measurements of the TRANC conducted above a remote mixed forest for 2.5 years and focused on the temporal dynamics of concentrations, fluxes, and depositions velocities.

- Wintjen, P., Schrader, F., Schaap, M., Beudert, B., Kranenburg, R., and Brümmer, C.: Forest-atmosphere exchange of reactive nitrogen in a remote region – Part II: Modeling annual budgets, Biogeosciences Discuss. [preprint], https://doi.org/10.5194/bg-2022-72, in review, 2022.
    - In this article, I compared N dry deposition determined from EC flux measurements (Part I) with modeled dry deposition fluxes of an in-situ application of DEPAC,

DEPAC-1D, and the chemical transport model LOTOS-EUROS. In addition, a comparison to an ecological method based on estimating nitrogen deposition from canopy throughfall measurements was made.

No further modifications were made to these articles. They are presented in the same way as made by the respective journal apart from figure and table formatting and minor changes to typesetting and language editing. In chapter 5, I provide a summary of the key findings of each article and finally give recommendations to the analysis of EC fluxes and an outlook to a further development of the TRANC in chapter 6.

Additional contributions to the field of EC flux measurements were made leading to co-authorships on the works of Zöll et al. (2019), in which we analyzed controlling factors of the ΣN_r and CO_2 exchange using artificial neural networks, Brümmer et al. (2022), in which we described and provided access to flux measurement data of ΣN_r and NH_3 conducted at different ecosystems, and Swaart et al. (2022), in which we compared NH_3 flux measurements of two novel open-path instruments using the AGM and the EC method.

2. Correcting high-frequency losses of reactive nitrogen flux measurements

Abstract. Flux measurements of reactive nitrogen compounds are of increasing importance to assess the impact of unintended emissions on sensitive ecosystems and to evaluate the efficiency of mitigation strategies. Therefore, it is necessary to determine the exchange of reactive nitrogen gases with the highest possible accuracy. This study gives insight into the performance of flux correction methods and their usability for reactive nitrogen gases. The eddy-covariance (EC) technique is today widely used in experimental field studies to measure land surface–atmosphere exchange of a variety of trace gases. In recent years, applying the EC technique to reactive nitrogen compounds has become more important since atmospheric nitrogen deposition influences the productivity and biodiversity of (semi)natural ecosystems and their carbon dioxide (CO_2) exchange. Fluxes, which are calculated by EC, have to be corrected for setup-specific effects like attenuation in the high-frequency range. However, common methods for correcting such flux losses are mainly optimized for inert greenhouse gases like CO_2 and methane or water vapor. In this study, we applied a selection of correction methods to measurements of total reactive nitrogen (ΣN_r) conducted in different ecosystems using the Total Reactive Atmospheric Nitrogen Converter (TRANC) coupled to a chemiluminescence detector (CLD). Average flux losses calculated by methods using measured cospectra and ogives were approximately 26 % – 38 % for a seminatural peatland and about 16 % – 22 % for a mixed forest. The investigation of the different methods showed that damping factors calculated with measured heat and gas flux cospectra using an empirical spectral transfer function were most reliable. Flux losses of ΣN_r with this method were on the upper end of the median damping range, i.e., 38 % for the peatland site and 22 % for the forest site. Using modified Kaimal cospectra for damping estimation worked well for the forest site but underestimated damping for the peatland site by about 12 %. Correction factors of methods based on power spectra or on site-specific and instrumental parameters were mostly below 10 %. Power spectra of ΣN_r were heavily affected – likely by white noise – and deviated substantially at lower frequencies from the respective temperature (power) spectra. Our study supports the use of an empirical method for estimating flux losses of ΣN_r or any reactive nitrogen compound and the use of locally measured cospectra.

Published as: Wintjen, P., Ammann, C., Schrader, F., and Brümmer, C.: Correcting high-frequency losses of reactive nitrogen flux measurements, Atmos. Meas. Tech., 13, 2923–2948, https://doi.org/10.5194/amt-13-2923-2020, 2020.

2.1 Introduction

The eddy-covariance (EC) method is widely applied for determining turbulent exchange of trace gases and energy between the biosphere and atmosphere (Aubinet et al., 2012; Burba, 2013). EC is mainly used for long-lived, stable gases like carbon dioxide (CO_2), water vapor (H_2O), and methane (CH_4). Only a few studies concentrated on reactive, short-lived gases like reactive nitrogen compounds (N_r). In our study, N_r covers species like nitrogen monoxide (NO), nitrogen dioxide (NO_2), nitric acid (HNO_3), nitrous acid (HONO), peroxyacetyl nitrate (PAN), ammonia (NH_3), and particulate ammonium nitrate (NH_4NO_3). The sum of these species is called total reactive nitrogen (ΣN_r). Nitrous oxide (N_2O), sometimes also considered to be a reactive N compound, is not detected with our system (see Sect. 2.2.1) and is excluded from ΣN_r here and not taken into account. Application of the EC technique to N_r or NH_3 is challenging, because most N_r compounds are highly reactive and water soluble, and background concentrations are typically low. In close proximity to sources like stables, managed fields (Sutton et al., 2011; Flechard et al., 2013), traffic, or industry (Sutton et al., 2011; Fowler et al., 2013), compounds of N_r like NH_3 or NO_2 can reach high concentrations. In the past, low-cost measurement devices like passive samplers (Tang et al., 2009), DELTA samplers (DEnuder for Long-Term Atmospheric sampling) (Sutton et al., 2001), or wet chemistry analyzers (von Bobrutzki et al., 2010) were mainly used in N_r measurement studies. However, these instruments typically have a low time resolution and require inferential modeling for estimating fluxes (e.g., Hurkuck et al., 2014). Recently, new measurement techniques for N_r compounds were developed, such as quantum cascade lasers (QCLs) using tunable-infrared-laser differential absorption spectroscopy (TILDAS), mainly for NH_3 (Ferrara et al., 2012; Zöll et al., 2016; Moravek et al., 2019), or the total reactive nitrogen converter (TRANC) (Marx et al., 2012; Ammann et al., 2012; Brümmer et al., 2013; Zöll et al., 2019) coupled to a fast-response chemiluminescence detector (CLD). Both measurement systems have a certain robustness and a high sampling frequency and are sensitive enough to allow EC measurements of NH_3 or ΣN_r.

Evaluating fluxes with these closed-path EC systems leads to underestimation of fluxes due to damping in the high- and low-frequency ranges. An EC setup, like any measurement setup, is comparable with a filter which removes high- and low-frequency parts from measured signals. High-frequency losses are, for example, related to sensor separation (Lee and Black, 1994), air transport through tubes in closed-path systems (Leuning and Moncrieff, 1990; Massman, 1991; Lenschow and Raupach, 1991; Leuning and Judd, 1996), different response characteristics of the instruments, and phaseshift mismatching (Ammann, 1999). These processes inducing flux losses are usually described by spectral transfer functions (Moore, 1986; Zeller et al., 1988; Aubinet et al., 1999).

The magnitude of the high-frequency flux loss depends on the trace gas of interest, the experimental setup, wind speed, and atmospheric stability. In recent literature, different estimates of flux losses due to high-frequency damping have been reported. For example Zöll et al. (2016) found flux losses of 33 % for NH_3 at an ombrotrophic, moderately drained peatland site. Ferrara et al. (2012) used the same QCL instrument and estimated flux losses from 23 % to 43 % depending on the correction method. Moravek et al. (2019) proposed a new approach for correcting high-frequency flux losses of NH_3 measured by a QCL. The method is based on frequently measuring the analyzer's time response. The application of this method resulted in 46 % flux loss. Ammann et al. (2012) measured ΣN_r with a TRANC–CLD system at an intensively managed grassland site and estimated flux losses between 19 % and 26 %. Brümmer et al. (2013) operated a TRANC–CLD system at a managed agricultural site and calculated flux losses of roughly 10 %. Stella et al. (2013) calculated flux losses of 12 % – 20 % for NO and 16 % – 25 % for NO_2. Evidently, the range and magnitude of flux losses of ΣN_r and several compounds is quite large. Correction factors for CO_2 and H_2O are usually lower. CO_2 shows attenuation factors from 2 % up to 15 % for a closed-path EC setup (Su et al., 2004; Ibrom et al., 2007; Mammarella et al., 2009; Burba et al., 2010; Butterworth and Else, 2018). H_2O shows a stronger damping than CO_2 that depends on humidity and age of intake tube due to interactions of sample air water vapor with the inner tube surfaces. The corresponding flux loss varies from 10 % to 42 % (Su et al., 2004; Ibrom et al.,

2007; Mammarella et al., 2009; Burba et al., 2010). Mammarella et al. (2009) reported that strong damping (up to 40 %) of H_2O occurs in wintertime and during the night due to high relative humidity and only 10 % to 15 % during summertime.

In the past decades, several methods for calculating spectral correction factors have been proposed based on theoretical cospectra (Kaimal et al., 1972; Moore, 1986; Moncrieff et al., 1997), measured power spectra (Ibrom et al., 2007; Fratini et al., 2012), and measured cospectra or ogives (Ammann et al., 2006). Some of these methods are implemented in ready-to-use eddy-covariance post-processing packages like EddyPro (LI-COR Biosciences, Lincoln, USA). In principle, it is possible to calculate flux losses without measuring trace gas concentrations, if all physical parameters of the setup and process losses are known. Such a method does not consider gas-specific properties and may not be suitable for highly reactive gases. In general, all these methods are optimized for inert greenhouse gases and not for N_r species. It is therefore questionable if common methods for spectral correction are applicable for N_r given the high reactivity and chemical characteristics of single compounds. Recently, Polonik et al. (2019) found that the applied correction method depends strongly on the gas of interest (CO_2 and H_2O) and the type of gas analyzer used. They suggest that high-frequency attenuation of closed and enclosed devices measuring H_2O should be corrected empirically. Consequently, common methods are not perfectly suited for dealing with specific EC setups. In this study, we test five different spectral damping correction methods for EC fluxes of ΣN_r that were measured at two different sites using a TRANC–CLD system. We investigate (1) quantitative differences between the methods, (2) their sensitivity to the input data, and (3) dependencies on meteorological conditions (wind speed, atmospheric stability, etc.) and measurement height.

2.2 Methods

2.2.1 Sites and experimental setup

We analyzed data from two measurement sites. At both sites we installed a custom-built ΣN_r converter (total reactive atmospheric nitrogen converter, TRANC) after Marx et al. (2012), a 3-D ultrasonic anemometer (GILL-R3, Gill Instruments, Lymington, UK), a fast-response chemiluminescence detector (CLD 780 TR, ECO PHYSICS AG, Dürnten, Switzerland), and a dry vacuum scroll pump (BOC Edwards XDS10, Sussex, UK).

The first site (52°39’ N, 7°11’ E, 19 m a.s.l.) is a seminatural peatland in northwest Germany, called “Bourtanger Moor” (BOG). It is an ombrotrophic, moderately drained bog with high ambient NH_3 concentrations (Zöll et al., 2016) dominating the local deposition of ΣN_r (Hurkuck et al., 2014). Average NH_3 concentrations ranged from 8 to 22 ppb, HONO was mostly below 0.1 ppb, HNO_3 had an average concentration of 0.04 ppb, NO was approximately 3.6 ppb, and NO_2 was 8.6 ppb on average (Hurkuck et al., 2014; Zöll et al., 2016). Averaged values refer to the entire measurement campaign of the cited publications. Concentrations of NO and NO_2 were requested from the “Air Quality Monitoring Lower Saxony” (Lower Saxony Ministry of Environment, Energy and Climate Protection) (for data availability please see https://www.umwelt.niedersachsen.de/startseite/themen/ luftqualitat/lufthygienische_uberwachung_niedersachsen/ aktuelle_messwerte_messwertarchiv/, last access: 4 May 2020). A detailed description of the site is given in Hurkuck et al. (2014, 2016). The EC system was operated from October 2012 to the middle of July 2013.

The TRANC and sonic anemometer were installed at 2.50 m above ground. The sampling inlet was designed after Marx et al. (2012) and Ammann et al. (2012). The inlet tube was 15 cm long, consisted of FeNiCr, had an outer diameter of 0.25 in., and was actively heated from the edge of the tube. Inner temperatures were higher than 100°C. While passing through the TRANC, air samples undergo two conversion steps. The first one is a thermal pathway inside an iron–nickel–chrome (FeNiCr) alloy tube at approximately 870°C. Inside the FeNiCr tube, NH_4NO_3 is thermally split up into gaseous NH_3 and

HNO_3. HNO_3 is thermally converted to NO_2, H_2O, and O_2. NH_3 reacts at a platinum gauze with O_2 to NO and H_2O. HONO is thermally split up to NO and a hydroxyl radical. In a passively heated gold tube (approx. 300°C) a catalytic conversion follows. Before reaching the gold tube, carbon monoxide (CO) is applied as a reducing agent resulting in a reduction of the remaining nitrogen compounds, NO_2 and other higher nitrogen oxides, to NO inside the gold tube. To sum it up, all ΣN_r (except for N_2O and N_2) are converted to NO. At the end of the converter a critical orifice was mounted, which ensured a pressure reduction at a constant flow rate of ~ 2.0 L min^{-1}. After passing through a 12 m opaque polytetrafluoroethylene (PTFE) tube, the sample air was analyzed in the CLD with a sampling frequency of 20 Hz. The GILL-R3 was installed next to the inlet of the TRANC (Table 1). The CLD and pump were located in an air-conditioned box. For further details of converter and field applications, we refer to Marx et al. (2012), Ammann et al. (2012), and Brümmer et al. (2013). It was shown that concentrations measured by the CLD are affected by water vapor due to quantum mechanical quenching. To compensate for this effect, calculated fluxes were corrected following the approach by Ammann et al. (2012) and Brümmer et al. (2013). Another EC system for CO_2 and H_2O measurements was placed next to the ΣN_r setup (Hurkuck et al., 2016) using a GILL-R3 and a fast-response, open-path infrared gas analyzer (IRGA, LI-7500, LI-COR Biosciences, Lincoln, USA).

Our second site (48°56' N, 13°25' E, 807 m a.s.l.) was located in the Bavarian Forest (FOR) National Park, Germany. The same TRANC and sonic anemometer were mounted on different booms next to each other at a height of 30 m above ground and approximately 10 m above the forest canopy. Next to the sonic anemometer, an open-path LI-7500 infrared gas analyzer (IRGA) for measuring CO_2 and H_2O concentrations was installed. The CLD and pump were placed in an air-conditioned box at the bottom of the tower. A 45 m long, opaque PTFE tube connected the TRANC with the CLD. A critical orifice at the end of the TRANC restricted the flow to 2.1 L min^{-1} and assured low pressure along the tube. Air temperature and relative humidity sensors (HC2S3, Campbell Scientific, Logan, Utah, USA) were mounted at four different heights along a vertical gradient (10, 20, 40, and 50 m). The site was located in a remote area, next to the Czech border, with no local industrial and agricultural emission hot spots (Beudert et al., 2018). Therefore, concentrations of N_r species such as NH_3 (1.3 ppb), NO (0.4–1.5 ppb), and NO_2 (1.9–4.4 ppb) were very low (Beudert and Breit, 2010). A detailed description of the forest site can be found in Zöll et al. (2019). For the attenuation analysis, data from June 2016 to the end of June 2018 were selected. Important site-specific parameters of both measurement sites are listed in Table 2.1. Table 2.2 gives an overview about abbreviations used in this study.

2.2.2 Calculation and quality selection of fluxes and spectra

Data were collected with the software EddyMeas, included in the software EddySoft (Kolle and Rebmann, 2007), with time resolutions of 20 Hz at BOG and 10 Hz at FOR. Analog signals from CLD and LI-7500 were sampled by the interface of the anemometer and combined with the ultrasonic wind components and temperature data to a common data stream. Periods of maintenance and insufficient instrument performance were removed from damping analysis based on manual screening and monitoring performance parameters such as TRANC heating temperature or flow rate. The software EddyPro 6.2.1 (LI-COR Biosciences, 2017) was used for raw data processing and flux calculation. A 2-D coordinate rotation of the wind vector was selected (Wilczak et al., 2001), spikes were detected and removed after Vickers and Mahrt (1997), and block averaging was applied.

The recorded datasets show a time lag between the measurements of the sonic anemometer and the gas analyzers due to sampling of air through the inlet system (converter, tube, analyzer cell), the processing of signals within the analyzers, and the distance between the two instruments.

Table 2.1: Physical parameters of the EC setups.

Parameter	Bourtanger Moor (BOG)	Bavarian Forest (FOR)
Canopy height	0.4 m	20 m
Measurement height (from ground)	2.5 m	31 m
Displacement height	0.268 m	13.4 m
Tube length	12 m	48 m
Tube diameter (OD)	6.4 mm	6.4 mm
Flow rate	2.0 L min^{-1}	2.1 L min^{-1}
Horizontal sensor separation	5 cm	32 cm
Vertical sensor separation (below the sonic anemometer)	20 cm	20 cm
Sonic path length	15 cm	15 cm
CLD analyzer response time ($\tau_{r,a}$)	0.3 s	0.3 s
Acquisition frequency	20 Hz	10 Hz
Kinematic viscosity	1.46×10^{-5} m^2 s^{-1}	1.46×10^{-5} m^2 s^{-1}
Schmidt number for NO	0.87	0.87
Time delay	2.5 s	20 s

Table 2.2: Important terms and corresponding shortcuts used in this study.

Parameter or term	Abbreviation
Theoretical damping calculation	THEO
In situ cospectral method	ICO
Semi-in situ cospectral method	sICO
In situ ogive method	IOG
In situ power spectral method	IPS
(Power) spectrum	Ps(..)
Cospectrum	Co(..)
Ogive	Og(..)
Transfer function	TF
Response time	τ_r
Damping factor	α
Bourtanger Moor (seminatural peatland)	BOG
Bavarian Forest (mixed forest)	FOR
Total Reactive Atmospheric Nitrogen Converter	TRANC
Chemiluminescence detector	CLD

The time lag was estimated with the covariance maximization method (Aubinet et al., 2012; Burba, 2013), which is based on shifting the time series of vertical wind and concentration against each other to determine the lag time, at which the covariance between the two is maximized. At BOG the time lag was around 2.5 s, and at FOR the time lag was around 20 s. Accordingly, the time lag computation method in EddyPro was set to covariance maximization with the default. Based on theoretical considerations, we restricted the range for time lag computation from 15 to 25 s for the FOR data and from 0 to 5 s for the BOG data. The default value was set to 20 s for FOR and to 2.5 s for BOG. The windows for the time lag compensation were chosen in such a way because estimated lags were broadly distributed around the physical (default) lag. The chosen range for the time lag computation coincides with the range of the highest time lag density. The variation in time lags around the physical lag was almost constant for both measurement campaigns and not correlated to the temporal variation in the damping factors. The difference in ranges may be related to different site characteristics, different mixing ratio fluctuations of ΣN_r compounds at the sites, and performance of the TRANC–CLD setup. Time lags, estimated with a stand-alone script, are used as filtering criteria for the damping analysis. For the CO_2 and H_2O measurements, time lags were mostly negligible.

For the high-frequency damping analysis, we selected time series of vertical wind, temperature, and ΣN_r concentrations. These raw data were corrected for several effects in the following order: despiking (Vickers and Mahrt, 1997), crosswind correction (Liu et al., 2001), angle of attack correction (Nakai et al., 2006), tilt correction (Wilczak et al., 2001), time lag compensation, and block averaging. As the next

step, the time series were subject to a fast Fourier transformation (FFT) that yielded the power spectra of individual quantities like the temperature (power) spectrum Ps(T) and the cospectra of two quantities like the heat flux cospectrum Co(w, T) (Aubinet et al., 2012). The same was done for CO_2, H_2O, and ΣN_r, resulting in Co(w, CO_2), Co(w, H_2O), and Co(w, ΣN_r) and Ps(CO_2), Ps(H_2O), and Ps(ΣN_r), respectively. From the cospectra, flux-normalized ogives (Og) (Ammann et al., 2006) as the cumulative cospectrum (Desjardins et al., 1989; Oncley et al., 1996). The ogives and cospectra consisted of 40 log-spaced frequency bins.

For a quantitative evaluation of the high-frequency damping from the half-hourly flux (co)spectra, a quality flagging has to be applied. Flagging of (co)spectra is done automatically in EddyPro. However, the criteria are usually optimized for inert gases like CO_2 and H_2O that show characteristic daily flux cycles and magnitudes. They are much less specific and were not very successful for filtering ΣN_r fluxes and spectra. Therefore, we performed a two-stage quality selection. First, common criteria were applied: discarding cases with (i) insufficient turbulence ($u_* < 0.1$ m s^{-1}), (ii) low flux quality (flag = 2) after Mauder and Foken (2006), (iii) variances of T and ΣN_r exceeding a threshold of 1.96σ, and (iv) a time lag outside the predefined range (see above). Next, we checked with manual screening whether the shapes of ogives and cospectra were relatively smooth and not influenced by considerable noise or outliers. A total of 821 cospectra passed the flagging criteria at BOG, and 872 cospectra passed the flagging criteria at FOR. With common selection criteria, 3232 cases at BOG and 9889 at FOR would have been retrieved. Another possibility for the characterization of the quality or influence of noise on power spectra and cospectra is the determination of the decline in the inertial subrange following the power law. Therefore, the slope of the decrease was evaluated on a double logarithmic scale by a linear regression. The theoretical slope for power spectra of temperature and inert trace gas concentrations is –2/3.

2.2.3 High-frequency damping and determination of correction factor

We used four different cospectral approaches for the computation of high-frequency losses. The fifth approach of Ibrom et al. (2007) is based on power spectral analysis and implemented in EddyPro. The majority of the approaches determine the damping factor of a trace gas flux as an integral of the frequency-dependent attenuation of the corresponding cospectrum. With Co(f) being the true undamped cospectrum, the flux damping factor(s) α, or its inverse, the correction factor α^{-1} can be described in the following way, e.g., (Moore, 1986):

$$\alpha^{-1} = \frac{\overline{w's'}^{\mathrm{m}}}{\overline{w's'}} = \frac{\int_{f=0}^{\infty} \mathrm{Co}_{w,s}^{\mathrm{m}}(f)\,\mathrm{d}f}{\int_{f=0}^{\infty} \mathrm{Co}_{w,s}(f)\,\mathrm{d}f} = \frac{\int_{f=0}^{\infty} \mathrm{TF}(f)\,\mathrm{Co}(f)\,\mathrm{d}f}{\int_{f=0}^{\infty} \mathrm{Co}(f)\,\mathrm{d}f} \tag{2.1}$$

The flux attenuation factor is the ratio of the measured flux covariance $\overline{w's'}^{\mathrm{m}}$ of vertical wind $w'$and scalar s' to the true covariance $\overline{w's'}$, where the prime denotes fluctuations of the scalars. $\overline{w's'}$ is evaluated by the integral of Co(f) over the frequency. Also, $\overline{w's'}^{\mathrm{m}}$ can be expressed by the integral of frequency, but it has to consider a transfer function. TF is the overall spectral transfer function of the EC setup and is usually a product of several individual damping processes with specific transfer functions TF_i. In the following subsections we describe the methods in detail.

2.2.3.1 Theoretical damping calculation (THEO)

The theoretical damping calculation (THEO) is the most commonly applied method (Spank and Bernhofer, 2008). It is independent of any measured data and works for open-path as well as closed-path EC systems (Leuning and Moncrieff, 1990; Lenschow and Raupach, 1991; Massman, 1991;

Leuning and Judd, 1996; Moncrieff et al., 1997). It is based on the assumption that all relevant attenuation processes are known and can be quantitatively described by spectral transfer functions TF_i. Detailed descriptions of the TF_i are given in Moore (1986), Moncrieff et al. (1997), Ammann (1999), and Aubinet et al. (1999, 2012). The TF_i and physical parameters for the EC setups used here, like the analyzer response time $\tau_{r,a}$, flow rate, tube length, and sensor separation, are listed in Tables A2.1 and 2.1. All TF_i functions were merged into a single total transfer function (TF_{theo}), which was applied to theoretical (modified) Kaimal cospectra (from the original Kaimal et al., 1972). Subsequently, α was calculated after Eq. (2.1) for every quality-selected flux averaging interval. Kaimal cospectra exclusively depend on stability, wind speed, and measurement height above canopy (Moore, 1986; Ammann, 1999). Further in situ measurements were not used for this approach.

In order to prevent a misunderstanding between $\tau_{r,a}$ and the later introduced parameter τ_r, we state their differences here. Physically, the analyzer response time $\tau_{r,a}$ represents the time at which the difference between the measured quantity and the analyzer output signal is reduced by 1/*e* after a step change. Thus, it is also called *e*-folding time. If it is zero, changes will be recognized instantaneously. This is mostly not possible for common gas analyzers. Our TRANC–CLD system, which has proven to be suitable for EC measurements (Marx et al., 2012; Brümmer et al., 2013), has an *e*-folding time of about 0.3–0.35 s. $\tau_{r,a}$ is used for the first-order filter transfer function (Table A2.1) in the THEO approach. In this paper τ_r, which is also called response time, is a fitting parameter used in Eq. (2.2). It is linked to the cutoff frequency $f_c = 1/2\pi\tau_r$, at which the cospectrum is damped to 1/2 ≈ 0.71 or the power spectrum to 50 %.

2.2.3.2 In situ cospectral method (ICO)

Theoretical cospectra could deviate from site-specific characteristics of the turbulent transfer, while theoretical transfer functions could miss important chemical or microphysical processes, which are more important for ΣN_r than for inert gases like CO_2, H_2O, CH_4, or N_2O. In the exemplary case of Fig. 2.1, the prescribed cospectrum of Kaimal corresponds generally well with Co(*w*, *T*), but a systematic deviation may exist in the low-frequency range for BOG. At both sites, differences to Co(*w*, ΣN_r) are also visible in the high-frequency range right of the cospectral maximum, which is around 0.2 Hz for BOG and around 0.02 Hz for FOR in the present example.

Cospectra of FOR are shifted to the left due to the larger measurement height above canopy and the increased contribution of low-frequency, large-scale eddies with height (Burba, 2013). The wind speed and stability values of the shown example are in close agreement with long-term, daytime averages of the corresponding sites. On average, wind speed and stability were approximately 1.65 m s^{-1} and –0.22 at BOG during daytime. At FOR, the average wind speed and stability were 1.91 m s^{-1} and –0.44 during daytime. Wind speed conditions of the cospectra displayed in Fig. 2.1 are similar to the average values during daytime for the entire period. Stability values of the displayed case are in agreement with the daytime average for BOG. At FOR, the shown example refers to stable conditions, whereas an unstable average is exhibited during daytime. In general, daytime stability values of both sites are rather low and close to neutral conditions. At both sites, approximately 10 % of the analyzed cospectra were in the range of ±0.5 m s^{-1} for the average wind speed and ±0.15 for the average stability. Using only the wind speed restriction resulted in 40 % agreement at FOR and 55 % at BOG. It seems that the stability is more diverse and not correlated to wind speed. The correlation between wind speed and stability for the analyzed cospectra used for the damping analysis is rather low for both sites (0.26 for BOG and 0.15 for FOR). In conclusion, the shown example represents a common case of the selected cospectra, which were used for the empirical approaches, especially for wind speed.

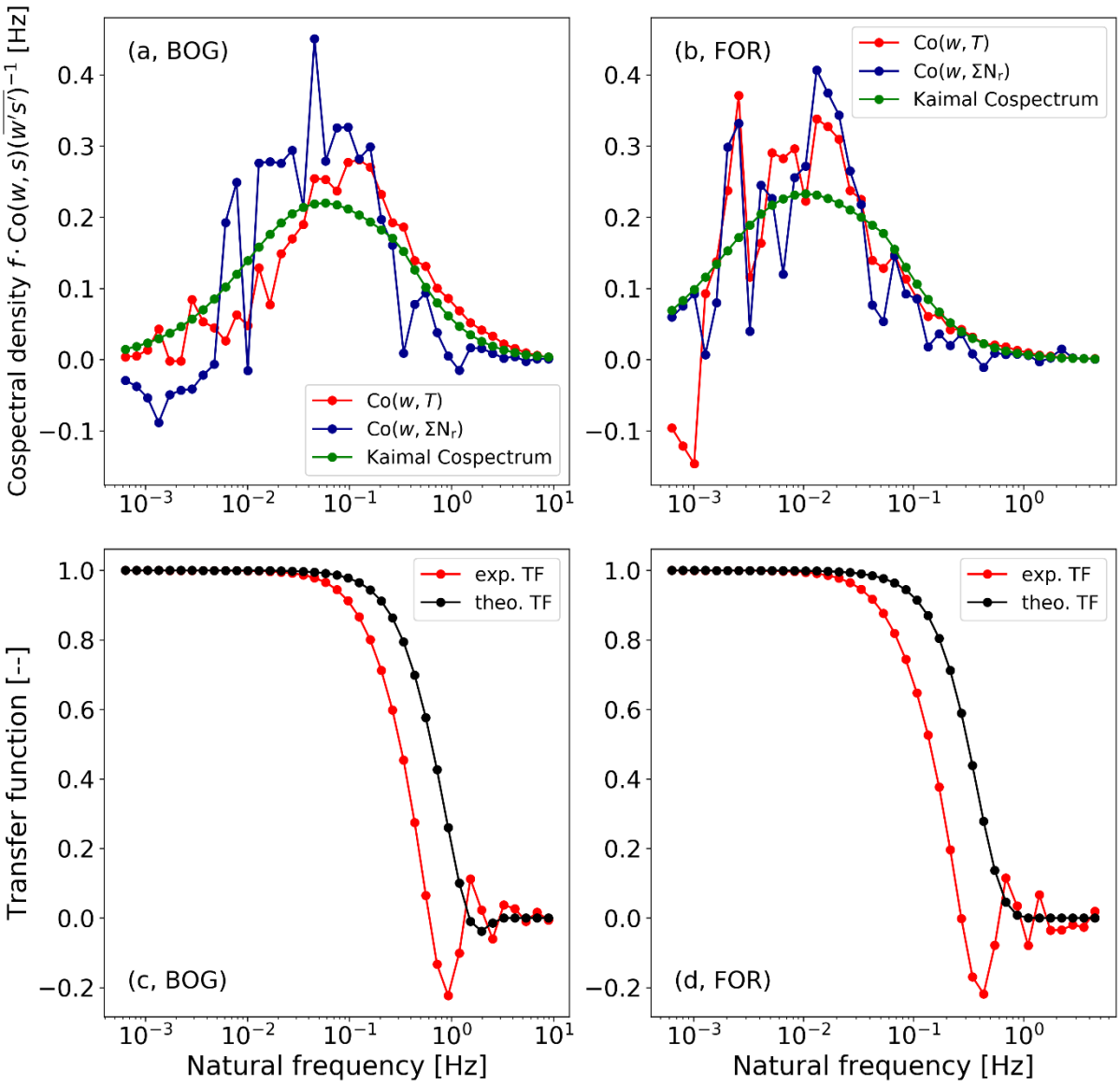

Figure 2.1: Comparison of observed normalized cospectra with modified Kaimal cospectra (green) for similar wind speed and stability and their theoretical and experimental transfer functions at BOG (a, c) ($\zeta = -0.23$, $\bar{u} = 1.38$ m s^{-1}) and FOR (b, d) ($\zeta = 0.17$, $\bar{u} = 2.04$ m s^{-1}). Panels (c, d) show the theoretical cospectral transfer function (TF_{theo}) (black) and the experimental transfer function (TF_{exp}) (red). The experimental transfer functions were determined with the cospectra in (a, b). The displayed cospectra of heat (red) and ΣN_r mass flux (blue) are averaged over half-hourly measurements on 10 October 2012 between 09:30 and 14:00 CET and on 28 October 2016 between 10:00 and 15:30 CET for BOG and FOR, respectively. The choice of different days was caused by data gaps in the measurements.

The in situ cospectra method (ICO) utilizes Co(w, T) instead of the Kaimal cospectrum in Eq. (2.1). Co(w, T) is used as the reference cospectrum because it is almost unaffected by damping processes. Assuming spectral similarity between Co(w, T) and Co(w, ΣN_r), we can derive TF_{exp} as follows (Aubinet et al., 1999; Su et al., 2004):

$$\alpha \cdot \frac{\mathrm{Co}(w, \Sigma N_r)}{\overline{w' \Sigma N_r'}} = TF_{exp} \cdot \frac{\mathrm{Co}(w, T)}{\overline{w' T'}} \tag{2.2}$$

In principle, this equation compares the ratio of the cospectra, which corresponds to the cospectral transfer function, to the empirical transfer function $TF_{exp}(f)$. Equation (2.2) allows us to determine τ_r.

TF_{exp} consists of a first-order filter TF_R combined with a mismatching phase-shift $TF_{\Delta R}$ for first-order systems (Ammann, 1999) (Table A1):

$$TF_{exp} = TF_R \cdot TF_{\Delta R} \tag{2.3}$$

The approach used in this study is somewhat different to other methods that are also based on using measured cospectra of heat and gas flux, for example the method of Aubinet et al. (1999). The latter uses a normalization factor, which corresponds to the ratio of the heat flux cospectrum to gas flux cospectrum. Both cospectra are integrated until frequency f_0, which should not be affected by high-frequency damping but is high enough to allow an accurate calculation of the normalization factor. However, the definition of f_0 is rather imprecise, and thus an incorrect setting of f_0 can lead to significant uncertainties in the damping analysis. In our approach cospectra are normalized by their corresponding total covariance. In order to consider the damping of the gas flux cospectrum and its covariance, the damping factor is introduced in Eq. (2.2). Thus, we assume that both approaches give similar results, since both approaches cover the damping of the gas flux cospectrum. The procedure of solving Eq. (2.2) is not straightforward. Thus, a flow chart of the important calculation steps is shown in Fig. 2.2.

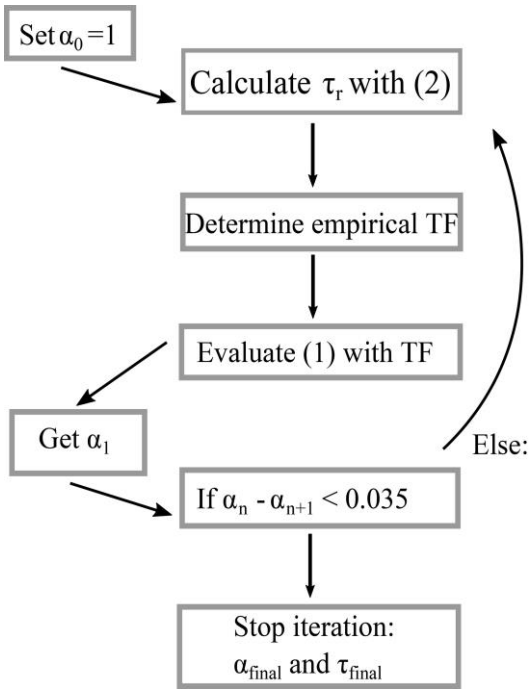

Figure 2.2: Illustration of the calculation of α and τ_r by ICO.

The iteration was started with $\alpha_0 = 1$. Afterwards, a nonlinear least-square fit of Eq. (2.2) was performed. For minimizing both sides of Eq. (2.2), τ_r was used as the optimization parameter. After τ_r was calculated, $TF_{exp}(f)$ could be determined and inserted into Eq. (2.1). α_1 was estimated by Eq. (2.1) using Co(*w*, *T*) as the reference. Finally, the process was terminated if the difference between the first guess and α_1 was sufficiently low (< 0.035). Otherwise, the whole process was repeated. Equation (2.2) was solved iteratively until α converged. Our experience was that three iteration steps were mostly enough to fulfill the termination criterion. The nonlinear fit (Eq. 2.2) was performed for frequencies larger than 0.055 Hz for the BOG campaign. This frequency range is assumed to be affected by damping effects. A similar frequency limit had been used in the damping analysis of Zöll et al. (2016) for the same site. For the FOR campaign the lower frequency limit was set to 0.025 Hz. The decision of the lower frequency limits was further proven by the examination of the ogives ratio, which shows constant

values in a certain frequency range. The position exhibits the frequency at which high-frequency attenuation mostly starts to increase. Figure 2.1c, d show examples of the theoretical and experimentally determined transfer functions for the two measurement sites. In both cases the experimental transfer function drops earlier than the theoretical transfer function and reveals a significant variation in the high-frequency range.

2.2.3.3 Semi-in-situ cospectra method (sICO)

The semi-in-situ cospectra approach is similar to the one described in Sect. 2.2.3.2. The determination of τ_r follows the same procedure as for ICO, but, instead of using Co(*w*, *T*) in Eq. (2.1), this approach uses Kaimal cospectra (Eqs. A2.1 and A2.2) as the reference. This method is useful if the quality of Co(*w*, *T*) is not sufficient for estimating the damping factors, especially in the low-frequency range.

2.2.3.4 In situ ogive method (IOG)

The in situ ogive method (IOG) is based on Ammann et al. (2006) and Ferrara et al. (2012). An ogive is defined as the cumulative integral of the cospectrum from the lowest frequency f_0, which is given by the averaging interval, to the highest frequency, the Nyquist frequency f_N. The Nyquist frequency is half of the sampling frequency.

$$\mathrm{Og}(f) = \int_{f_0}^{f_N} \mathrm{Co}(f)\mathrm{d}f \tag{2.4}$$

This method is similar to ICO, but does not rely on a specific form for the spectral transfer functions or cospectra and only requires Og(*w*, *T*) and Og(*w*, ΣN_r). Again, spectral similarity between Og(*w*, *T*) and Og(w, ΣN_r) is assumed. For estimating the damping, a linear regression between Og(*w*, *T*) and Og(*w*, ΣN_r) was performed in a specific frequency range. The range was constrained by frequencies for which Og(*w*, *T*) > 0.2 and Og(*w*, ΣN_r) < 0.85 were fulfilled. Frequencies lower than 0.002 Hz were excluded. The difference between the regression line and Og(w, ΣN_r) was calculated, and points exceeding a difference of 0.1 or frequencies above which the signal is totally damped were not considered for a linear least-square fit of Og(*w*, ΣN_r) and Og(*w*, *T*). The former criterion was applied for discarding spikes. Finally, the optimization factor, which minimizes the difference between Og(w, ΣN_r) against Og(*w*, *T*), is the result of the least-squares problem and corresponds to the damping factor.

2.2.3.5 In situ power spectral method (IPS)

Application of the in situ power spectral method (IPS) after Ibrom et al. (2007) was executed using EddyPro. It uses measured power spectra of a reference scalar and of the trace gas of interest, here Ps(*T*) and Ps(ΣN_r). The first step – the estimation of τ_r or the cutoff frequency f_c – is similar to the in situ cospectra method (Eq. 2.2), but the transfer function is different.

$$\frac{\mathrm{Ps}(\Sigma N_r)}{\mathrm{Ps}(T)} = \frac{1}{1 + \left(\frac{f}{f_c}\right)^2} \tag{2.5}$$

For estimating f_c EddyPro uses quality-selected and averaged power spectra. We set 0.4 Hz as the lowest noise frequency in the option "removal of high frequency noise" and adjusted the threshold values for removing power spectra and cospectra from the analysis accordingly. The value for the "lowest noise frequency", which was set in EddyPro for running IPS, was a subjective decision based on visual screening through power spectra. Therefore, we calculated slopes of ΣN_r power spectra in the inertial subrange and estimated the frequency at which noise started to increase and slopes became positive.

Additionally, we forced EddyPro to filter the spectra after statistical (Vickers and Mahrt, 1997) and micrometeorological (Mauder and Foken, 2004) quality criteria. We applied the correction of instrument separation after Horst and Lenshow (2009) for crosswind and vertical wind and took the suggested lowest and highest frequencies (0.006 and 5 Hz) as the fitting range for Ps(T) and Ps(ΣN_r) for FOR. Applying the IPS through EddyPro for ΣN_r at BOG requires CO_2 and H_2O measurements. Since both inert gases were not measured at the ΣN_r tower, we used high-frequency CO_2 and H_2O data from the EC setup described in Hurkuck et al. (2016), which was placed next to the ΣN_r setup. Then, the application of IPS to ΣN_r at BOG was performed, thereby inducing additional uncertainty. We changed the highest frequency to 8 Hz and took the lowest frequency from standard settings (0.006 Hz). For comparing the results of IPS to our cospectral methods, we chose the same half hours which passed the automatic selection criteria and the manual screening (see Sect. 2.2.2). In general, the idea of IPS is that the EC system can be simulated by a recursive filter. Thereby, α^{-1} is determined by the ratio of the unfiltered covariance $\overline{w'T'}$ to the filtered covariance $\overline{w'T_f'}$ and applying the recursive filter to degrade the time series of sonic temperature (Ibrom et al., 2007). However, Ibrom et al. (2007) argued that this ratio gives erroneous results for small fluxes. Therefore, they parameterized α by the mean horizontal wind speed (u), stability, and f_c. Ibrom et al. (2007) investigated a proportionality between α^{-1} and $u \cdot f_c^{-1}$. By introducing a proportionality constant A_1 and a second constant A_2, which should account for spectral properties of the time series, the following equation for calculating the correction factor was proposed (for details see Ibrom et al., 2007, Sect. 2.4):

$$\alpha^{-1} = \frac{A_1 \, \bar{u}}{A_2 + f_c} + 1 \tag{2.6}$$

A_1 and A_2 were estimated for stable and unstable stratification using degraded time series of sonic temperature. The degradation was carried out using a varying low-pass recursive filter (Ibrom et al., 2007; Sabbatini et al., 2018). A general summary of processing eddy-covariance data including high-frequency spectral correction methods is given in Sabbatini et al. (2018).

2.3 Results

2.3.1 Characterization of power spectra and cospectra

Figure 2.3 shows exemplary cospectra and power spectra of the two measurement sites. We compare cospectra which were measured during unstable daytime conditions and at similar wind speeds. All in all, the cospectral densities of the gas and heat fluxes are quite similar. This indicates that the chosen sampling interval and frequency were sufficient to capture flux-carrying eddies. However, Co(w, ΣN_r) shows a stronger variation than the other cospectra. The effect of different measurement heights is quite obvious. It results in a shift of all cospectra to the left for the FOR site. The stronger drop of Co(w, ΣN_r) compared to Co(w, CO_2) and Co(w, H_2O) in the high-frequency range is likely related to damping by the ΣN_r inlet tubes, which did not affect the CO_2 and H_2O open-path measurements. It also appears that the damping (difference of cospectra in the high-frequency range) at BOG is higher than that at FOR for the selected averaging interval.

The shapes of the power spectra for T, CO_2, and H_2O are comparable to those found in other studies (e.g., Ammann, 1999; Ibrom et al., 2007; Rummel et al., 2002; Aubinet et al., 2012; Ferrara et al., 2012; Fratini et al., 2012; Min et al., 2014). For Ps(T) a slope of –0.62 (BOG) and –0.63 (FOR) was determined in the inertial subrange. The fitting range used for the derivation of the slopes is smaller than the inertial subrange, for example, to exclude slightly positive slopes of the inert trace gases at the very high frequencies. Differences to the theoretical shape, –2/3 for power spectra, may be related to slight damping of Ps(T) in the high frequency range. A slight high-frequency damping of Ps(T) can be caused by the path averaging of the sonic anemometer (e.g., Moore, 1986). In addition, the observed shape of the spectrum (slope) can deviate from the theoretical shape due to nonideal environmental conditions (e.g., nonhomogeneous turbulence, influence of roughness sublayer). The stronger drop of Co(w, ΣN_r), compared to Co(w, CO_2) and Co(w, H_2O) in the high-frequency range, is likely related to damping by the tubes, which is not relevant for open-path instruments. Ps(CO_2) and Ps(H_2O) have nearly the same slope in the inertial subrange and exhibit the excepted shape.

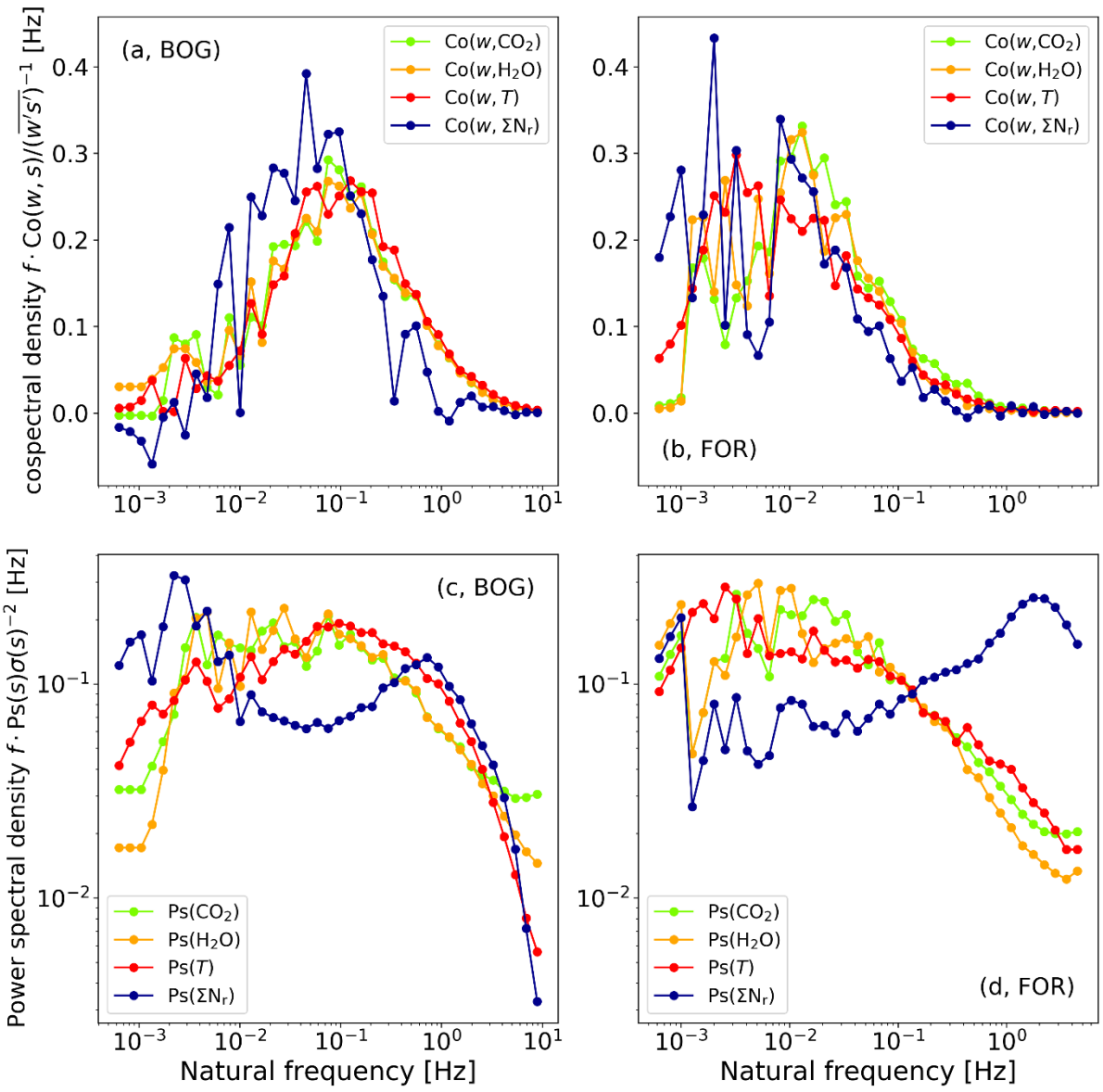

Figure 2.3: Normalized cospectra and power spectra T (red), ΣN_r (blue), CO_2 (green), and H_2O orange at BOG (a, c) and FOR (b, d). (Co)spectra were averaged at BOG from 11 October 2012 09:00 CET to 11 October 2012 16:30 CET ($\zeta = 0.31, \bar{u} = 1.36$ m s^{-1}) and at FOR from 16 October 2016 10:00 CET to 16 October 2016 15:30 CET ($\zeta = 3.27$, $\bar{u} = 1.89$ m s^{-1}). CO2 and H2O (co)spectra of BOG were adjusted to the aerodynamic measurement height of the ΣN_r setup. Note that the time period used for averaging is different from the periods of Fig. 2.1.

In contrast, Ps(ΣN_r) is lower than Ps(CO_2), and Ps(H_2O) at lower frequencies (< 0.1 Hz) starts to rise afterwards and reaches a maximum around 1Hz. This phenomenon was found in almost all Ps(ΣN_r) spectra at the measurement sites, for which we estimated the slope of Ps(ΣN_r) in the high-frequency range. However, the number of Ps(CO_2) measurements that were affected by this phenomenon was rather small compared to Ps(ΣN_r). For an in-depth investigation of slope we applied a variance filter of *w*, *T*, and ΣN_r and excluded Ps if the variance was higher than 1.96σ, which corresponds to a confidence limit of 95 %. Additionally, we excluded low-quality fluxes (flag = 2) of sensible heat and ΣN_r after Mauder and Foken (2006) and applied the time lag filtering criteria. These criteria were used to exclude periods of rather low fluxes, instrument performance issues, and conditions of insufficient turbulence. We used equivalent filtering criteria for CO_2 and additionally applied a precipitation filter due to the open-path characteristics of the LI-7500. The precipitation filter was also applied for filtering the lower-quality cases of CO_2 and H_2O shown in Fig. 2.3. Figure 2.4 shows a distribution of the estimated slopes at both measurement sites.

The slopes of Ps(*T*) are between –0.5 and –0.7, which is close to the theoretical value, and the shape of the histogram seems to be narrower around the theoretical value at BOG than at FOR. The distribution of the Ps(CO_2) slopes is rather bimodal at BOG but coincides well with the slope shape of the Ps(*T*) slopes at FOR. In volume terms, most slopes of Ps(CO_2) are negative at both sites (70 % for BOG and nearly all for BOG, 95 %), but their maximum is slightly higher than –2/3 (–0.53 for BOG and –0.58 for FOR). More Ps(CO_2) slopes of BOG exhibit a positive slope between 0.50 and 0.75 (24 %) than the Ps(CO_2) slopes of FOR (2 %) in the same range. In contrast, the slopes of Ps(ΣN_r) are mostly positive at both sites (88 % at BOG and 97 % at FOR). Also at BOG, the slopes of Ps(ΣN_r) exhibit a slight bimodal distribution. The second maximum is observed at around –0.45.

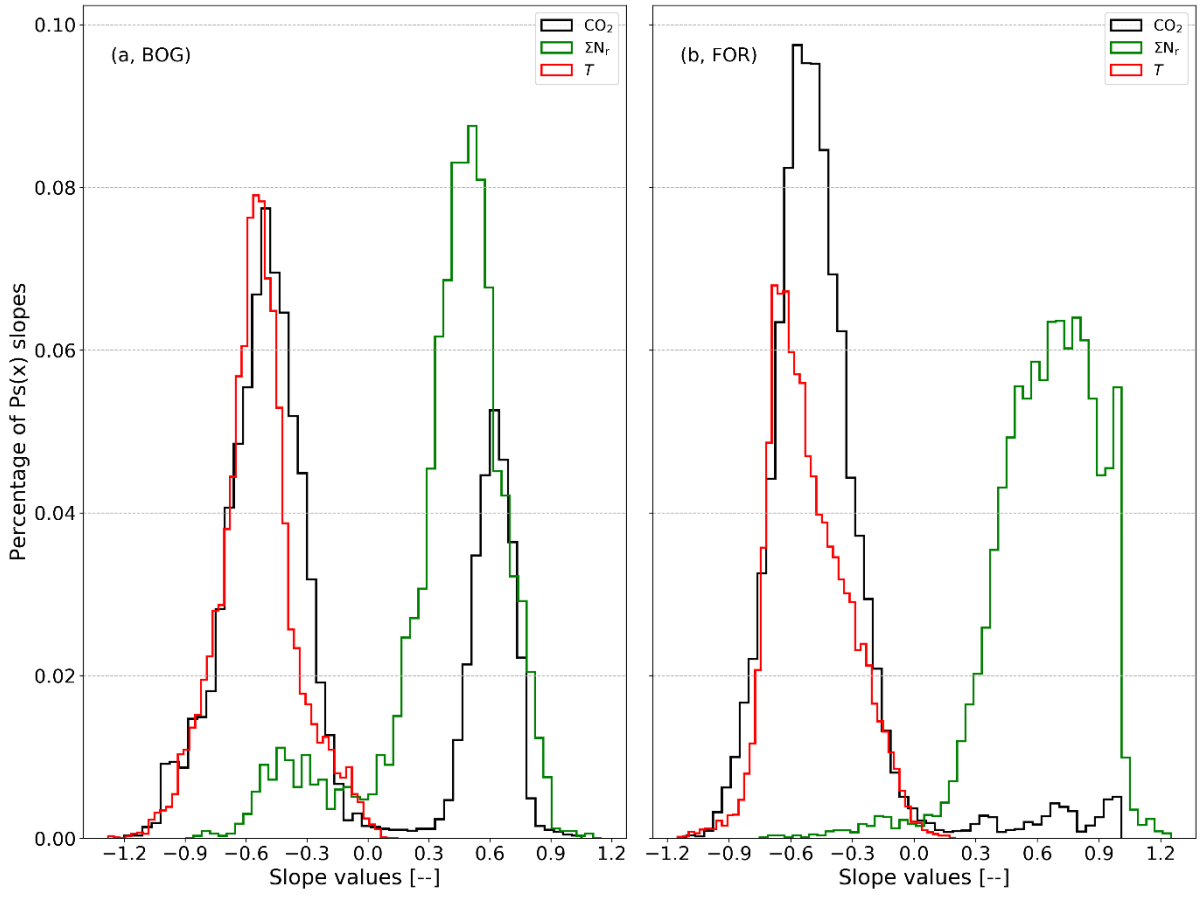

Figure 2.4: Distribution of spectral slopes in the high-frequency range (> 0.1 Hz) of Ps(ΣN_r) (green), Ps(CO_2) (black), and Ps(*T*) (red) for the BOG site (a) and for the FOR site (b). Slopes were estimated for half-hourly power spectra from 2 October 2012 to 17 July 2013 and from 1 June 2016 to 28 June 2018 at BOG and FOR, respectively.

The number of $Ps(\Sigma N_r)$ slopes around –2/3 is rather small at BOG (fewer than 10% are lower than –0.25) and even negligible at FOR (fewer than 1 % are lower than –0.25). A positive slope for nearly all power spectra value of a certain trace gas is rather unexpected.

2.3.2 Comparison of different damping correction methods

In the following, we present the results of the damping correction methods introduced in Sect. 2.2.3. Firstly, we describe the results of the in situ power spectral method (IPS) and the four cospectral methods. Secondly, we demonstrate findings of dependencies on meteorological variables. Figures 2.5 and 2.6 show statistical analyses of α which were calculated by each method on a monthly (BOG) or bimonthly (FOR) basis depicted as box plots. It was possible to estimate α with all methods for 816 half hours for BOG and 811 half hours for FOR. All damping correction methods were evaluated for the same half hours.

Monthly α values calculated with the IPS method show no temporal drift at FOR (Fig. 2.6). The median α is around 0.95 for nearly every month. Additionally, the interquartile range (IQR; 25 % to 75 % quartiles) is very small (0.01 to 0.02). At BOG, monthly median α values calculated with IPS were also mostly around 0.95; only the first 3 months were sightly lower by ~ 0.04. Their IQR is around 0.04 on average. It is obvious that α of IPS is the highest compared to the cospectral methods, and it exhibits the lowest IQR during the measurement period.

At both sites, the median α of the in situ cospectral methods ICO, sICO, and IOG show only moderate temporal variations during the entire measurement campaign. While slightly higher values in summer and lower values in winter were found at the FOR site (Fig. 2.6), the opposite pattern was observed at the BOG site (Fig. 2.5). Their IQR is more variable and ranges from 0.13 to 0.26 at BOG and from 0.16 to 0.31 at FOR. Changes in the range of the IQR and fluctuations of the medians may be related to different meteorological conditions, to changes in composition of ΣN_r, or to a degeneration of instrumental response. During field visits for maintenance, parts of the TRANC like the heating tube or platinum gauze were exchanged or cleaned, which could influence the results. At both sites, α values by THEO were always higher than those from in situ cospectral methods (IOG, ICO, sICO), and their medians were about 0.90 at BOG and about 0.95 at FOR. Their IQR is smaller than those of IOG, ICO, and sICO, too.

At FOR, the median α values of ICO and sICO are similar for every month, showing a difference of 0.03 on average, and their IQRs cover mostly the same range (Table 2.3 and Fig. 2.6). Values for α by IOG are mostly higher and exhibit a difference of 0.06 on average to sICO and ICO. The IQR by IOG is roughly half of the IQR of ICO and sICO (Table 2.3). During the month of December in 2016 and 2017, as well as January in 2017 and 2018, and April to May in 2018, IQR of ICO and sICO is relatively large.

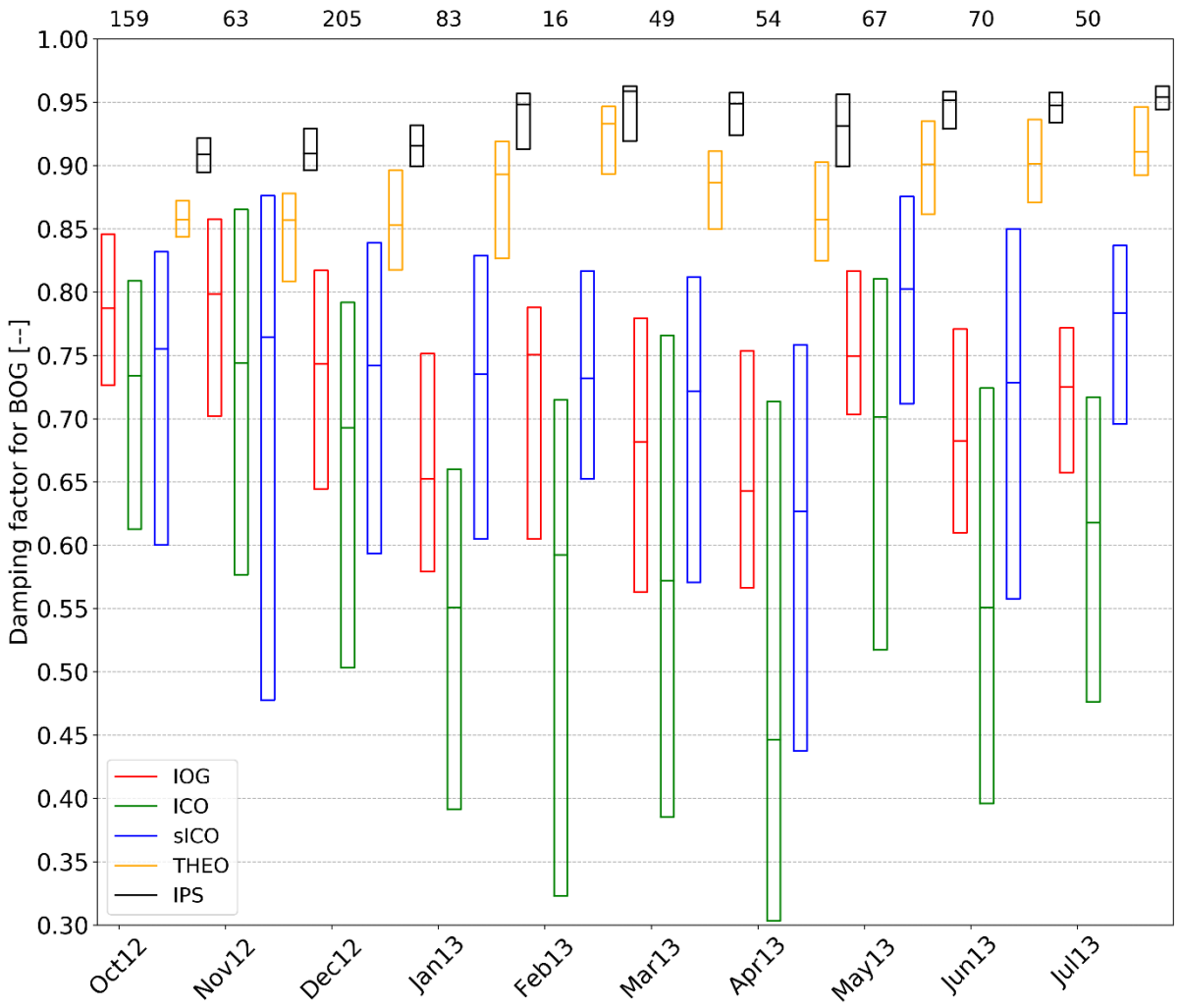

Figure 2.5: Boxplots of the flux damping factor (α) for BOG without whiskers and outliers (the box frame is the 25 % to 75 % interquartile ranges (IQR); the bold line is the median). The number of observations which are displayed at the top of the plot is the same for every method.

Common to both periods, the average vertical wind was quite low in January 2017 and 2018 (less than 0.01 m s^{-1}). Additionally, we had some instrumental performance problems (exchange of the pump and heating tube, power failure) with the TRANC in the mentioned months. As mentioned in Sect. 2.2.2, these periods were not considered in the flux analysis. As a matter of fact, not all affected fluxes can be excluded by the selection criteria. Thus, an influence on the quality of the cospectra and ogives can not be excluded. Consequently, IOG, ICO, and sICO exhibit a wide IQR from 0.15 to 0.40 and differences in the median from 0.06 to 0.16, which could be related to the low number of valid cospectra and ogives. Therefore, classifying α at FOR bimonthly (Fig. 2.6) was a necessary approach to enhance the quality when the number of valid cospectra is not enough for a robust estimation of α. Overall, a good agreement of IOG, ICO, and sICO was found.

At BOG, the median α values of ICO are the lowest, and the median α values of sICO and IOG are nearly the same for every month (Table 2.3 and Fig. 2.5). The difference of ICO to IOG varies by 0.05 and 0.20 and to sICO by 0.02 and 0.18. A systematic difference in α between ICO and sICO was not observed for FOR. At the beginning of the measurements the difference was rather small, but it started increasing after December 2012. The range of the quartiles is similar for IOG and sICO for certain months (see Table 2.3 and Fig. 2.5), but their IQR is lower than the IQR of ICO. Again, the IQR of IOG is roughly half of ICO IQR. It seems that theoretical cospectra could not reproduce the shape of Co(w, T) well under certain site conditions, although τ_r values of sICO and ICO were quite similar. They show

a correlation of 0.75 and an average absolute difference of 0.48. Comparing α between the sites shows that the damping is stronger at BOG than at FOR. Table 2.3 shows the averaged α at FOR and BOG.

By subtracting α from an ideal, unattenuated system, which has a damping factor of 1, the result will be the flux loss value (= 1–α). This loss value shows how much of the signal is lost from the inlet to the analysis of the signal by the instrument. Thus, flux losses calculated by IPS for our TRANC–CLD setup are around 6 % at BOG and around 5 % at FOR. The flux loss after THEO was approximately 12 % at BOG and about 5 % at FOR. The methods using measured cospectra or ogives (ICO, sICO, and IOG) showed a flux loss of roughly 16 %–22 % for FOR and around 26 %–38 % for BOG. ICO shows the strongest damping at both sites. These values are in common with other EC studies conducted on ΣN_r and other reactive nitrogen compounds (Ammann et al., 2012; Ferrara et al., 2012; Brümmer et al., 2013; Stella et al., 2013; Zöll et al., 2016; Moravek et al., 2019).

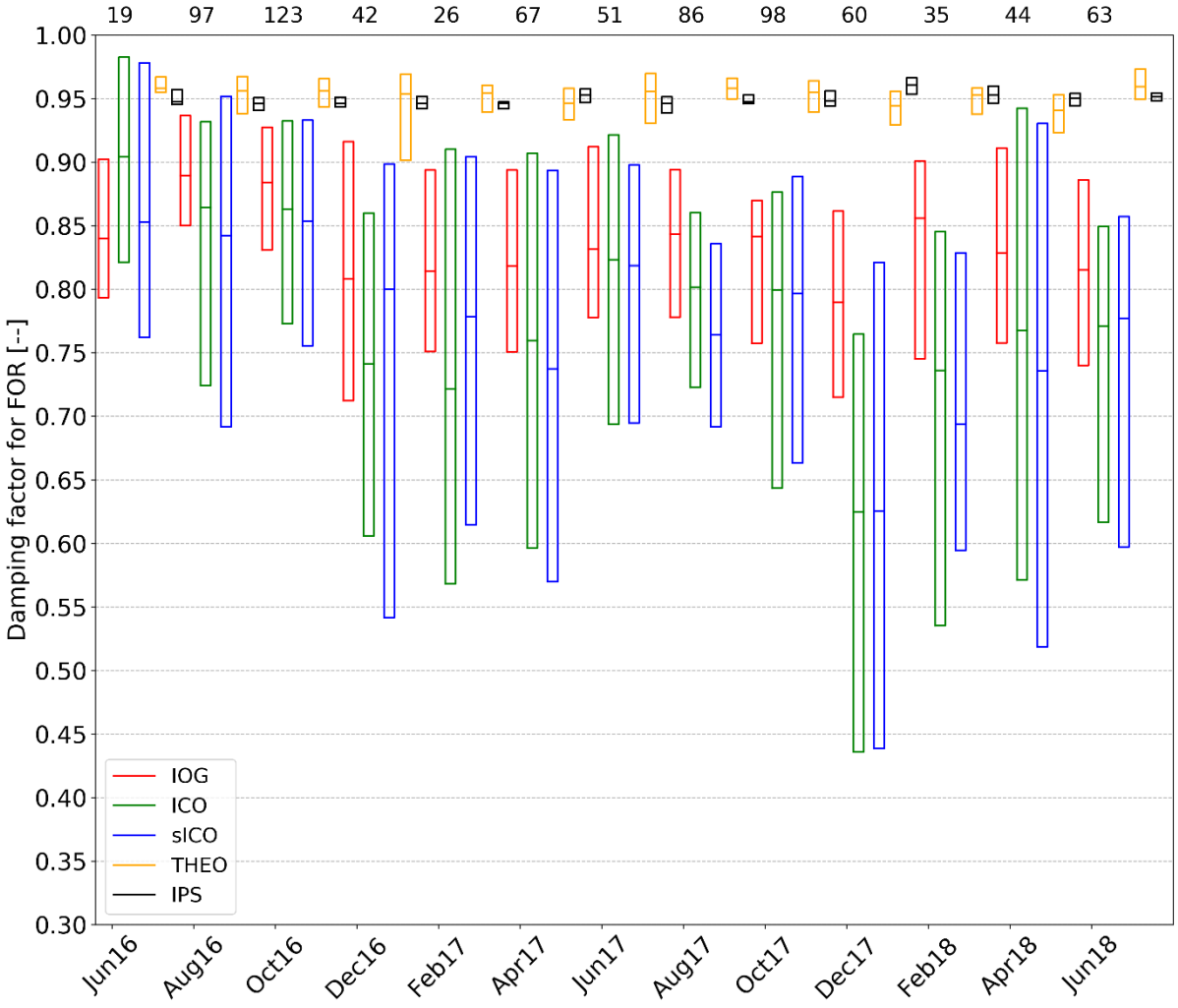

Figure 2.6: Box plots of the flux damping factor (α) for FOR without whiskers and outliers (the box frame is the 25 % to 75 % interquartile ranges (IQR); the bold line is the median). The number of observations displayed at the top of the plot is the same for every method.

Table 2.3: Averages of monthly medians and lower and upper quartiles of α over the whole measurement period for all applied methods at both sites.

Site	Method	Median	Lower quartile	Upper quartile
Bourtanger Moor (BOG)	IOG	0.72	0.64	0.80
	ICO	0.62	0.45	0.76
	sICO	0.74	0.59	0.83
	THEO	0.88	0.85	0.91
	IPS	0.94	0.91	0.95
Bavarian Forest (FOR)	IOG	0.84	0.77	0.90
	ICO	0.78	0.64	0.89
	sICO	0.78	0.63	0.89
	THEO	0.95	0.93	0.96
	IPS	0.95	0.94	0.95

For investigating deviations of the different methods more precisely, we computed correlation, bias, and precision as the standard deviation of the difference for each pair of methods. The results are summarized in Table B2.1. IOG exhibits a bias of not more than 0.10 to ICO and sICO and is rather small at BOG (0.03). The bias and precision between sICO and ICO is lowest at FOR. Additionally, the scattering of sICO α is more pronounced, which results in a lower precision of sICO compared with the IOG α. Common to both sites, the correlation of IOG with sICO was inferior to ICO. Checking ICO α against sICO α demonstrates a high correlation at both sites (0.78 for FOR and 0.66 for BOG). This is excepted since theoretical cospectra are based on Co(w, T). IOG, ICO, and sICO show a strong bias, low precision, and nearly no correlation to THEO. The correlation between sICO and THEO is somewhat higher because of utilizing Kaimal cospectra for both methods. IPS shows a negative bias and high precision against IOG, ICO, and sICO at FOR. At BOG, IPS exhibits a negative bias against THEO of approximately –0.05. The correlation of IPS with THEO is quite high at both sites, which is reasonable since bias and precision are quite low. Both methods give almost equal α.

For investigating a trend in meteorological variables such as temperature, relative humidity, stability, and wind speed, we classified them into bins, calculated α for each bin, and display them as box plots (Fig. 2.7). In the following figure, only wind speed and stability are shown. These are two variables for which we except a dependence, since the shape and position of a Kaimal cospectrum varies with wind speed and stability. We checked for dependencies on the other variables such as global radiation, temperature, and humidity, but no significant influence was found.

A slight dependence on wind speed for BOG α is starting to be relevant at wind speeds above 1 ms^{-1}, which is confirmed by IOG, ICO, and sICO. The influence on wind speed predicted by THEO already begins at low wind speed, which means that stronger damping was found at higher wind speed values. It shows a (linear) decrease from the beginning. A bias of IOG, ICO, and sICO to THEO (Fig. 2.7) exists for all wind speed classes. Considering the medians, we observe an increase in attenuation from 0.15 till 0.20 over the whole wind speed regime. The bias of IOG and ICO with sICO (Fig. 2.7) is mostly visible for wind speeds up to 1.5 m s^{-1} and becomes negligible afterwards.

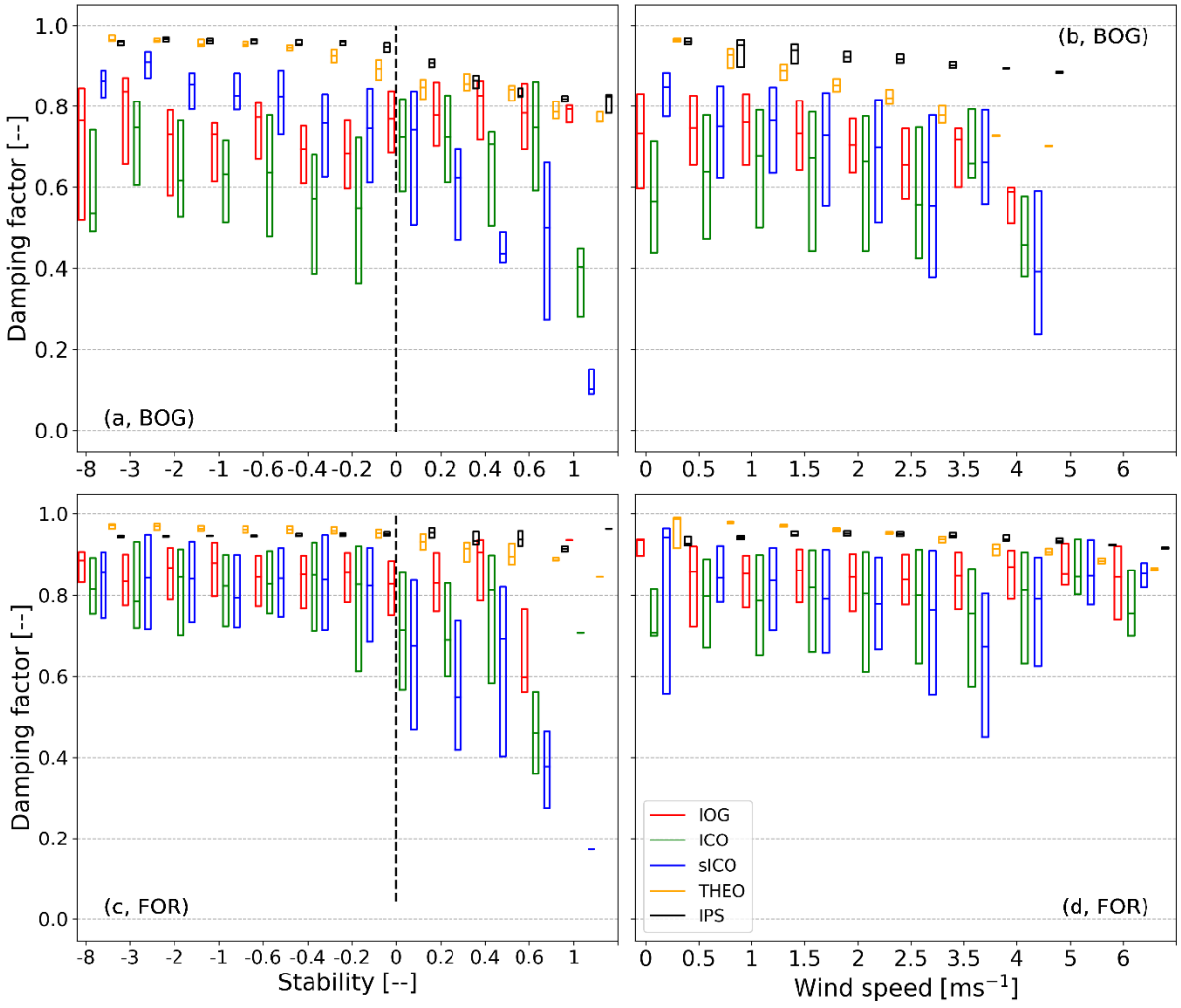

Figure 2.7: Dependency of the flux damping factor (α) on stability and wind speed classes as box plots without whiskers and outliers (box frame is the 25 % to 75 % interquartile ranges (IQR); the bold line is the median). Each damping estimation method is assigned a different color (red: IOG, green: ICO, blue: sICO, orange: THEO, black: IPS). Panels (a, b) refer to the BOG site and (c, d) to the FOR site.

α values of IOG, ICO, and sICO are nearly invariant to changes in wind speed at FOR. The predicted drop due to wind speed by THEO is roughly 0.10 at FOR. The difference of the empirical cospectral methods with THEO diminished for wind speeds larger than 4 m s^{-1}. IPS shows the weakest α for all wind speed classes at both sites. The decrease in α with wind speed is less than 0.10 at BOG and hence lower than the cospectral methods. IPS exhibits no significant drop in α with wind speed at FOR.

Values of α estimated by THEO are almost equal for unstable conditions and decline for stable situations. As before, the theoretical drop in attenuation is stronger at BOG (up to 0.20) than at FOR (not exceeding 0.10). At FOR, α values of IOG, ICO, and sICO are nearly equal ($\sim$ 0.85) for unstable cases. ICO, IOG, and sICO exhibit no distinct trend through all positive stability classes. Only for stability values above 0.4 is a decrease in α visible. However, this decline in α is rather uncertain since the IQR is relatively large compared to the unstable classes, and the number of cospectra that are attributed to stable conditions is relatively small.

At BOG, the linear decline in α is given for sICO but does not exist for IOG and ICO. α values of IOG and ICO are similar for unstable cases but show no clear decrease with increasing stability. The IQR of the sICO increases for positive stability and is smaller than IOG and ICO for negative values. The bias of sICO to IOG and ICO is obvious for the negative stability values. Similar to THEO, IPS shows a drop of α with increasing stability at BOG, but values are higher than for the cospectral methods. As observed for wind speed at FOR, no significant drop in α for IPS occurs under stable conditions.

2.3.3 Analysis of response time

After comparing α of the individual methods, we focus on variation in τ_r in time. Therefore, we show statistical analyses of τ_r of both measurement sites. Figure 8 shows statistical analyses of τ_r, which were calculated by ICO on a bimonthly basis depicted as box plots.

It is obvious that medians of τ_r of FOR are generally larger than medians of τ_r of BOG. The averaged median τ_r is 1.37 s for BOG and 3.13 s for FOR (Table B2.2). Common to both sites, τ_r was sightly lower at the start of the measurements and the medians were quite constant until December 2012 at BOG and October–November 2016 at FOR. Afterwards τ_r and its IQR increased significantly, especially at FOR. The variation in τ_r follows no trend and seems to be rather random. The IQR of FOR was larger, indicating that scattering of τ_r was enhanced at FOR. On average, τ_r increased from 0.74 to 1.63 s at BOG and from 1.85 to 3.51 s at FOR (Table B2.2).

We further determined the correlation between monthly averaged τ_r and α. Correlations of –0.83 for BOG and –0.72 for FOR show that there is a significant inverse relation between both parameters, which is expected due to the inverse dependency of τ_r in the empirical transfer function. The analysis of τ_r stratified by meteorological variables can be useful in order to investigate whether the scattering in α is related either to the variability in cospectra or to the instrument performance. τ_r is mostly a device-specific parameter. It should have a higher affinity to instrument or measurement setup parameters such as measurement height, pump and heating efficiency, altering of the inlet, and sensitivity of the analyzer than to turbulent atmospheric variations. Changes in gas concentrations may also affect τ_r. Therefore, we classified the meteorological parameters into bins, calculated τ_r for each bin, and display them as box plots (Fig. B2.1). τ_r is mostly constant for medium and high wind speed at BOG and exhibits slightly higher values at low wind speeds (0–0.5 m s^{-1}). During highly stable and unstable conditions τ_r reaches up to 3.50 s. It seems rather constant during medium unstable conditions but increases under stable conditions. The same is valid for τ_r at FOR. τ_r exhibits the highest values under both highly unstable and stable conditions. However, τ_r is strongly affected by wind speed at FOR. It decreases with wind speed and seems to follow a nonlinear relationship.

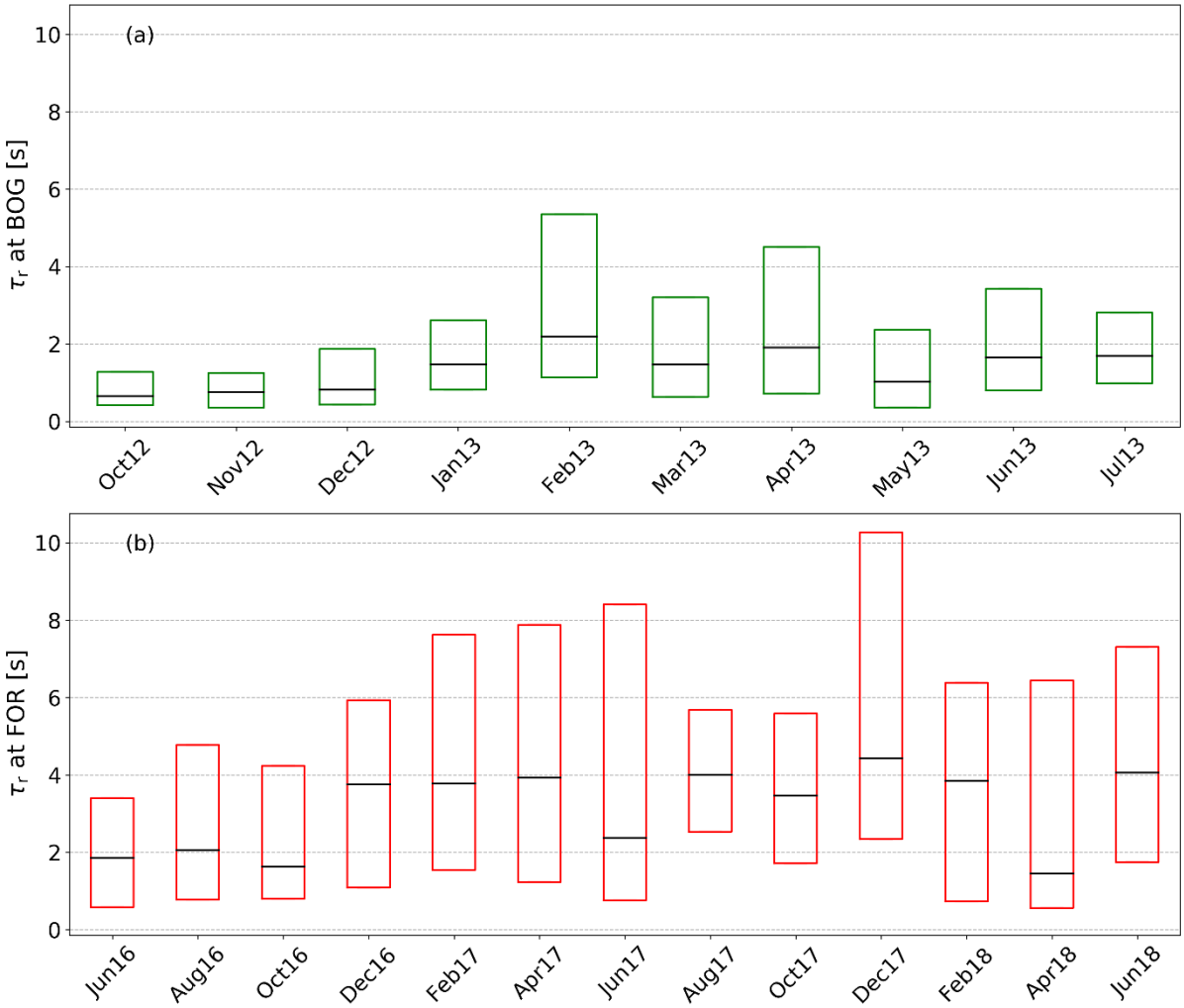

Figure 2.8: Statistical analysis of the response time (τ_r) depicted as a box plot without whiskers and outliers (the box frame is the 25 % to 75 % interquartile ranges (IQR); the bold line is the median) for the BOG site (a) and the FOR site (b).

2.4 Discussion

2.4.1. Noise effects on power spectra and cospectra

2.4.1.1 Sources of spectral noise

Measured fluxes of ΣN_r are heavily affected by white and red noise. They are caused by low and nonstationary ambient trace gas concentrations and fluxes, typically low fluxes due to weak sources and inhomogeneously distributed N sources, limited resolution and precision of the CLD, and varying proportions of different N_r compounds. This leads to a high rejection rate of cospectra and power spectra during quality screening, which is challenging for every spectral analysis using in situ measurements. While the influence on cospectra is mainly limited to the low-frequency range, power spectra show systematic deviations in the low- and high-frequency ranges. The positive slope (Figs. 2.3 and 2.4) is related to white noise which compromises the $Ps(\Sigma N_r)$ in the high-frequency domain. White and red noise are more present at FOR, because the site was located in a remote area with no nearby anthropogenic sources of ΣN_r (Zöll et al., 2019), resulting in low concentrations of N_r compounds (see Sect. 2.2.1). At BOG white noise is weaker since more sources of ΣN_r were next to the EC station. As

shown by Hurkuck et al. (2014), N_r concentrations at BOG were relatively high and showed a distinct diurnal cycle due to intensive livestock and crop production in the surrounding region. The disturbance due to red noise is also visible in Fig. 2.3. The variability (scattering) of cospectra and power spectra is more pronounced at FOR than at BOG in the low-frequency range as visible in the shown example.

Some Ps(ΣN_r) measurements in Fig. 2.4, mainly at BOG, show a slope near the theoretical value of –2/3 and were not affected by white noise. Therefore, we examined the environmental conditions such as wind speed, friction velocity, concentration, and flux values at that site during half hours, which were attributed to slopes less than –0.25, and compared them to half hours with a slope greater than –0.25. Only the distribution of concentration was different for the two regimes: most Ps(ΣN_r) measurements with a slope less than –0.25 were associated with concentration values between 25 and 40ppb, whereas Ps(ΣN_r) power spectra with a slope greater than –0.25 were associated with concentration values between 10 and 25 ppb, which is in common with the background concentration level of ΣN_r at BOG. It was about 21 ppb, whereas only 5 ppb on average was measured at FOR. Thus, it seems that the concentration is an important factor for regulating the quality of Ps(ΣN_r). The slope of Ps(T) shows a clear peak between –0.5 and –0.7 for both sites, which is close to the theoretical value of –2/3. The differences in the distribution may be related to different site characteristics like surface roughness length, inhomogeneous canopy height, or turbulence or to large-scale eddies which gain more influence on the fluxes at higher aerodynamic measurement height. Before, we argued that concentration of ΣN_r leads to differences in the slope distribution (Fig. 2.4). Concentrations of CO_2 were not significantly different between the sites. As a consequence, there has to be another parameter responsible for discrepancy in the contribution of positive Ps(CO_2) slopes at the measurement sites. We suppose that the discrepancy of positive Ps(CO_2) slopes corresponds to different levels of humidity at the measurement sites. Humid conditions could reduce the sensitivity of the open-path instrument and introduce noise in power spectra. Above the forest the air was less humid and consequentially fewer Ps(CO_2) measurements were affected by white noise.

2.4.1.2 Impact of noise on power spectra and cospectra

Removing high-frequency variations which consist mainly of white noise is easier for Ps(CO_2) measurements because their signal is higher than those of Ps(ΣN_r) in the low-frequency domain, and the observed noise is limited to the highest frequencies (> 2 Hz at FOR and > 5 Hz at BOG). Additionally, the noise is strictly linear and exhibits no parabolic structure like for Ps(ΣN_r) (Fig. 2.3). The observed parabolic shape in Ps(ΣN_r), which occurs around 1 Hz, is most likely caused by uncorrelated noise, which is induced by some components of the setup like pump, air-conditioning system, or electrical components, and decreased towards the highest frequencies. Handling the impact of unknown noise on power spectra is challenging for common linear noise compensation methods. Thus, it is probably not possible to remove the uncorrelated noise from Ps(ΣN_r) completely.

Wolfe et al. (2018) installed an EC setup in an aircraft and measured CO_2, H_2O, and CH_4 with Los Gatos Research analyzers and H_2O with an open-path infrared absorption spectrometer. They found a slope of ~ 1 in Ps(CO_2), Ps(H_2O), and Ps(CH_4) above 0.4 Hz but not in the Ps(H_2O) of the open-path analyzer. They concluded that the white noise was related to insufficient precision of the closed-path analyzers at higher frequencies. No white noise was detected in the corresponding cospectra, because it does not correlate with w.

Kondo and Tsukamoto (2007) performed CO_2 flux measurements above the equatorial Indian Ocean. They concluded that white noise was related to a lack of sensitivity to small CO_2 density fluctuations. Density fluctuations of CO_2 above open-ocean surfaces are much smaller than over vegetation. Similar to the present study, they detected no white noise in Co(w, CO_2). Their site characteristics and related low fluctuations of trace gas are comparable to those of the forest site. The latter was located in a remote area and therefore far away from potential (anthropogenic) nitrogen sources. This led to low

concentrations and less variability in concentrations and deposition fluxes. Very small fluctuations of ΣN_r are probably not detectable by the instrument. This is further confirmed by the time lag analysis we did before flux estimation. The broad shape of the empirical lag distribution around the physical lag (not shown) and the random time lag scattering demonstrated that most of the fluxes were near or below the detection limit, and thus quality of (co)spectra suffered from noise. Instrumental noise also affects the shape of the covariance function. It can lead to a broadening of the covariance peak and generally enhances the scattering of the covariance values. Both effects are already enlarged in the case of small mixing ratio fluctuations. Thus, instrumental noise further compromises the time lag estimation and leads to additional noise in cospectra. Due to the applied time lag criterion, the effect of instrumental noise is mostly canceled out. The position of the cospectral peak is less impacted, and thus instrumental noise can only lead to an enhancement of scattering of cospectral values, preferentially in the low-frequency range of the cospectrum. In other words, instrumental noise mostly contributes to the low-frequency noise, the red noise. Additionally, physical reasons, such as an inhomogeneous surface roughness length, canopy height in the footprint of the tower, and different range of relevant eddy sizes, may have been reasons for fewer valid high-quality (co)spectra compared to the BOG site.

2.4.1.3 Impact of noise on IPS

The findings indicate that using Ps for estimating correction factors of gases with low turbulent fluctuations, which are measured by a closed-path instrument, can be problematic. Therefore, we recommend using cospectra to estimate τ_r and α of reactive gases, since these gases normally exhibit low density fluctuations. However, Fig. 2.3 reveals that Ps(ΣN_r) shows a steep decline in the high-frequency range after the peak at BOG, which is similar to the decline of Ps(T). ΣN_r concentration was 24.4 ppb on average and exhibits a standard deviation of 9.6 ppb for the averaging period in Fig. 2.3, suggesting significant differences in concentration levels. It confirms the statement that the concentration is an important driver for the quality of Ps(ΣN_r). This leads us to the assumption that the instrument was in principle able to capture differences in concentration levels in the high-frequency range if mixing ratio fluctuations are relatively high.

White noise was observed in power spectra of CO_2 and H_2O, too. Both gases were measured with an open-path analyzer, but their concentrations are higher and the variability in concentrations of these gases is much larger than for ΣN_r. It indicates that Ps(CO_2) values are clearly less affected by white noise, and the instrument is able to capture the high-frequency variability of CO_2 well. The assumption of spectral similarity, which is a critical assumption for all in situ methods, was valid for Ps(CO_2) but was not fulfilled for Ps(ΣN_r) due to the influence of red and white noise. Consequentially, an optimization fit with an infinite impulse response function gives unrealistic results for τ_r. Most likely, automatic filtering criteria are not sufficient enough to extract good quality (co)spectra of ΣN_r efficiently, and thereby the averaged Ps(ΣN_r) used for the fitting procedure is dominated by low-quality and invalid cases. However, using more restrictive quality selection criteria or narrowing the frequency range for the fitting of the transfer function produced rapidly changing values or even negative values for τ_r. This demonstrates that the estimation of τ_r with Ps(ΣN_r) via IPS is very uncertain, and the number of Ps(ΣN_r) measurement with sufficient quality was not high enough for a robust fitting. Consequently, for estimating damping factors with IPS certain conditions seem to be fulfilled. For example, (i) instruments need a low detection limit and (ii) influence of noise on (co)spectra has to be reduced to a minimum, for instance by optimizing the positions of the sonic anemometer and gas analyzer. In addition, (iii) strategies for the elimination of noise have to be aligned with the design of the instrument and trace gas of interest. The latter should be (iv) rather inert, i.e., little interaction with surfaces or other chemical compounds, and, in the case of IPS, (v) trace gases should exhibit a wind speed dependency on damping factors. Similar to cospectral methods, IPS will also benefit from a well-defined footprint, equal canopy height, and sufficient turbulence. Satisfying these aspects is quite difficult for a custom-built EC system, for which not all attenuation processes are identified yet. In addition, measuring and

analyzing ΣN_r is challenging since the concentrations of the several compounds contributing to ΣN_r are unknown, and the compounds exhibit complex reaction pathways and generally low fluctuations.

The number of good quality (co)spectra for CO_2 and H_2O was at least 1 order of magnitude higher than for ΣN_r. Monthly averaged α values for CO_2 and H_2O by IPS were in the range of 0.95 and 0.90, which is quite reasonable for an open-path instrument and in agreement with studies dealing with the same instrument (Burba et al., 2010; Butterworth and Else, 2018).

2.4.2 Assessment of cospectral approaches

2.4.2.1 THEO vs. (semi)empirical approaches

In general, α values determined by the (semi)empirical cospectral methods (sICO, ICO, and IOG) were considerably lower than the results of THEO. The difference indicates a strong additional damping effect whose impact on ΣN_r fluxes is not detected by the fluid-dynamics-related transfer functions used in THEO. This additional damping must be caused by adsorption processes at the inner surfaces of the inlet system, for example in the converter or the sample lines or the CLD. Studies from Aubinet et al. (1999), Bernhofer et al. (2003), Ammann et al. (2006), and Spank and Bernhofer (2008) have also shown that the damping factor by the THEO approach is often too high. Besides disregarded damping processes, this could have also been caused by deviations of the site-specific cospectra from theoretical cases. Therefore, it is advisable to apply empirical methods to measurements of gases with unknown properties or to setups and instrument devices with flux loss sources which are difficult to quantify. Empirical methods take the sum of all potential flux losses into account and do not take care of an individual or specific flux loss. The difference between THEO and empirical methods in total flux losses at the two study sites can be explained by the different aerodynamic measurement heights. With increasing measurement height, turbulence cospectra are shifted to lower frequencies (Figs. 2.1 and 2.3), and hence a weaker high-frequency damping is expected. Vertical sensor separation was not considered by the spectral transfer function in the THEO approach. However, the impact of vertical sensor separation on the flux loss is very low if the gas analyzer is placed below the anemometer as in the present study. Kristensen et al. (1997) determined a flux loss of only 2 % at the vertical separation of 20 cm and measurement height of 1 m. This effect becomes even smaller with increasing measurement height. Besides the measurement height, the wind speed and stability are also expected to have an influence on the position and shape of the cospectrum and thus on the damping factor. Yet, no clear systematic dependencies of (s)ICO and IOG results on these parameters were found. At BOG, the dependency on wind speed is only valid for medium- and high-wind-speed classes. α values of IOG and ICO appear to be invariant to changes in stability at BOG, whereas α values of the cospectral empirical approaches are quite constant under unstable conditions at FOR. In contrast, sICO follows the expected drop at stable conditions as observed for THEO at both sites. The reason for the difference between sICO and ICO is discussed in Sect. 2.4.2.2.

There could be other effects which superpose the wind speed and stability dependencies, for example, (chemical) damping processes occurring inside the TRANC–CLD system. Humidity and ΣN_r could affect the aging of the tube and consequentially the adsorption at inner tube walls. However, we found no dependency of these parameters on damping factor and time response. Interactions with tube walls is probably less important, especially for the tube connecting the end of the TRANC to the CLD, because the main trace gas within the line is NO, which acts rather inertly in the absence of ozone and NO_2. Because NO_2 and O_3 are converted in the TRANC, it can be assumed that the influence of interaction with tube walls on time response and high-frequency flux losses is mostly negligible compared to effects that happen in the CLD and TRANC. The CLD contributes more to the total attenuation than the tubing, but supposedly not as much as the TRANC. Rummel et al. (2002) also used the CLD 780 TR as a device for measuring NO fluxes. High-frequency flux losses were rather low and ranged between 21 % (close

to the ground) and 5 % (11 m above ground). Also, Wang et al. (2020) observed low flux losses of NO by approximately 12 % by measuring with a QCL (1.7 m above ground).

Consequently, the strongest contributor to the overall damping has to be the TRANC. NH_3 is, considering all possible convertible compounds, the most abundant in certain ecosystems, highly reactive, and rather "sticky". In absolute terms it has the highest influence on the damping of ΣN_r. QCL devices, which may be used for the detection of NH_3 (Ferrara et al., 2012; Zöll et al., 2016; Moravek et al., 2019), were equipped with a special designed, heated, and opaque inlet to avoid sticking of NH_3 at tube walls and water molecules and preventing unwanted molecules entering the analyzer cell. Thus, NH_3 has high flux loss factors ranging from 33 % to 46 % (Ferrara et al., 2012; Zöll et al., 2016; Moravek et al., 2019). These damping factors are closer to the damping factors of ΣN_r, in particular for BOG, at which high NH_3 concentrations were measured, and most of ΣN_r can be attributed to NH_3 (Hurkuck et al., 2014; Zöll et al., 2016). At FOR, flux losses were lower due to physical reasons and due to a lower contribution of NH_3 to ΣN_r at FOR. According to DELTA-Denuder measurements presented in Zöll et al. (2019), NH_3 concentrations were relatively low at the FOR site (Beudert and Breit, 2010). A fraction of 33 % of ΣN_r was NH_3 and 32% NO_2. NH_3 is converted inside the TRANC at the platinum gauze after passing through the actively heated inlet and iron–nickel–chrome (FeNiCr) alloy tube. Since the main part of the pathway is heated and isolated against environmental impacts, the inlet of the TRANC and the distance to the sonic anemometer seem to be critical for the detection and attenuation of NH_3. Finally, we suppose that the response time and attenuation of our TRANC–CLD system is more similar to that of an NH_3 analyzer under a high ambient NH_3 load.

2.4.2.2 ICO vs. sICO approach

The difference between the ICO and sICO method is the usage of Kaimal cospectra for determining α after Eq. (2.1). One reason for using theoretical cospectra is that it lowers the computation time for estimation of α. Moreover, due to site or experimental setup reasons, the Co(w, T) may be influenced by noise in the low-frequency range, which compromises the determination of α. In such cases, using Kaimal cospectra can be a good alternative. The usage of standard Kaimal cospectra leads to a loss of site-specific information. Differences to measured Co(w, T) can lead to uncertainties in the damping estimation of sICO. The consequence is an observed bias of unstable α between sICO and ICO at BOG (Fig. 2.7) or wind speed and stability dependencies induced by the usage of Kaimal cospectra, which are not confirmed by ICO or IOG. Mamadou et al. (2016) computed α of CO_2 with locally measured cospectra and Kansas cospectra (Kaimal et al., 1972), which are slightly different from the theoretical cospectra used in this study. They found that theoretical and measured Co(w, T) differ significantly in shape, which resulted in large differences of correction factors during stable conditions, although their investigated site exhibited no complex terrain or vegetation. This led to an overestimation of nighttime fluxes of 14 %–28 % if Kansas cospectra were used. Therefore, we selected α of ICO and sICO estimated at stable conditions during day and nighttime. Comparing stable ($\zeta > 0.05$) nighttime–dawn ($R_g < 20$ W m^{-2}) α with stable daytime half-hourly α showed that stable nighttime α had a higher variability and were mostly overestimated by 0.14– 0.35, whereas stable daytime α values were overestimated by 0.10–0.20 if Kaimal cospectra (sICO) were used. Some α values were underestimated by sICO, but the discrepancy was about 0.15 on average. Using Kaimal cospectra can be problematic for estimating α under stable conditions. If typical wind speed or stability dependencies are not approved by other cospectral methods, we do not recommend the usage of theoretical methods such as Kaimal cospectra since it may lead to a bias or unproven dependency.

2.4.2.3 ICO vs. IOG approach

The main difference between ICO and the IOG method is that IOG utilizes the low-frequency part and (s)ICO the high-frequency part of the cospectrum. The low-frequency part is much more variable than the high-frequency one, especially on a half-hourly basis. As a consequence, the ratio between Og(w, ΣN_r) and Og(w, T) is often not well-defined in the fitting range and hence the linear regression between Og(w, ΣN_r) and Og(w, T) gives erroneous results. Strong attenuation is possibly underestimated by IOG because damping can extend into the fit range. IOG may perform better for averaged cospectra since the impact of scattering in the low-frequency part of the spectrum would be reduced. The variability (scattering) of cospectra in the high-frequency part is comparatively small, and differences in the decay of Co(w, ΣN_r) and Co(w, T) are easier to identify than differences in the low-frequency part. The transfer function used in the ICO fitting routine has to consider the relevant damping processes. While the transfer functions for physical damping effects are relatively well defined (see Mamadou et al., 2016; Table A2.1), chemical damping effects are rather unknown, although they can be very important for reactive gases such as NH_3 or ΣN_r. The empirical transfer function was chosen with regard to different response times of the individual sensors. Since both sensors are first-order system filters, the dynamic frequency response can be described by the first-order filter transfer function (Eq. A2.1). Additionally, the TRANC–CLD has a slower response than the sonic anemometer. The mismatch in the response times introduces a phase shift in the time series, which is accounted for by applying the phase-shift mismatch function (Table A2.1) after Zeller et al. (1988), and Ammann (1999). The inclusion of the shift mismatch in Eq. (2.3) leads to a steeper slope in the empirical transfer function and variations around zero at higher frequencies (see Fig. 2.1) compared to a first-order function alone (not shown). If α is calculated without including the phase-shift effect, we get an overestimation of the damping of up to 10 % for both sites. This could be expected and indicates that most of the damping is related to a time shift. Until now, there is no ideal transfer function which can capture all damping processes. The transfer function can differ depending on trace gas and site setup. Our empirical transfer function was chosen especially for reactive gases such as ΣN_r or NH_3 measured with a closed-path instrument. The usage of Eq. (2.3) for other gases like CO_2 or H_2O is not recommended without knowing any spectral characteristics. In the case of CO_2 and H_2O measured with Li-7500 at FOR and BOG, we have to modify Eq. (2.3). We would leave out the phase-shift mismatch since the Li-7500 has a faster response and consider using the sensor separation and/or path-averaging transfer function (Moore, 1986).

2.4.3 Recommendations for correcting high-frequency flux losses of N_r compounds

ΣN_r is a complex trace gas signal since it consists of many reactive N gases, which have various reaction pathways, and concentrations of the single compounds are unknown. We have shown that very low concentration differences of ΣN_r are difficult to detect for the CLD. This has an influence on the variability of (co)spectra, strengthens their susceptibility to noise, and reduces the number of high-quality (co)spectra. Since power spectra had a strong affinity to white noise and exhibited no spectral similarity to temperature spectrum due to red noise, we recommend using cospectra for estimating α. We found that flux loss is rather chemical driven, in particular determined by the dimensions of the inlet and ambient NH_3 load. It could lead to an invariance in wind speed and stability. As a consequence, common approaches, which are based on theoretical, physical assumptions or established dependencies on environmental dependencies, are not suitable for our EC system. Specifying the flux loss of the different compounds is rather difficult due to the measurement of the sum of individual N_r compounds. Thus, we can only roughly estimate the contribution of individual species to the flux and its high-frequency loss. At BOG, mostly NH_3 seems to influence the damping of ΣN_r. At FOR, NH_3 as well as NO_2 were the main ΣN_r flux contributors, thereby playing an important role in the detected flux loss at the forest site (see Sect. 2.4.2.1). Due to the unknown physical and chemical characteristics of ΣN_r, an empirical approach seems to be the best solution for capturing attenuation processes of ΣN_r and its complex compounds. Having carefully considered all pros and cons of the used approaches, our method of choice will be ICO.

A general or site-specific parameterization of the damping as a function of wind speed and stability was not possible for the entire wind speed and stability range. A parameterization would be possible only for certain wind speed and stability ranges. For example, a parameterization can be performed for unstable conditions and for wind speeds above 1.5 m s^{-1} at BOG. As mentioned in Sect. 2.3.2, other parameters such as global radiation showed no clear dependency on α. No significant difference between day and nighttime α values was found. The exchange pattern of ΣN_r is rather bidirectional during the entire day. The exchange pattern of inert gases like CO_2 is largely related to photosynthesis and respiration. During daytime CO_2 also exhibits bidirectional exchange characteristics. During nighttime the exchange of CO_2 is mostly unidirectional. Thus, we would expect a diurnal variation in the CO_2 attenuation. The influence of global radiation on the biosphere–atmosphere exchange of ΣN_r and CO_2 was explicitly shown by Zöll et al. (2019) for FOR. They also investigated drivers of ΣN_r. However, global radiation explained only 22 % of the variability in ΣN_r fluxes, whereas 66% of the variability in CO_2 fluxes was related to global radiation. ΣN_r had the concentration as a second driver, which was approximately 24 %. Consequently, there are additional factors controlling the biosphere–atmosphere exchange of total reactive nitrogen, which may be of a chemical nature and challenging to quantify. Thus, a flux loss correction of ΣN_r after meteorologically classified parameters is not provided.

For an aspired correction of the determined fluxes, half-hourly estimated α values of the empirical methods will not be used due to their variation with time and to the limited number of high-quality ΣN_r cospectra. Therefore, it is advisable to use averages over certain time periods. We decided to use monthly median values for correcting fluxes at BOG. A bimonthly classification was conducted for FOR because the rejection rate was higher due to higher uncertainty of cospectra in the low-frequency range. For estimating α, a reliable determination of τ_r is needed. Using a constant τ_r is possible but not recommended for our ΣN_r setup since τ_r varied with time and started to increase after a few months. It seems that the variation in α in time was mainly driven by the change in τ_r. The increase in τ_r and the enhanced variation in τ_r after a few months could be related to instrumental performance problems caused by aging of the inlet, tubes, and filters, reducing pump performance; problems with the CO supply and TRANC temperature; or a sensitivity loss of the CLD. The variability in τ_r also has an influence on the meteorological classification of α. Generally, it is not known how much the variability in τ_r contributes to the scattering in α for certain wind speeds or stability values. Thus, usage of τ_r and the corresponding α classified by meteorological parameters is only recommended for medium or high wind speeds at BOG or near-neutral and unstable atmospheric conditions at both sites. Finally, it seems that the attenuation of the TRANC–CLD system is mainly driven by the performance of the EC setup and by changes in the composition of ΣN_r.

2.5 Conclusions

We investigated flux losses of total reactive nitrogen (ΣN_r) measured with a custom-built converter (TRANC) coupled to a fast-response CLD above a mixed forest and a seminatural peatland. We compared five different methods for the quantification and correction of high-frequency attenuation: the first is adapted from Moore (1986) (THEO), the second uses measured cospectra of sensible heat and trace gas flux (ICO), the third uses response time calculated from measured cospectra and estimate damping with modified Kaimal cospectra (Ammann, 1999) (sICO), the fourth uses the measured ogives (IOG), and the fifth method is the power spectral method by Ibrom et al. (2007) (IPS). The flux losses by IPS for our closed-path eddy-covariance setups were around 6 % at the peatland site (BOG) and around 5 % at the forest site (FOR). The attenuation after THEO was about 12 % at BOG and about 5 % at FOR. The methods using measured cospectra or ogives (ICO, sICO, and IOG) showed a flux loss of roughly 16 %–22 % for the forest measurements and around 26 %–38 % for the peatland measurements, with ICO showing the strongest damping at both sites. Flux losses of the empirical approaches are comparable to other EC studies on ΣN_r and other reactive nitrogen compounds.

We found that Ps(ΣN_r) was heavily affected by white and red noise. No robust estimation of the response time (τ_r) by using measured power spectra was possible. THEO could not capture strong damping processes of ΣN_r fluxes, which are likely caused by adsorption processes occurring at inner surfaces of the inlet system or missing information about the contribution of specific gases to ΣN_r. Consequently, THEO and IPS are not recommended for estimating reliable flux losses of ΣN_r.

Differences in flux losses are related to measurement height and hence to the variable contribution of small- and large-scale eddies to the flux. No systematic or only partly significant dependencies of the empirical methods (ICO, sICO, and IOG) on parameters such as atmospheric stability and wind speed, which have an influence on the shape and position of cospectrum, were observed. In the case of the empirical methods, we found a wind speed dependency on damping factors (α), apparently a linear decrease in α with increasing wind speed at BOG. However, the trend is limited to wind speeds higher than 1.5 m s^{-1}. At FOR, α values of IOG, sICO, and ICO seem to be invariant to changes in wind speed. For unstable cases, α values are rather constant at FOR ($\sim$ 0.85). At BOG, α values of IOG and ICO were similar and vary between 0.60 and 0.80 at unstable conditions, whereas sICO values were higher by approximately 0.05–0.15. The expected decline of α with increasing stability was only observed in sICO at both sites, probably related to the usage of Kaimal cospectra. IOG and ICO showed no clear trend for stable cases. We suppose that other factors like varying atmospheric concentration, distribution, and strength of sources and sinks; enhanced chemical activity of ΣN_r compared to CO_2 and H_2O; aging of the TRANC inlet; varying CLD performance; and vegetation could influence α more strongly and may superpose slight effects of wind speed and stability. Thus, a general or site-specific parameterization of the damping for the complete wind speed and stability range was not possible.

The empirical methods perform well at both sites and median α values are in the range of former studies about reactive nitrogen compounds. However, we detected significant discrepancies to ICO which were related to site-specific problems or to using different frequency ranges of the cospectrum for the assessment. We discovered a bias between α computed with ICO and sICO for the BOG measurements. No significant bias for ICO and sICO was detected at the FOR site. We supposed that Kaimal cospectra may underestimate the attenuation of fluxes under certain site conditions (see Mamadou et al., 2016). Differences in α to IOG are induced by utilizing the low-frequency part of the cospectrum. The low-frequency part is more variable than the high-frequency part on a half-hourly basis. Strong attenuation cases could be underestimated by IOG since damping already occurs in the fit range.

Our investigation of different spectral correction methods showed that ICO is most suitable for capturing damping processes of ΣN_r. However, not all damping processes of reactive gases are fully understood yet, and current correction methods have to be improved with regard to quality selection of cospectra. Power spectral and purely theoretical methods which are established in flux calculation software worked well for inert gases, but they are not suitable for reactive nitrogen compounds. Estimating damping of EC setups designed for highly reactive gases with an empirical method may be a considerable and reliable option. For further correction of fluxes, we will use monthly median α since half-hourly values will lead to significant uncertainties in fluxes. Using a constant τ_r is not recommended as we noticed variation in τ_r with time, which is caused by altering the inlet system. Correcting fluxes after meteorologically classified α is possible if dependencies are exhibited by the EC setup.

Appendix A

A2.1 Transfer functions of the ΣN_r setup

Transfer functions used for validation of α after THEO, ICO, and sICO are listed in Table A2.1. A detailed description is given in the mentioned literature. Table 2.1 contains physical parameters of the setup which are necessary to estimate α.

Table A2.1: Transfer functions used for evaluation of the ΣN_r damping factors.

Transfer function	Physical parameters
First-order filter $\mathrm{TF_R}(f) = \frac{1}{\sqrt{1 + (2\pi\tau_r f)^2}}$	response time τ_r; the THEO approach uses the analyzer response time $\tau_{r,a}$ (Moore, 1986; Moncrieff et al., 1997)
Sensor separation $\mathrm{TF_S}(f) = \exp(-9.9(f\, d_s/u)^{1.5})$ with $d_s = d_{sa}\lvert\sin(\alpha_d)\rvert$	wind speed u, effective lateral separation distance d_s,measured separation distance d_{sa}, angle between the line joining the sensors and wind direction α_d (Moore, 1986; Aubinet et al., 2012)
Path-averaging anemometer $\mathrm{TF_w}(f_p) = \frac{2}{\pi f_p}\left(1 + \frac{1}{2}\exp(-2\pi f_p) - 3\frac{1-\exp(-2\pi f_p)}{4\pi f_p}\right)$; $f_p = \frac{f\, p_1}{u}$	p_1 sonic path length (Moore, 1986; Moncrieff et al., 1997; Aubinet et al., 2012)
Tube attenuation $\mathrm{TF_{t,lam}}(f) = \exp(-0.82 ReSc\, f_t^2)$ with $f_t = f \cdot (0.5DL)^{0.5}/v_t$	D diameter of tube, L length of tube, Sc Schmidt number, Re Reynolds number, v_t flow speed inside the tube (Ammann, 1999; Aubinet et al., 1999, 2012)
Phase-shift mismatch $\mathrm{TF_{\Delta R}}(f) \approx \cos[\arctan(2\pi f\tau_r) - 2\pi f\tau_r]$	τ_r response time (Zeller et al., 1988; Ammann, 1999)

A2.2 Kaimal cospectrum used in THEO and sICO

The cospectrum for stable conditions after Ammann (1999) has the following form:

$$\mathrm{Co_{mod}}(f,a,u) = \frac{f \cdot (a/u)}{0.284 \cdot (1 + 6.4 \cdot \zeta)^{0.75} + 9.345 \cdot (1 + 6.4 \cdot \zeta)^{-0.825} \cdot \left(f \cdot (a/u)\right)^{2.1}} \quad \text{(A2.7)}$$

where a is the aerodynamic measurement height and is given by the difference of measurement height z and the zero-plane displacement height d with $a = z–d$ (Spank and Bernhofer, 2008). ζ is the stability parameter and is defined by $\zeta = a/L$. L is the Obukhov length. The cospectrum for unstable conditions is determined by two parts:

$$\mathrm{Co_{mod}}(f,a,u) = \begin{cases} 12.92 \cdot f \cdot (a/u) \cdot \left(1 + 26.7 \cdot f \cdot (a/u)\right)^{-1.375} & f \cdot (a/u) < 0.54 \\ 4.378 \cdot f \cdot (a/u) \cdot \left(1 + 3.8 \cdot f \cdot (a/u)\right)^{-2.4} & f \cdot (a/u) \geq 0.54 \end{cases} \quad \text{(A2.2)}$$

Appendix B

B2.1 Results of different damping correction methods

Table B2.1: Result of the comparison between different damping determination methods at the two measurement sites. Bias (1) is computed as the averaged difference between α values. Precision is given as 1.96 standard deviation of the difference. r is the correlation coefficient.

Method	Bavarian Forest			Bourtanger Moor		
	Δ	1.96σ	r	Δ	1.96σ	r
ICO,IOG	-0.07	0.33	0.50	-0.10	0.31	0.67
ICO,sICO	0.0	0.25	0.78	-0.07	0.33	0.66
ICO,THEO	-0.19	0.37	0.09	-0.25	0.43	-0.08
ICO,IPS	-0.19	0.38	-0.09	-0.30	0.43	-0.14
sICO,IOG	-0.07	0.36	0.36	-0.03	0.36	0.42
sICO,THEO	-0.20	0.33	0.22	-0.18	0.37	0.36
sICO,IPS	-0.20	0.37	-0.05	-0.23	0.38	0.38
IOG,THEO	-0.12	0.22	0.0	-0.15	0.26	0.01
IOG,IPS	-0.12	0.22	-0.08	-0.20	0.26	-0.16
THEO,IPS	0.0	0.05	0.47	-0.05	0.07	0.70

Table B2.2: Median τ_r averaged over certain measurement periods at both sites.

Site	Time period	Averaged τ_r (s)	Lower quartile (s)	Upper quartile (s)
Bavarian	Jun 2016–Nov 2016	1.85	0.72	4.14
Forest	Dec 2016–Jun 2018	3.51	1.43	7.15
	whole period	3.13	1.26	6.46
Bourtanger	Oct 2012–Dec 2012	0.74	0.40	1.47
Moor	Jan 2013–Jul 2013	1.63	0.78	3.47
	whole period	1.37	0.67	2.87

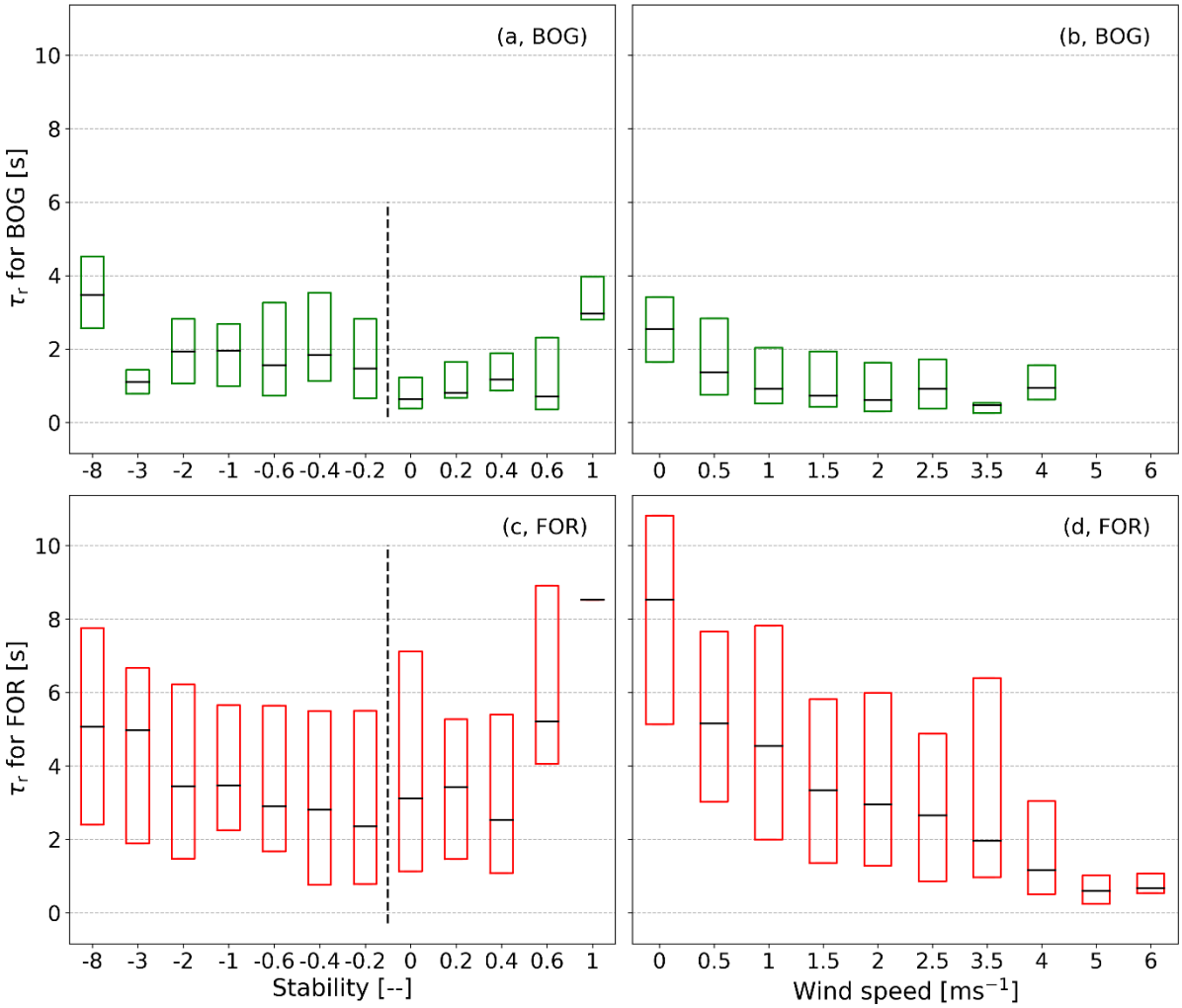

Figure B2.1: Dependency of the response time (τ_r) on stability and wind speed classes as box plots without whiskers and outliers (the box frame is the 25 % to 75 % interquartile ranges (IQR), and the bold line is the median). Panels (a, b) refer to the BOG site and (c, d) to the FOR site.

Code and data availability. All data are available upon request from the first author of this study (pascal.wintjen@thuenen.de). Also, Python 3.7 code for damping factor calculation as well as the data analysis code can be requested from the first author. All necessary equations for determining the damping factors are given in this paper.

Author contributions. PW wrote the manuscript, carried out the measurements at the forest site, and performed data analysis and interpretation. CA gave scientific advice. FS helped with coding and evaluated meteorological measurements. CB conducted the measurements at the peatland site and gave scientific advice. All authors discussed the results, and FS, CA, and CB reviewed the manuscript.

Competing interests. The authors declare that they have no conflict of interest.

Acknowledgements. We thank Undine Zöll for scientific and logistical help; Jeremy Rüffer and Jean-Pierre Delorme for excellent technical support, particularly during the field campaigns; and the Bavarian Forest National Park Administration, namely Burkhard Beudert, Wilhelm Breit, and Ludwig Höcker, for technical and logistical support at the site. We further thank the two anonymous reviewers for valuable comments that helped improve the quality of the manuscript.

Financial support. This research has been supported by the German Environment Agency (UBA) (FORESTFLUX project, support code FKZ 3715512110) and the German Federal Ministry of Education and Research (BMBF) (Junior Research Group NITROSPHERE, support code FKZ 01LN1308A).

Review statement. This paper was edited by Thomas F. Hanisco and reviewed by two anonymous referees.

References

Ammann, C.: On the applicability of relaxed eddy accumulation and common methods for measuring trace gas fluxes, PhD thesis, ETH Zurich, https://doi.org/10.3929/ethz-a-002031554, 1999

Ammann, C., Brunner, A., Spirig, C., and Neftel, A.: Technical note: Water vapour concentration and flux measurements with PTR-MS, Atmos. Chem. Phys., 6, 4643–4651, https://doi.org/10.5194/acp-6-4643-2006, 2006.

Ammann, C., Wolff, V., Marx, O., Brümmer, C., and Neftel, A.: Measuring the biosphere-atmosphere exchange of total reactive nitrogen by eddy covariance, Biogeosciences, 9, 4247–4261, https://doi.org/10.5194/bg-9-4247-2012, 2012.

Aubinet, M., Grelle, A., Ibrom, A., Rannik, U., Moncrieff, J., Foken, T., Kowalski, A. S., Martin, P. H., Berbigier, P., Bernhofer, C., Clement, R., Elbers, J., Granier, A., Grünwald, T., Morgenstern, K., Pilegaard, K., Rebmann, C., Snijders, W., Valentini, R., and Vesala, T.: Estimates of the Annual Net Carbon and Water Exchange of Forests: The EUROFLUX Methodology, Adv. Ecol. Res., 30 113–175, https://doi.org/10.1016/S00652504(08)60018-5, 1999.

Aubinet, M., Vesala, T., and Papale, D. (Eds.): Eddy Covariance: A Practical Guide to Measurement and Data Analysis, Springer Science+Business Media B.V., Dordrecht, The Netherlands, 2012.

Bernhofer, C., Feigenwinter, C., Grünwald, T., and Vogt, R.: Spectral Correction of Water and Carbon Flux for EC Measurements at the Anchor Station Tharandt, in: Flussbestimmung an komplexen Standorten, edited by: Bernhofer, C., Tharandter Klimaprotokolle Band 8, 1–13, 2003.

Beudert, B. and Breit, W.: Integrated Monitoring Programm an der Meßstelle Forellenbach im Nationalpark Bayerischer Wald, Untersuchungen zum Stickstoffeintrag und zum wassergebundenen Stickstoffhaushalt des Forellenbachgebiets, Förderkennzeichen 351 01 012, Nationalparkverwaltung Bayerischer Wald, Sachgebiet IV, techreport, Umweltbundesamt, available at: https://www.umweltbundesamt.de/sites/default/files/medien/370/dokumente/ece_im_forellenbach_berichtsjahr_2009.pdf (last access: 4 May 2020), 2010.

Beudert, B., Bernsteinová, J., Premier, J., and Bässler, C.: Natural disturbance by bark beetle offsets climate change effects on streamflow in headwater catchments of the Bohemian Forest, Silva Gabreta, 24, 21–45, available at: https://www.npsumava.cz/ wp-content/uploads/2019/06/2_sg_24_beudertetal.pdf, (last access: 4 May 2020), 2018.

Brümmer, C., Marx, O., Kutsch, W., Ammann, C., Wolff, V., Flechard, C. R., and Freibauer, A.: Fluxes of total reactive atmospheric nitrogen (ΣN_r) using eddy covariance above arable land, Tellus B, 65, 19770, https://doi.org/10.3402/tellusb.v65i0.19770, 2013.

Burba, G.: Eddy Covariance Method for Scientific, Industrial, Agricultural and Regulatory Applications: A Field Book on Measuring Ecosystem Gas Exchange and Areal Emission Rates, LICOR Biosciences, Lincoln, Nebraska, USA, 2013.

Burba, G. G., Mcdermitt, D. K., Anderson, D. J., Furtaw, M. D., and Eckles, R. D.: Novel design of an enclosed CO_2/H_2O gas analyser for eddy covariance flux measurements, Tellus B, 62, 743– 748, https://doi.org/10.1111/j.1600-0889.2010.00468.x, 2010.

Butterworth, B. J. and Else, B. G. T.: Dried, closed-path eddy covariance method for measuring carbon dioxide flux over sea ice, Atmos. Meas. Tech., 11, 6075–6090, https://doi.org/10.5194/amt-11-6075-2018, 2018.

Desjardins, R. L., MacPherson, J. I., Schuepp, P. H., and Karanja, F.: An evaluation of aircraft flux measurements of CO_2, water vapor and sensible heat, Bound.-Lay. Meteorol., 47, 55–69, https://doi.org/10.1007/BF00122322, 1989.

Ferrara, R. M., Loubet, B., Di Tommasi, P., Bertolini, T., Magliulo, V., Cellier, P., Eugster, W., and Rana, G.: Eddy covariance measurement of ammonia fluxes: Comparison of high frequency correction methodologies, Agr. Forest Meteorol., 158-159, 30– 42, https://doi.org/10.1016/j.agrformet.2012.02.001, 2012.

Flechard, C. R., Massad, R.-S., Loubet, B., Personne, E., Simpson, D., Bash, J. O., Cooter, E. J., Nemitz, E., and Sutton, M. A.: Advances in understanding, models and parameterizations of biosphere-atmosphere ammonia exchange, Biogeosciences, 10, 5183–5225, https://doi.org/10.5194/bg-10-5183-2013, 2013.

Fowler, D., Coyle, M., Skiba, U., Sutton, M. A., Cape, J. N., Reis, S., Sheppard, L. J., Jenkins, A., Grizzetti, B., Galloway, J. N., Vitousek, P., Leach, A., Bouwman, A. F., Butterbach-Bahl, K., Dentener, F., Stevenson, D., Amann, M., and Voss, M.: The global nitrogen cycle in the twenty-first century, Philos. T. Roy. Soc. B, 368, 20130164, https://doi.org/10.1098/rstb.2013.0164, 2013.

Fratini, G., Ibrom, A., Arriga, N., Burba, G., and Papale, D.: Relative humidity effects on water vapour fluxes measured with closed-path eddy-covariance systems with short sampling lines, Agr. Forest Meteorol., 165, 53–63, https://doi.org/10.1016/j.agrformet.2012.05.018, 2012.

Horst, T. W. and Lenshow, D. H.: Attenuation of Scalar Fluxes Measured with Spatially-displaced Sensors, Bound.-Lay. Meteorol., 130, 275–300, https://doi.org/10.1007/s10546-008-9348-0, 2009.

Hurkuck, M., Brümmer, C., Mohr, K., Grünhage, L., Flessa, H., and Kutsch, W. L.: Determination of atmospheric nitrogen deposition to a semi-natural peat bog site in an intensively managed agricultural landscape, Atmos. Environ., 97, 296–309, https://doi.org/10.1016/j.atmosenv.2014.08.034, 2014.

Hurkuck, M., Brümmer, C., and Kutsch, W. L.: Near-neutral carbon dioxide balance at a seminatural, temperate bog ecosystem, J. Geophys. Res.-Biogeo., 121, 370–384, https://doi.org/10.1002/2015jg003195, 2016.

Ibrom, A., Dellwick, E., Flyvbjerg, H., Jensen, N. O., and Pilegaard, K.: Strong low-pass filtering effects on water vapour flux measurements with closed-path eddy correlation systems, Agr. Forest Meteorol., 147, 140–156, https://doi.org/10.1016/j.agrformet.2007.07.007, 2007.

Kaimal, J. C., Wyngaard, J. C., Izumi, Y., and Coté, O. R.: Spectral characteristics of surface-layer turbulence, Q. J. Roy. Meteor. Soc., 98, 563–589, https://doi.org/10.1002/qj.49709841707, 1972.

Kolle, O. and Rebmann, C.: EddySoft Documentation of a Software Package to Acquire and Process Eddy Covariance Data, techreport, MPI-BGC, available at: https://repository.publisso.de/resource/frl:4414276-1/data (last access: 4 May 2020), 2007.

Kondo, F. and Tsukamoto, O.: Air-Sea CO_2 Flux by Eddy Covariance Technique in the Equatorial Technique in the Equatorial, J. Oceanogr., 63, 449–456, available at: https://www.terrapub. co.jp/journals/JO/pdf/6303/63030449.pdf (last access: 4 May 2020), 2007.

Kristensen, L., Mann, J., Oncley, S. P., and Wyngaard, J. C.: How Close is Close Enough When Measuring Scalar Fluxes with Displaced Sensors?, J. Atmos. Ocean. Tech., 14, 814–821, https://doi.org/10.1175/15200426(1997)014<0814:HCICEW>2.0.CO;2, 1997.

Lee, X. and Black, T. A.: Relating eddy correlation sensible heat flux to horizontal sensor separation in the unstable atmospheric surface layer, J. Geophys. Res., 99, 18545–18553, https://doi.org/10.1029/94JD00942, 1994.

Lenschow, D. H. and Raupach, M. R.: The attenuation of fluctuations in scalar concentrations through sampling tubes, J. Geophys. Res., 96, 15259–15268, https://doi.org/10.1029/91JD01437, 1991.

Leuning, R. and Judd, M. J.: The relative merits of open and closed-path analysers for measurement of eddy fluxes, Glob. Change Biol., 2, 241–253, https://doi.org/10.1111/j.13652486.1996.tb00076.x, 1996.

Leuning, R. and Moncrieff, J.: Eddy-covariance CO_2 flux measurements using open- and closed-path CO_2 analysers: Corrections for analysers water vapour sensitivity and damping of fluctuations in air sampling tubes, Bound.-Lay. Meteorol., 53, 63–76, https://doi.org/10.1007/BF00122463, 1990.

Liu, H., Peters, G., and Foken, T.: New equations for sonic temperature variance and buoyancy heat flux with an omnidirectional sonic anemometer, Bound.-Lay. Meteorol., 100, 459–468, https://doi.org/10.1023/A:1019207031397, 2001.

Mamadou, O., de la Motte, L. G., De Ligne, A., Heinisch, B., and Aubinet, M.: Sensitivity of the annual net ecosystem exchange to the cospectral model used for high frequency loss corrections at a grazed grassland site, Agr. Forest Meteorol., 228–229, 360–369, https://doi.org/10.1016/j.agrformet.2016.06.008, 2016.

Mammarella, I., Launiainen, S., Gronholm, T., Keronen, P., Pumpanen, J., Rannik, U., and Vesala, T.: Relative Humidity Effect on the High-Frequency Attenuation of Water Vapor Flux Measured by a Closed-Path Eddy Covariance System, J. Atmos. Ocean. Tech., 26, 1856–1866, https://doi.org/10.1175/2009JTECHA1179.1, 2009.

Marx, O., Brümmer, C., Ammann, C., Wolff, V., and Freibauer, A.: TRANC – a novel fast-response converter to measure total reactive atmospheric nitrogen, Atmos. Meas. Tech., 5, 1045–1057, https://doi.org/10.5194/amt-5-1045-2012, 2012.

Massman, W. J.: The attenuation of concentration fluctuations in turbulent flow through a tube, J. Geophys. Res., 96, 15269–15274, https://doi.org/10.1029/91JD01514, 1991.

Mauder, M. and Foken, T.: Documentation and instruction manual of the eddy covariance software package TK2, 26, Arbeitsergebnisse, Universität Bayreuth, Abt. Mikrometeorologie, Bayreuth, Germany, 2004.

Mauder, M. and Foken, T.: Impact of post-field data processing on eddy covariance flux estimates and energy balance closure, Meteorol. Z., 15, 597–609, https://doi.org/10.1127/09412948/2006/0167, 2006.

Min, K.-E., Pusede, S. E., Browne, E. C., LaFranchi, B. W., and Cohen, R. C.: Eddy covariance fluxes and vertical concentration gradient measurements of NO and NO_2 over a ponderosa pine ecosystem: observational evidence for within-canopy chemical removal of NO_x, Atmos. Chem. Phys., 14, 5495–5512, https://doi.org/10.5194/acp-14-5495-2014, 2014.

Moncrieff, J. B., Massheder, J. M., deBruin, H., Elbers, J., Friborg, T., Heusinkveld, B., Kabat, P., Scott, S., Soegaard, H., and Verhoef, A.: A system to measure surface fluxes of momentum, sensible heat, water vapour and carbon dioxide, J. Hydrol., 188, 589–611, https://doi.org/10.1016/S0022-1694(96)03194-0, 1997.

Moore, C. J.: Frequency response corrections for eddy correlation systems, Bound.-Lay. Meteorol., 37, 17–35, https://doi.org/10.1007/BF00122754, 1986.

Moravek, A., Singh, S., Pattey, E., Pelletier, L., and Murphy, J. G.: Measurements and quality control of ammonia eddy covariance fluxes: a new strategy for high-frequency attenuation correction, Atmos. Meas. Tech., 12, 6059–6078, https://doi.org/10.5194/amt-12-6059-2019, 2019.

Nakai, T., van der Molen, M. K., Gash, J. H. C., and Kodama, Y.: Correction of sonic anemometerangle of attack errors, Agr. Forest Meteorol., 136, 19–30, https://doi.org/10.1016/j.agrformet.2006.01.006, 2006.

Oncley, S. P., F. C. A., Larue, J. C., Businger, J. A., Itsweire, E. C., and Chang, S. S.: Surface-Layer Fluxes, Profiles, and Turbulence Measurements over Uniform Terrain under Near-Neutral Conditions, J. Atmos. Sci., 53, 1029–1044, https://doi.org/10.1175/15200469(1996)053<1029:SLFPAT>2.0.CO;2, 1996.

Polonik, P., Chan, W. S., Billesbach, D. P., Burba, G., Nottrott, A., Bogoev, I., Conrad, B., and Biraud, S. C.: Comparison of gas analyzers for eddy covariance: Effects of analyzer type and spectral corrections on fluxes, Agr. Forest Meteorol., 272–273, 128–142, https://doi.org/10.1016/j.agrformet.2019.02.010, 2019.

Rummel, U., Ammann, C., Gut, A., Meixner, F. X., and Andreae, M. O.: Eddy covariance measurements of nitric oxide flux within an Amazonian rain forest, J. Geophys. Res., 107, 8050, https://doi.org/10.1029/2001JD000520, 2002.

Sabbatini, S., Mammarella, I., Arriga, N., Fratini, G., Graf, A., Hörtnagel, L., Ibrom, A., Longdoz, B., Mauder, M., Merbold, L., Metzger, S., Montagnani, L., Pitacco, A., Rebmann, C., Sedlák, P., Sigut, L., Vitale, D., and Papale, D.: Eddy covariance raw data processing for CO_2 and energy fluxes calculation at ICOS ecosystem stations, Int. Agrophys., 32, 495–515, https://doi.org/10.1515/intag-2017-0043, 2018.

Spank, U. and Bernhofer, C.: Another Simple Method of Spectral Correction to Obtain Robust Eddy-Covariance Results, Bound.Lay. Meteorol., 128, 403–422, https://doi.org/10.1007/s10546008-9295-9, 2008.

Stella, P., Kortner, M., Ammann, C., Foken, T., Meixner, F. X., and Trebs, I.: Measurements of nitrogen oxides and ozone fluxes by eddy covariance at a meadow: evidence for an internal leaf resistance to NO_2, Biogeosciences, 10, 5997–6017, https://doi.org/10.5194/bg-10-5997-2013, 2013.

Su, H.-B., Schmid, H. P., Grimmond, C. S. B., Vogel, C. S., and Oliphant, A. J.: Spectral characteristics and correction of long-term eddy-covariance measurements over two mixed hardwood forests in non-flat terrain, Bound.-Lay. Meteorol., 110, 213–253, https://doi.org/10.1023/A:1026099523505, 2004.

Sutton, M. A., Tang, Y. S., Miners, B., and Fowler, D.: A New Diffusion Denuder System for Long-Term, Regional Monitoring of Atmospheric Ammonia and Ammonium, Water, Air and Soil Pollution: Focus, 1, 145–156, https://doi.org/10.1023/a:1013138601753, 2001.

Sutton, M. A., Howard, C. M., Erisman, J. W., Billen, G., Bleeker, A., Grennfelt, P., van Grinsven, H., and Grizzetti, B. (Eds.): The European Nitrogen Assessment: sources, effects and policy perspectives, Cambridge University Press, Cambridge, UK, 2011.

Tang, Y. S., Simmons, I., van Dijk, N., Di Marco, C., Nemitz, E., Dämmgen, U., Gilke, K., Djuricic, V., Vidic, S., Gliha, Z., Borovecki, D., Mitosinkova, M., Hanssen, J. E., Uggerud, T. H., Sanz, M. J., Sanz, P., Chorda, J. V., Flechard, C. R., Fauvel, Y., Ferm, M., Perrino, C., and Sutton, M. A.: European scale application of atmospheric reactive nitrogen measurements in a low-cost approach to infer dry deposition fluxes, Agr. Ecosyst. Environ., 133, 183–195, https://doi.org/10.1016/j.agee.2009.04.027, 2009.

Vickers, D. and Mahrt, L.: Quality Control and Flux Sampling Problems for Tower and Aircraft Data, J. Atmos. Ocean. Tech., 14, 512–526, https://doi.org/10.1175/15200426(1997)014<0512:QCAFSP>2.0.CO;2, 1997.

von Bobrutzki, K., Braban, C. F., Famulari, D., Jones, S. K., Blackall, T., Smith, T. E. L., Blom, M., Coe, H., Gallagher, M., Ghalaieny, M., McGillen, M. R., Percival, C. J., Whitehead, J. D., Ellis, R., Murphy, J., Mohacsi, A., Pogany, A., Junninen, H., Rantanen, S., Sutton, M. A., and Nemitz, E.: Field inter-comparison of eleven atmospheric ammonia measurement techniques, Atmos. Meas. Tech., 3, 91–112, https://doi.org/10.5194/amt-3-91-2010, 2010.

Wang, K., Wang, D., Zheng, X., and Nelson, D. D.: Applicability of a closed-path quantum cascade laser spectrometer for eddy covariance (EC) flux measurements of nitric oxide (NO) over a cropland during a low emission period, Agr. Forest Meteorol., 282–283, 107855, https://doi.org/10.1016/j.agrformet.2019.107855, 2020.

Wilczak, J. M., Oncley, S. P., and Stage, S. A.: Sonic Anemometer Tilt Correction Algorithms, Bound.-Lay. Meteorol., 99, 127– 150, https://doi.org/10.1023/A:1018966204465, 2001.

Wolfe, G. M., Kawa, S. R., Hanisco, T. F., Hannun, R. A., Newman, P. A., Swanson, A., Bailey, S., Barrick, J., Thornhill, K. L., Diskin, G., DiGangi, J., Nowak, J. B., Sorenson, C., Bland, G., Yungel, J. K., and Swenson, C. A.: The NASA Carbon Airborne Flux Experiment (CARAFE): instrumentation and methodology, Atmos. Meas. Tech., 11, 1757–1776, https://doi.org/10.5194/amt-11-1757-2018, 2018.

Zeller, K. F., Massman, W. J., Stocker, D. W., Fox, D. A., and Stedman, D. H.: Initial results from the Pawnee Eddy Correlation system for dry acid-deposition research, United States Department of Agriculture, Forest Service, Rocky Mountain Forest and Range Experiment Station Fort Collins, CO, Forest Service research paper, Report No., RM-282, 30 pp., 1988.

Zöll, U., Brümmer, C., Schrader, F., Ammann, C., Ibrom, A., Flechard, C. R., Nelson, D. D., Zahniser, M., and Kutsch, W. L.: Surface–atmosphere exchange of ammonia over peatland using QCL-based eddy-covariance measurements and inferential modeling, Atmos. Chem. Phys., 16, 11283–11299, https://doi.org/10.5194/acp-16-11283-2016, 2016.

Zöll, U., Lucas-Moffat, A. M., Wintjen, P., Schrader, F., Beudert, B., and Brümmer, C.: Is the biosphere-atmosphere exchange of total reactive nitrogen above forest driven by the same factors as carbon dioxide? An analysis using artificial neural networks, Atmos. Environ., 206, 108–118, https://doi.org/10.1016/j.atmosenv.2019.02.042, 2019.

3. Forest–Atmosphere exchange of reactive nitrogen in a remote region – Part I: Measuring temporal dynamics

Abstract. Long-term dry deposition flux measurements of reactive nitrogen based on the eddy covariance or the aerodynamic gradient method are scarce. Due to the large diversity of reactive nitrogen compounds and high technical requirements for the measuring devices, simultaneous measurements of individual reactive nitrogen compounds are not affordable. Hence, we examined the exchange patterns of total reactive nitrogen (ΣN_r) and determined annual dry deposition budgets based on measured data at a mixed forest exposed to low air pollution levels located in the Bavarian Forest National Park (NPBW), Germany. Flux measurements of ΣN_r were carried out with the Total Reactive Atmospheric Nitrogen Converter (TRANC) coupled to a chemiluminescence detector (CLD) for 2.5 years. The average ΣN_r concentration was 3.1 µg N m^{-3}. Denuder measurements with DELTA samplers and chemiluminescence measurements of nitrogen oxides (NO_x) have shown that NO_x has the highest contribution to ΣN_r (~ 51.4%), followed by ammonia (NH_3) (~ 20.0%), ammonium (NH_4^+) (~ 15.3%), nitrate NO_3^- (~ 7.0%), and nitric acid (HNO_3) (~ 6.3%). Only slight seasonal changes were found in the ΣN_r concentration level, whereas a seasonal pattern was observed for the contribution of NH_3 and NO_x. NH_3 showed highest contributions to ΣN_r in spring and summer, NO_x in autumn and winter. We observed deposition fluxes at the measurement site with median fluxes ranging from –15 to –5 ng N m^{-2} s^{-1} (negative fluxes indicate deposition). Median deposition velocities ranged from 0.2 to 0.5 cm s^{-1}. In general, highest deposition velocities were recorded during high solar radiation, in particular from May to September. Our results suggest that seasonal changes in composition of ΣN_r global radiation (R_g), and other drivers correlated with R_g were most likely influencing the deposition velocity (v_d). We found that from May to September higher temperatures, lower relative humidity and dry leaf surfaces increase v_d of ΣN_r. At the measurement site, ΣN_r concentration did not emerge as a driver of the ΣN_r v_d. No significant influence of temperature, humidity, friction velocity, or wind speed on ΣN_r fluxes when using the mean-diurnal variation (MDV) approach for filling gaps of up to 5 days was found. Remaining gaps were replaced by a monthly average of the specific half-hourly value From June 2016 to May 2017 and June 2017 to May 2018, we estimated dry deposition sums of 3.8 and 4.0 kg N ha^{-1} a^{-1}, respectively. Adding results from wet deposition measurements, we determined 12.2 and 10.9 kg N ha^{-1} a^{-1} as total nitrogen deposition in the 2 years of observation. This work encompasses (one of) the first long-term flux measurements of ΣN_r using novel measurements techniques for estimating annual nitrogen dry deposition to a remote forest ecosystem.

Published as: Wintjen, P., Schrader, F., Schaap, M., Beudert, B., and Brümmer, C.: Forest–atmosphere exchange of reactive nitrogen in a remote region – Part I: Measuring temporal dynamics, Biogeosciences, 19, 389–413, https://doi.org/10.5194/bg-19-389-2022, 2022.

3.1 Introduction

Reactive nitrogen (N_r) compounds are essential nutrients for plants However, an intensive supply of nitrogen by fertilization or atmospheric deposition is harmful for natural ecosystems and leads to a loss of biodiversity through soil acidification, eutrophication (Krupa, 2003; Galloway et al., 2003), and may also threaten human health by acting as precursors for ozone (O_3) and $PM_{2.5}$ (Erisman et al., 2013). Atmospheric nitrogen load increased significantly during the last century due to intensive crop production and livestock farming (Sutton et al., 2011, 2013; Flechard et al., 2011, 2013) (mainly through ammonia) and fossil fuel combustion by traffic and industry (mainly through nitrogen dioxide and nitric oxide). The additional amount of N_r enhances biosphere–atmosphere exchange of N_r (Flechard et al., 2011), affects plant health (Sutton et al., 2011) and influences the carbon sequestration of ecosystems such as forests (Magnani et al., 2007; Högberg, 2007; Sutton et al., 2008; Flechard et al., 2020), although the impact of increasing nitrogen deposition on forests carbon sequestration is still under investigation.

For estimating the biosphere–atmosphere exchange of N_r compounds such as nitrogen dioxide (NO_2), nitric oxide (NO), ammonia (NH_3), nitrous acid (HONO), nitric acid (HNO_3), and particulate ammonium (NH_4^+) and nitrate (NO_3^-), micrometeorological methods such as the eddy covariance (EC), and the aerodynamic gradient method (AGM) have proven their applicability on various ecosystems. The sum of these compounds is called total reactive nitrogen (ΣN_r) throughout this article. The EC method is the common method for estimating greenhouse gas fluxes (Aubinet et al., 1999; Baldocchi, 2003) in flux monitoring networks (FLUXNET Baldocchi et al., 2001, ICOS Heiskanen et al., 2021) and also suitable for measuring the exchange of N_r compounds. However, the EC method requires fast-response analyzers. For evaluating fluxes of NO and NO_2 the EC technique has been tested in earlier studies (Delany et al., 1986; Eugster and Hesterberg, 1996; Civerolo and Dickerson, 1998; Li et al., 1997; Rummel et al., 2002; Horii et al., 2004; Stella et al., 2013; Min et al., 2014). In recent years, progress has been made in EC measurements of NH_3 (Famulari et al., 2004; Whitehead et al., 2008; Ferrara et al., 2012; Zöll et al., 2016; Moravek et al., 2019). First attempts in applying EC had been made on HNO_3, organic nitrogen molecules, nitrate (NO_3^-), and ammonium aerosols (NH_4^+) (Farmer et al., 2006, 2011; Nemitz et al., 2008; Farmer and Cohen, 2008). Due to typically low concentrations, high reactivity, and water solubility, measuring fluxes of N_r compounds is still challenging since instruments need a low detection limit and a response time of < 1 s (Ammann et al., 2012). Thus, fast-response instruments for measuring N_r compounds like HNO_3 or NH_3 are equipped with a special inlet and short heated tubes to prevent interaction with tube walls (see Farmer et al., 2006; Zöll et al., 2016). However, these instruments need regular maintenance, have a high power consumption, and need a temperature-controlled environment for a stable performance. Considering the high technical requirements of these instruments, measuring fluxes of HNO_3 or NH_3 with these instrument is still challenging.

The Total Reactive Atmospheric Nitrogen Converter (TRANC) (Marx et al., 2012) converts all above mentioned N_r compounds to NO. In combination with a fast-response chemiluminescence detector (CLD), the system allows measurements of ΣN_r with a high sampling frequency. Due to a low detection limit and a response time of about 0.3 s, the TRANC-CLD system can be used for flux calculation based on the eddy-covariance (EC) technique. The key advantage of the TRANC is that only one device is needed for a quantification of the nitrogen dry deposition instead of running several instruments for each compound individually. The TRANC-CLD system has been shown to be suitable for EC measurements above a number of different ecosystems (see Ammann et al., 2012; Brümmer et al., 2013; Zöll et al., 2019; Wintjen et al., 2020).

Only a few long-term studies have been conducted to derive annual inputs with micrometeorological methods at (remote) forest ecosystems. Munger et al. (1996) conducted EC measurements of NO_y, which refers to the sum of all oxidized N_r compounds, e.g., NO_2, NO, HNO_3, dinitrogen pentoxide (N_2O_5), peroxyacyl nitrates (PAN), aerosol nitrates, above a mixed deciduous forest for 5 years. Averaged NO_x concentrations were at 0.62 and 4.26 ppb (0.36 and 2.44 µg N m^{-3}) during summer and winter,

respectively, if wind was blowing from the northwest. During southwesterly winds, mean NO_x concentrations were 1.25 and 9.48 ppb (0.72 and 5.43 µg N m^{-3}) during summer and winter, respectively, indicating a varying pollution climate. The authors reported an annual net dry deposition of NO_y covering 1990 to 1994 of 2.49 kg N ha^{-1} a^{-1}. Munger et al. (1998) reported an annual reactive N deposition of wet+dry deposition measurements of 6.4 kg N ha^{-1} a^{-1} for the period 1990 to 1996 at the same site. Dry deposition of NO_y contributed 34 % to total deposition. Wet deposition of NH_4^+ was comparatively low estimated to 1.1 kg N ha^{-1} a^{-1}. Neirynck et al. (2007) and Erisman et al. (1996) conducted AGM measurements in order to estimate dry deposition of NO_x and NH_3. Neirynck et al. (2007) published AGM measurements from July 1999 to November 2001 above mixed coniferous–deciduous forest, which was in close proximity of a highway and the city of Antwerp leading to mean NO_2 and NH_3 concentrations of 8.7 and 3.0 µg N m^{-3}, respectively. The authors determined an annual NH_3 dry deposition of 19.6 kg N ha^{-1} a^{-1} and NO_x emission of 2.7 kg N ha^{-1} a^{-1}. NO_x emissions were probably related to a strong contribution of soil-emitted NO. Erisman et al. (1996) reported NO_x and NH_3 fluxes above a Douglas fir stand of 2.5 ha surrounded by a larger forested area of 50 km^2 for 1995. Mean NH_3 concentration was 4.5 µg N m^{-3} possibly related to livestock farming in the surroundings of the site. They estimated annual dry depositions of 17.9 and 2.8 kg N ha^{-1} a^{-1} for NH_3 and NO_x, respectively. These long-term micrometeorological measurements of N_r species above forests were made more than 20 years ago, and no recent reports on long-term flux measurements of N_r are currently available. Since several N_r compounds contribute to ΣN_r each with different chemical and physical properties, a complex arrangement of different, highly specialized measurement devices would be needed for quantifying ΣN_r exchange. To our knowledge, there is no publication available reporting annual ΣN_r deposition at (remote) forest ecosystems using micrometeorological methods. As stated above, the outstanding benefit of the TRANC is that the most relevant N_r species are converted, and a single instrument is sufficient for deriving dry nitrogen deposition. During a measurement campaign instrumental performance issues and/or periods of insufficient turbulence arise, which require a quality flagging of processed fluxes. Afterwards, the resulting gaps in the measured time series need to be filled in order to properly estimate long-term deposition budgets. Known gap-filling strategies include the mean-diurnal-variation (MDV) method, look-up tables (LUTs), non-linear regression (NLR) (Falge et al., 2001), marginal distribution sampling (MDS) (Reichstein et al., 2005), and artificial neural networks (Moffat et al., 2007). However, most of these methods have in common that they were originally designed for carbon dioxide (CO_2) or other inert gases. MDS requires a short-term stability of fluxes and micrometeorological parameters. This condition is not necessarily fulfilled for ΣN_r and its components. Their exchange patterns are characterized by a higher variability for different timescales leading to a lower autocorrelation and non-stationarities in flux time series compared to inert gases like CO_2. It is, on the other hand, possible to use statistical methods like MDV or linear interpolation to fill short gaps in flux time series. This was done by Brümmer et al. (2013), but filling long gaps with this technique is not recommended. Since exchange patterns of ΣN_r can substantially vary each day depending on the composition of ΣN_r and micrometeorology, it is questionable if statistical methods are suitable for ΣN_r considering the high reactivity and chemical properties of its compounds.

Our study is the first one presenting long-term EC flux measurements of ΣN_r above a remote forest. Based on the successful implementation of the TRANC methodology, our objectives are the following:

1. a discussion of observed concentration and flux patterns of ΣN_r in the context of different temporal scales
2. an investigation of the influence of micrometeorology on deposition velocities
3. an assessment of annual N deposition using both gap-filling for the dry deposition eddy flux data and complementary wet-deposition estimates from local samplers.

A companion paper will investigate the usage of the acquired dataset in a modeling framework to estimate annual N budgets.

3.2 Materials and Methods

3.2.1 Site and meteorological conditions

Measurements were made in the Bavarian Forest National Park (NPBW) (48°56' N, 13°25' E; 807 m a.s.l.) in southeast Germany. The unmanaged site is located in the Forellenbach catchment (~ 0.69 km^2 Beudert and Breit, 2010) is surrounded by a natural, mixed forest and is about 3km away from the Czech border. Due to the absence of emission sources of N_r in the surroundings of the measurement site, mean annual concentrations of NO_2 (2.1–4.8 ppb (1.2–2.8 µg N m^{-3})), NO (0.4–1.6 ppb (0.2–0.9 µg N m^{-3})), and NH_3 (1.4 ppb (0.8 µg N m^{-3})) are low (Beudert and Breit, 2010). The site is characterized by low annual temperatures (6.1°C) and high annual precipitation (1327 mm) measured at 945 m a.s.l. Annual temperature in 2016, 2017, and 2018 was 6.8, 6.9, and 8.0°C, and precipitation was 1208, 1345, and 1114 mm, respectively. There are no industries or power plants nearby, only small villages with moderate animal housing and farming (Beudert et al., 2018). Due to these site characteristics, measurements of the ΣN_r background deposition are possible. For monitoring air quality and micrometeorology a 50 m tower was installed in the 1980s. Measurements of ozone, sulfur dioxide, and NO_x, the sum of NO and NO_2, have been conducted since 1990 (Beudert and Breit, 2010). The Forellenbach site is part of the International Cooperative Program on Integrated Monitoring of Air pollution Effects on Ecosystems (ICP IM) within the framework of the Geneva Convention on Long-Range Transboundary Air Pollution (UNECE, 2021) and belongs to the Long Term Ecological Research (LTER) network (LTER, 2021). The Federal Environment Agency (UBA) and NPBW Administration have been carrying out this monitoring program in the Forellenbach catchment. The flux footprint consists of Norway spruce (*Picea abies*) and European beech (*Fagus sylvatica*) covering approximately 80 % and 20 % of the footprint, respectively (Zöll et al., 2019). During the study period, maximum stand height was less than 20m since the dominating Norway spruce is recovering from a complete dieback by bark beetle in the mid-1990s and 2000s (Beudert and Breit, 2014).

3.2.2 Experimental setup

Flux measurements of ΣN_r were made from January 2016 until end of June 2018 at a height of 30 m above ground. A custom-built ΣN_r converter (Total Reactive Atmospheric Nitrogen Converter, TRANC) after Marx et al. (2012) and a 3-D ultrasonic anemometer (GILL-R3, Gill Instruments, Lymington, UK) were attached on different booms close to each other at 30 m height. The horizontal and vertical sensor separations were 32 and 20 cm, respectively (Wintjen et al., 2020). The TRANC was connected via a 45 m opaque PTFE tube to a fast-response chemiluminescence detector (CLD 780 TR, ECO PHYSICS AG, Dürnten, Switzerland), which was housed in an air-conditioned box at the bottom of the tower. The CLD was coupled to a dry vacuum scroll pump (BOC Edwards XDS10, Sussex, UK), which was placed at ground level, too. The inlet of the TRANC is designed after Marx et al. (2012) and Ammann et al. (2012). The conversion of ΣN_r to NO is split in two steps. First, a thermal conversion occurs in an iron–nickel–chrome tube at 870°C leading to a split-up of NH_4^+ and NO_3^- aerosols such as ammonium sulfate, ammonium nitrate, sodium, and calcium nitrate into their subcomponents. In case of NH_4NO_3, it is thermally converted to NH_3 and HNO_3 (Marx et al., 2012). The latter is split up into to NO_2, H_2O, and O_2. NH_3 is oxidized by O_2 at a platinum gauze to NO. HONO is split up to NO and a hydroxyl radical (OH). In a second step, a gold tube passively heated to 300°C catalytically converts the remaining oxidized N_r species to NO. In this process, carbon monoxide (CO) is acting as a reducing agent. More details about the chemical conversion steps can be found in Marx et al. (2012). A critical orifice was mounted at the TRANC's outlet and restricted the mass flow to 2.1 L min^{-1} after the critical orifice assuring low pressure along the tube. The pressure gradient from the critical orifice to the CLD was not measured. Thus, only assumptions about the turbulent flow regime can be made. Considering tube length

and lag time minus residence time in the converter, the latter assumed to 2 s at maximum due to tube length and platinum mesh as an additional flow resistance, flow speed was at 2.7 m s^{-1} at maximum. Using an inner diameter of 4.4 mm and a kinematic viscosity at 15°C (1.485×10^{-5} m^2 s^{-1}), we calculated a Reynolds number of 800 indicating an overall laminar flow. We cannot provide a reasonable explanation to the low Reynolds number since pressure gradient was not measured. Generally, the flow type inside the tube affects high-frequency attenuation (Massman, 1991; Lenshow and Raupach, 1991; Moncrieff et al., 1997). High-frequency attenuation was corrected with an empirical method based fully on measured cospectra (Wintjen et al., 2020). Since an empirical approach was used to estimate the high-frequency damping, effects originating from the low Reynolds number and from physical and chemical processes occurred after the critical orifice were considered in the flux analysis.

The conversion efficiency of the TRANC had been investigated by Marx et al. (2012). They found 99 % for NO_2, 95 % for NH_3, and 97 % for a gas mixture of NO_2 and NH_3. Conversion efficiencies for sodium nitrate ($NaNO_3$), ammonium nitrate (NH_4NO_3), and ammonium sulfate ($(NH_4)_2SO_4$) were 78 %, 142 %, and 91 %, respectively. Overall, the results indicate that the TRANC is able to convert aerosols and gases efficiently to NO. For further details we refer to the publication of Marx et al. (2012).

For investigating the local meteorology, air temperature and relative humidity sensors (HC2S3, Campbell Scientific, Logan, Utah, USA) were mounted at four different heights (10, 20, 40, and 50 m above ground). At the same levels, wind propeller anemometers (R.M. Young, Wind Monitor Model 05103VM-45, Traverse City, Michigan, USA) were mounted on booms. Leaf wetness sensors designed after the shape of a leaf (Decagon, LWS, n = 6, Pullman, Washington, USA) were attached to branches of a spruce and a beech tree near the tower. Sensors of the beech tree were at heights of approximately 2.1, 5.6, and 6.1 m; sensors of the spruce tree were at heights of 2.1, 4.6, and 6.9 m. These measurements started in April 2016. Due to a wetting of the sensor's surface, the electric conductivity of the material changes. This signal, the leaf wetness, was converted by the instrument to dimensionless counts. Based on the number and range of counts, different wetness states could be defined. Half-hourly leaf wetness values were in the range from 0 to 270. In this study, we defined the wetness states "dry" and "wet". The condition wet can be induced by the accumulation of hygroscopic particles extending the duration of the wetness state or water droplets. In order to classify a leaf as dry or wet, we determined a threshold value based on the medians of leaf wetness values. During daylight (global radiation > 20 W m^{-2}), medians ranged from 1.1 to 2.0 and were between 4.1 and 9.4 during nighttime. During nighttime, medians are higher due to dew formation. According to the values determined during daylight, we set the threshold value to 1.5 for all sensors. If the leaf wetness value was lower than 1.5, the leaf was considered as dry. Otherwise, the leaf surface was considered wet. To take differences between the sensors into account, all sensors were used to derive a common wetness Boolean. Therefore, the number of dry sensors was counted for each half-hour: if at least three sensors were considered dry, the corresponding half-hour was considered mostly dry. A cleaning of sensors was not conducted because contamination effects could be corrected by implemented algorithms. The derived wetness Boolean was used in the analysis of deposition velocities (Sect. 3.3.3).

Ambient NH_3 was collected by passive samplers at ground level (1.5), 10, 20, 30, and 50 m from January 2016 to June 2018. Measurements at 40 m started in July 2016. The collector at ground level was moved to 40 m. Passive samplers of the IVL type (Ferm, 1991) were used for NH_3, and the exposure duration was approximately one month at a time. DELTA measurements (DEnuder for Long-Term Atmospheric sampling e.g., Sutton et al., 2001; Tang et al., 2009) of NH_3, HNO_3, SO_2, NO_3^-, and NH_4^+ were taken at the 30 m platform. The DELTA measurements had the same sampling duration as the passive samplers. The denuder preparation and subsequent analyzing of the samples was identical to the procedure for KAPS denuders (Kananaskis Atmospheric Pollutant Sampler, Peake, 1985; Peake and Legge, 1987) given in Dämmgen et al. (2010) and Hurkuck et al. (2014). Basic denuders were coated with sodium carbonate to collect HNO_3, SO_2, and HCl. Citric acid was applied to acid denuders for removing NH_3. Two cellulose filter papers (Whatman No. 1, 25 mm diameter) were used for collecting aerosols. The first filter was prepared with potassium carbonate in glycerol, the second filter with citric acid. During

operation, we controlled the pump to keep flow at a constant level and checked the pipes for contamination effects before analyzing. Blank values were used as additional quality control.

Additionally, fast-response measurements of NH_3 were performed with a NH_3 quantum cascade laser (QCL) (model mini QC-TILDAS-76 from Aerodyne Research, Inc. (ARI, Billerica, MA, USA)) at 30 m height. The setup of the QCL was the same as described in Zöll et al. (2016). In contrast to Zöll et al. (2016), we were not able to calculate NH_3 fluxes with the QCL using the EC method (see Sect. 3.2.3). Further details about the location and specifications of the installed instruments can be found in Zöll et al. (2019) and Wintjen et al. (2020).

At the top of the tower (50 m platform), measurements of NO_2 and NO were conducted by the NPBW using a chemiluminescence detector (APNA-360, HORIBA, Tokyo, Japan). The instrument was equipped with a thermal NO_x converter resulting in cross-sensitivity to higher oxidized nitrogen compounds. Measurements of global radiation and atmospheric pressure were also conducted at 50 m. Above the canopy, the concentration gradients of NO_2 and NO were probably not significant. Seok et al. (2013) found highest NO_x concentrations above the canopy, but concentration gradients were negligible at this height. Since both measurement heights were above the canopy, no correction was applied to NO_2 and NO concentration measurements. Precipitation was measured at a location in 1 km southwest distance from the tower according to WMO (World Meteorological Organization) guidelines (Jarraud, 2008). Wet deposition was collected as bulk and wet-only samples in weekly intervals in close vicinity to the tower using four samplers, three bulk samplers and one wet-only sampler, at an open site. A detailed description of the wet deposition measurements is given as Supplement A3.1.

3.2.3 Flux calculation and post-processing

The software package EddyMeas, included in EddySoft (Kolle and Rebmann, 2007), was used to record the data with a time resolution of 10 Hz. Analog signals from CLD, LI7500, and the sonic anemometer were collected at the interface of the anemometer and joined to a common data stream. Flux determination covered the period from 1 January 2016 to 30 June 2018. Half-hourly fluxes were calculated by the software EddyPro 7.0.4 (LI-COR Biosciences, 2019). For flux calculation a 2-D coordinate rotation of the wind vector was selected (Wilczak et al., 2001), spikes were detected and removed from time series after Vickers and Mahrt (1997), and block averaging was applied. Due to the distance from the TRANC inlet to the CLD, a time lag between concentration and sonic data was inevitable. The covariance maximization method allows the estimation of the time lag via shifting the time series of vertical wind and concentration against each other until the covariance is maximized (Aubinet et al., 2012; Burba, 2013). The time lag was found to be approximately 20 s (see Fig. S3.1 in the Supplement). We instructed EddyPro to compute the time lag after covariance maximization with default setting while using 20 s as a default value and set the range from 15 to 25 s (for details see Wintjen et al., 2020). For correcting flux losses in the high-frequency range we used an empirical method suggested by Wintjen et al. (2020), which uses measured cospectra of sensible heat (Co(w,T)) and ΣN_r flux (Co(w, ΣN_r)) and an empirical transfer function. We followed their findings and used medians of the damping factors calculated for correcting calculated fluxes since the chemical composition of ΣN_r exhibits seasonal differences (see Fig. 3 and Brümmer et al., 2013). Each damping factor (median) refers to a period of 2 months. On average, the damping factor was 0.78, which corresponds to flux loss of 22 % (Wintjen et al., 2020). The authors determined flux loss factors for two different ecosystems, which are different, for example, in the composition of ΣN_r. They assumed that the differences in flux losses are also related to the chemical composition of ΣN_r. The low-frequency flux loss correction was done with the method of Moncrieff et al. (2004), and the random flux error was calculated after Finkelstein and Sims (2001).

Previous measurements with the same CLD model by Ammann et al. (2012) and Brümmer et al. (2013) revealed that the device is affected by ambient water vapor due to quantum mechanical quenching.

Excited NO_2 molecules can reach ground state without emitting a photon by colliding with a H_2O molecule; thereby no photon is detected by the photo cell. It results in a sensitivity reduction of 0.19 % per 1 mmol mol^{-1} water vapor increase. Thus, calculated fluxes were corrected after the approach by Ammann et al. (2012) and Brümmer et al. (2013) using the following equation:

$$F_{\mathrm{NO,int}} = -0.0019 \cdot c_{\Sigma \mathrm{N_r}} \cdot F_{\mathrm{H_2O}} \quad (3.1)$$

The NO interference flux $F_{\mathrm{NO,int}}$ has to be added to every estimated flux value. $c_{\Sigma \mathrm{N_r}}$ is the measured concentration of the CLD and $F_{\mathrm{H_2O}}$ the estimated H_2O flux from the LI-7500 eddy-covariance system. The correction contributed approximately 132 g N ha^{-1} to 2 years of TRANC flux measurements if the mean-diurnal-variation (MDV) approach was used as a gap-filling approach. Half-hourly interference fluxes were between –3 and +0.3 ng N m^{-2} s^{-1}. Their random flux uncertainty ranged between 0.0 and 0.5 ng N m^{-2} s^{-1}. Since we measured H_2O fluxes with an open-path system and used them for correcting ΣN_r fluxes, density corrections following the Webb–Pearman–Leuning correction for H_2O fluxes measured with closed-path systems (Ibrom et al., 2007) were not accounted for. The impact on the correction is likely small, but the determined interference flux correction should be seen as an upper estimate.

After flux calculation, we applied different criteria to identify low-quality fluxes. We removed fluxes, which were outside the predefined flux range of –520 to 420 ng N m^{-2} s^{-1} (I), discarded periods with insufficient turbulence ($u_* < 0.1$ m s^{-1}) (see Zöll et al., 2019) (II), and fluxes with a quality flag of "2" (Mauder and Foken, 2006) (III). In order to avoid uncertainties due to the washout process as it introduces an additional sink below the measurement height leading to a height dependent flux, we applied a precipitation filter on ΣN_r flux measurements (IV). These criteria ensure the quality of the fluxes but lead to systematic data gaps in flux time series. Flux data with applied u_* filter were used for investigating the flux pattern of ΣN_r. Figures 3.4, 3.5, 3.7, S3.5, S3.6, S3.9, S3.10, S3.12, and S3.13 in the Supplement, and associated descriptions are based on this flux dataset. Instrumental performance problems led to further gaps in the time series. Most of them were related to maintaining and repairing of the TRANC and/or CLD, for example, heating and pump issues, broken tubes, empty O_2 gas tanks (O_2 is required for CLD operation), power failure, or a reduced sensitivity of the CLD. The reduction in sensitivity may be caused by reduced pump performance leading to an increase in sample cell pressure. If pressure in the sampling cell is outside the regular operating range, low pressure conditions needed for the detection of photons emitted by excited NO_2 molecules may not hold. We checked the pressure in the sample cell of the CLD during each, at least monthly, site visit. If the sample cell pressure was outside the allowed range, tip seals of the pump were replaced. The sensitivity of the CLD could also be reduced by changes in the O_2 supply from gas tanks to ambient, dried box air if O_2 gas tanks were empty. Issues in the air-conditioning system of the box could also affect the sensitivity of the CLD. An influence of aging on the inlet, tubes, and filters may also affect the measurements. In order to minimize an impact on the measurements, half-hourly raw concentrations were carefully checked for irregularities like spikes or drop-outs by visual screening. Considering the time period of ongoing measurements from the beginning of January 2016 till June 2018, the quality flagging resulted in 58.6 % missing data. The loss in flux data is higher than values reported by Brümmer et al. (2013). They reported a flux loss of 24 % caused by u_* filtering. In this study, the same u_* threshold caused a flux loss of approximately 15.5 %. A total of 32.7 % data loss from January 2016 to June 2018 was caused by instrumental performance problems showing that TRANC-CLD system was overall operating moderately stable. For gap-filling we applied the MDV approach to gaps in the ΣN_r flux time series. The window for filling each gap was set to ±5 d. Remaining, long-term gaps were filled by a monthly average of the specific half-hour value estimated from non-gap-filled fluxes (Fig. 3.5) in order to estimate ΣN_r dry-deposition sums from June 2016 to May 2017 and from June 2017 to May 2018. Uncertainties of the gap-filled fluxes are estimated by the standard error of the mean.

Hereafter, we named this MDV approach "original" (OMDV). To examine the impact of the u_* filter as it may remove preferentially smaller fluxes occurring at low turbulent conditions, we compared dry deposition sums calculated with and without u_* filter while using OMDV. On both datasets, flux filters (I), (III), and (IV) were applied (see Fig. 3.8 and associated text). Seasonal and annual ΣN_r dry depositions shown in Table 3.1 refer to flux data with u_* filter and were calculated by using OMDV.

In addition to u_*, other micrometeorological parameters may also bias annual dry deposition. Therefore, we examined the impact of temperature, relative humidity, and wind speed on the dry deposition sums of ΣN_r compared to the dry deposition when using OMDV as a gap-filling approach. We named this gap-filling approach as "conditional" MDV (CMDV) and applied it to flux data with and without u_* filter. For CMDV, we considered only fluxes in the time frame of ±5 d, at which temperature agreed within ±3°C, relative humidity by ±5 %, or wind speed by ±1.5 m s^{-1}. Remaining, long-term gaps were treated similarly to OMDV.

As outlined in Sect. 3.2.2, measurements of NH_3 were made with a QCL at high temporal resolution. In combination with the sonic anemometer, it gives the opportunity to determine NH_3 fluxes and to further investigate the non-NH_3 component of the ΣN_r flux. However, a calculation of the NH_3 fluxes with the EC method was not possible in this study. No consistent NH_3 time lag was found making flux evaluation impossible. Due to regular pump maintenance, cleaning of the inlet and absorption cell, issues related to the setup of the QCL were unlikely to be the cause. We suppose that the variability in the measured NH_3 concentrations was not sufficiently detectable by the instrument. Significant short-term variability in the ΣN_r raw concentrations was not found in the NH_3 signal even in spring or summer. Thus, no robust time lag estimation could be applied to the vertical wind component of the sonic anemometer and the NH_3 concentration. Recently, Ferrara et al. (2021) found large uncertainties for low NH_3 fluxes measured with the same QCL model. Cross-covariance functions had a low signal-to-noise ratio, indicating that most of the fluxes were close to the detection limit.

3.2.4 Determining deposition velocity of ΣN_r from measurements

In surface–atmosphere exchange models of N_r species like NO_2, NO, NH_3, HNO_3, or related aerosol compounds, the flux (F_t) is calculated by multiplying concentrations of a trace gas modeled or measured at a reference height ($\chi_a(z-d)$) with a so-called deposition velocity ($v_d(z-d)$), where z is measurement height and d the zero-plane displacement height (van Zanten et al., 2010). The deposition velocity can be described by an electrical analogy and is defined as the inverse of the sum of three resistances (Wesely, 1989; Erisman and Wyers, 1993). According to its definition a positive v_d indicates deposition, a negative v_d emission. Note that, strictly speaking, for bidirectional exchange v_d needs to be interpreted as an "exchange velocity"; i.e., it can technically become negative during emission phases. Equations are the same as for v_d (van Zanten et al., 2010).

$$F_t = -v_d \cdot \chi_a(z-d) \text{ with } v_d = (R_a(z-d) + R_b + R_c)^{-1} \quad (3.2)$$

R_a is the aerodynamic resistance, R_b is the quasi-laminar boundary layer resistance, and R_c is the canopy resistance. R_a is influenced by turbulent characteristics (Paulson, 1970; Webb, 1970; Garland, 1977), and R_b (Jensen and Hummelshøj, 1995, 1997) depends on surface characteristics and chemical properties of the gas or particle of interest. Both have in common that they are proportional to the inverse of u_*. R_c consists of several parallel connected resistances describing the exchange with the vegetated surface (van Zanten et al., 2010).

3.3 Results

3.3.1 Measured concentrations of ΣN_r and individual N_r compounds

Figure 3.1 shows ambient concentrations of ΣN_r (black), NH_3 (red), and NO_x (blue) as half-hourly averages for the entire measurement campaign. Data gaps were related to instrumental performance problems. No ΣN_r measurements were possible until end of May 2016 due to heating problems of the TRANC. The contribution of individual compounds to the ΣN_r concentration pattern is shown in Fig. 3.2, which illustrates a comparison of ΣN_r concentrations with DELTA denuder and NO_x measurements on a monthly basis.

ΣN_r concentrations exhibited highest values during the winter months. For example, values were higher than 10 µg N m^{-3} during January 2017 and February 2018. NO_x also showed a relatively high concentration level during winter. During spring and summer, NO_x values were lower

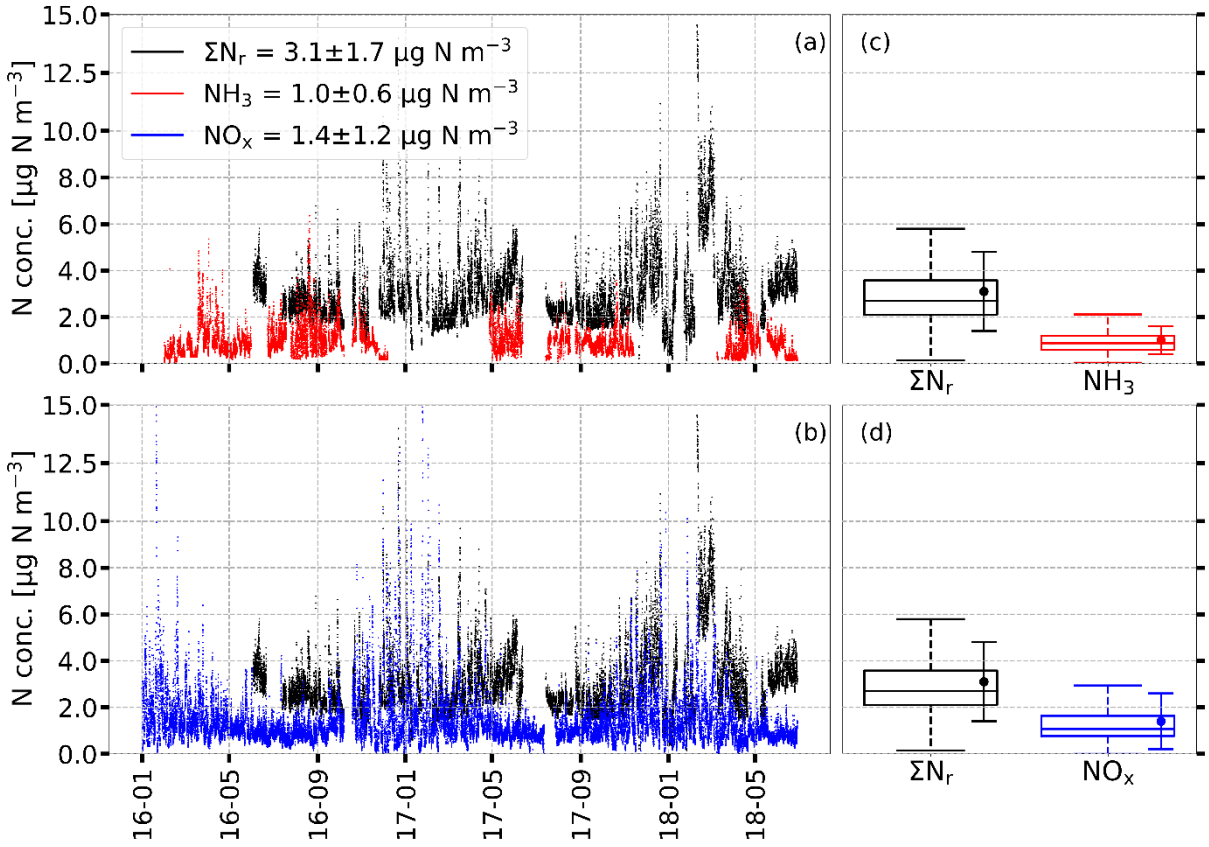

Figure 3.1: Half-hourly averaged concentrations of ΣN_r (black), NH_3 (red), and NO_x (blue) in µg N m^{-3} from 1 January 2016 to 30 June 2018 displayed in (a, b). Box plots (box frame = 25 % to 75 % interquartile range (IQR), bold line=median, whisker = 1.5 · IQR) with average values (dots) shown in (c, d) refer to the entire campaign. Error bars represent 1 standard deviation. Y axis is capped at 15 µg N m^{-3}.

than 2 µg N m^{-3}, and hence their contribution to ΣN_r decreased. However, ΣN_r values remained around 3 µg N m^{-3} and reached values of up to 6 µg N m^{-3}, which was related to higher NH_3 concentrations during these periods. The ΣN_r concentration was 3.1 µg N m^{-3} on average, NH_3 was 1.0 µg N m^{-3}, and NO_x was 1.4 µg N m^{-3} on average with the latter values being in agreement with concentrations reported by Beudert and Breit (2010). Averaged NH_3 concentrations of the QCL agreed well with NH_3 from passive samplers and DELTA measurements (Fig. S3.2 in the Supplement). Overall, the agreement in the annual pattern was reasonable, but a bias between the QCL and the diffusion samplers was found. From passive sampler measurements, an increase in the NH_3 concentration with measurement height was observed. At 10 m (in the canopy), the lowest NH_3 concentrations were measured. No systematic

difference was found between 20 and 30 m. At 50 m, the NH_3 concentration exceeded that at 30 m by 0.1 µg N m^{-3}. During winter, the difference in measurement heights diminished.

The seasonal variations of the half-hourly ΣN_r concentrations are represented by box-and-whisker plots including monthly medians in Fig. S3.3 in the Supplement. In general, median concentrations were comparable for the entire campaign with slight differences between the years. Medians ranged between 2 and 3.5 µg N m^{-3}. From July to September, concentrations were slightly higher in 2016 than in 2017. During this period, interquartile ranges (IQRs) and whiskers were the smallest for the entire year showing less variability in ΣN_r concentrations. In spring and winter, median concentrations were higher, and concentrations covered a wider range compared to the summer months. Figure S3.4 in the Supplement shows the corresponding diurnal patterns for each month. During the entire day, ΣN_r concentrations exhibited variations of less than 1 µg N m^{-3}. If concentrations were averaged for each season (not shown), higher concentrations were observed from 09:00 to 15:00 LT and lower values during the night.

Figure 3.2 shows absolute concentrations of individually measured N_r compounds as stacked bars and ΣN_r from the TRANC from January 2016 to June 2018. TRANC and NO_x measurements were averaged to exposure periods of DELTA measurements. DELTA measurements recorded at an insufficient pump flow were excluded from the analysis. Missing NH_3 values in the DELTA time series were filled by NH_3 data determined from the passive sampler mounted at 30 m. Remaining data gaps in the DELTA time series of NH_3, HNO_3, NH_4^+, and NO_3^- were replaced by monthly averages from other years.

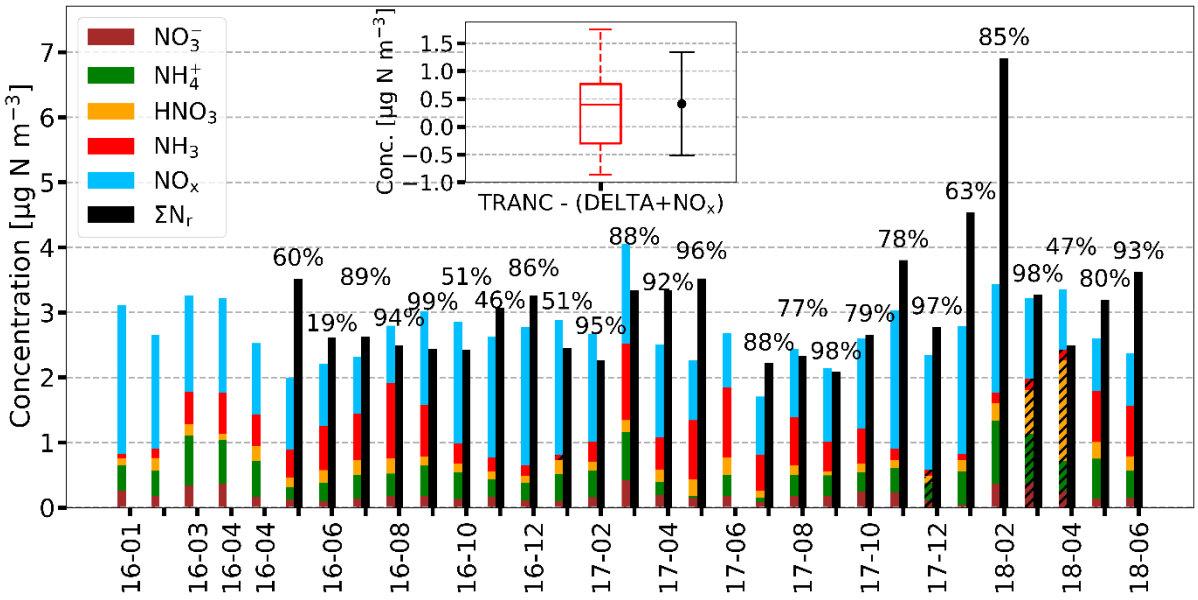

Figure 3.2: Monthly stacked concentration of TRANC, DELTA, and NO_x in µg N m^{-3} for the entire measurement campaign. Missing NH_3 values from the DELTA measurements caused by a low pump flow were filled with passive sampler values from 30 m. This procedure was done for December 2016 and 2017, March 2018, and April 2018. Remaining gaps in the time series of HNO_3, NH_4^+, and NO_3^- were replaced by monthly averages estimated from other years if possible. In the case of NH_3, the procedure was applied to January 2017. For the other compounds, the gap-filling was done for December 2017, March 2018, and April 2018. Gap-filled bars are hatched. NO_x and ΣN_r were averaged to the exposure periods of the DELTA samplers. Numbers above the bars indicate the relative coverage of TRANC measurements during each exposure period.

The comparison of the TRANC with DELTA+NO_x revealed overestimations by the latter from August 2016 to October 2016 and from January to March 2017. On average, an underestimation by DELTA+NO_x of approximately 0.41 µg N m^{-3} with a standard deviation of 0.93 µg N m^{-3} was observed. The median value was about 0.4 µg N m^{-3}.

HNO_3, NH_4^+, and NO_3^- concentrations were nearly equal through the entire measurement campaign. Seasonal differences existed mainly for NH_3 and NO_x. We measured average concentrations of 0.55,

0.17, 0.42, 0.19, and 1.40 µg N m^{-3} for NH_3, HNO_3, NH_4^+, NO_3^-, and NO_x for the entire campaign, respectively. On average, the relative contribution of NH_3, HNO_3, NH_4^+, and NO_3^- to ΣN_r was less than 50 % for the entire measurement campaign as visualized by Fig. 3.3. We further observed a low particle contribution to the ΣN_r concentrations (~ 22 % on average) showing that the ΣN_r concentration pattern was significantly influenced by gaseous N_r compounds.

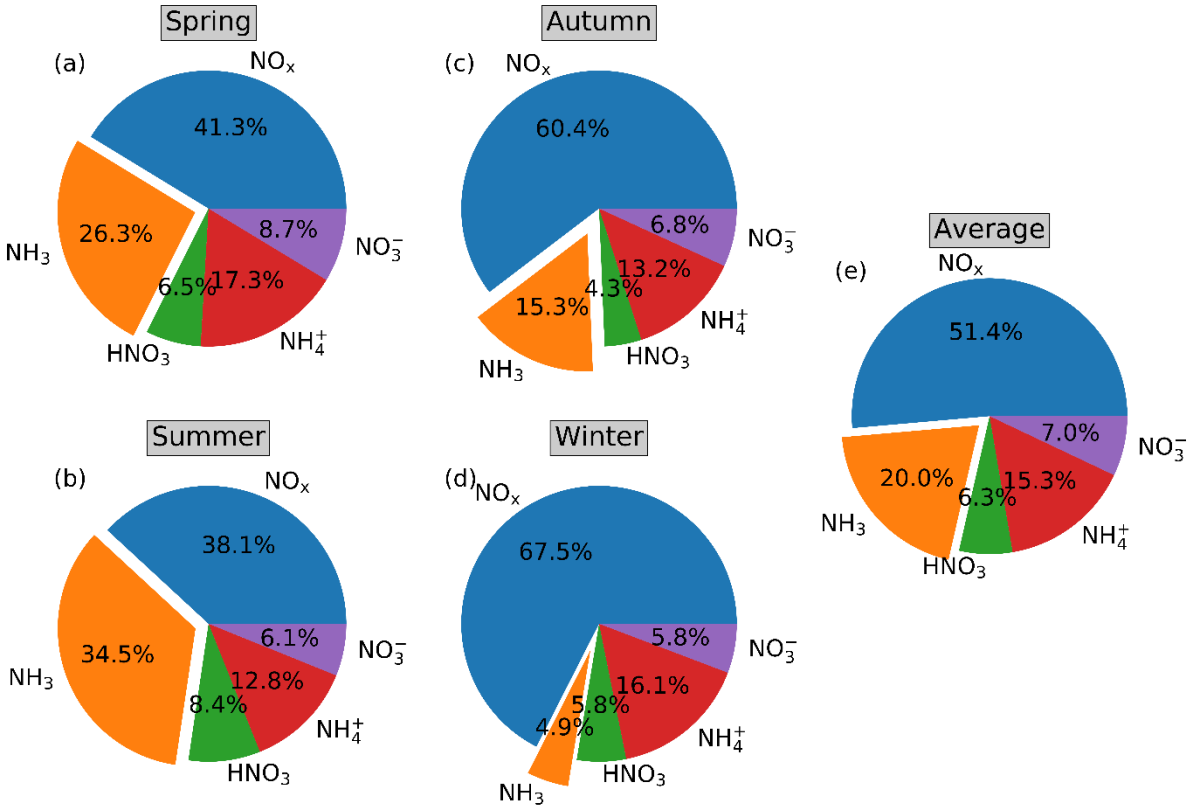

Figure 3.3: Pie charts showing the relative contribution of concentrations for NO_x, NH_3, NO_3^-, NH_4^+, and HNO_3 to ΣN_r based on DELTA samplers and NO_x measurements for different seasons of the year. NO_x measurements are averaged to exposure periods of the DELTA samplers. Panels (a)–(d) refer to spring, summer, autumn, and winter, respectively. Panel (e) shows the average relative contribution to ΣN_r for the entire measurement period.

In general, NO_x showed the highest contribution to ΣN_r and followed seasonal changes with highest values during winter and lowest values in summer. NH_3 also featured seasonal variations with concentrations lowest in winter and highest values in spring and summer. Seasonal contributions of HNO_3 varied by less than 2 % compared to the average.

The highest relative contribution of HNO_3 was found for summer. NO_3^- and NH_4^+ exhibited highest values for spring. The excess of NH_4^+ over NO_3^- is obvious. Similar to HNO_3, the seasonal contribution of NH_4^+ and NO_3^- deviated only by ±2 % from their averages. Only small seasonal changes in the overall ΣN_r concentration were observed. As shown in Fig. 3.2, ΣN_r concentrations were between 2 and 4.5 µg N m^{-3} excluding February 2018. We measured 3.3, 2.6, 2.5, and 3.0 µg N m^{-3} with the TRANC system for spring, summer, autumn, and winter, respectively.

3.3.2 Measured exchange fluxes and deposition velocities of ΣN_r

Figure 3.4 shows the non-gap-filled ΣN_r fluxes depicted as box plots on a monthly timescale. The convention is as follows: negative fluxes represent deposition, positive fluxes emission.

Except for February 2018, all ΣN_r flux medians were between –15 and –5 ng N m^{-2} s^{-1}, indicating that deposition of ΣN_r predominated at our measurement site. Quality-assured half-hourly fluxes showed 80 % deposition and 20 % emission fluxes. On a half-hourly basis, fluxes were in the range from –516 to 399 ng N m^{-2} s^{-1}. On a monthly basis, random flux error medians were between 3 and 6 ng N m^{-2} s^{-1}. According to Langford et al. (2015), the limit of detection (LOD) is calculated by multiplying the random flux error (95 % confidence limit) with 1.96. The comparison of half-hourly fluxes with their individual LOD revealed that 79 % of the measured fluxes were above their detection limits. Deposition fluxes contributed with 84 % to fluxes above the LOD. The fraction of emission was estimated to 16 %. The relative contribution of emission fluxes to measured fluxes decreased under the consideration of the LOD. This indicates that emission fluxes were closer to the flux detection limit of the instrument.

In general, median deposition was within the same range for the entire campaign with only small seasonal differences. For instance, median deposition was higher during spring and summer than during winter for 2016. However, median deposition during winter 2017 was comparable to median deposition in summer 2017. Median deposition was significantly increased from June 2016 till September 2016 compared to the same period in 2017, and IQR and whiskers also covered a wider range in 2016. The pattern changed for the time period from October to December. In December 2017, the IQR expanded in the positive range indicating emission events for a significant time period. The largest median deposition with 25 ng N m^{-2} s^{-1} and the widest range in IQR reaching approximately –80 ng N m^{-2} s^{-1} were registered in February 2018, indicating strong deposition phases during that month with sporadic emission events. Such phenomena were not observed in the years before. In the following month, the deposition was higher from March to April 2017 than for the same period in 2018. Figure 3.5 shows averaged diurnal cycles of measured ΣN_r fluxes for every month.

In general, the ΣN_r diurnal cycle exhibited low deposition or fluxes close to zero during nighttime/evening and increasing deposition during daytime. Deposition fluxes were similar during the night for the entire campaign except for February 2018. Maximum deposition was reached between 09:00 and 15:00 LT. Deposition is enhanced from May until September showing fluxes between –40 and –20 ng N m^{-2} s^{-1}. From October to November and from December to February, the diurnal cycle weakened with near-zero or small negative fluxes, which were lower than

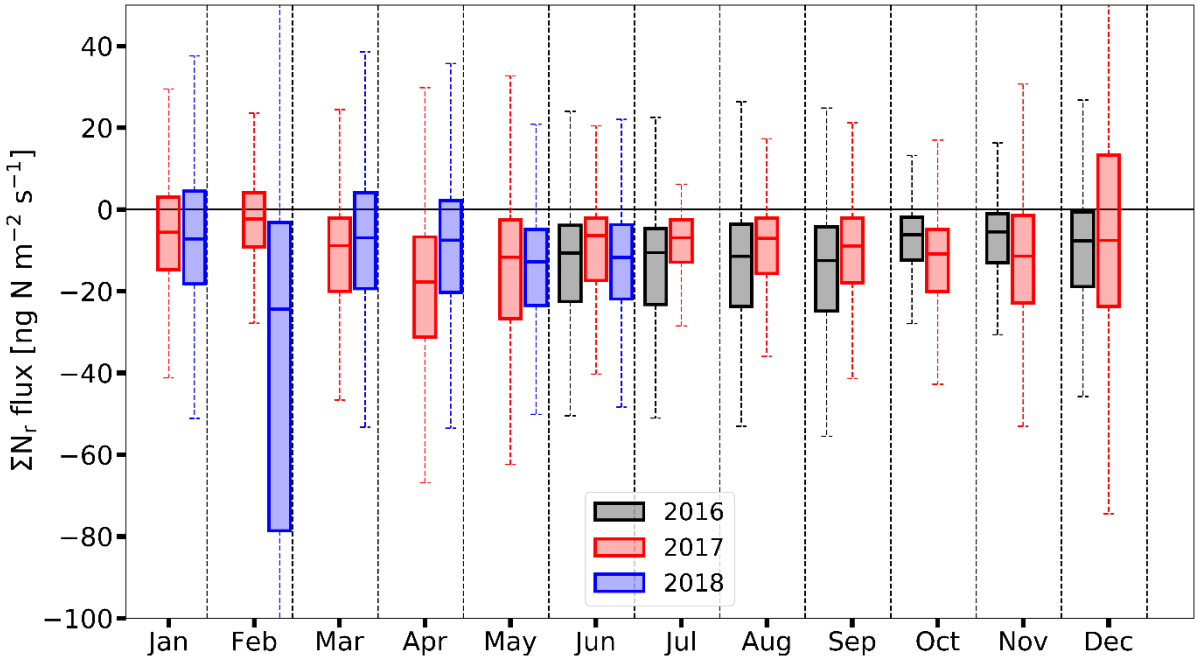

Figure 3.4: Time series of measured high-quality (flags "0" and "1") ΣN_r fluxes depicted as box-and-whisker plots on a monthly basis (box frame = 25 % to 75 % interquartile ranges (IQR), bold line = median, whisker = 1.5 · IQR) in ng N m^{-2} s^{-1}. Colors indicate different years. The whiskers in February 2018 cover the range from –191 to 105 ng N m^{-2} s^{-1}; the upper whisker of December 2017 was at 69 ng N m^{-2} s^{-1}.

–10 ng N m^{-2} s^{-1}. The diurnal cycles of the respective same months were comparable. However, during certain months, which differ in their micrometeorology and/or in the composition of ΣN_r, differences can be significant. For example, the diurnal cycles of March and April 2017 were clearly different to the diurnal cycles of March and April 2018. During spring 2017, deposition fluxes were found whereas the ΣN_r exchange was close to zero one year later. The median deposition was also larger in March and April 2017 than in the year after (Fig. 3.4). In December 2017, the diurnal cycle was close to the zero line and positive fluxes were observed, although standard errors were relatively large (±11.5 ng N m^{-2} s^{-1} on average). In December 2016, small deposition fluxes were observed for the entire diurnal cycle. The diurnal cycle of February 2018 showed highest deposition values during the entire day, even the highest values during the measurement campaign. Again, the average standard error was relatively large (±19.9 ng N m^{-2} s^{-1}) for February 2018 compared to February 2017.

Figure S3.5 shows the median v_d for the corresponding fluxes. Values ranged between 0.2 and 0.5 cm s^{-1} for the entire campaign. In general, median v_d followed closely the seasonality of their corresponding fluxes (Fig. 3.4). During autumn and winter, v_d remained stable. From May to September, a continuous increase in v_d was observed from 06:00 until noon. A decrease in v_d followed in the late afternoon (15:00 to 18:00 LT). Similar to the diurnal fluxes, maximum v_d values were reached between 09:00 and 15:00 LT. During that time, values of v_d were close to 1 cm s^{-1} or even higher (Fig. S3.6).

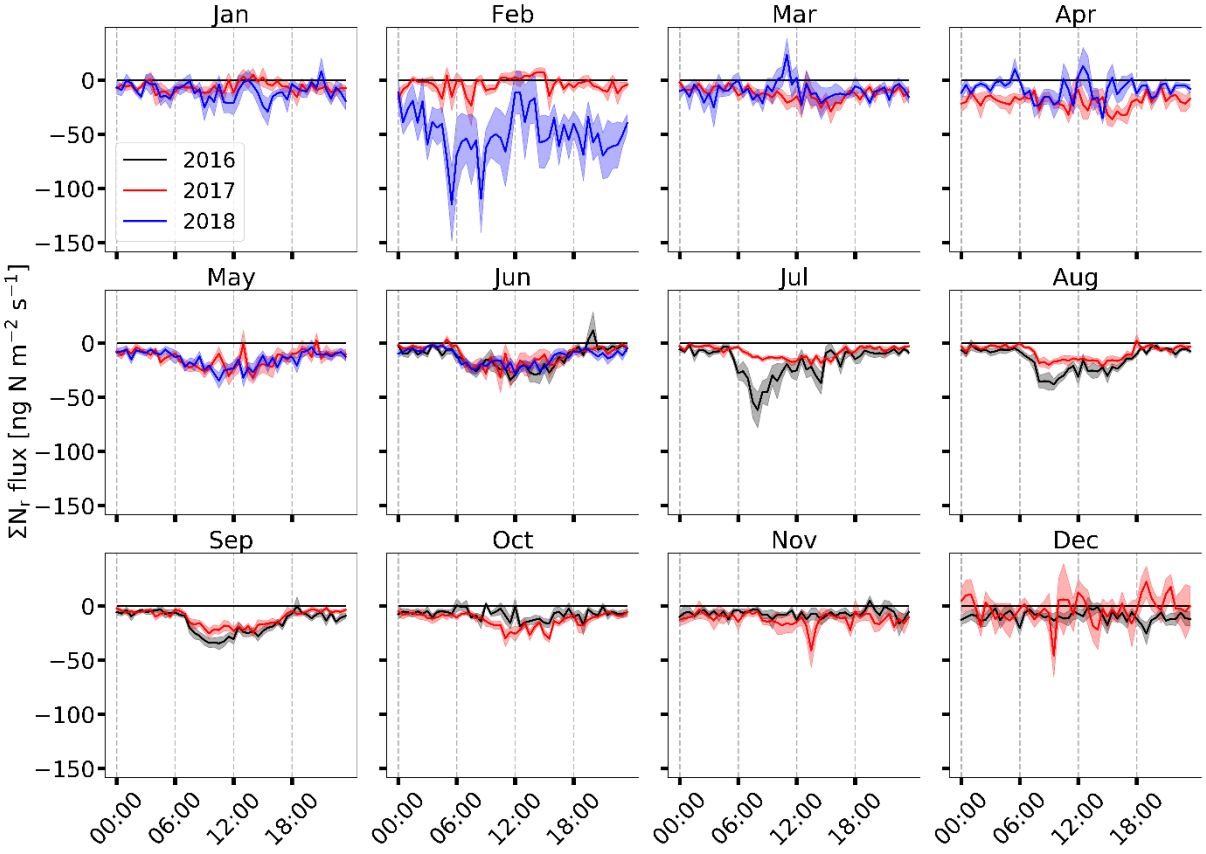

Figure 3.5: Mean diurnal cycle of ΣN_r fluxes (ng N m^{-2} s^{-1}) based on half-hourly measurements for every month from June 2016 to June 2018. The shaded area represents the standard error of the mean. Colors indicate different years.

3.3.3 Controlling factors of measured ΣN_r deposition velocities

From May to September, a clear diurnal pattern was found for v_d and their corresponding fluxes (Figs. 3.5 and S3.6). It was characterized by lower deposition during the night and highest values around noon (Fig. S3.9). During winter, deposition fluxes were close to zero and showed no diurnal variation leading

to a constantly low v_d except for midday (Fig. S3.10). During that time, a strong decrease in v_d was found with near-zero or even small negative values around 12:00 LT. Micrometeorological parameters such as global radiation (R_g) (Zöll et al., 2019), temperature and turbulence (Wolff et al., 2010), humidity (Wyers and Erisman, 1998; Milford et al., 2001), dry/wet leaf surfaces (Wyers and Erisman, 1998; Wentworth et al., 2016), and the concentration of ΣN_r, especially changes in the concentration of the individual nitrogen compounds (Brümmer et al., 2013; Zöll et al., 2016), were reported to control the deposition of ΣN_r.

In order to investigate the influence of u_* on the ΣN_r exchange, Fig. S3.7 in the Supplement illustrates the dependency of v_d on u_* for deposition and emission fluxes during day and night. The R_g threshold for day and nighttime fluxes was set to 10 W m^{-2}. For better visibility, we binned data in 0.1 m s^{-1} increments of u_*. Since bins are not equal in size, we added corresponding half-hourly fluxes to the plots. Red dots represent averages of each bin and error bars correspond to their standard error. We found that v_d increased slightly with u_* due to dependency of v_d on R_a and R_b. The latter are proportional to the inverse of u_*, suggesting that the increase with u_* should follow a power law. In the case of particles, linear relationships between u_* and v_d were found by Gallagher et al. (1997), Lavi et al. (2013), and Donateo and Contini (2014). Although uncertainties of the binned averages were large, a relationship between v_d and u_* seems to exist as suggested by the correlations (r), but no clear functional relationship could be identified due to the large scattering of half-hourly v_d.

For visualizing the impact of the concentration on v_d (Fig. 3.6), we plotted the ΣN_r concentration against the ratio v_d/u_* in order to reduce the influence of R_a and R_b on v_d. The threshold for R_g was set to 10 W m^{-2}, and we binned data in 0.5 µg N m^{-3} increments of the ΣN_r concentration.

It is obvious that v_d/u_* exhibited no significant dependence on the ΣN_r concentration as shown by the low values for r. The ratio appeared to be constant across the (entire) concentration range. It demonstrates that the ΣN_r concentration had no significant influence on their v_d. In the case of particles, the ratio v_d/u_* depends on Obukhov length (L) and particle size according to Gallagher et al. (1997) and Lavi et al. (2013). In the case of deposition fluxes measured during daytime, we found that the ratio decreased for $-0.2 > L^{-1} < 0$ up to a minimum if L^{-1} reaches zero (neutral stratification) (Fig. S3.8 in the Supplement). This relationship was observed by Gallagher et al. (1997) and Lavi et al. (2013). Although the scattering of half-hourly ratios is large, the decrease of the ratio with increasing L^{-1} and the dependence of v_d on u_* demonstrate that v_d was more influenced by micrometeorological variables than by the ΣN_r concentration.

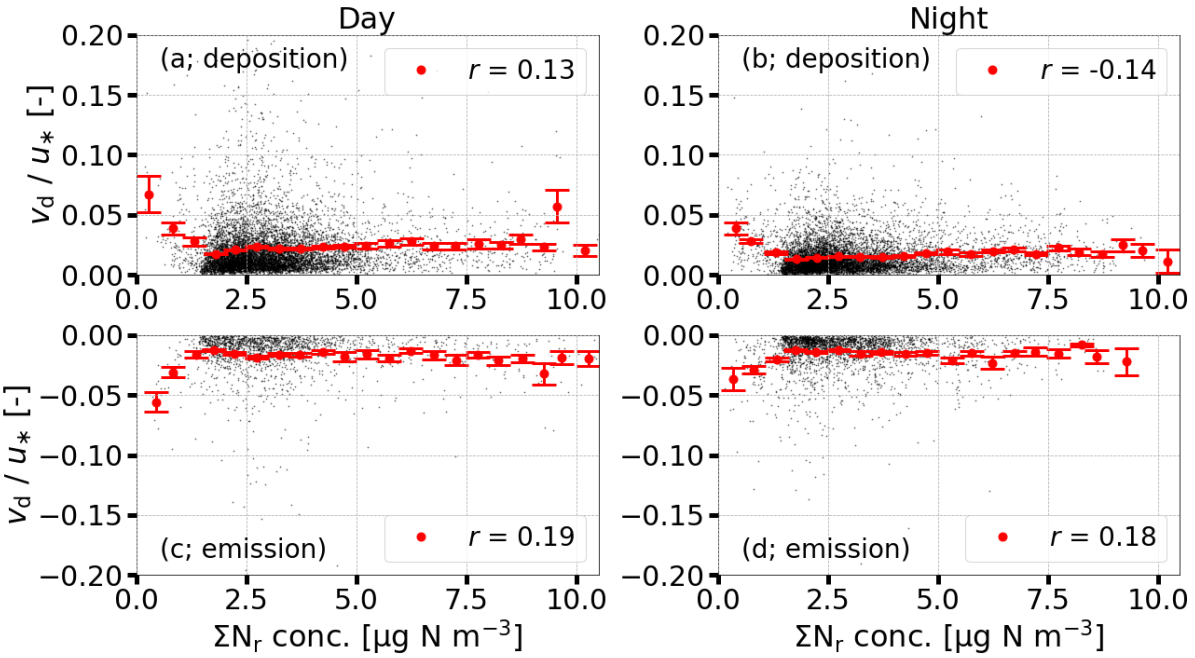

Figure 3.6: Relationships between measured ΣN_r concentrations and corresponding ratios v_d/u_* separated in emission and deposition during day (a, c) and night (b, d). Half-hourly data are displayed in black; red dots represent averages binned in increments of 0.5 µg N m^{-3}. Error bars indicate the standard error of the averages. The threshold for identifying day and nighttime v_d was set to 10 W m^{-2}. *r* represents the measure of correlation evaluated for the binned data.

From the analysis of Figs. 3.6, S3.7, and S3.8, it is impossible to state u_* or L as the controlling variable of the ΣN_r exchange since turbulence, stratification, R_g, sensible heat flux, air temperature, and relative humidity are highly correlated with each other. Figure S3.9 shows the diurnal cycle of concentration, R_g, u_*, air temperature (T_{air}), and v_d for the period from May to September. During that period, a clear diurnal pattern in v_d was observed with largest values around noon and lowest values during the night. During winter (December, January, and February) (Fig. S3.10), v_d was almost equal and even lower during the day, which resulted in a lower deposition of ΣN_r during winter. The different shapes of the diurnal variations of v_d could be induced by micrometeorological variables, which change the composition of available ΣN_r compounds during the day (e.g., Munger et al., 1996; Horii et al., 2004, 2006; Wyers and Duyzer, 1997; Van Oss et al., 1998) and promote photosynthesis (e.g., stomatal uptake or release of NO_2 Thoene et al., 1996 and NH_3 Wyers and Erisman, 1998).

Within the period of enhanced ΣN_r exchange, in particular from May to September, we investigated the dependency of the ΣN_r deposition velocities on T_{air}, relative humidity (RH), dry/wet leaf surface, and ΣN_r concentration. We separated half-hourly v_d into groups of low and high T_{air}, and concentration according to their median. In the case of separating v_d into groups of dry and wet leaf surfaces, we used the proposed calculation scheme of a leaf wetness Boolean (see Sect. 3.2.2). No significant influence of the different installation heights on leaf surface wetness was found (see Fig. S3.11 and corresponding description in the Supplement). Figure 3.7 shows the results for v_d.

In general, higher air temperatures, lower relative humidity, and dry leaf surfaces were associated with enhanced deposition of ΣN_r, and a clear diurnal pattern was observed for v_d with high values around noon and low, non-zero values in the night.

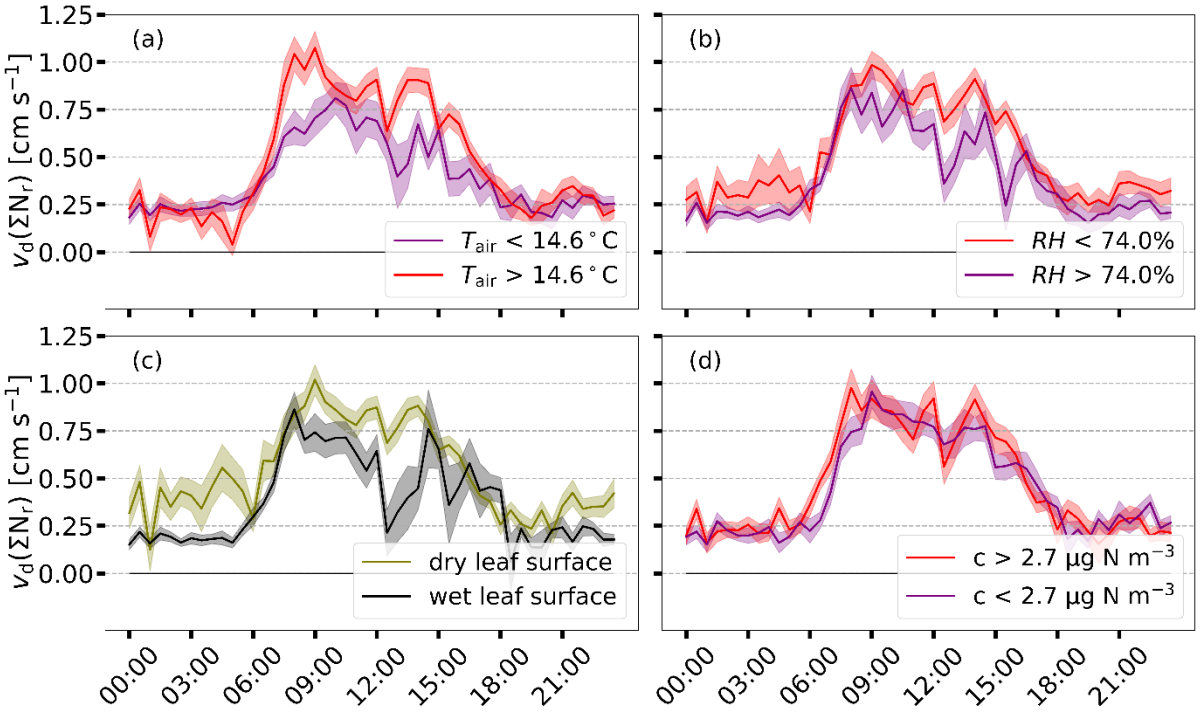

Figure 3.7: Mean diurnal cycle of v_d from May to September for low and high temperature (a), relative humidity (b), and concentration (c). Median values of temperature, humidity, and concentration, which are derived for the same time period, are used as threshold values for separating v_d. In panel (d), the mean diurnal cycle of v_d for dry and wet leaf surfaces is shown. For classifying leaf surfaces as dry or wet, the scheme proposed in Sect. 3.2.2 is applied. The shaded areas represent the standard error of the mean.

During dawn/nighttime, deposition velocities exhibited no significant difference between the applied temperature and humidity thresholds. In the presence of dry leaf surfaces, v_d was higher by approximately 0.2 cm s^{-1} compared to wet leaf surfaces during the night. During the entire day, no difference was found for low and high concentration regimes. During other times of the year, no diurnal pattern was observed. In those periods, v_d was almost constant and exhibited lower values during daylight compared to the May to September period. Occasionally, negative deposition velocities referring to emission of ΣN_r were recorded during times of lower radiation.

3.3.4 Dependence of ΣN_r dry deposition sums on micrometeorological variables

We found that preferentially micrometeorological variables enhance deposition velocities and fluxes. The application of data-driven gap-filling methods like MDV (Falge et al., 2001) for estimating dry deposition could lead to biased results if micrometeorological conditions of the certain gap are different to fluxes used for filling the gap. Therefore, we determined dry deposition budgets with and without u_* filter and conducted gap-filling with additional conditions for temperature, relative humidity, and wind speed.

Figure 3.8 shows the non-gap-filled ΣN_r fluxes depicted as box and their cumulative sums with and without a u_* filter if OMDV is used as a gap-filling approach. For details to the implementation of OMDV, we refer to Sect. 3.2.3.

The difference in dry deposition was approximately 400 g N ha^{-1} after 2 years and corresponds to 6% of the cumulative sum with u_* filter. Figure 3.8a shows that median deposition of ΣN_r

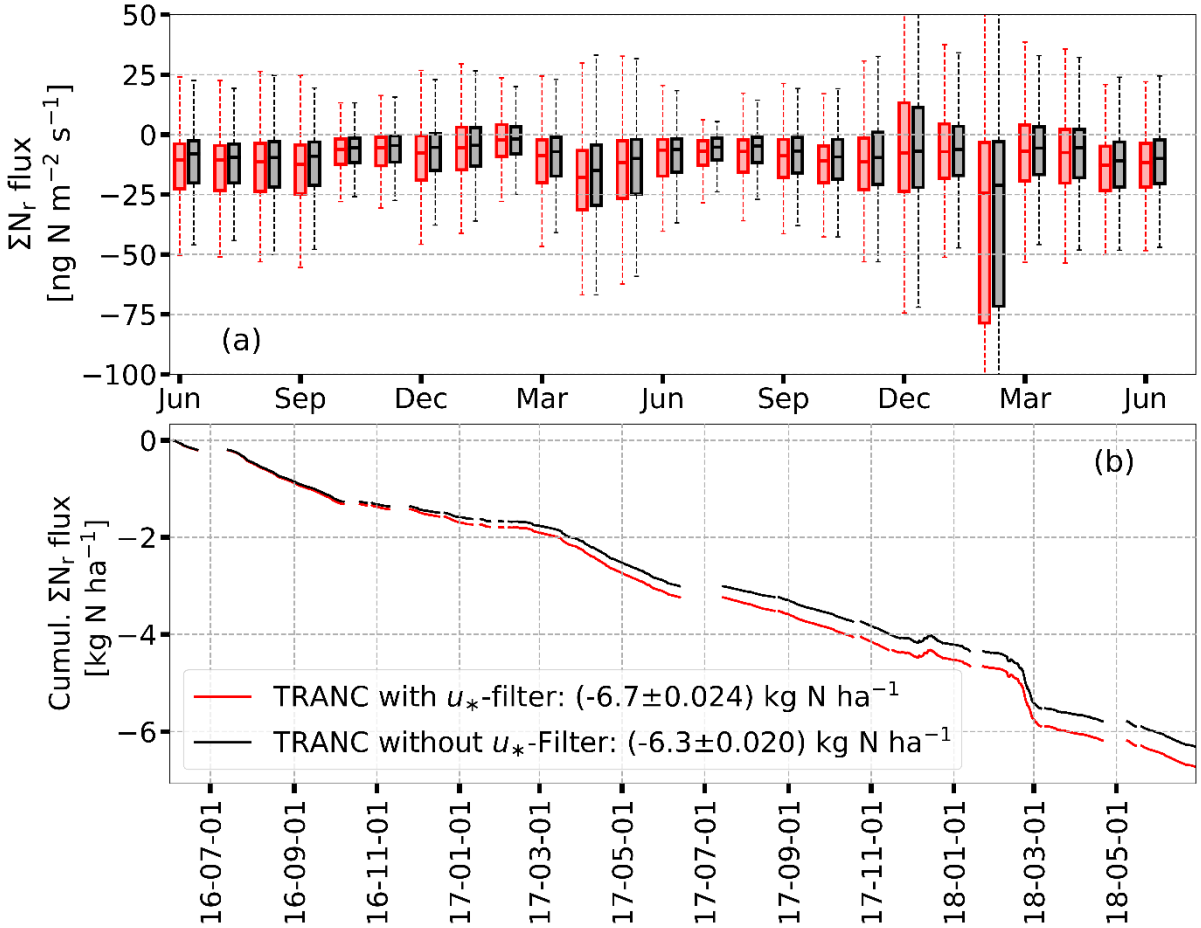

Figure 3.8: Panel (a) shows the non-gap-filled ΣN_r fluxes represented by box-and-whisker plots with (red) and without (black) u_* filter in ng N m^{-2} s^{-1} (box frame = 25 % to 75 % interquartile ranges (IQR), bold line = median, whisker = 1.5 · IQR). The threshold for u_* was set to 0.1 m s^{-1}. In panel (b), the cumulative dry deposition of ΣN_r is plotted for both cases in kg N ha^{-1}. For determining the cumulative curves, OMDV was used as a gap-filling method, and gaps were filled with fluxes being in a range of ±5 d. Remaining gaps were not filled. In the legend of panel (b), cumulative ΣN_r deposition and the total uncertainty of the gap-filled fluxes according to Eq. (3.3) (see Sect. 3.4.3) are shown.

with u_* filter was equal to or larger than the median deposition without u_* filter. Thus, the applied u_* threshold removed not only small fluxes resulting in a consistent bias between the median deposition. The contribution of the water vapor correction (Eq. 3.1) to the estimated dry deposition was very low. ΣN_r interference fluxes were between –3 and –0.3 ng N m^{-2} s^{-1}. The uncertainty ranged between 0.0 and 0.5 ng N m^{-2} s^{-1}. Considering 2 years of TRANC flux measurements with OMDV as a gap-filling approach, the correction contributed with 131 g N ha^{-1} to the estimated dry deposition of 6.7 kg N ha^{-1}.

In order to evaluate the influence of micrometeorological variables such as temperature (*T*), RH, and wind speed (wsp) on annual ΣN_r dry deposition, we compared the deposition estimates of OMDV with CMDV in regard to the measurement years from the beginning of June to the end of May (Fig. 3.9). Details about the implementation of CMDV are given in Sect. 3.2.3.

No significant difference could be found between the dry deposition sums and their cumulative uncertainties related to gap-filling for both measurement years. Consequently, the applied selection criteria did not lead to biased sums compared to the dry deposition calculated with OMDV. The relative contribution to dry deposition related to temperatures, relative humidity, and wind speeds above their respective medians was at 60 % and at 55 % in the first and second measurement year, respectively.

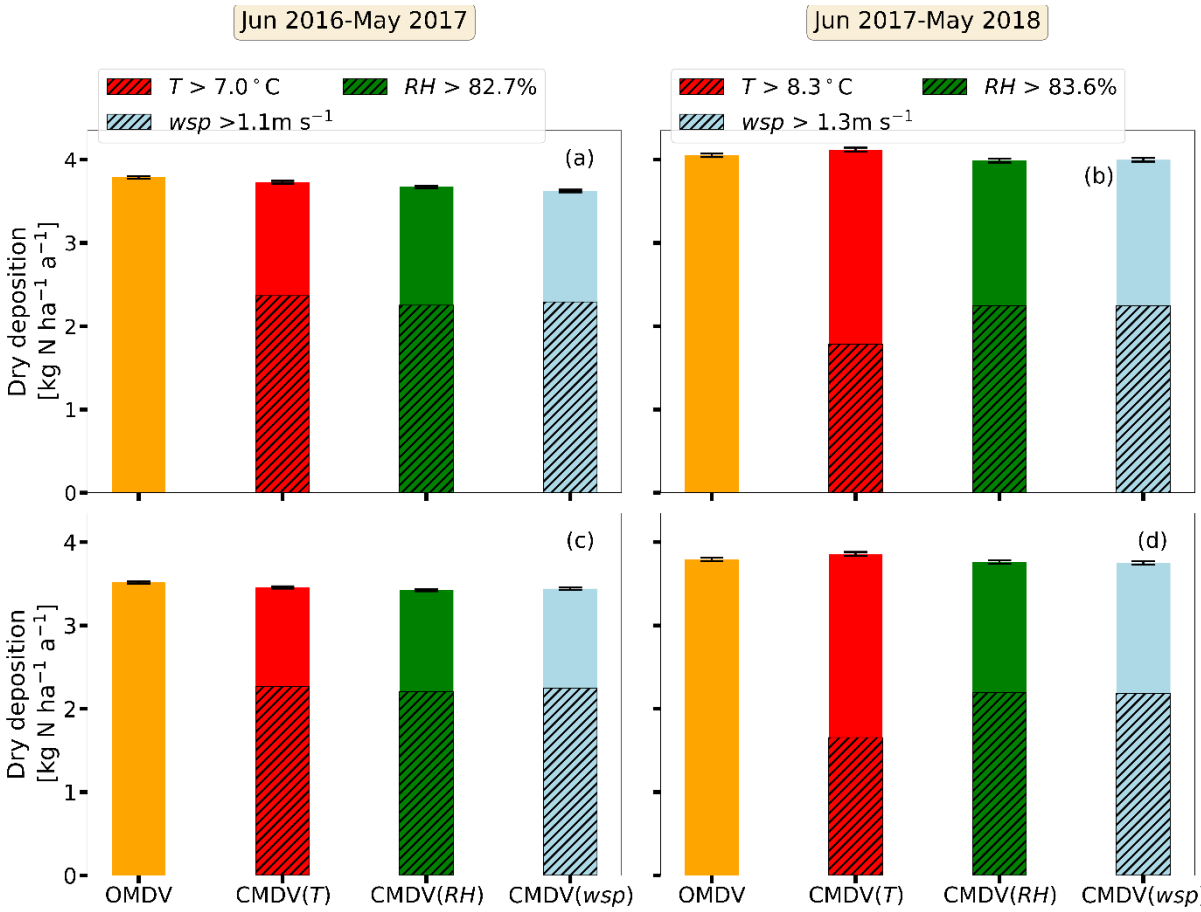

Figure 3.9: Annual ΣN_r dry deposition shown as bar graphs from June to May in kg N ha^{-1} a^{-1}. For the orange bar, short-term gaps were filled with the OMDV approach while using only fluxes in the time frame of ±5 d. In the case of the red, green, and blue bars, the CMDV approach is applied for temperature (*T*), relative humidity (RH), and wind speed (wsp), respectively. Fluxes used for CMDV have to additionally be in a range for *T* (±3°C), RH (±5 %), or wsp (±1.5 m s^{-1}). For OMDV and CMDV, remaining gaps were replaced by monthly averages estimated for each half-hour calculated from the non-gap-filled fluxes. Panels (a, b) were made for fluxes with u_* filter, (c, d) without it. The hatched area of the bars represents the dry deposition for *T*, RH, and wsp values higher than the annual median shown in the legend. Error bars correspond to the total uncertainty of the gap-filled fluxes (see Eq. 3.3).

As shown before, a difference in the application of a u_* filter exists but is within the uncertainty range. Dry deposition was higher in 2017/2018, which was related to the large deposition fluxes observed in February 2018. Still, differences between the years were within their uncertainty ranges. In total, we estimated 3.8 and 4.0 kg N ha^{-1} a^{-1} with the OMDV approach (orange bar) and u_* filter for 2016/17 and 2017/18, respectively.

3.5 Wet and total nitrogen deposition

Wet deposition was estimated from measurements of bulk and wet-only samplers. Table 3.1 shows estimated ΣN_r dry depositions, the deposition estimates of NH_4^+–N, NO_3^-–N, dissolved organic nitrogen (DON), and the resulting total nitrogen from wet deposition (TWD) for all seasons and both measurement years. Please note that the sum of all seasons corresponds to the sum of both measurement years.

Table 3.1: Annual and seasonal sums of dry-deposition estimates (DD) and NH_4^+–N, NO_3^-–N, dissolved organic nitrogen (DON), and the resulting total wet deposition (TWD) from wet-deposition samplers (bulk (BD) and wet-only (WD)) in kg N ha^{-1} per period.

Time	DD [kg N ha^{-1} per period]	WD [kg N ha^{-1} per period]				BD [kg N ha^{-1} per period]			
		NO_3^-–N	NH_4^+–N	DON	TWD	NO_3^-–N	NH_4^+–N	DON	TWD
Winter	2.0	1.5	0.9	0.4	2.8	1.7	1.3	0.5	3.5
Spring	2.2	1.8	2.3	0.1	4.2	1.9	2.4	0.1	4.4
Summer	2.0	1.9	2.6	0.2	4.7	1.6	2.2	0.6	4.4
Autumn	1.7	1.5	1.4	0.6	3.5	1.4	1.4	0.6	3.4
16 June-17 May	3.8	3.8	4.2	0.4	8.4	3.5	4.2	1.0	8.7
17 June-18 May	4.0	2.9	3.1	0.9	6.9	3.0	3.1	0.9	7.0

Small seasonal and annual differences in dry deposition were determined (approx. 200 g N ha^{-1} per period). Total seasonal and annual uncertainties related to gap-filling (Eq. 3.3) were between 7 and 21 g N ha^{-1} per period. Dry deposition contributed approximately one-third to total deposition except for winter (Fig. S3.12). In the second year, the contribution of dry deposition was higher than in the first year. Higher fractions of dry deposition were related to the large dry deposition occurring in late February 2018. Thus, dry deposition and its uncertainty were remarkably high during winter. Total wet deposition (TWD) was highest in spring and summer (Figs. 3.2 and S3.2). During those periods, NH_4^+–N contributed most to TWD, which was probably related to high NH_3 concentrations. Interseasonal differences for NO_3^-–N were found but were lower compared to changes in NH_4^+–N. DON deposition was lowest and was between 0.1 and 0.6 kg N ha^{-1} a^{-1}. Overall, differences in TWD for both sampler types were less than 300 g N ha^{-1} a^{-1} except for winter. Total wet+dry deposition was equivalent to 12.2 kg N ha^{-1} a^{-1} for 2016/17 and 10.9 kg N ha^{-1} a^{-1} for 2017/18.

3.4 Discussion

3.4.1 Interpretation of measured concentrations and fluxes

Measured half-hourly ΣN_r concentrations were low relative to sites exposed to agricultural activities or urban environments. On average, we measured 5.5 ppb (3.1 µg N m^{-3}) ΣN_r, 1.8 ppb (1.0 µg N m^{-3}) NH_3, and 2.5 ppb (1.4 µg N m^{-3}) NO_x. Wintjen et al. (2020) determined an average ΣN_r concentration level of 21 ppb (12 µg N m^{-3}) for a seminatural peatland, Brümmer et al. (2013) measured between 7 and 23 ppb (4 and 13 µg N m^{-3}) as monthly averages above a cropland site, and Ammann et al. (2012) measured half-hourly ΣN_r concentrations ranging from less than 1 to 350 ppb (0.6 to 201 µg N m^{-3}) for a grassland site. Only for certain time periods, ΣN_r concentrations reached significantly higher values. During winter, NO_x increased due to emission from heating with fossil fuels and from combustion processes, for example through traffic and power plants. A generally lower mixing height, which is often observed during winter, also leads to higher ground level concentrations of air pollutants. In spring and autumn, higher ΣN_r concentrations can be attributed to NH_3 emission from the application of fertilizer and livestock farming in the surrounding environment (Beudert and Breit, 2010). NH_3 emissions from livestock farming in rural districts around the NPBW are approximately half of the emissions compared to rural districts located in the Danube–Inn valley (Beudert and Breit, 2010). The authors measured concentrations of NO_2 (2.1–4.8 ppb (1.2–2.8 µg N m^{-3})), NO (0.4–1.6 ppb (0.2–0.9 µg N m^{-3})) and NH_3 (1.4 ppb (0.8 µg N m^{-3})) at the same site. Those values for NO_2 and NO refer to 1992 until the end of 2008; NH_3 was measured from mid-2003 to 2005. The low concentration level and seasonal variability of the ΣN_r compounds, in particular NH_3 and NO_2, are in agreement with Beudert and Breit (2010). Low concentration values of NH_3 and NO_x are reasonable for a site, which is some kilometers away from anthropogenic emission sources. Studies like Wyers and Erisman (1998), Horii et al. (2004), and Wolff

et al. (2010) conducted measurements of NH_3 and NO_2 above remote (mixed) forests and reported similar concentrations for those gases.

Our measurements further indicated that NO_x made the highest contribution to the measured ΣN_r concentrations. At the measurement height, the contribution of NO to NO_x was negligible. Median contribution of NO to NO_x concentrations was approximately 10 % at 50 m. NO exhibits higher concentrations and fluxes close to the forest floor as shown by Rummel et al. (2002). Even if soil NO was converted to NO_2 it could still contribute to the measured ΣN_r flux except for the fraction that is removed by the canopy. As mentioned in Sect. 3.2.2, NO_2 concentrations had been measured at 50m. Seok et al. (2013) reported marginal differences in NO_2 concentrations above the canopy at a remote site. Above the canopy, height differences in NO_2 concentrations were probably not relevant for the measurement site. The NO_x analyzer was equipped with a thermal converter and likely cross-sensitive to other NO_y compounds. However, measured concentrations of HNO_3 or NO_3^- were comparatively low as seen in Fig. 3.2. Thus, their influence on NO_x measurements was most likely small. In the context of height differences, we found no systematic difference between NH_3 concentrations within the canopy and just above the canopy. Only for short time periods, for example in summer 2016 and 2017, differences in passive samplers were found indicating a small NH_3 flux. Considering the LOD of IVL passive samplers for NH_3 of 0.4 µg N m^{-3} determined by Dämmgen et al. (2010) shows that passive sampler measurements were conducted close to their LOD. It suggests that the uncertainty of the passive samplers was too large to resolve flux gradients. Still, NH_3 had a strong presence in the ΣN_r concentration within the growing period of the plants, in particular during spring and summer. DELTA measurements further suggested that the ΣN_r concentration pattern was mainly influenced by gaseous N_r.

The increase in the relative contributions of HNO_3 from spring to summer compared to the decrease of NH_4^+ and NO_3^- (Fig. 3.3) can be related to the evaporation of NH_4NO_3 (Wyers and Duyzer, 1997; Van Oss et al., 1998; Schaap et al., 2002). However, the findings of Tang et al. (2015) and Tang et al. (2021) revealed that HNO_3 concentrations measured by the DELTA system using carbonate coated denuders may be significantly overestimated (45 % on average) since HONO sticks also at those prepared surfaces. Thus, the measured HNO_3 concentrations should be seen as an upper estimate. Due to the reaction of NH_3 with HNO_3 and sulfuric acid particulate NH_4^+ is formed, available as $(NH_4)_2SO_4$ or NH_4NO_3 (Trebs et al., 2005).

These aerosols are mainly in the fine mode and associated with aerodynamic diameters less than 2.5 µm ($PM_{2.5}$) (Kundu et al., 2010; Putaud et al., 2010; Schwarz et al., 2016). Since the DELTA cut-off size is approximately 4.5 µm (Tang et al., 2015), fine accumulated particles could be adequately detected. Coarse-mode NO_3^- aerosols like sodium nitrate ($NaNO_3$) are formed in the presence of sea salt (Na^+ and Cl^-) or other geological minerals or biological particles like pollen (Lee et al., 2008; Putaud et al., 2010). Generally, concentrations of Na^+, Ca^{2+}, and Mg^{2+} were close to zero during the entire campaign. On average, we measured 0.08 µg m^{-3} for Na^+ and 0.01 µg m^{-3} for Ca^{2+} and Mg^{2+}. Although these concentrations were close to and lower than the LOD of DELTA (Tang et al., 2021) and partly underestimated by the filters of the DELTA system due to the cutoff size of approximately 4.5 µm, it illustrates that coarse mode nitrate levels are not expected to be significant at the measurement site. As noted in Sect. 3.2.2, cellulose filters were used for collecting NO_3^- and SO_4^{2-}. According to Tang et al. (2015), cellulose filters underestimate NO_3^- and SO_4^{2-} ions, sulfate by 11%, and nitrate by 37 %. However, Schaap et al. (2004) found that cellulose filters are appropriate for capturing NO_3^-.

Inside of the TRANC, high temperatures (≥ 870°C) probably led to a chemical decomposition of coarse aerosols (Yuvaraj et al., 2003). Marx et al. (2012) found that the TRANC is able to convert $NaNO_3$. Thus, we assume that the TRANC's cut-off size was higher resulting in a higher sensitivity to aerosols in the coarse mode. Still, we observed a clear excess of NH_4^+ over NO_3^-. Presumably, the contribution of NO_3^- aerosols to TRANC measurements was not significant. In addition, higher oxidized compounds

like N_2O_5 or peroxyacetyl nitrates could not be collected by DELTA but were probably converted by the TRANC. Issues in the temperature stability or CO supply leading to instabilities in the conversion efficiency of the TRANC may be responsible for disagreements to the collection efficiency of the denuders. A key uncertainty was the data coverage of the TRANC, which was 78 % on average during the exposure periods. In total, the comparison of the total N concentrations shows that the TRANC can adequately measure ΣN_r concentration.

In general, a comparison of ΣN_r concentrations and fluxes to other studies is difficult due to the measurement of the total nitrogen. Most studies that have been published so far focused only on a single or a few compounds of ΣN_r and are limited to selected sites and time periods of a few days or months. Only a few studies had been focusing on ΣN_r flux measurements using the EC method (see Ammann et al., 2012; Brümmer et al., 2013; Zöll et al., 2019; Wintjen et al., 2020). Brümmer et al. (2013) measured ΣN_r exchange above an agricultural land. During unmanaged phases, fluxes were between –20 and 20 ng N m^{-2} s^{-1}. Apart from management events, fluxes above the arable field site were closer to zero compared to our unmanaged forest site, which is dominated by deposition fluxes and is therefore a larger sink for reactive nitrogen. Ammann et al. (2012) measured ΣN_r fluxes above a managed grassland. In the growing season, deposition fluxes of –40 ng N m^{-2} s^{-1} were measured. The authors reported increased deposition due to weak NO emission during that period. Similar to Brümmer et al. (2013), the flux pattern observed by Ammann et al. (2012) is influenced by fertilizer application and thus, varying contributions of N_r compounds, for instance by bidirectionally exchange of NH_3 leading to both periods of net emission and deposition of ΣN_r. Despite the low signal-to-noise ratio of emission fluxes and data coverage of 50 % from June 2016 to June 2018 at the measurement site, we were able to investigate the exchange pattern of ΣN_r and could estimate reliable dry deposition sums. To our knowledge, flux measurements of ΣN_r above mixed forests have not been carried out so far. We found that the flux magnitude and diurnal flux pattern were similar to observations reported for individual N_r species above forests, e.g., NH_3 (Wyers and Erisman, 1998; Hansen et al., 2013, 2015), NO_2 (Horii et al., 2004; Geddes and Murphy, 2014), HNO_3 (Munger et al., 1996; Horii et al., 2006), and total ammonium (tot-NH_4^+) and total nitrate (tot-NO_3^-) (Wolff et al., 2010). As seen by the flux values and measurements of individual compounds, deposition prevails in the reported flux pattern, which corresponds to our measurements.

However, under certain circumstances regarding micrometeorology or the availability of ΣN_r compounds large deposition or emission fluxes can be observed. In February 2018, remarkably high ΣN_r concentrations and depositions were measured.

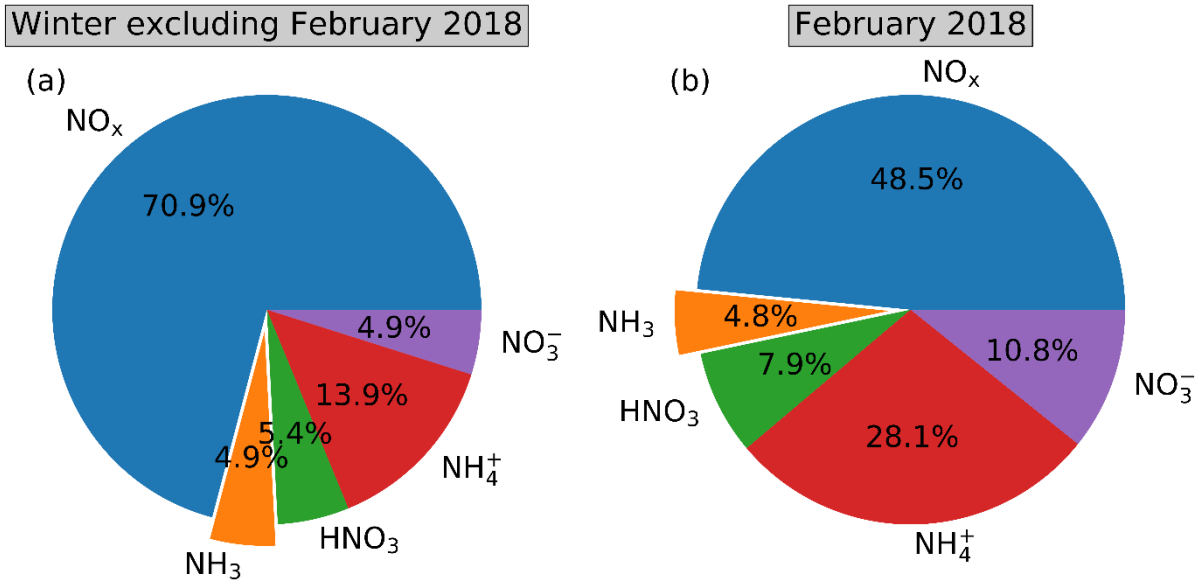

Figure 3.10: Relative contribution of concentrations for NO_x, NH_3, HNO_3, NO_3^-, and NH_4^+ to ΣN_r estimated from DELTA and NO_x measurements for winter and separately for February 2018. NO_x measurements are averaged to exposure periods of the DELTA samplers.

During the exposure period of the DELTA samplers, we found 0.96, 0.17, 0.37, 0.27, and 1.70 µg N m^{-3} for NH_4^+, NH_3, NO_3^-, HNO_3, and NO_x, respectively. The aerosol concentrations were exceptionally large in February 2018, which have affected these averages considerably. Averaged NH_4^+ concentration during winter excluding February 2018 was only 0.38 µg N m^{-3} in comparison to 0.96 µg N m^{-3} for February 2018. The concentration in this month results in a NH_4^+ concentration 2.5 times higher than the average. Also, the SO_2 concentration was much larger (1.54 µg N m^{-3}) in this month compared to the other winter months (0.37 µg N m^{-3}). Figure 3.10 shows the relative contributions of each N_r compound for February 2018 compared to averaged fractions during winter excluding February 2018.

During February 2018, NH_4^+ made a significant contribution to the ΣN_r concentration. The measured NH_4^+ value is an integrated value over approximately one month. Thus, daily contributions of NH_4^+ could have been even higher. Earlier studies by, e.g., Wolff et al. (2010) report events with large aerosol deposition. During their campaign, wind speeds were relatively high. Largest aerosol deposition occurred during dry conditions, e.g., low RH, no rain, and high visibility. Figure S3.13 shows micrometeorological parameters, deposition velocities, and gap-filled ΣN_r fluxes from the 12 February to 6 March. Large deposition fluxes were accompanied by high wsp and u_* values, high R_g indicating high visibility, and low RH. The observed conditions are typical for cold air streams with high aerosol loads coming from northeast and led to a reduction in turbulent resistances resulting in a high v_d, which is due to efficient turbulent mixing. Hence, even at low concentrations of NH_4^+ significant aerosol deposition is possible if R_a and the surface resistance are reduced. In conclusion, particulate NH_4^+ was mainly responsible for the large ΣN_r deposition due to its excess over aerosol NO_3^-. Since we had no

high-resolution flux measurements of any ΣN_r compound, we have no evidence which aerosol predominated the ΣN_r flux.

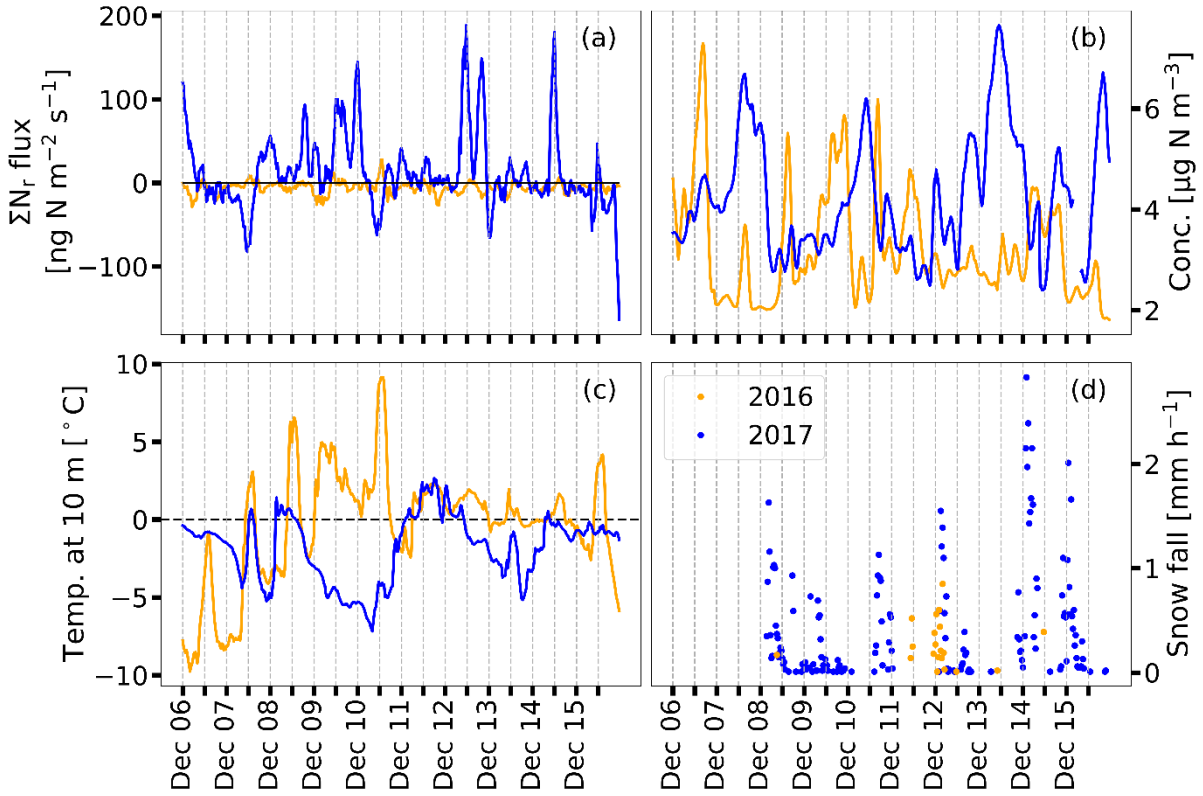

Figure 3.11: ΣN_r gap-filled fluxes (a), ΣN_r concentrations (b), air temperature at 10 m height above ground (c), and snowfall (d) from 6 to 15 December for 2016 (orange) and 2017 (blue). Gaps are filled with the OMDV approach with fluxes being in a range of ±3 d. Fluxes and concentrations of ΣN_r were smoothed with a 3 h running mean for better visualization.

In December 2017, large emission fluxes were measured. Compared to 2016, significant differences in temperature and snow depth were observed. Figure 3.11 shows recorded temperature, snowfall, concentrations, and estimated fluxes of ΣN_r from 6 to 15 December for 2016 and 2017. Here, ±3 d was chosen for filling the gaps in order to keep the short-term variability of the fluxes.

In 2017, we observed substantial snowfall and a more slowly varying temperature compared to 2016, leading to significant snow depths compared to 2016. On the 1 December, 1 and 20 cm snow depth were measured in the fetch of the tower for 2016 and 2017, respectively. Two weeks later, snow depth increased to 5 and 60 cm, respectively. In addition, temperatures alternated around 0°C with minimum and maximum values close to ±10°C in December 2016. In 2017, temperatures were below 0°C and only for one day above 0°C, and global radiation was below 100 W m^{-2}.

The decomposition of organic matter, e.g., leaves, occurring on the topsoil could be responsible for the observed ΣN_r emission fluxes. Due to the large snow depth in December 2017, the snow pack could act as an isolator, inhibit soil frost penetration, and therewith promote decomposition processes. In December 2016, decomposition rates were likely reduced compared to 2017 since snow depth was smaller (e.g., Bokhorst et al., 2013; Kreyling et al., 2013; Saccone et al., 2013). The influence of snow cover on soil emissions of N_r compounds, for example NO, is still under discussion (Medinets et al., 2016). As stated by the authors, different results had been published about the origin of NO emissions from snow-covered soils (see Medinets et al., 2016, and references therein). Since we conducted no measurements of NO close to or at the forest floor, we were not able to examine the influence NO emissions from soil or snow on the ΣN_r measurements. Since soil-emitted NO is rapidly converted to NO_2 (Rummel et al., 2002), the measured ΣN_r emissions were unlikely to be solely caused by NO. The low correlations of the ΣN_r fluxes to micrometeorological variables could be related to, for example,

time shifts between exchange processes and micrometeorological variations, multiple (chemical) interactions between the N_r compounds, and feedback mechanisms, which are difficult to quantify.

3.4.2 Influence of micrometeorology and nitrogen concentrations on deposition and emission

Figures S3.9 and S3.10 show that the variability of v_d and other micrometeorological variables were highly correlated with each other. Thus, we could not examine the mechanistic micrometeorological driver of the ΣN_r flux. The dependencies on u_* or L (Figs. S3.7 and S3.8) could also be related to effects of sensible heat flux, R_g, or T_{air}. Surely, micrometeorological parameters such as R_g and T_{air} promote photosynthesis of plants (Jarvis, 1976), i.e., lower the stomatal resistance, which is essential for the stomatal uptake of ΣN_r compounds such as NO_2 (e.g., Thoene et al., 1996) and NH_3 (e.g., Wyers and Erisman, 1998). Stomatal uptake of N_r compounds was possible during periods of photosynthetic activity, leading to high values of v_d during the summer months (Fig. S3.9). Figure S3.10 reveals that a certain degree of ΣN_r uptake still occurred in winter, but deposition decreased strongly during midday, and even periods of emission were observed. These emissions may be due to the decomposition of leaves, leading to a release NH_3 in late autumn/early winter (Hansen et al., 2013), or from snow-covered soils (see Sect. 3.4.1).

The analysis of Fig. 3.6 revealed that deposition velocities were independent of the ΣN_r concentration. However, the impact of increasing concentrations on nitrogen (deposition) fluxes is well documented, for example, by Ammann et al. (2012) and Brümmer et al. (2013) for ΣN_r above grassland and arable land, respectively, by Horii et al. (2006) for NO_y and Horii et al. (2004) for NO_x above a mixed forest, and by Zöll et al. (2016) for NH_3 above a seminatural peatland.

Since we had no possibility to determine the actual contribution of the individual compounds to the ΣN_r flux, comparing micrometeorological dependencies of v_d to observations made for individual compounds is not possible. In the case of NH_3, surface wetness was identified as a controlling factor for the NH_3 uptake in previous studies (Wyers and Erisman, 1998; Milford et al., 2001; Wentworth et al., 2016). For total ammonium and total nitrate (tot-NH_4^+ and tot-NO_3^-, respectively), Wolff et al. (2010) found that tot-NO_3^- exchange was nearly zero and emission was observed for tot-NH_4^+ during rain or fog. Highest deposition was observed during sunny days. For the actual compound mix at our measurement site, high temperatures (> 14.6°C), low relative humidity (< 74.0 %), and dry leaf surfaces were found to enhance the surface uptake of ΣN_r from May to September. Since the actual composition of the ΣN_r flux is not known, no arguments about an agreement or disagreement to the cited publications can be made.

We further found that the ΣN_r concentration did not change significantly through the year. The difference between lowest and highest seasonal concentration means was only 0.8 µg N m^{-3}. However, DELTA measurements demonstrated that the contribution of individual compounds does show a seasonal cycle. Since the ΣN_r compounds differ in their v_d, the observed seasonality in the dry deposition flux is related to the availability of ΣN_r compounds. For example, in spring and summer, NH_3 had probably the largest contribution on the ΣN_r flux. Elevated NH_3 concentrations were likely caused by emissions from agricultural management in the surrounding region (Ge et al., 2020). The concentration of NH_3 was still lower than of NO_2, but the v_d of NH_3 is significantly higher than of NO_2 for woodland. Deposition velocities of NH_3 range between 1.1 and 2.2 cm s^{-1} (see Schrader and Brümmer, 2014, and references therein), and values between 0.015 and 0.51 c ms^{-1} were reported for NO_2 (e.g., Rondon et al., 1993; Horii et al., 2004; Breuninger et al., 2013; Delaria et al., 2018, 2020). However, variations in the composition of ΣN_r may correlate with micrometeorological parameters. For example, the formation of HNO_3 is correlated with R_g. The solar radiation responsible for the stomatal opening also promotes the formation hydroxyl radicals, which react with NO_2 to form HNO_3 (e.g., Munger et al., 1996; Horii et al., 2004, 2006; Seinfeld and Pandis, 2006). T_{air} influences the diurnal pattern of NH_4NO_3, which may also

volatilize close to the surface due to the depletion of its precursors and in the case the temperature gradient is large enough (Wyers and Duyzer, 1997; Van Oss et al., 1998). Thus, part of the NH_4^+ and NO_3^- in the aerosol phase may be converted to NH_3 and HNO_3, which deposits faster to surfaces than aerosols. For tot-NH_4^+ and tot-NO_3^-, mean v_d of 3.4 and 4.2 cm s^{-1} were determined by Wolff et al. (2010). In the case of HNO_3, mean values between 2 and 8 cm s^{-1} were published by Pryor and Klemm (2004), Horii et al. (2006), and Farmer and Cohen (2008).

In conclusion, the variability in micrometeorological controls such as R_g, T_{air}, u_*, or RH in combination with changes in ambient concentration levels of the ΣN_r compounds explains the observed variation in the ΣN_r flux pattern.

3.4.3 Uncertainties in dry deposition estimates

Fluxes determined with the EC method are exposed to systematic and random errors. Systematic errors are related to the design of the measurement setup and the instruments, data processing steps including calibration, tilt correction, detrending, and corrections due to low- and high-frequency attenuation (Wintjen et al., 2020), and advection fluxes originating preferentially from non-homogeneous surfaces. Uncertainties from the measurement setup were likely caused by an insufficient pump performance, issues in temperature stability of the TRANC and CLD, sensitivity loss of the CLD, and problems in the O_2 and CO supply. Therefore, regular maintenance and continuous observation of instrument performance parameters such as TRANC temperature and flow rate were made. With manual screening of measured half-hourly values and the recording of these parameters, low-quality half-hourly values were effectively excluded from analysis. A basic assumption for the EC method is that the terrain needs to be flat, and the canopy height and density should be uniform (Burba, 2013). These site criteria are not perfectly fulfilled at our measurement site. The site is located in a low mountain range, and tree density is rather sparse south of the flux tower. Such diverse terrain characteristics could lead to unwanted turbulent fluctuations (non-stationarity of time series), which introduce noise in the cross-covariance function. A 2D-footprint analysis exemplarily made for the year 2016 showed that the 70 % isoline of the flux had an extension of approximately 300 m. In southwest direction of the tower (approx. distance 100 to 300 m), tree density and height were lower than to the northeast of the tower. Due to the high surface roughness, the flux footprint is limited in its size but the footprint represents the typical forest structure of the NPBW. Thus, we did not filter half-hourly fluxes from certain wind direction sectors.

Random errors are related to turbulence sampling errors (Finkelstein and Sims, 2001; Hollinger and Richardson, 2005; Loescher et al., 2006). An inadequate sample size results in an incomplete sampling of large-scale eddies, which compromises the cross-covariance of the vertical wind and the scalar of interest. The method of Finkelstein and Sims (2001) allows one to quantify the random error of the measured fluxes ($F_{unc,meas}$). In order to determine the effect of the random flux error on the estimated dry deposition sums, we used the method proposed by Pastorello et al. (2020):

$$F_{unc,cum_i} = \sqrt{\sum_i^n \left(F_{unc,meas_i}\right)^2} \tag{3.3}$$

Using Eq. (3.3), we determined an uncertainty of 9 g N ha^{-1} a^{-1} for 2016/17 and 21 g N ha^{-1} a^{-1} for 2017/18 due to insufficient sampling of turbulent motions. The uncertainty related to u_* filtering is difficult to quantify since common approaches for estimating u_* thresholds, i.e., moving point threshold (Reichstein et al., 2005) or change point detection (Barr et al., 2013), are designed for CO_2. Applying these threshold detection algorithms to N_r species is not suggested since their exchange patterns are characterized by a higher variability for different timescales. The chosen u_* threshold of 0.1 cm s^{-1} should be interpreted as minimal filter to exclude periods of insufficient turbulence (for details see Zöll et al., 2019, Sect. 2.4). In combination with the MDV approach as the gap-filling method, the applied

threshold may lead to biased dry deposition sums. As shown in Fig. 3.8, the difference between dry deposition sums was small compared to estimated dry deposition after 2 years. Presumably, not only small fluxes were removed from the analysis by the u_* filter. We further showed that the contribution of the water vapor correction was negligible. Brümmer et al. (2013) and Ammann et al. (2012) reported a low contribution of the correction to their observed TRANC fluxes.

The uncertainty related to gap-filling of a certain half-hourly value was determined by the standard error of the averaged flux, and their annual and seasonal uncertainties were determined by Eq. (3.3). Both random errors, the random uncertainty of Finkelstein and Sims (2001) and the uncertainty due to the MDV approach, are negligible. Presumably, systematic errors affected the TRANC measurements at most. However, estimating a total systematic uncertainty is not possible since the contribution of individual systematic errors is not known and their quantification is difficult.

Regarding the gap-filling technique, we showed that the results when applying the MDV method were independent of the applied micrometeorological criteria. The differences in v_d to micrometeorology were observed for a limited time period of the year. During other months, we found no influence of micrometeorological variables such as temperature, humidity, and wet/dry leaf surfaces on diurnal pattern of the ΣN_r fluxes. Thus, the dry deposition sums exhibited no significant differences for the applied micrometeorological criteria. The difference in the annual dry deposition estimates was likely related to the large deposition occurring in February 2018.

Using the MDV approach is recommended for gaps spanning over no more than a few days. Using statistical gap-filling approaches such as look-up tables, non-linear regression, or MDV (Falge et al., 2001) for longer gaps is not suggested. Statistical methods like MDV assume a periodic variability with high auto-correlation of fluxes. This assumption is valid for CO_2, which has a distinct diurnal cycle. Reactive gases do not exhibit a clearly predictable flux pattern. Their flux variability depends on micrometeorological conditions and their chemical and physical properties sometimes leading to instationarities in data time series. Gap-filling methods based on inferential modeling or artificial neural networks may be a further valuable option, especially for long-term gaps – if models are available. Monthly averages estimated for each half-hour do not account for short-term deposition or emission events. Since 80 % of measured half-hourly fluxes were deposition fluxes at the measurement site, the applied gap-filling method for long-term gaps is somewhat justified.

The results of wet deposition have shown that dry deposition contributes approximately one-third to the total deposition, which is comparable to previous nitrogen deposition estimates obtained by canopy budget models at the same site (Beudert and Breit, 2014). As shown in Table 1, differences between bulk and wet-only deposition were negligible. Small differences between TWD from wet-only and bulk measurements were related to the sedimentation of inorganic and organic dust particles or to dry deposition of NH_3 and HNO_3 (Staelens et al., 2005). The effects were not relevant for the annual nitrogen deposition at the measurement site. Estimated total N deposition was in the range of critical loads for *Picea abies* and *Fagus sylvatica* reaching from 10 to 15 kg N ha^{-1} a^{-1} and 10 to 20 kg N ha^{-1} a^{-1}, respectively (Bobbink and Hettelingh, 2011). Since the forest stand consists of approximately 80% of Norway spruce in the footprint and the surrounding forest stand is predominated by Norway spruce, the critical load for the forest stand is probably closer to the values of *Picea abies*. It suggests that the forest is currently close to the limit of receiving too much nitrogen from the atmosphere, assuming that the critical load of the forest site is at the upper end of the reported ranges.

3.5 Conclusions

Our study is the first one presenting 2.5 years of flux measurements of total reactive atmospheric nitrogen (ΣN_r) measured with a custom-built converter called Total Relative Atmospheric Nitrogen

Converter (TRANC) coupled to fast response chemiluminescence detector (CLD) above a protected temperate mixed forest, which is located in a remote area.

A comparison of monthly averaged ΣN_r concentrations from the TRANC and DELTA (DEnuder for Long-Term Atmospheric sampling) and chemiluminescence measurements of nitric oxide (NO) and nitrogen dioxide (NO_2) showed a reasonable agreement in their seasonal patterns. On average, concentrations by the TRANC-CLD system were higher by ~ 0.41 µg N m^{-3}, showing that the TRANC-CLD system can adequately measure ΣN_r concentrations. Differences could be related to higher oxidized nitrogen compounds, which are not detected by the DELTA system, an insufficient data coverage of TRANC measurements during the exposure periods, the presumably lower aerosol cut-off size of DELTA, issues in the conversion efficiency of the TRANC, etc. Only nitrogen oxides (NO_x) and ammonia (NH_3) showed distinct seasonal changes in their concentrations, whereas ΣN_r concentration remained stable throughout the year. NO_x exhibited highest concentrations during winter, NH_3 during spring and summer. In total, the sum of both gases had a mean contribution of 71.0 % to the ΣN_r concentrations, highlighting their importance for the observed ΣN_r exchange pattern.

During 2.5 years of flux measurements, median deposition ranged from –15 to –5 ng N m^{-2} s^{-1}. Deposition velocities followed the diurnal pattern of the fluxes, and median values ranged between 0.2 and 0.5 cm s^{-1}. Highest deposition was observed during periods of high solar radiation, in particular from May to September. Our findings suggest that seasonal changes in the contributions of the individually measured N_r compounds, global radiation (R_g), and micrometeorological controls correlated with R_g were most likely responsible for the observed pattern of the deposition velocity (v_d). From May to September, v_d was elevated in presence of dry leaf surfaces, at a low humidity level, and at higher temperatures. No relationship between ΣN_r concentration and corresponding deposition velocities was found. These findings are exclusively related to the composition of the ΣN_r flux at the measurement site. Comparing results to other sites is challenging due to a different mixture of compounds in the ΣN_r flux.

From June 2016 to May 2017 and June 2017 to May 2018, we estimated dry deposition sums of 3.8 and 4.0 kg N ha^{-1} a^{-1}, respectively. No significant influence of micrometeorological parameters on ΣN_r fluxes when using the mean-diurnal-variation approach for filling short-term gaps (up to five days) was found. Remaining half-hourly gaps were replaced by monthly averages of the specific half-hour. In the first and second measurement year, we determined 12.2 and 10.9 kg N ha^{-1} a^{-1} as total nitrogen deposition, respectively. Thus, dry deposition contributed approximately 1⁄3 to the total N deposition. A review of published critical loads show that estimated total deposition were at the upper end of the critical load range.

The dataset presented in this study provides an unique opportunity for a comparison to deposition models. In a follow-up paper, a comparison of the acquired dataset to the performance of deposition models will be made. Modeled exchange dynamics will be discussed in regard to their biophysical controlling factors. Annual N budgets from measurements, modeling approaches using in situ and modeled input parameters, and canopy outflow measurements will be shown.

Code and data availability. Concentration, flux, micrometeorological, and ecological data can be accessed in the following repository: https://doi.org/10.5281/zenodo.4513854 (Brümmer et al., 2022). All data are available upon request from the first author of this study (pascal.wintjen@thuenen.de). Also, Python 3.7 code for flux data analysis can be requested from the first author.

Supplement. The supplement related to this article is available online at: https://doi.org/10.5194/bg-19-389-2022-supplement.

Author contributions. PW, FS, and CB conceived the study. PW wrote the manuscript, carried out the measurements at the forest site, and conducted flux data analysis and interpretation. FS evaluated meteorological measurements. FS and MS provided insights in interpreting deposition velocities. BB performed the wet deposition analysis. CB installed the flux tower equipment and gave scientific advise to the overall data analysis and interpretation. All authors discussed the results, and FS, MS, BB, and CB contributed to the manuscript.

Acknowledgements. We thank Undine Zöll for scientific and logistical help, Jeremy Rüffer and Jean-Pierre Delorme for excellent technical support, Ute Tambor, Andrea Niemeyer, and Dr. Daniel Ziehe for conducting laboratory analyses of denuder and filter samples, and the Bavarian Forest National Park (NPBW) Administration, namely Wilhelm Breit and Ludwig Höcker, for technical and logistical support at the measurement site. We further thank the anonymous reviewers and the editor for their valuable comments that helped improve the quality of the manuscript significantly.

Financial support. This research has been supported by the Umweltbundesamt (FORESTFLUX project (grant no. FKZ 3715512110)) and the Bundesministerium für Bildung und Forschung (Junior Research Group NITROSPHERE (grant no. FKZ 01LN1308A)).

Review statement. This paper was edited by Ivonne Trebs and reviewed by three anonymous referees.

References

Ammann, C., Wolff, V., Marx, O., Brümmer, C., and Neftel, A.: Measuring the biosphere-atmosphere exchange of total reactive nitrogen by eddy covariance, Biogeosciences, 9, 4247–4261, https://doi.org/10.5194/bg-9-4247-2012, 2012.

Aubinet, M., Grelle, A., Ibrom, A., Rannik, U., Moncrieff, J., Foken, T., Kowalski, A. S., Martin, P. H., Berbigier, P., Bernhofer, C., Clement, R., Elbers, J., Granier, A., Grünwald, T., Morgenstern, K., Pilegaard, K., Rebmann, C., Snijders, W., Valentini, R., and Vesala, T.: Estimates of the Annual Net Carbon and Water Exchange of Forests: The EUROFLUX Methodology, Adv. Ecol. Res., 30, 113–175, https://doi.org/10.1016/S00652504(08)60018-5, 1999.

Aubinet, M., Vesala, T., and Papale, D. (Eds.): Eddy Covariance: A Practical Guide to Measurement and Data Analysis, Springer Science+Business Media B.V., Dordrecht, the Netherlands, 2012.

Baldocchi, D., Falge, E., Gu, L., Olson, R., Hollinger, D., Running, S., Anthoni, P., Bernhofer, C., Davis, K., Evans, R., Fuentes, J., Goldstein, A., Katul, G., Law, B., Lee, X., Malhi, Y., Meyers, T., Munger, W., Oechel, W., Paw, K. T., Pilegaard, K., Schmid, H. P., Valentini, R., Verma, S., Vesala, T., Wilson, K., and Wofsy, S.: FLUXNET: A New Tool to Study the Temporal and Spatial Variability of Ecosystem–Scale Carbon Dioxide, Water Vapor, and Energy Flux Densities, B. Am. Meteorol. Soc., 82, 2415–2434, https://doi.org/10.1175/15200477(2001)082<2415:Fantts>2.3.Co;2, 2001.

Baldocchi, D. D.: Assessing the eddy covariance technique for evaluating carbon dioxide exchange rates of ecosystems: past, present and future, Glob. Change Biol., 9, 479–492, https://doi.org/10.1046/j.1365-2486.2003.00629.x, 2003.

Barr, A., Richardson, A., Hollinger, D., Papale, D., Arain, M., Black, T., Bohrer, G., Dragoni, D., Fischer, M., Gu, L., Law, B., Margolis, H., McCaughey, J., Munger, J., Oechel, W., and Schaeffer, K.: Use of change-point detection for friction–velocity threshold evaluation in eddy-covariance studies, Agr. Forest Meteorol., 171–172, 31–45, https://doi.org/10.1016/j.agrformet.2012.11.023, 2013.

Beudert, B. and Breit, W.: Integrated Monitoring Programm an der Meßstelle Forellenbach im Nationalpark Bayerischer Wald, Untersuchungen zum Stickstoffeintrag und zum wassergebundenen Stickstoffhaushalt des Forellenbachgebiets, Förderkennzeichen 351 01 012. Nationalparkverwaltung Bayerischer Wald, Sachgebiet IV, technical report, Umweltbundesamt, Dessau-Roßlau, Germany, available at: https://www.umweltbundesamt.de/sites/default/files/medien/370/dokumente/ece_im_forellenbach_berichtsjahr_2009.pdf (last access: 8 December 2021), 2010.

Beudert, B. and Breit, W.: Kronenraumbilanzen zur Abschätzung der Stickstoffgesamtdeposition in Waldökosysteme des Nationalparks Bayerischer Wald, techninal report, Umweltbundesamt, Dessau-Roßlau, Germany, available at: https://www.umweltbundesamt.de/sites/default/files/medien/370/dokumente/kronenraumbilanzen_stickstoffgesamtdeposition_nationalpark_bayerisches_wald_-_berichtsjahr_2013_im_forellenbach.pdf (last access: 8 December 2021), 2014.

Beudert, B., Bernsteinová, J., Premier, J., and Bässler, C.: Natural disturbance by bark beetle offsets climate change effects on streamflow in headwater catchments of the Bohemian Forest, Silva Gabreta, 24, 21–45, available at: https://www.npsumava.cz/ wp-content/uploads/2019/06/2_sg_24_beudertetal.pdf (last access: 8 December 2021), 2018.

Bobbink, R. and Hettelingh, J.-P.: Review and revision of empirical critical loads and dose-response relationships, Tech. Rep. RIVM report 680359002, National Institute for Public Health and the Environment (RIVM), available at: https://www.rivm.nl/ bibliotheek/rapporten/680359002.pdf (last access: 8 December 2021), 2011.

Bokhorst, S., Metcalfe, D. B., and Wardle, D. A.: Reduction in snow depth negatively affects decomposers but impact on decomposition rates is substrate dependent, Soil Biol. Biochem., 62, 157– 164, https://doi.org/10.1016/j.soilbio.2013.03.016, 2013.

Breuninger, C., Meixner, F. X., and Kesselmeier, J.: Field investigations of nitrogen dioxide (NO_2) exchange between plants and the atmosphere, Atmos. Chem. Phys., 13, 773–790, https://doi.org/10.5194/acp-13-773-2013, 2013.

Brümmer, C., Marx, O., Kutsch, W., Ammann, C., Wolff, V., Flechard, C. R., and Freibauer, A.: Fluxes of total reactive atmospheric nitrogen (ΣN_r) using eddy covariance above arable land, Tellus B, 65, 19770, https://doi.org/10.3402/tellusb.v65i0.19770, 2013.

Brümmer, C., Rüffer, J. J., Delorme, J.-P., Wintjen, P., Schrader, F., Beudert, B., Schaap, M., and Ammann, C.: Reactive nitrogen fluxes over peatland (Bourtanger Moor) and forest (Bavarian Forest National Park) using micrometeorological measurement techniques, Zenodo [data set], https://doi.org/10.5281/zenodo.4513854, 2022.

Burba, G.: Eddy Covariance Method for Scientific, Industrial, Agricultural and Regulatory Applications: A Field Book on Measuring Ecosystem Gas Exchange and Areal Emission Rates, LICOR Biosciences, Lincoln, Nebraska, USA, 2013.

Civerolo, K. L. and Dickerson, R. R.: Nitric oxide soil emissions from tilled and untilled cornfields, Agr. Forest Meteorol., 90, 307–311, https://doi.org/10.1016/S0168-1923(98)00056-2, 1998.

Dämmgen, U., Thöni, L., Lumpp, R., Gilke, K., Seitler, E., and Bullinger, M.: Feldexperiment zum Methodenvergleich von Ammoniak- und Ammonium-Konzentrationsmessungen in der Umgebungsluft, 2005 bis 2008 in Braunschweig, vol. 337 of Landbauforschung: Sonderheft, Johann Heinrich von Thünen Institut, Braunschweig, jahresberichtskategorie: 10-M4;10-3, available at: https://www.openagrar.de/receive/timport_mods_ 00006160 (last access: 21 January 2022), 2010.

Delany, A. C., Fitzjarrald, D. R., Lenschow, D. H., Pearson, R., Wendel, G. J., and Woodrufl, B.: Direct measurements of nitrogen oxides and ozone fluxes over grassland, J. Atmos. Chem., 4, 429–444, https://doi.org/10.1007/BF00053844, 1986.

Delaria, E. R., Vieira, M., Cremieux, J., and Cohen, R. C.: Measurements of NO and NO_2 exchange between the atmosphere and *Quercus agrifolia*, Atmos. Chem. Phys., 18, 14161–14173, https://doi.org/10.5194/acp-18-14161-2018, 2018.

Delaria, E. R., Place, B. K., Liu, A. X., and Cohen, R. C.: Laboratory measurements of stomatal NO2 deposition to native California trees and the role of forests in the NO_x cycle, Atmos. Chem. Phys., 20, 14023–14041, https://doi.org/10.5194/acp-20-140232020, 2020.

Donateo, A. and Contini, D.: Correlation of Dry Deposition Velocity and Friction Velocity over Different Surfaces for $PM_{2.5}$ and Particle Number Concentrations, Adv. Meteorol., 2014, 1– 12, https://doi.org/10.1155/2014/760393, 2014.

Erisman, J. W. and Wyers, G. P.: Continuous measurements of surface exchange of SO_2 and NH_3; Implications for their possible interaction in the deposition process, Atmos. Environ. A-Gen., 27, 1937–1949, https://doi.org/10.1016/0960-1686(93)90266-2, 1993.

Erisman, J. W., Mennen, M. G., Fowler, D., Flechard, C. R., Spindler, G., Grüner, A., Duyzer, J. H., Ruigrok, W., and Wyers, G. P.: Towards development of a deposition monitoring network for air pollution in Europe, resreport Report no. 722108015, RIVM, the Netherlands, available at: https://rivm.openrepository.com/ bitstream/handle/10029/10432/722108015.pdf;jsessionid= 532211C11FE7D0487F070927B24AE8ED?sequence=1 (last access: 8 December 2021), 1996.

Erisman, J. W., Galloway, J. N., Seitzinger, S., Bleeker, A., Dise, N. B., Petrescu, A. M., Leach, A. M., and de Vries, W.: Consequences of human modification of the global nitrogen cycle, Philos. T. R. Soc. B, 368, 20130116, https://doi.org/10.1098/rstb.2013.0116, 2013.

Eugster, W. and Hesterberg, R.: Transfer resistances of NO_2 determined from eddy correlation flux measurements over a litter meadow at a rural site on the swiss plateau, Atmos. Environ., 30, 307–311, https://doi.org/10.1016/1352-2310(95)00418-1, 1996.

Falge, E., Baldocchi, D., Olson, R., Anthoni, P., Aubinet, M., Bernhofer, C., Burba, G., Ceulemans, R., Clement, R., Dolman, H., Granier, A., Gross, P., Grünwald, T., Hollinger, D., Jensen, N.-O., Katul, G., Keronen, P., Kowalski, A., Lai, C. T., Law, B. E., Meyers, T., Moncrieff, J., Moors, E., Munger, J., Pilegaard, K., Üllar Rannik, Rebmann, C., Suyker, A., Tenhunen, J., Tu, K., Verma, S., Vesala, T., Wilson, K., and Wofsy, S.: Gap filling strategies for defensible annual sums of net ecosystem exchange, Agr. Forest Meteorol., 107, 43–69, https://doi.org/10.1016/S0168-1923(00)00225-2, 2001.

Famulari, D., Fowler, D., Hargreaves, K., Milford, C., Nemitz, E., Sutton, M. A., and Weston, K.: Measuring Eddy Covariance Fluxes of Ammonia Using Tunable Diode Laser Absorption Spectroscopy, Water, Air, and Soil Pollution: Focus, 4, 151–158, https://doi.org/10.1007/s11267-004-3025-1, 2004.

Farmer, D. K. and Cohen, R. C.: Observations of HNO_3, Σ AN, Σ PN and NO_2 fluxes: evidence for rapid HO_x chemistry within a pine forest canopy, Atmos. Chem. Phys., 8, 3899–3917, https://doi.org/10.5194/acp-8-3899-2008, 2008.

Farmer, D. K., Wooldridge, P. J., and Cohen, R. C.: Application of thermal-dissociation laser induced fluorescence (TD-LIF)

to measurement of HNO_3, Σ alkyl nitrates, Σ peroxy nitrates, and NO_2 fluxes using eddy covariance, Atmos. Chem. Phys., 6, 3471–3486, https://doi.org/10.5194/acp-6-3471-2006, 2006.

Farmer, D. K., Kimmel, J. R., Phillips, G., Docherty, K. S., Worsnop, D. R., Sueper, D., Nemitz, E., and Jimenez, J. L.: Eddy covariance measurements with high-resolution time-of-flight aerosol mass spectrometry: a new approach to chemically resolved aerosol fluxes, Atmos. Meas. Tech., 4, 1275–1289, https://doi.org/10.5194/amt-4-1275-2011, 2011. Ferm, M.: A Sensitive Diffusional Sampler, Report L91-172, Swedish Environmental Research Institute, Gothenburg, 1991.

Ferrara, R. M., Loubet, B., Di Tommasi, P., Bertolini, T., Magliulo, V., Cellier, P., Eugster, W., and Rana, G.: Eddy covariance measurement of ammonia fluxes: Comparison of high frequency correction methodologies, Agr. Forest Meteorol., 158–159, 30– 42, https://doi.org/10.1016/j.agrformet.2012.02.001, 2012.

Ferrara, R. M., Di Tommasi, P., Famulari, D., and Rana, G.: Limitations of an Eddy-Covariance System in Measuring Low Ammonia Fluxes, Bound.-Lay. Meteorol., 180, 173–186, https://doi.org/10.1007/s10546-021-00612-6, 2021.

Finkelstein, P. L. and Sims, P. F.: Sampling error in eddy correlation flux measurements, J. Geophys. Res.-Atmos., 106, 3503–3509, https://doi.org/10.1029/2000JD900731, 2001.

Flechard, C. R., Nemitz, E., Smith, R. I., Fowler, D., Vermeulen, A. T., Bleeker, A., Erisman, J. W., Simpson, D., Zhang, L., Tang, Y. S., and Sutton, M. A.: Dry deposition of reactive nitrogen to European ecosystems: a comparison of inferential models across the NitroEurope network, Atmos. Chem. Phys., 11, 2703–2728, https://doi.org/10.5194/acp-112703-2011, 2011.

Flechard, C. R., Massad, R.-S., Loubet, B., Personne, E., Simpson, D., Bash, J. O., Cooter, E. J., Nemitz, E., and Sutton, M. A.: Advances in understanding, models and parameterizations of biosphere-atmosphere ammonia exchange, Biogeosciences, 10, 5183–5225, https://doi.org/10.5194/bg-10-5183-2013, 2013.

Flechard, C. R., Ibrom, A., Skiba, U. M., de Vries, W., van Oijen, M., Cameron, D. R., Dise, N. B., Korhonen, J. F. J., Buchmann, N., Legout, A., Simpson, D., Sanz, M. J., Aubinet, M., Loustau, D., Montagnani, L., Neirynck, J., Janssens, I. A., Pihlatie, M., Kiese, R., Siemens, J., Francez, A.-J., Augustin, J., Varlagin, A., Olejnik, J., Juszczak, R., Aurela, M., Berveiller, D., Chojnicki, B. H., Dämmgen, U., Delpierre, N., Djuricic, V., Drewer, J., Dufrêne, E., Eugster, W., Fauvel, Y., Fowler, D., Frumau, A., Granier, A., Gross, P., Hamon, Y., Helfter, C., Hensen, A., Horváth, L., Kitzler, B., Kruijt, B., Kutsch, W. L., Lobo-do-Vale, R., Lohila, A., Longdoz, B., Marek, M. V., Matteucci, G., Mitosinkova, M., Moreaux, V., Neftel, A., Ourcival, J.-M., Pilegaard, K., Pita, G., Sanz, F., Schjoerring, J. K., Sebastià, M.-T., Tang, Y. S., Uggerud, H., Urbaniak, M., van Dijk, N., Vesala, T., Vidic, S., Vincke, C., Weidinger, T., Zechmeister-Boltenstern, S., Butterbach-Bahl, K., Nemitz, E., and Sutton, M. A.: Carbon–nitrogen interactions in European forests and semi-natural vegetation – Part 1: Fluxes and budgets of carbon, nitrogen and greenhouse gases from ecosystem monitoring and modelling, Biogeosciences, 17, 1583–1620, https://doi.org/10.5194/bg-17-1583-2020, 2020.

Gallagher, M., Beswick, K., Duyzer, J., Westrate, H., Choularton, T., and Hummelshøj, P.: Measurements of aerosol fluxes to speulder forest using a micrometeorological technique, Atmos. Environ., 31, 359–373, https://doi.org/10.1016/S13522310(96)00057-X, 1997.

Galloway, J. N., Aber, J. D., Erisman, J. W., Seitzinger, S. P., Howarth, R. W., Cowling, E. B., and Cosby, B. J.: The Nitrogen Cascade, Bio-Science, 53, 341–356, https://doi.org/10.1641/00063568(2003)053[0341:TNC]2.0.CO;2, 2003.

Ge, X., Schaap, M., Kranenburg, R., Segers, A., Reinds, G. J., Kros, H., and de Vries, W.: Modeling atmospheric ammonia using agricultural emissions with improved spatial variability and temporal dynamics, Atmos. Chem. Phys., 20, 16055–16087, https://doi.org/10.5194/acp-20-16055-2020, 2020.

Geddes, J. A. and Murphy, J. G.: Observations of reactive nitrogen oxide fluxes by eddy covariance above two midlatitude North American mixed hardwood forests, Atmos. Chem. Phys., 14, 2939–2957, https://doi.org/10.5194/acp-14-2939-2014, 2014.

Hansen, K., Sørensen, L. L., Hertel, O., Geels, C., Skjøth, C. A., Jensen, B., and Boegh, E.: Ammonia emissions from deciduous forest after leaf fall, Biogeosciences, 10, 4577–4589, https://doi.org/10.5194/bg-10-4577-2013, 2013.

Hansen, K., Pryor, S. C., Boegh, E., Hornsby, K. E., Jensen, B., and Sorensen, L. L.: Background concentrations and fluxes of atmospheric ammonia over a deciduous forest, Agr. Forest Meteorol., 214–215, 380–392, https://doi.org/10.1016/j.agrformet.2015.09.004, 2015.

Heiskanen, J., Brümmer, C., Buchmann, N., Calfapietra, C., Chen, H., Gielen, B., Gkritzalis, T., Hammer, S., Hartman, S., Herbst, M., Janssens, I., Jordan, A., Juurola, E., Karstens, U., Kasurinen, V., Kruijt, B., Lankreijer, H., Levin, I., Linderson, M.-L., Loustau, D., Merbold, L., Lund Myhre, C., Papale, D., Pavelka, M., Pilegaard, K., Ramonet, M., Rebmann, C., Rinne, J., Rivier, L., Saltikoff, E., Sanders, R., Steinbacher, M., Steinhoff, T., Watson, A., Vermeulen, A., Vesala, T., Vítková, G., and Kutsch, W.: The Integrated Carbon Observation System in Europe, B. Am. Meteorol. Soc., 1–54, https://doi.org/10.1175/BAMS-D-19-0364.1, 2021.

Högberg, P.: Nitrogen impacts on forest carbon, Nature, 447, 781– 782, https://doi.org/10.1038/447781a, 2007.

Hollinger, D. Y. and Richardson, A. D.: Uncertainty in eddy covariance measurements and its application to physiological models, Tree Physiol., 25, 873–885, https://doi.org/10.1093/treephys/25.7.873, 2005.

Horii, C. V., Munger, J. W., Wofsy, S. C., Zahniser, M., Nelson, D., and McManus, J. B.: Fluxes of nitrogen oxides over a temperate deciduous forest, J. Geophys. Res.-Atmos., 109, D08305, https://doi.org/10.1029/2003JD004326, 2004.

Horii, C. V., Munger, J. W., Wofsy, S. C., Zahniser, M., Nelson, D., and McManus, J. B.: Atmospheric reactive nitrogen concentration and flux budgets at a Northeastern US forest site, Agr. Forest Meteorol., 136, 159–174, https://doi.org/10.1016/j.agrformet.2006.03.005, 2006.

Hurkuck, M., Brümmer, C., Mohr, K., Grünhage, L., Flessa, H., and Kutsch, W. L.: Determination of atmospheric nitrogen deposition to a semi-natural peat bog site in an intensively managed agricultural landscape, Atmos. Environ., 97, 296–309, https://doi.org/10.1016/j.atmosenv.2014.08.034, 2014.

Ibrom, A., Dellwick, E., Flyvbjerg, H., Jensen, N. O., and Pilegaard, K.: Strong low-pass filtering effects on water vapour flux measurements with closed-path eddy correlation systems, Agr. Forest Meteorol., 147, 140–156, https://doi.org/10.1016/j.agrformet.2007.07.007, 2007.

Jarraud, M.: Guide to meteorological instruments and methods of observation (WMO-No. 8), World Meteorological Organization, Geneva, Switzerland, 2008.

Jarvis, P. G.: The Interpretation of the Variations in Leaf Water Potential and Stomatal Conductance Found in Canopies in the Field, Philos. T. R. Soc. B, 273, 593–610, https://doi.org/10.1098/rstb.1976.0035, 1976.

Jensen, N. and Hummelshøj, P.: Derivation of canopy resistance for water vapor fluxes over a spruce forest, using a new technique for the viscous sublayer resistance (correction to vol. 73, p. 339, 1995), Agr. Forest Meteorol., 85, 289, https://doi.org/10.1016/S0168-1923(97)00024-5, 1997.

Jensen, N. O. and Hummelshøj, P.: Derivation of canopy resistance for water-vapor fluxes over a spruce forest, using a new technique for the viscous sublayer resistance, Agr. Forest Meteorol., 73, 339–352, https://doi.org/10.1016/0168 1923(94)05083-I, 1995.

Kolle, O. and Rebmann, C.: EddySoft Documentation of a Software Package to Acquire and Process Eddy Covariance Data, techreport, MPI-BGC, available at: https://repository.publisso. de/resource/frl:4414276-1/data (last access: 21 January 2022), 2007.

Kreyling, J., Haei, M., and Laudon, H.: Snow removal reduces annual cellulose decomposition in a riparian boreal forest, Can. J. Soil Sci., 93, 427–433, https://doi.org/10.4141/CJSS2012-025, 2013.

Krupa, S. V.: Effects of atmospheric ammonia (NH_3) on terrestrial vegetation: a review, Environ. Pollut., 124, 179–221, https://doi.org/10.1016/S0269-7491(02)00434-7, 2003.

Kundu, S., Kawamura, K., and Lee, M.: Seasonal variation of the concentrations of nitrogenous species and their nitrogen isotopic ratios in aerosols at Gosan, Jeju Island: Implications for atmospheric processing and source changes of aerosols, J. Geophys. Res.-Atmos., 115, D20305, https://doi.org/10.1029/2009JD013323, 2010.

Langford, B., Acton, W., Ammann, C., Valach, A., and Nemitz, E.: Eddy-covariance data with low signal-to-noise ratio: time-lag determination, uncertainties and limit of detection, Atmos. Meas. Tech., 8, 4197–4213, https://doi.org/10.5194/amt-8-4197-2015, 2015.

Lavi, A., Farmer, D., Segre, E., Moise, T., Rotenberg, E., Jimenez, J. L., and Rudich, Y.: Fluxes of Fine Particles Over a Semi-Arid Pine Forest: Possible Effects of a Complex Terrain, Aerosol Sci. Tech., 47, 906–915, https://doi.org/10.1080/02786826.2013.800940, 2013.

Lee, T., Yu, X.-Y., Ayres, B., Kreidenweis, S. M., Malm, W. C., and Collett, J. L.: Observations of fine and coarse particle nitrate at several rural locations in the United States, Atmos. Environ., 42, 2720–2732, https://doi.org/10.1016/j.atmosenv.2007.05.016, vienna Visibility Conference 2006, 2008.

Lenshow, D. H. and Raupach, M. R.: The attenuation of fluctuations in scalar concentrations through sampling tubes, J. Geophys. Res., 96, 15259–15268, https://doi.org/10.1029/91JD01437, 1991.

Li, Y., Aneja, V. P., Arya, S. P., Rickman, J., Brittig, J., Roelle, P., and Kim, D. S.: Nitric oxide emission from intensively managed agricultural soil in North Carolina, J. Geophys. Res.-Atmos., 104, 26115–26123, https://doi.org/10.1029/1999JD900336, 1997.

Loescher, H. W., Law, B. E., Mahrt, L., Hollinger, D. Y., Campbell, J., and Wofsy, S. C.: Uncertainties in, and interpretation of, carbon flux estimates using the eddy covariance technique, J. Geophys. Res.-Atmos., 111, D21S90, https://doi.org/10.1029/2005JD006932, 2006.

LTER: Long Term Ecological Research (LTER) network, available at: https://deims.org/993ed2fc-1cb0-4810-a619 8bcf78b6ecee, last access: 8 December 2021.

Magnani, F., Mencuccini, M., Borghetti, M., Berbigier, P., Berninger, F., Delzon, S., Grelle, A., Hari, P., Jarvis, P. G., Kolari, P., Kowalski, A. S., Lankreijer, H., Law, B. E., Lindroth, A., Loustau, D., Manca, G., Moncrieff, J. B., Rayment, M., Tedeschi, V., Valentini, R., and Grace, J.: The human footprint in the carbon cycle of temperate and boreal forests, Nature, 447, 848–850, https://doi.org/10.1038/nature05847, 2007.

Marx, O., Brümmer, C., Ammann, C., Wolff, V., and Freibauer, A.: TRANC – a novel fast-response converter to measure total reactive atmospheric nitrogen, Atmos. Meas. Tech., 5, 1045–1057, https://doi.org/10.5194/amt-5-1045-2012, 2012.

Massman, W. J.: The attenuation of concentration fluctuations in turbulent flow through a tube, J. Geophys. Res., 96, 15269–15274, https://doi.org/10.1029/91JD01514, 1991.

Mauder, M. and Foken, T.: Impact of post-field data processing on eddy covariance flux estimates and energy balance closure, Meteorol. Z., 15, 597–609, https://doi.org/10.1127/09412948/2006/0167, 2006.

Medinets, S., Gasche, R., Skiba, U., Schindlbacher, A., Kiese, R., and Butterbach-Bahl, K.: Cold season soil NO fluxes from a temperate forest: drivers and contribution to annual budgets, Environ. Res. Lett., 11, 114012, https://doi.org/10.1088/17489326/11/11/114012, 2016.

Milford, C., Hargreaves, K. J., Sutton, M. A., Loubet, B., and Cellier, P.: Fluxes of NH3 and CO2 over upland moorland in the vicinity of agricultural land, J. Geophys. Res.-Atmos., 106, 24169–24181, https://doi.org/10.1029/2001jd900082, 2001.

Min, K.-E., Pusede, S. E., Browne, E. C., LaFranchi, B. W., and Cohen, R. C.: Eddy covariance fluxes and vertical concentration gradient measurements of NO and NO_2 over a ponderosa pine ecosystem: observational evidence for within-canopy chemical removal of NO_x, Atmos. Chem. Phys., 14, 5495–5512, https://doi.org/10.5194/acp-14-5495-2014, 2014.

Moffat, A. M., Papale, D., Reichstein, M., Hollinger, D. Y., Richardson, A. D., Barr, A. G., Beckstein, C., Braswell, B. H., Churkina, G., Desai, A. R., Falge, E., Gove, J. H., Heimann, M., Hui, D. F., Jarvis, A. J., Kattge, J., Noormets, A., and Stauch, V. J.: Comprehensive comparison of gap-filling techniques for eddy covariance net carbon fluxes, Agr. Forest Meteorol., 147, 209–232, https://doi.org/10.1016/j.agrformet.2007.08.011, 2007.

Moncrieff, J., Clement, R., Finnigan, J., and Meyers, T.: Averaging, Detrending, and Filtering of Eddy Covariance Time Series, Kluwer Academic, Dordrecht, 7–31, https://doi.org/10.1007/14020-2265-4_2, 2004.

Moncrieff, J. B., Massheder, J. M., deBruin, H., Elbers, J., Friborg, T., Heusinkveld, B., Kabat, P., Scott, S., Soegaard, H., and Verhoef, A.: A system to measure surface fluxes of momentum, sensible heat, water vapour and carbon dioxide, J. Hydrol., 188, 589–611, https://doi.org/10.1016/S0022-1694(96)03194-0, 1997.

Moravek, A., Singh, S., Pattey, E., Pelletier, L., and Murphy, J. G.: Measurements and quality control of ammonia eddy covariance fluxes: a new strategy for high-frequency attenuation correction, Atmos. Meas. Tech., 12, 6059–6078, https://doi.org/10.5194/amt-12-6059-2019, 2019.

Munger, J. W., Wofsy, S. C., Bakwin, P. S., Fan, S. M., Goulden, M. L., Daube, B. C., Goldstein, A. H., Moore, K. E., and Fitzjarrald, D. R.: Atmospheric deposition of reactive nitrogen oxides and ozone in a temperate deciduous forest and a subarctic woodland: 1. Measurements and mechanisms, J. Geophys. Res.-Atmos., 101, 12639–12657, https://doi.org/10.1029/96JD00230, 1996.

Munger, J. W., Fan, S.-M., Bakwin, P. S., Goulden, M. L., Goldstein, A. H., Colman, A. S., and Wofsy, S. C.: Regional budgets for nitrogen oxides from continental sources: Variations of rates for oxidation and deposition with season and distance from source regions, J. Geophys. Res.-Atmos., 103, 8355–8368, https://doi.org/10.1029/98JD00168, 1998.

Neirynck, J., Kowalski, A. S., Carrara, A., Genouw, G., Berghmans, P., and Ceulemans, R.: Fluxes of oxidised and reduced nitrogen above a mixed coniferous forest exposed to various nitrogen emission sources, Environ. Pollut., 149, 31–43, https://doi.org/10.1016/j.envpol.2006.12.029, 2007.

Nemitz, E., Jimenez, J. L., Huffman, J. A., Ulbrich, I. M., Canagaratna, M. R., Worsnop, D. R., and Guenther, A. B.: An Eddy-Covariance System for the Measurement of Surface/Atmosphere Exchange Fluxes of Submicron Aerosol Chemical Species–First Application Above an Urban Areas, Aerosol Sci. Tech., 42, 636–657, https://doi.org/10.1080/02786820802227352, 2008.

Pastorello, G., Trotta, C., and Canfora, E. e. a.: The FLUXNET2015 dataset and the ONEFlux processing pipeline for eddy covariance data, Scientific Data, 7, 225, https://doi.org/10.1038/s41597020-0534-3, 2020.

Paulson, C. A.: The Mathematical Representation of Wind Speed and Temperature Profiles in the Unstable Atmospheric Surface Layer, J. Appl. Meteorol., 9, 857–861, https://doi.org/10.1175/15200450(1970)009<0857:Tmrows>2.0.Co;2, 1970.

Peake, E. and Legge, A. H.: Evaluation of methods used to collect air quality data at remote and rural sites in Alberta, Canada, in: Proc. 1987 EPA/APCA Symposium on Measurements of Toxic and Related Air Pollutants, APCA, Research Triangle Park, North Carolina (NC), 3–6 May 1987, 174–182, 1987.

Peake, M.: A Preliminary Report on the Design and Testing of the KAPS (Kananaskis Atmospheric Pollutant Sampler) for the Collection of Acidic and Basic Gases and Fine Particles, Document 0012e/July 8/85, Typskript University Calgary, 1985.

Pryor, S. and Klemm, O.: Experimentally derived estimates of nitric acid dry deposition velocity and viscous sub-layer resistance at a conifer forest, Atmos. Environ., 38, 2769–2777, https://doi.org/10.1016/j.atmosenv.2004.02.038, 2004.

Putaud, J.-P., Van Dingenen, R., Alastuey, A., Bauer, H., Birmili, W., Cyrys, J., Flentje, H., Fuzzi, S., Gehrig, R., Hansson, H., Harrison, R., Herrmann, H., Hitzenberger, R., Hüglin, C., Jones, A., Kasper-Giebl, A., Kiss, G., Kousa, A., Kuhlbusch, T., Löschau, G., Maenhaut, W., Molnar, A., Moreno, T., Pekkanen, J., Perrino, C., Pitz, M., Puxbaum, H., Querol, X., Rodriguez, S., Salma, I., Schwarz, J., Smolik, J., Schneider, J., Spindler, G., ten Brink, H., Tursic, J., Viana, M., Wiedensohler, A., and Raes, F.: A European aerosol phenomenology – 3: Physical and chemical characteristics of particulate matter from 60 rural, urban, and kerbside sites across Europe, Atmos. Environ., 44, 1308–1320, https://doi.org/10.1016/j.atmosenv.2009.12.011, 2010.

Reichstein, M., Falge, E., Baldocchi, D., Papale, D., Aubinet, M., Berbigier, P., Bernhofer, C., Buchmann, N., Gilmanov, T., Granier, A., Grünwald, T., Havránková, K., Ilvesniemi, H., Janous, D., Knohl, A., Laurila, T., Lohila, A., Loustau, D., Matteucci, G., Meyers, T., Miglietta, F., Ourcival, J.-M., Pumpanen, J., Rambal, S., Rotenberg, E., Sanz, M., Tenhunen, J., Seufert, G., Vaccari, F., Vesala, T., Yakir, D., and Valentini, R.: On the separation of net ecosystem exchange into assimilation and ecosystem respiration: review and improved algorithm, Glob. Change Biol., 11, 1424–1439, https://doi.org/10.1111/j.1365-2486.2005.001002.x, 2005.

Rondon, A., Johansson, C., and Granat, L.: Dry Deposition of Nitrogen-Dioxide and Ozone to Coniferous Forests, J. Geophys. Res.-Atmos., 98, 5159–5172, https://doi.org/10.1029/92jd02335, 1993.

Rummel, U., Ammann, C., Gut, A., Meixner, F. X., and Andreae, M. O.: Eddy covariance measurements of nitric oxide flux within an Amazonian rain forest, J. Geophys. Res.-Atmos., 107, LBA 17-1–LBA 17-9, https://doi.org/10.1029/2001JD000520, 2002.

Saccone, P., Morin, S., Baptist, F., Bonneville, J.-M., Colace, M.P., Domine, F., Faure, M., Geremia, R., Lochet, J., Poly, F., Lavorel, S., and Clèment, J.-C.: The effects of snowpack properties and plant strategies on litter decomposition during winter in subalpine meadows, Plant Soil, 363, 215–229, https://doi.org/10.1007/s11104-012-1307-3, 2013.

Schaap, M., Müller, K., and ten Brink, H.: Constructing the European aerosol nitrate concentration field from quality analysed data, Atmos. Environ., 36, 1323–1335, https://doi.org/10.1016/S1352-2310(01)00556-8, 2002.

Schaap, M., Spindler, G., Schulz, M., Acker, K., Maenhaut, W., Berner, A., Wieprecht, W., Streit, N., Müller, K., Brüggemann, E., Chi, X., Putaud, J.-P., Hitzenberger, R., Puxbaum, H., Baltensperger, U., and ten Brink, H.: Artefacts in the sampling of nitrate studied in the "INTERCOMP" campaigns of EUROTRAC-AEROSOL, Atmos. Environ., 38, 6487–6496, https://doi.org/10.1016/j.atmosenv.2004.08.026, 2004.

Schrader, F. and Brümmer, C.: Land Use Specific Ammonia Deposition Velocities: a Review of Recent Studies (2004–2013), Water Air Soil Poll., 225, 2114, https://doi.org/10.1007/s11270-0142114-7, 2014.

Schwarz, J., Cusack, M., Karban, J., Chalupnícková,˘ E., Havránek, V., Smolík, J., and Ždímal, V.: PM2.5 chemical composition at a rural background site in Central Europe, including correlation and air mass back trajectory analysis, Atmos. Res., 176–177, 108–120, https://doi.org/10.1016/j.atmosres.2016.02.017, 2016.

Seinfeld, J. H. and Pandis, S. N.: Atmospheric Chemistry and Physics – From Air Pollution to Climate Change, 2 edn., John Wiley and Sons, New York, USA, 2006.

Seok, B., Helmig, D., Ganzeveld, L., Williams, M. W., and Vogel, C. S.: Dynamics of nitrogen oxides and ozone above and within a mixed hardwood forest in northern Michigan, Atmos. Chem. Phys., 13, 7301–7320, https://doi.org/10.5194/acp-137301-2013, 2013.

Staelens, J., De Schrijver, A., Van Avermaet, P., Genouw, G., and Verhoest, N.: A comparison of bulk and wet-only deposition at two adjacent sites in Melle (Belgium), Atmos. Environ., 39, 7– 15, https://doi.org/10.1016/j.atmosenv.2004.09.055, 2005.

Stella, P., Kortner, M., Ammann, C., Foken, T., Meixner, F. X., and Trebs, I.: Measurements of nitrogen oxides and ozone fluxes by eddy covariance at a meadow: evidence for an internal leaf resistance to NO_2, Biogeosciences, 10, 5997–6017, https://doi.org/10.5194/bg-10-5997-2013, 2013.

Sutton, M. A., Tang, Y. S., Miners, B., and Fowler, D.: A New Diffusion Denuder System for Long-Term, Regional Monitoring of Atmospheric Ammonia and Ammonium, Water, Air and Soil Pollution: Focus, 1, 145–156, https://doi.org/10.1023/a:1013138601753, 2001.

Sutton, M. A., Simpson, D., Levy, P. E., Smith, R. I., Reis, S., van Oijen, M., and de Vries, W.: Uncertainties in the relationship between atmospheric nitrogen deposition and forest carbon sequestration, Glob. Change Biol., 14, 2057–2063, https://doi.org/10.1111/j.1365-2486.2008.01636.x, 2008.

Sutton, M. A., Howard, C. M., Erisman, J. W., Billen, G., Bleeker, A., Grennfelt, P., van Grinsven, H., and Grizzetti, B. (Eds.): The European Nitrogen Assessment: sources, effects and policy perspectives, Cambridge University Press, Cambridge, UK, 2011.

Sutton, M. A., Reis, S., Riddick, S. N., Dragosits, U., Nemitz, E., Theobald, M. R., Tang, Y. S., Braban, C. F., Vieno, M., Dore, A. J., Mitchell, R. F., Wanless, S., Daunt, F., Fowler, D., Blackall, T. D., Milford, C., Flechard, C. R., Loubet, B., Massad, R., Cellier, P., Personne, E., Coheur, P. F., Clarisse, L., Van Damme, M., Ngadi, Y., Clerbaux, C., Skjoth, C. A., Geels, C., Hertel, O., Wichink Kruit, R. J., Pinder, R. W., Bash, J. O., Walker, J. T., Simpson, D., Horvath, L., Misselbrook, T. H., Bleeker, A., Dentener, F., and de Vries, W.: Towards a climate-dependent paradigm of ammonia emission and deposition, Philos. T. . Soc. B, 368, 20130166, https://doi.org/10.1098/rstb.2013.0166, 2013.

Tang, Y. S., Simmons, I., van Dijk, N., Di Marco, C., Nemitz, E., Dämmgen, U., Gilke, K., Djuricic, V., Vidic, S., Gliha, Z., Borovecki, D., Mitosinkova, M., Hanssen, J. E., Uggerud, T. H.,
Sanz, M. J., Sanz, P., Chorda, J. V., Flechard, C. R., Fauvel, Y., Ferm, M., Perrino, C., and Sutton, M. A.: European scale application of atmospheric reactive nitrogen measurements in a low-cost approach to infer dry deposition fluxes, Agr. Ecosyst. Environ., 133, 183–195, https://doi.org/10.1016/j.agee.2009.04.027, 2009.

Tang, Y. S., Cape, J. N., Braban, C. F., Twigg, M. M., Poskitt, J., Jones, M. R., Rowland, P., Bentley, P., Hockenhull, K., Woods, C., Leaver, D., Simmons, I., van Dijk, N., Nemitz, E., and Sutton, M. A.: Development of a new model DELTA sampler and assessment of potential sampling artefacts in the UKEAP AGANet DELTA system: summary and technical report, Tech. rep., London, available at: https://uk-air.defra.gov.uk/ library/reports?report_id=861 (last access: 8 December 2021), 2015.

Tang, Y. S., Flechard, C. R., Dämmgen, U., Vidic, S., Djuricic, V., Mitosinkova, M., Uggerud, H. T., Sanz, M. J., Simmons, I., Dragosits, U., Nemitz, E., Twigg, M., van Dijk, N., Fauvel, Y., Sanz, F., Ferm, M., Perrino, C., Catrambone, M., Leaver, D., Braban, C. F., Cape, J. N., Heal, M. R., and Sutton, M. A.: Pan-European rural monitoring network shows dominance of NH_3 gas and NH_4NO_3 aerosol in inorganic atmospheric pollution load, Atmos. Chem. Phys., 21, 875–914, https://doi.org/10.5194/acp-21-875-2021, 2021.

Thoene, B., Rennenberg, H., and Weber, P.: Absorption of atmospheric NO_2 by spruce (Picea abies) trees, New Phytol., 134, 257–266, https://doi.org/10.1111/j.1469-8137.1996.tb04630.x, 1996.

Trebs, I., Metzger, S., Meixner, F. X., Helas, G., Hoffer, A., Rudich, Y., Falkovich, A. H., Moura, M. A. L., da Silva Jr., R. S., Artaxo, P., Slanina, J., and Andreae, M. O.: The NH_4^+-NO_3^--Cl^--SO_4^{2-}-H_2O aerosol system and its gas phase precursors at a pasture site in the Amazon Basin: How relevant are mineral cations and soluble organic acids?, J. Geophys. Res.-Atmos., 110, D07303, https://doi.org/10.1029/2004JD005478, 2005.

UNECE: International Cooperative Program on Integrated Monitoring of Air pollution Effects on Ecosystems (ICP IM) within the framework of the Geneva Convention on Long-Range Transboundary, available at: http://www.unece.org/env/lrtap/, last access: 8 December 2021.

Van Oss, R., Duyzer, J., and Wyers, P.: The influence of gas-to-particle conversion on measurements of ammonia exchange over forest, Atmos. Environ., 32, 465–471, https://doi.org/10.1016/S1352-2310(97)00280-X, 1998.

van Zanten, M. C., Sauter, F. J., Wichink Kruit, R. J., van Jaarsveld, J. A., and van Pul, W. A. J.: Description of the DEPAC module; Dry deposition modeling with DEPAC_GCN2010, Tech. rep., RIVM, Bilthoven, NL, 2010.

Vickers, D. and Mahrt, L.: Quality Control and Flux Sampling Problems for Tower and Aircraft Data, J. Atmos. Ocean. Tech., 14, 512–526, https://doi.org/10.1175/15200426(1997)014<0512:QCAFSP>2.0.CO;2, 1997.

Webb, E. K.: Profile relationships: The log-linear range, and extension to strong stability, Q. J. Roy. Meteor. Soc., 96, 67–90, https://doi.org/10.1002/qj.49709640708, 1970.

Wentworth, G. R., Murphy, J. G., Benedict, K. B., Bangs, E. J., and Collett Jr., J. L.: The role of dew as a night-time reservoir and morning source for atmospheric ammonia, Atmos. Chem. Phys., 16, 7435–7449, https://doi.org/10.5194/acp-167435-2016, 2016.

Wesely, M. L.: Parameterization of Surface Resistances to Gaseous Dry Deposition in Regional-Scale Numerical-Models, Atmos. Environ., 23, 1293–1304, https://doi.org/10.1016/00046981(89)90153-4, 1989.

Whitehead, J. D., Twigg, M., Famulari, D., Nemitz, E., Sutton, M. A., Gallagher, M. W., and Fowler, D.: Evaluation of laser absorption spectroscopic techniques for eddy covariance flux measurements of ammonia, Environ. Sci. Technol., 42, 2041–6, https://doi.org/10.1021/es071596u, 2008.

Wilczak, J. M., Oncley, S. P., and Stage, S. A.: Sonic Anemometer Tilt Correction Algorithms, Bound.-Lay. Meteorol., 99, 127– 150, https://doi.org/10.1023/A:1018966204465, 2001.

Wintjen, P., Ammann, C., Schrader, F., and Brümmer, C.: Correcting high-frequency losses of reactive nitrogen flux measurements, Atmos. Meas. Tech., 13, 2923–2948, https://doi.org/10.5194/amt-13-2923-2020, 2020.

Wolff, V., Trebs, I., Foken, T., and Meixner, F. X.: Exchange of reactive nitrogen compounds: concentrations and fluxes of total ammonium and total nitrate above a spruce canopy, Biogeosciences, 7, 1729–1744, https://doi.org/10.5194/bg-7-1729-2010, 2010.

Wyers, G. and Duyzer, J.: Micrometeorological measurement of the dry deposition flux of sulphate and nitrate aerosols to coniferous forest, Atmos. Environ., 31, 333–343, https://doi.org/10.1016/S1352-2310(96)00188-4, 1997.

Wyers, G. P. and Erisman, J. W.: Ammonia exchange over coniferous forest, Atmos. Environ., 32, 441–451, https://doi.org/10.1016/S1352-2310(97)00275-6, 1998.

Yuvaraj, S., Fan-Yuan, L., Tsong-Huei, C., and Chuin-Tih, Y.: Thermal Decomposition of Metal Nitrates in Air and Hydrogen Environments, J. Phys. Chem B, 107, 1044–1047, https://doi.org/10.1021/jp026961c, 2003.

Zöll, U., Brümmer, C., Schrader, F., Ammann, C., Ibrom, A., Flechard, C. R., Nelson, D. D., Zahniser, M., and Kutsch, W. L.: Surface–atmosphere exchange of ammonia over peatland using QCL-based eddy-covariance measurements and inferential modeling, Atmos. Chem. Phys., 16, 11283–11299, https://doi.org/10.5194/acp-16-11283-2016, 2016.

Zöll, U., Lucas-Moffat, A. M., Wintjen, P., Schrader, F., Beudert, B., and Brümmer, C.: Is the biosphere-atmosphere exchange of total reactive nitrogen above forest driven by the same factors as carbon dioxide? An analysis using artificial neural networks, Atmos. Environ., 206, 108–118, https://doi.org/10.1016/j.atmosenv.2019.02.042, 2019.

4. Forest-atmosphere exchange of reactive nitrogen in a remote region – Part II: Modeling annual budgets

Abstract. To monitor the effect of current nitrogen emissions and mitigation strategies, total (wet+dry) atmospheric nitrogen deposition to forests is commonly estimated using chemical transport models or canopy budget models in combination with throughfall measurements. Since flux measurements of reactive nitrogen (N_r) compounds are scarce, dry deposition process descriptions as well as the calculated flux estimates and annual budgets are subject to considerable uncertainties. In this study, we compared four different approaches to quantify annual dry deposition budgets of total reactive nitrogen (ΣN_r) at a mixed forest site situated in the Bavarian Forest National Park, Germany. Dry deposition budgets were quantified based on (I) 2.5 years of eddy-covariance flux measurements with the Total Reactive Atmospheric Nitrogen Converter (TRANC), (II) an in-situ application of the bidirectional inferential flux model DEPAC (Deposition of Acidifying Compounds), here called DEPAC-1D, (III) a simulation with the chemical transport model LOTOS-EUROS (LOng Term Ozone Simulation – EUROpean Operational Smog) v2.0 using DEPAC as dry deposition module, and (IV) a canopy budget technique (CBT).

Averaged annual ΣN_r dry deposition estimates determined from TRANC measurements were 4.7±0.2 and 4.3±0.4 kg N ha^{-1} a^{-1} depending on the gap-filling approach. DEPAC-1D modeled dry deposition, using concentrations and meteorological drivers measured at the site, was 5.8±0.1 kg N ha^{-1} a^{-1}. In comparison to TRANC fluxes, DEPAC-1D estimates were systematically higher during summer, and in close agreement in winter. Modeled ΣN_r deposition velocities (v_d) of DEPAC-1D were found to increase with lower temperatures, higher relative humidity, and in the presence of wet leaf surfaces, in particular from May to September. This observation was in contradiction to TRANC-observed fluxes. LOTOS-EUROS modeled annual dry deposition was 6.5±0.3 kg N ha^{-1} a^{-1} for the site-specific weighting of land-use classes within the site's grid cell. LOTOS-EUROS showed substantial discrepancies to measured ΣN_r deposition during spring and autumn, which was related to an overestimation of ammonia (NH_3) concentrations by a factor of two to three compared to measured values as a consequence of a mismatch between gridded input NH_3 emissions and the site's actual, rather low, pollution climate. According to LOTOS-EUROS predictions, ammonia contributed most to modeled input ΣN_r concentrations, whereas measurements showed NO_x as the prevailing compound in ΣN_r concentrations. Annual deposition estimates from measurements and modeling were in the range of minimum and maximum estimates determined from CBT being at 3.8±0.5 and 6.7±0.3 kg N ha^{-1} a^{-1}, respectively. By adding locally measured wet-only deposition, we estimated an annual total nitrogen deposition input between 11.5 and 14.8 kg N ha^{-1} a^{-1}, which is within the critical load ranges proposed for deciduous and coniferous forests.

Published as: Wintjen, P., Schrader, F., Schaap, M., Beudert, B., Kranenburg, R., and Brümmer, C.: Forest-atmosphere exchange of reactive nitrogen in a remote region – Part II: Modeling annual budgets, Biogeosciences Discuss. [preprint], https://doi.org/10.5194/bg-2022-72, in review, 2022.

4.1 Introduction

In the last century, global nitrogen emissions have increased significantly due to anthropogenic activities (Fowler et al., 2013). Reactive nitrogen compounds, such as ammonia (NH_3) and nitrogen oxides (NO_x), contribute most to the emissions. Ammonia emissions originate mostly from animal husbandry and fertilizer application (Sutton et al., 2011, 2013), whereas NO_x emissions are mainly related to combustion processes in, e.g., transport and industry (Erisman et al., 2011, 2013). Although fertilizer use and the internal combustion engine are vital for world's food security and the economy, the release of these compounds into the atmosphere has a wide range of negative effects (Krupa, 2003; Galloway et al., 2003; Erisman et al., 2013). Deposition of reactive nitrogen into ecosystems has been identified as a reduction factor for biodiversity (Bobbink et al., 1998; Krupa, 2003; Galloway et al., 2003; Sutton et al., 2011). Especially ecosystems with nutrient poor soils are highly sensitive to additional nitrogen inputs resulting in a change in plant species (Damgaard et al., 2011; Paulissen et al., 2016) and species composition in forests (Dirnböck et al., 2014, 2018; Roth et al., 2022). Critical loads are used to show at which level long-term nitrogen deposition may lead to adverse impacts (Hettelingh et al., 1995). Investigations by Hettelingh et al. (2013) have shown that half of the European ecosystems receive nitrogen above the critical level. In Germany, the fraction of ecosystems with a critical load exceedance is estimated to be about 70 % (Schaap et al., 2018).

Quantitative estimation of the total nitrogen deposition is needed to assess exceedances of critical loads and to develop successful mitigation strategies. Although wet deposition is relatively straightforward to measure, the accurate quantification of dry N deposition remains a challenge. Recent progress in fast and robust measurement techniques allowed to investigate the temporal dynamics in concentrations and dry deposition fluxes (using the eddy-covariance (EC) approach) for total reactive nitrogen (ΣN_r) (Marx et al., 2012; Ammann et al., 2012; Brümmer et al., 2013, 2022; Zöll et al., 2019; Ammann et al., 2019; Wintjen et al., 2020, 2022) and its individual compounds, e.g. for NH_3 (Whitehead et al., 2008; Ferrara et al., 2012, 2021; Zöll et al., 2016; Moravek et al., 2020). For ΣN_r, the total reactive atmospheric nitrogen converter (TRANC) (Marx et al., 2012) coupled to a chemiluminescence detector (CLD) has shown its suitability for flux measurements in various field applications (see references for ΣN_r above). Despite the recent progress, the number and temporal coverage of available datasets remains small. As these in-situ measurements are only valid for the ecosystem where the specific observations took place, a large-scale assessment based on observations alone is not feasible without a dense observation network.

Chemical transport models (CTMs) are used to assess nitrogen deposition over large regions. For Germany, the CTM LOTOS-EUROS (Wichink Kruit et al., 2012; Manders et al., 2017; van der Graaf et al., 2020) is applied for the mapping of nitrogen deposition fluxes across the country. LOTOS-EUROS predicts the dry deposition of various N_r compounds, namely nitrogen dioxide (NO_2), nitric oxide (NO), nitric acid (HNO_3), ammonia (NH_3), and particulate ammonium (NH_4^+) and nitrate (NO_3^-), in each grid cell by utilizing meteorological data from the European Centre for Medium Range Weather Forecasts (ECMWF), modeled concentrations of the mentioned compounds based on their emission sources and chemical processing, as well as information about the land-use distribution within each grid cell. The deposition module DEPAC (Deposition of Acidifying Compounds) is applied for calculating dry deposition velocities of those compounds (Erisman et al., 1994). DEPAC is a dry deposition inferential scheme featuring bidirectional NH_3 exchange (van Zanten et al., 2010; Wichink Kruit et al., 2012), which is also implemented in the Operational Priority Substance (OPS) model (van Jaarsveld, 2004; Sauter et al., 2020). DEPAC can be used as stand-alone model for estimating dry deposition of N_r compounds. For site-based modeling with DEPAC, decoupled from a CTM and henceforth called DEPAC-1D, only measurements of common micrometeorological variables and concentrations of the individual N_r compounds are needed. In the past, deposition estimates have often been obtained through such an inferential modeling approach (Flechard et al., 2011, 2020; Li et al., 2016; Schwede et al., 2011).

To evaluate modeled annual total dry deposition and seasonal patterns in modeled fluxes and deposition velocities, a careful comparative analysis to flux measurements may provide feedback on the representativeness of the input data and the bidirectional parameterizations (Wichink Kruit et al., 2010; Wichink Kruit et al., 2017). Wintjen et al. (2022) presented and analyzed novel flux measurements of ΣN_r and several subcomponents focusing on temporal dynamics above a remote, mixed forest site spanning a 2.5-year period. This dataset provides a unique opportunity for the evaluation of different approaches to quantify dry deposition fluxes. Such comparisons with novel measurement techniques are sparse and only available from few field campaigns (Ammann et al., 2012; Brümmer et al., 2013, 2022; Zöll et al., 2019). Since the adoption of the Geneva Convention on Long-Range Transboundary Air Pollution (CLRTAP) in 1979, throughfall measurements have been carried out at many sites of the International Co-operative Programmes on Assessment and Monitoring of Air Pollution Effects on Forests (ICP Forests, www.icp-forests.net, last access: 14 March 2022) and forested catchments (ICP Integrated Monitoring, http://www.syke.fi/nature/icpim, last access: 14 March 2022) according to standardized protocols. Using the so-called canopy budget technique (CBT), throughfall measurements also allow to give an estimate of the annual nitrogen dry deposition (Draaijers and Erisman, 1995; de Vries et al., 2003).

In this study, we provide a comparison of four independent methods for estimating nitrogen dry deposition for a remote mixed forest site in the Bavarian Forest National Park. The comparison is made for a 2.5 year period for which novel flux measurements were available (see companion paper Wintjen et al., 2022). The aim of this measurement campaign covering the time frame from January 2016 to June 2018 was to quantify background concentration and deposition levels as well as their temporal dynamics for further improvements in modeling nitrogen deposition that may be used for further defining environmental protection guidelines. Therefore, (1) we present modeled concentrations, deposition velocities, and fluxes of ΣN_r and compare them to measurements of the same compounds , (2) discuss the influence of micrometeorological parameters on modeled deposition velocities and the impact of measured and modeled input parameters on modeled fluxes , (3) compare annual N_r budgets of LOTOS-EUROS with DEPAC-1D, flux measurements, and nitrogen deposition estimates based on CBT and review them in the context of critical loads and (4) finally discuss uncertainties affecting modeled dry deposition estimates.

4.2 Materials and Methods

4.2.1 Data set description

For the comparison to modeled ΣN_r deposition fluxes, TRANC EC flux measurements described in detail in Wintjen et al. (2022) were used. These flux measurements were available at half-hourly resolution, carried out 30 m above the forest floor, and had a data coverage of 41.0 % considering the entire campaign period. Data gaps were related to violations of the EC theory and performance issues of the instruments.

For the application of DEPAC-1D, time series of micrometeorological parameters (i.e. temperature, atmospheric pressure, relative humidity, global radiation, Obukhov length (L), friction velocity (u_*)) and air pollutant concentrations (NO, NO_2, HNO_3, NH_3, pNO_3^-, pNH_4^+, and sulphur dioxide (SO_2)) are required for flux calculations. NH_3 concentrations obtained from Quantum cascade laser measurements taken at 30 m above ground, NO_2 and NO obtained from chemiluminescence measurements taken at 50 m above ground as well as micrometeorological parameters were aggregated at half-hourly resolution, whereas the remaining N_r species and an additional NH_3 determination were obtained from DELTA (DEnuder for Long-Term Atmospheric sampling, e.g., Sutton et al., 2001; Tang et al., 2009) and passive sampler (NH_3 only) measurements of the IVL type (Ferm, 1991) for on monthly basis. DELTA measurements were made at 30 m and passive sampler measurements at 10, 20, 30, 40, and 50 m above ground. Temperature and relative humidity were collected in a profile at 10, 20, 40, and 50 m above

ground. Pressure and global radiation measurements were taken at 50 m. Indicators of stability and turbulence such as L and u_* were obtained from momentum flux measurements of the sonic anemometer.

Gaps in DEPAC-1D were related to gaps in micrometeorological input data and issues in the measurements of N_r compounds. Respective half-hourly values in the flux time series of each gas (approx. 3.4% for NH_3, HNO_3, pNH_4^+, and pNO_3^- and 9.3% for NO and NO_2) were filled with results from LOTOS-EUROS. A detailed description of the site and the instrumentation is given in Wintjen et al. (2022). For LOTOS-EUROS flux modeling, modeled input data of the European Centre for Medium range Weather Forecast (ECMWF) and the national emission inventory of Germany (Schneider et al., 2016) were used to predict deposition fluxes for NO, NO_2, HNO_3, NH_3, pNO_3^-, and pNH_4^+. LOTOS-EUROS fluxes were resampled to half-hourly timestamps from the original hourly resolution and missing fluxes were linearly interpolated. For the canopy budget technique, hroughfall measurements under spruce and beech trees in close proximity to the station (Beudert et al., 2014) and bulk deposition measurements at an open site (Wintjen et al., 2022) were taken in weekly intervals and used for determination of total nitrogen dry deposition on annual basis (Sect. 4.2.3). An overview of all methods is given in Table 4.1.

Table 4.3: Overview of methods used for estimating ΣN_r dry deposition.

Method	**Primary input/observation variables and temporal resolution**	**Primary output variables and temporal resolution**
TRANC	Wind components (u,v,w), sonic temperature (T_s), and ΣN_r concentration at 10 Hz resolution	ΣN_r fluxes at half-hourly resolution, no gap-filling applied
DEPAC-1D	Measurements of micrometeorological variables at half-hourly resolution Measured NH_3, NO, NO_2 concentrations at half-hourly resolution Measured SO_2, HNO_3, NH_3, pNO_3^-, and pNH_4^+ concentrations at monthly resolution	Fluxes of NH_3, NO_2, NO, HNO_3, pNH_4^+, and pNO_3^- at continuous half-hourly resolution
TRANC (DEPAC-1D)	See above	Continuous ΣN_r fluxes at half-hourly resolution, only DEPAC-1D is used for gap-filling
TRANC (MDV+DEPAC-1D)	See above	Continuous ΣN_r fluxes at half-hourly resolution, gap-filled with a combination of MDV (window size of ±5 days) and DEPAC-1D for adding further missing fluxes
LOTOS-EUROS	Meteorological data from ECMWF weather forecasts and modeled concentrations of SO_2, NH_3, NO_2, NO, HNO_3, pNH_4^+, and pNO_3^- at hourly resolution for 7x7 km^2 grid cell; concentrations were linearly resampled to half-hourly resolution	Continuous fluxes of NH_3, NO_2, NO, HNO_3, pNH_4^+, and pNO_3^- at hourly resolution; fluxes were linearly resampled to half-hourly resolution
Canopy budget technique	Throughfall measurements from nearby spruce and beech trees and	Dissolved inorganic nitrogen deposition (DIN) based on the exchange of NO_3^- and NH_4^+ ions on

	bulk deposition measurements at an open-site in weekly intervals	monthly basis following the approaches of Draaijers and Erisman (1995) and de Vries et al. (2003), dissolved organic nitrogen (DON) corresponds to difference of DON fluxes between throughfall and bulk deposition

To compare dry deposition estimates from modeling to TRANC measurements, we filled gaps in the TRANC flux data with results from DEPAC-1D and henceforth, called this dataset TRANC(DEPAC-1D). In a second approach, we applied the mean-diurnal-variation (MDV) method to short-term gaps analogous to Wintjen et al. (2022) and replaced remaining gaps with results from DEPAC-1D. This approach was called TRANC(MDV+DEPAC-1D). Both approaches, DEPAC-1D alone and the combination of DEPAC-1D and MDV, were able to fill all gaps in TRANC flux time series. Uncertainties of the gap-filled fluxes determined by MDV were calculated as the standard error of the mean. Cumulative uncertainties of TRANC fluxes were solely based on the uncertainty of the gap-filling and were calculated according to Eq. (3) of Wintjen et al. (2022). The error calculation scheme proposed by Brümmer et al. (2022, Eq. (1)) was applied to fluxes filled with DEPAC-1D. Flux uncertainty of those half-hourly values was given as

$$F_{\mathrm{unc,DEPAC-1D}} = \frac{\tilde{X}}{F_{\mathrm{DEPAC-1D}}} \; ; \text{ with } \tilde{X} = \frac{F_{\mathrm{unc,meas}}}{F_{\mathrm{meas}}} \tag{4.8}$$

where $\tilde{X}$ represents the median of the ratio of the uncertainty of the measured fluxes ($F_{\mathrm{unc,meas}}$) to their corresponding flux values (F_{meas}). The uncertainty of the measured fluxes was estimated after Finkelstein and Sims (2001). Systematic uncertainties were not accounted in the error calculation. A discussion on systematic uncertainties is given in Wintjen et al. (2022).

4.2.2 Modeling reactive nitrogen fluxes

4.2.2.1 Bidirectional flux model DEPAC

In surface-atmosphere flux exchange models, fluxes are calculated by using resistance schemes. In case of gases exhibiting bidirectional exchange behavior, the flux F is defined as follows

$$F = -v_{\mathrm{d}}(z-d) \cdot (\chi_{\mathrm{a}}(z-d) - \chi_{\mathrm{tot}}) \tag{4.9}$$

The flux is a product of the deposition velocity (v_{d}) with the concentration difference between the atmospheric concentration, χ_{a}, and the compensation point, χ_{tot}, of the trace gas χ_{a}. In DEPAC, a compensation point is only implemented for NH_3. Both, the dry deposition or exchange velocity and the atmospheric concentration, are height dependent and given for an aerodynamic reference height ($z - d$) where z is the geometric height and d the zero-plane displacement height. The following convention is used for the fluxes: negative values represent deposition, positive values emission. Following the conductivity-resistance analogy, v_{d} is the inverse of the sum of the aerodynamic resistance (R_{a}), the quasi-laminar layer resistance (R_{b}), and the canopy resistance (R_{c}).

$$v_{\mathrm{d}} = (R_{\mathrm{a}} + R_{\mathrm{b}} + R_{\mathrm{c}})^{-1} \tag{4.10}$$

DEPAC (van Zanten, et al., 2010) can be used to calculate the dry deposition of reactive nitrogen gases. R_{a} and R_{b} are required by DEPAC as input variables. Hence, the module is oriented at determining R_{c}

for NO, NO_2, HNO_3, and NH_3. R_c is treated differently for each N_r compound but basically as the sum of parallel resistances, which model the exchange behavior of the atmosphere and vegetation:

$$R_c^{-1} = R_w^{-1} + R_{stom}^{-1} + (R_{inc} + R_{soil})^{-1} \quad (4.11)$$

The stomatal resistance (R_{stom}) is calculated following Emberson et al. (2000a, b). In this scheme, stomatal conductance is determined by vegetation type dependent on maximum conductance lowered by factors controlling stomatal opening, i.e., light intensity, ambient temperature, vapor pressure deficit, and soil water content, using well known Jarvis functions (Jarvis, 1976). For NH_3 a stomatal compensation point (χ_{stom}) is calculated following Wichink Kruit et al. (2010, 2017). The cuticular resistance (R_w) is described by Sutton and Fowler (1993) for NH_3 and the corresponding cuticular compensation point based on the works of Wichink Kruit et al. (2010, 2017). For NO and NO_2, R_w is set considerably high to 10000 and 2000 s m^{-1}, respectively, allowing hardly any deposition on external surfaces. The in-canopy resistance (R_{inc}) is given by van Pul and Jacobs (1994), and the soil resistance (R_{soil}) is described following Erisman et al. (1994). In the current version of DEPAC, the soil compensation point is set to zero for all surface types. In case of HNO_3, a fast uptake to any surface is assumed through a low, constant R_c of 10 s m^{-1}. The total compensation point (χ_{tot}) is determined as written in van Zanten et al. (2010).

$$\chi_{tot} = \frac{R_c}{R_w} \cdot \chi_w + \frac{R_c}{R_{inc} + R_{soil}} \cdot \chi_{soil} + \frac{R_c}{R_{stom}} \cdot \chi_{stom} \quad (4.12)$$

For further details to the documentation of DEPAC, we refer to the publication of van Zanten et al. (2010). Following implementation in LOTOS-EUROS, the version of DEPAC used in this study differs from the one documented in van Zanten et al. (2010) in two main aspects: Firstly, the implementation of a function considering co-deposition of SO_2 and NH_3 (Wichink Kruit et al., 2017) in the non-stomatal pathway and secondly, the usage of a monthly moving NH_3 average concentration for determining the stomatal compensation point (Wichink Kruit et al., 2017).

4.2.2.2 Modeling of ΣN_r deposition (LOTOS-EUROS)

LOTOS-EUROS (Manders et al., 2017) simulations were performed for the entire measurement period. For this purpose, a large-scale simulation was setup for Europe in which a second domain covering northwestern Europe at 7x7 km^2 was nested. The simulations were forced with weather data from the ECMWF and the CORINE-2012 land-use classification. For the European background simulation, the CAMS-REG European emission inventory (Kuenen et al., 2021) was used. For the inner domain the emission data for Germany were replaced by the national emission inventory. For Germany, the gridded emissions were obtained from the GrETa system (*GRETA – Gridding Emission Tool for ArcGIS v1.1*; Schneider et al., 2016). On hourly basis, the land-use specific total dry deposition was calculated in LOTOS-EUROS by applying DEPAC for NH_3, NO, NO_2, and HNO_3. Dry deposition of pNO_3^- and pNH_4^+ was calculated according to Zhang et al. (2001) (see Manders-Groot et al. (2016, Sect. 5.2)). In the model, the dry deposition velocity and flux are calculated for the mid-layer height of the first model layer, which has a depth of ca. 20 m. By assuming a constant flux and using the stability parameters, the concentrations can be estimated for the canopy top and the typical observation height (2.5 m above roughness length (z_0)) in air quality networks. The Corine Land Cover 2012 classification of the grid cell, in which the measurement site was located, was divided into 46.0 % seminatural vegetation, 37.2 % coniferous forest, 15.9 % deciduous forest, 0.7 % water bodies, and 0.2 % grassland. However, the actual structure of the forest stand showed 81.1 % coniferous forest and 18.9 % deciduous forest within the footprint of the flux measurements during the measurement campaign. Due to differences in the distribution of vegetation types in the footprint, results from LOTOS-EUROS were calculated with the

site-specific weighting of land-use classes of the flux tower's footprint. The low contribution of coniferous forest and deciduous forest within the grid cell may be related to the evaluation of older aerial photographs showing larger areas of deadwood. Finally, the dry deposition of ΣN_r was calculated as the sum of the individual N_r fluxes. A detailed documentation of LOTOS-EUROS is given in Manders-Groot et al. (2016) and Manders et al. (2017).

4.2.2.3 Site-based modeling of ΣN_r deposition (DEPAC-1D)

DEPAC-1D is a stand-alone version of LOTOS-EUROS' dry deposition module DEPAC using a FORTRAN90 wrapper program to accept arbitrary input datasets. DEPAC-1D used micrometeorological variables and parameters measured at the site to estimate R_c and the compensation point of NH_3. The atmospheric resistances – R_a and R_b – and the fluxes of NH_3, NO, NO_2, HNO_3, pNO_3^-, and pNH_4^+ were calculated outside DEPAC following Garland (1977) and Jensen and Hummelshøj (1995, 1997) with stability corrections after Webb (1970) and Paulson (1970). The deposition of particles was calculated following Zhang et al. (2001) (see also Manders-Groot et al. (2016, Sect. 5.2)) and therewith equal to LOTOS-EUROS. For the fine fraction of pNO_3^- and pNH_4^+, a mass median diameter of 0.7 µm was used. For the coarse fraction of pNO_3^-, 8 µm was taken (Manders-Groot et al. (2016, Sect. 5.2)). Note that particle deposition is strictly speaking not part of the DEPAC module and was modeled with a separate program implementing the particle deposition scheme used within LOTOS-EUROS.

Half-hourly gaps in the NH_3 QCL concentration time series were filled with their monthly integrated concentration value obtained from DELTA samplers. If these measurements were not available, missing values were replaced by monthly integrated results from passive sampler measurements of NH_3. During winter, the uncertainty introduced by this gap-filling approach seems to be low as suggested by Schrader et al. (2018). We did not superimpose gap-filled concentration values with a diurnal pattern or used monthly averages of half-hours to fill gaps in concentration time series, since abrupt changes in the NH_3 concentration pattern, i.e., periods of low auto-correlation could not be reproduced by a synthetic diurnal cycle or monthly averages of half-hourly values. Fluxes of HNO_3, pNO_3^-, and pNH_4^+ were solely based on monthly DELTA measurements. Gaps in time series of these compounds and SO_2 were replaced by monthly averages from adjacent years. NO and NO_2 fluxes were based on half-hourly concentration measurements. The difference in measuring height was considered in the calculation of R_a. SO_2 and NH_3 concentrations from gap-filled DELTA time series were used to determine compensation points and additional deposition corrections.

Since measurements of temperature and relative humidity data were not available at the measurement height of the EC system, we took the average of measurements from 20 m and 40 m height above ground. These profile measurements started in April 2016 (Wintjen et al., 2022), and thus measurements at 50 m were used until end of March 2016. For modeling R_a, the solar zenith angle, which is calculated by using celestial mechanic equations, z_0, and d are needed. We set z_0 to 2.0 m and d to 12.933 m for coniferous forest and to 11.60 m for deciduous forest, corresponding to LOTOS-EUROS defaults for these land-use classes. Leaf area index (LAI) was modeled as described by van Zanten et al. (2010). The LAI determined from the site-specific land-use class weighting ranged between 4.1 and 4.8 due to leaf growth and shedding.

The calculation of the dry deposition was made for NH_3, NO, NO_2, HNO_3, pNO_3^-, and pNH_4^+ with the mentioned input data on half-hourly basis. Results from DEPAC-1D were weighted with the site-specific land-use distribution within the flux measurement's footprint (81.1 % coniferous forest and 18.9 % deciduous forest).

4.2.3 Measuring nitrogen outflow from the canopy using the Canopy Budget Technique (CBT)

The canopy budget technique (CBT) is the most common method for estimating total (wet+dry) atmospheric deposition of dissolved inorganic nitrogen (DIN_t) based on wet inorganic nitrogen fluxes of NO_3^- and NH_4^+-ions estimated from open-site precipitation (bulk deposition) and throughfall of NO_3^- and NH_4^+-ions measurements (see Staelens et al., 2008, Table 1). DIN_t was estimated on monthly basis after the CBT approach of Draaijers and Erisman (1995) and de Vries et al. (2003). The results from the two methods differed only marginally and were therefore averaged. The biological conversion of deposited inorganic nitrogen into dissolved organic nitrogen (DON) in the phyllosphere (bacteria, yeasts, and fungi) or the dry deposition of atmospheric DON onto the canopy or the exudation of DON from plant tissues is not addressed in CBT. Here, it was estimated by the difference of DON fluxes between throughfall and bulk deposition, and henceforth called ΔDON. Adding ΔDON to throughfall DIN or to DIN_t reveals a frame of lower and upper estimates of total (wet+dry) nitrogen deposition (N_t) and, by subtracting DIN deposition at an open land site from these N_t, of lower and upper estimates of dry deposition (Beudert and Breit, 2014).

4.3 Results

4.3.1 Comparison of modeled and measured concentrations

4.3.1.1 High resolution concentration measurements of NH_3, NO_x, and ΣN_r

Figure 4.1 shows the comparison of measured half-hourly NH_3, NO_x, and ΣN_r concentrations (*cf.* Wintjen et al., 2022) to their modeled concentrations of LOTOS-EUROS represented as monthly box-whisker plots. From high-resolution concentration measurements, we found average concentrations and standard deviations of 1.0 ± 0.6, 1.4 ± 1.2, and 3.1 ± 1.7 μg N m^{-3} for NH_3, NO_x, and ΣN_r for the entire campaign, respectively. Corresponding averages of LOTOS-EUROS of NH_3 and ΣN_r were higher by 0.8 and 1.9 μg N m^{-3}, whereas NO_x was slightly underestimated. Substantial mismatches in standard deviations of NH_3 and ΣN_r indicate that the variability in concentrations of NH_3 and ΣN_r was overestimated by LOTOS-EUROS. In case of NH_3, largest discrepancies were observed for spring and partially for autumn. NO_x concentrations were systematically underestimated by LOTOS-EUROS in summer. During winter, difference between measured and modeled NO_x concentrations was lower than during summer time. Except for the summer, modeled half-hourly concentrations of ΣN_r were two to three times higher than the measured values. The slight seasonal differences in measured ΣN_r concentrations could not be reproduced by LOTOS-EUROS. The largest discrepancy during spring clearly correlates with the modeled NH_3 concentrations.

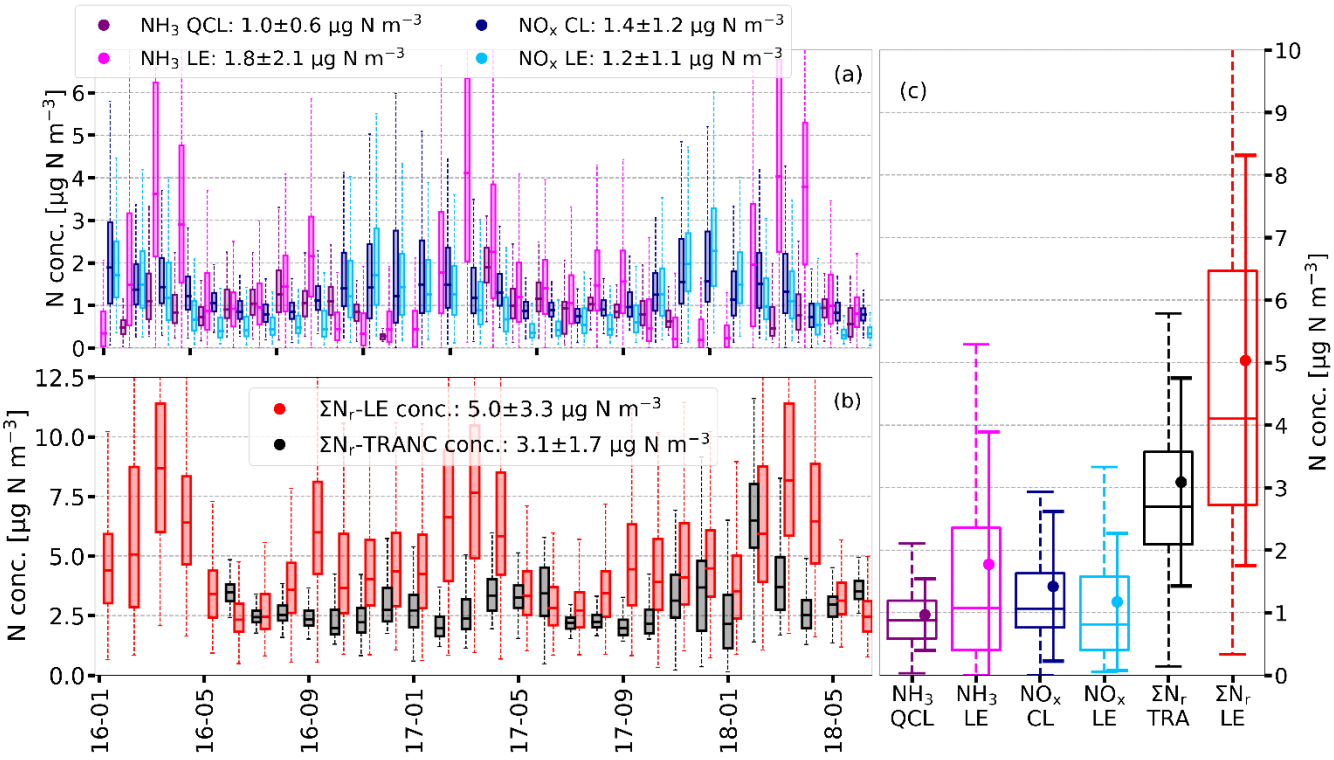

Figure 4.8: Half-hourly concentrations of NH_3, NO_X, and ΣN_r obtained from quantum-cascade-laser (QCL), chemiluminescence (CL), and TRANC (TRA) measurements compared to LOTOS-EUROS (LE) results displayed as box-whisker plots (box frame = 25 % to 75 % interquartile range (IQR), bold line = median, whisker = 1.5*IQR) on monthly basis ((a) and (b)) and for the entire duration of the campaign (January 2016 to end of June 2018) (c) in µg N m^{-3}. Darker colors represent the results from measurements, brighter colors from LOTOS-EUROS. In the legends, averages and standard deviations referring to the entire campaign for NH_3, NO_X, and ΣN_r are shown.

4.3.1.2 Passive samplers and DELTA measurements

The large modeled NH_3 concentrations by LOTOS-EUROS could also not be verified by the observed levels of the passive samplers, and the DELTA system. Figure S4.1 shows a comparison of the applied NH_3 measurement techniques with NH_3 concentrations predicted by LOTOS-EUROS. Figures and Tables denoted with a S can be found the supplement. A two- to threefold overestimation of NH_3 concentrations by LOTOS-EUROS is visible. In addition, the modeled seasonal pattern was also not in agreement with the results from wet chemical samplers.

A comparison of the individual measured N_r compounds by DELTA to LOTOS-EUROS is displayed in Fig. 4.2. Considering the entire campaign, we measured average concentrations of 0.55, 0.17, 0.42, and 0.19 µg N m^{-3} for NH_3, HNO_3, pNH_4^+, and pNO_3^-, respectively. For the same exposure periods, the concentration averages of LOTOS-EUROS for NH_3, HNO_3, pNH_4^+, and pNO_3^- were 1.8, 0.1, 1.2, and 0.8 µg N m^{-3}, respectively. Differences considering the entire campaign duration are shown in Fig. S4.2. Like NH_3, particulate nitrogen compounds concentrations were also higher in the LOTOS-EUROS simulations. Predicted seasonality for pNH_4^+ and pNO_3^- could only partially be verified by DELTA measurements. For HNO_3, concentrations were in close agreement. In total, ΣN_r values of DELTA and TRANC showed a reasonable agreement and ΣN_r concentrations showed only small seasonal differences whereas LOTOS-EUROS overestimated ΣN_r of the TRANC by ca. 2 µg N m^{-3} (Fig. S4.2).

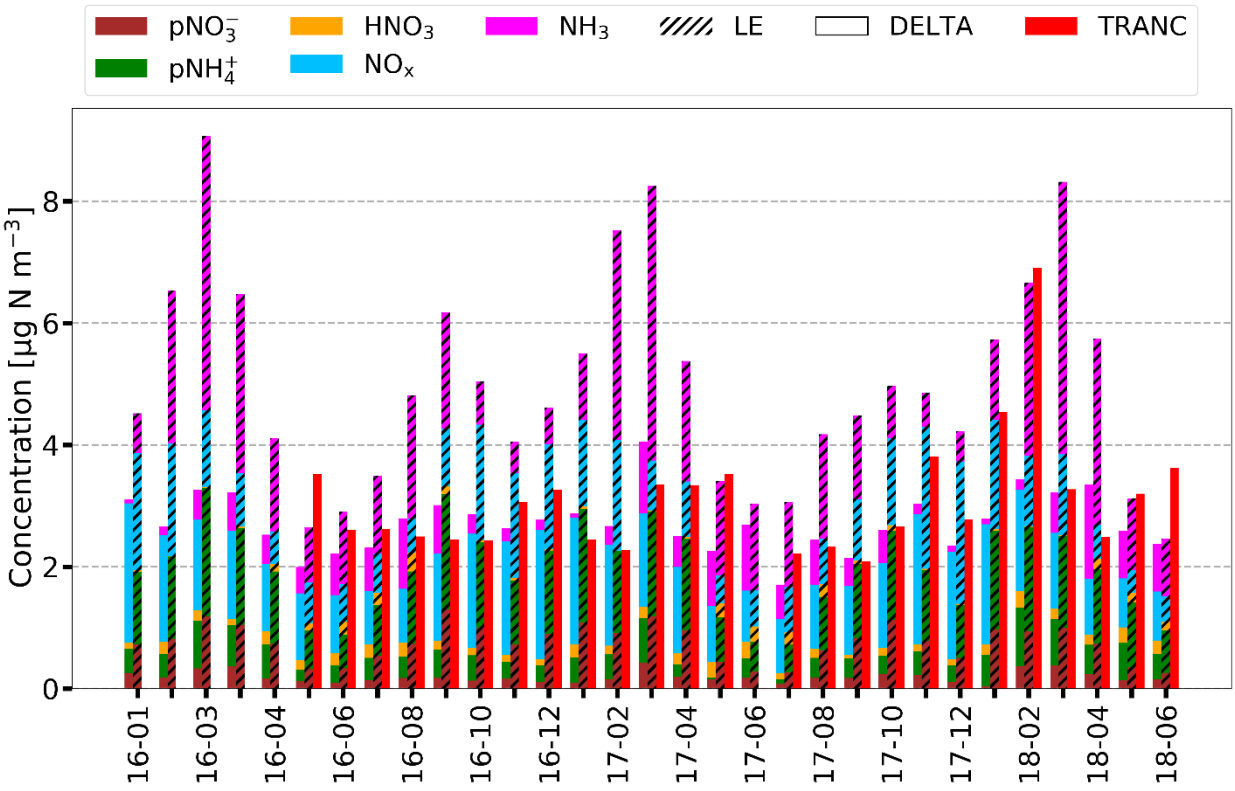

Figure 4.9: Monthly stacked concentration of LOTOS-EUROS (LE) (hatched), TRANC (red), DELTA, and NO_x in µg N m^{-3} for the entire measurement campaign. Gaps in the NH_3 timeseries caused by a low pump flow of the denuder pump were filled with passive sampler values from 30 m. This procedure was done for December 2016 and 2017, March 2018, and April 2018. Remaining gaps in the time series of HNO_3, pNH_4^+, and pNO_3^- were replaced by monthly averages estimated from other years if available. In case of NH_3, the procedure was applied to January 2017. For the other compounds, the gap-filling was done for December 2017, March 2018, and April 2018. Results from LOTOS-EUROS, TRANC, and NO_x measurements were averaged to the exposure periods of the DELTA samplers.

According to Wintjen et al. (2022), NO_x was the predominant compound in the ΣN_r concentrations. For the entire campaign, NO_x contributed 51.4 % and NH_3 20.0 % to measured ΣN_r, whereas LOTOS-EUROS predicted NH_3 as the most important compound (~ 35.7 %) contributing to ΣN_r followed by pNH_4^+ (~ 24.3 %), NO_x (~ 22.8 %), pNO_3^- (~ 15.2 %), and HNO_3 (~ 1.9 %) as shown by Fig. S4.3. Furthermore, LOTOS-EUROS showed deviations from measurements in seasonal contributions. During winter, the contribution of NH_3 to ΣN_r was surprisingly high (28.6 %) compared to the observations (4.9 %) during winter. HNO_3 contributions were comparable and on a low level between LOTOS-EUROS and DELTA. On average, particle contribution was higher in the model. Contributions of pNO_3^- and pNH_4^+ were highest during spring according to measurements but lowest in LOTOS-EUROS in that season. Apart from springtime, seasonal contributions of pNO_3^- and pNH_4^+ were higher by 6.6 to 14.4% in LOTOS-EUROS.

4.3.2 Comparison of modeled and measured deposition velocities

4.3.2.1 Comparison of modeled and measured deposition velocities for each N_r compound

NH_3 deposition velocities of LOTOS-EUROS and DEPAC-1D exhibited similar values in winter, but disagreements were found in summer and autumn. In summer, DEPAC-1D determined systematically larger median deposition velocities, whereas LOTOS-EUROS predicted a large variability in NH_3 deposition velocities during autumn, which was not supported by DEPAC-1D. For NO_2, deposition velocities of LOTOS-EUROS and DEPAC-1D agreed well in their temporal pattern and the median deposition velocities, but the variability in DEPAC-1D deposition velocities was slightly higher during

summer. In both model applications, NO deposition velocities were practically zero (medians always < 0.06 cm s^{-1}). For pNH_4^+, deposition velocities of DEPAC-1D and LOTOS-EUROS agreed well with median deposition velocities close to zero, but a large disagreement was found during winter. Deposition velocities of pNO_3^- were close to zero during the entire campaign in DEPAC-1D, but LOTOS-EUROS showed a large scattering of v_d in the winter months. For HNO_3, a discrepancy in v_d was also found during winter, and, similar to NH_3, deposition velocities of DEPAC-1D were generally larger from May to September. The comparison of the deposition velocities for each N_r compound modeled by DEPAC-1D and LOTOS-EUROS is shown in Fig. S4.4.

4.3.2.2 Comparison of modeled and measured ΣN_r deposition velocities

A comparison of the modeled and measured v_d for the ΣN_r flux is provided in Fig. 4.3. The modeled total nitrogen dry deposition velocities were obtained by dividing the modeled dry deposition flux for all compounds by the modeled total nitrogen concentrations in ambient air. Subtracting median v_d of TRANC from LOTOS-EUROS results, differences typically ranged between -0.3 and 1.0 cm s^{-1}. Especially during the summer months, an overestimation of v_d by DEPAC-1D was observed with respect to TRANC measurements. During those months, median v_d of DEPAC-1D was ca. 2 to 3 times higher than their measured entities. LOTOS-EUROS v_d of the ΣN_r flux were generally lower than DEPAC-1D but still larger than found in the measurements within that period. During the winter months, DEPAC-1D ΣN_r showed lowest median values and variability, whereas deposition velocities of TRANC and LOTOS-EUROS were comparable caused by influence of pNO_3^- and pNH_4^+ on LOTOS-EUROS v_d predictions. Modeled and measured medians v_d and their lower and upper quartiles are given in Table S4.1.

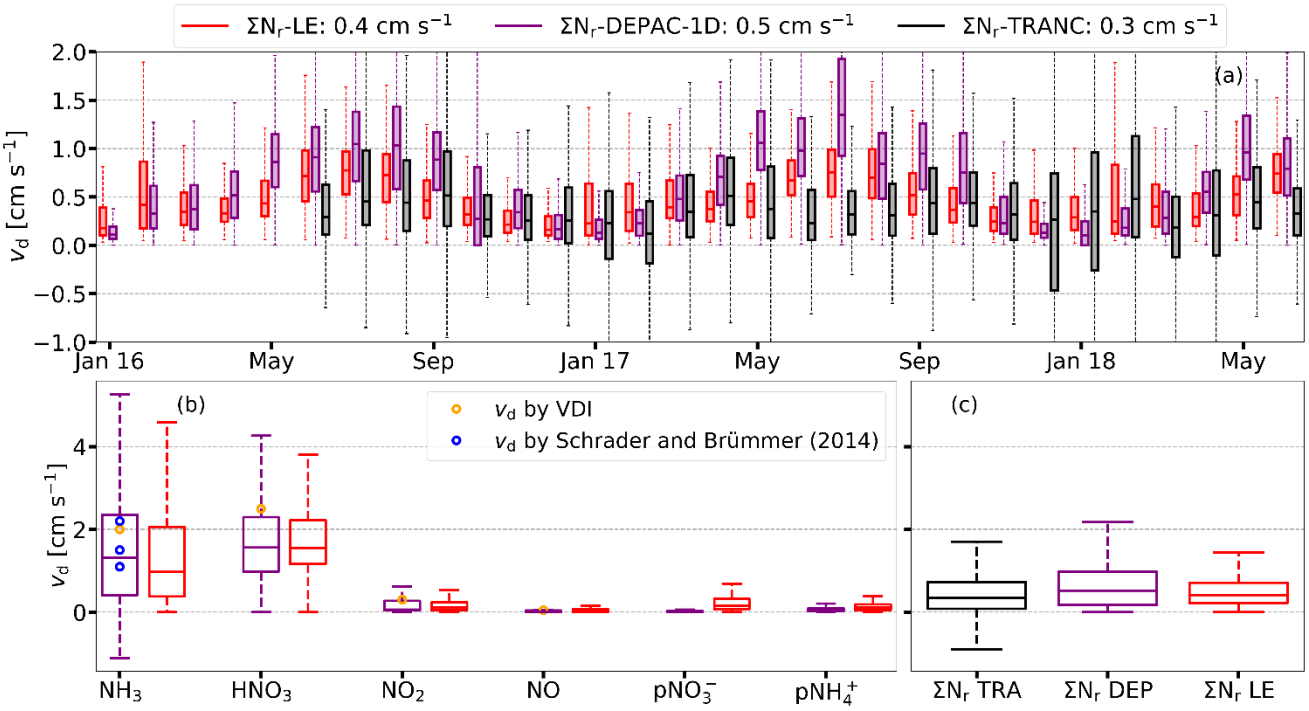

Figure 4.10: Monthly v_d of ΣN_r determined from TRANC (black) measurements, DEPAC-1D (purple), and LOTOS-EUROS (red) with the corrected land-use weighting in cm s^{-1} represented as box-and-whisker plots in the upper panel (a). In the corresponding legend median v_d related to the entire campaign are given. In the lower panels ((b) and (c)), box-and-whisker plots of v_d for each N_r compound and ΣN_r are shown based on the entire campaign (TRA=TRANC, DEP=DEPAC-1D, LE= LOTOS-EUROS). Blue circles are referring to NH_3 deposition velocities reported by Schrader and Brümmer (2014) for deciduous forest, mixed forest, and spruce forest (from low to high), orange circles show deposition velocities proposed by VDI (2006).

Inspection of the diurnal cycles of ΣN_r deposition velocities for May to September in the year 2017 (Fig. S4.7) shows that both, the DEPAC-1D and measured data, exhibit a clear diurnal pattern with lowest deposition during the night and highest values around noon. However, in those periods where the measured data are close to zero during the night, the modeled fluxes show considerable nighttime exchange with deposition velocities between 0.5 and 1 cm s^{-1}.

To further examine the reasons behind these discrepancies, we show the diurnal cycles of v_d after classifying the ΣN_r deposition velocities for half-hours without precipitation during May-September in two groups being below or above the median temperature (T_{air} =14.6°C), relative humidity (RH = 74.0 %), and total ΣN_r concentration (c(ΣN_r) = 2.7 µg N m^{-3}). Leaf surface wetness was measured at the site with sensors attached to a spruce and a beech tree. In order to classify the sensor as dry or wet, the half-hourly leaf wetness value was compared to a threshold value based on the calculation scheme given by Wintjen et al. (2022).

The diurnal cycles illustrate the same diurnal biases as discussed above. Figure 4.4 shows that DEPAC-1D results indicate that lower temperatures, higher relative humidity, and wet leaf surfaces enhance the ΣN_r dry deposition velocity. This behavior was expected based on the models' parameterization, but it is in contradiction to the TRANC measurements. Especially, the differences for the relative humidity regimes are remarkable. Smaller differences are observed for the dependency on temperature and the ΣN_r concentration, although both have a stronger influence in the model than on their measured counterpart.

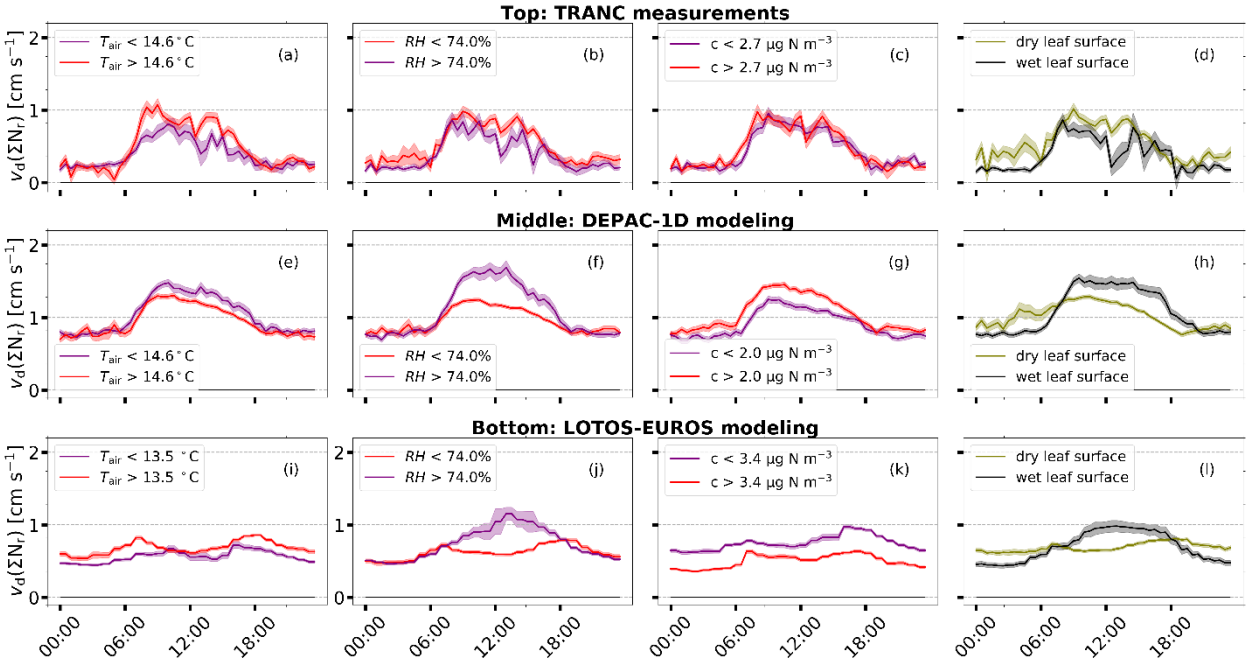

Figure 4.11: Averaged diurnal cycles of ΣN_r v_d for low and high temperature, relative humidity, concentration during the time frame May to September. The top row refers to TRANC measurements ((a) to (d)), the middle row refers to DEPAC-1D modeling ((e) to (h)), and the bottom row to LOTOS-EUROS simulations ((i) to (l)). Data was stratified after their median calculated for the entire period. Dry and wet leaf surfaces (Panel (d) , (h) and (l)) were identified following the calculation scheme of Wintjen et al. (2022). Shaded areas represent the standard error of the mean.

In case of LOTOS-EUROS, separating diurnal cycles of v_d led to similar observations made for DEPAC-1D regarding relative humidity and leaf surfaces. In addition, lower temperatures and concentration tend to increase v_d, which contradicts the results of DEPAC-1D. Generally, values of v_d are closer to TRANC deposition velocities, but the diurnal pattern differs from those of TRANC and DEPAC-1D showing maxima in the morning (~06:00 LT) and evening (~18:00 LT) and low values around noon except for high relative humidity and wet leaf surfaces.

4.3.3 Comparison of modeled and measured fluxes

4.3.3.1 Influence of input concentrations and meteorology on modeled fluxes

The statements made for v_d can be transferred to the flux predictions. Differences to the observations made for v_d (Fig. S4.4) are related to the concentration input data. For example, due to overestimations of modeled NH_3 concentrations in spring and autumn, differences in fluxes were higher during the same time. Modeled NO_2 and HNO_3 concentrations of LOTOS-EUROS were lower than their measured values resulting in flux underestimations by LOTOS-EUROS for NO_2 and HNO_3 during summer. High modeled input concentrations of particulate nitrogen led to substantial deposition fluxes in the LOTOS-EUROS simulations. Following the model predictions, NH_3 fluxes had the largest contribution to the modeled ΣN_r flux with an average flux of -12.5 and -13.0 ng N m^{-2} s^{-1} in the DEPAC-1D and LOTOS-EUROS applications, respectively, considering the entire campaign. Averaged fluxes of NO_2 and HNO_3 showed – although on a low level in absolute terms – higher deposition fluxes for DEPAC-1D, namely 2.0 and 1.3 ng N m^{-2} s^{-1}, respectively, compared to 1.2 and 0.3 ng N m^{-2} s^{-1} in case of LOTOS-EUROS. Substantial flux differences were found for particulate nitrogen. DEPAC-1D averaged fluxes were close to zero (0.9 and 0.1 ng N m^{-2} s^{-1} for pNH_4^+ and pNO_3^-, respectively), whereas LOTOS-EUROS showed substantial higher aerosol deposition with averaged fluxes of 3.7 and 2.2 ng N m^{-2} s^{-1} for pNH_4^+ and pNO_3^-, respectively. The comparison of fluxes for each N_r compound of LOTOS-EUROS and DEPAC-1D is shown in Figure S4.5.

Apart from concentrations being responsible for differences in modeled flux estimates, other parameters may have also been contributed to the deviations. To further investigate the impacts of the input data used in the LOTOS-EUROS simulations, we made a comparison of the measured and modeled input parameters used for the dry deposition modeling of NH_3 in LOTOS-EUROS (Fig. S4.6). The agreement of temperature and global radiation in terms of their coefficient of determination R^2 was good. We found differences of approximately 1.5°C and -6.1 W m^{-2} of modeled to measured values on average. High R^2 values were determined for the entire campaign duration using half-hourly values, namely 0.97 for temperature and 0.78 for global radiation. A slight difference was found for relative humidity during the first half of 2016. However, modeled values were higher by only 2.4 % on average, and the R^2 was still 0.67. In case of u_*, we found a systematic difference, and the seasonal pattern did not agree well resulting in a lower R^2 of 0.43 compared to the other micrometeorological parameters. In particular from November 2017 to February 2018, the difference between modeled and measured u_* values was considerably large.

The largest discrepancy was found for NH_3 concentration as illustrated by Fig. 4.2 and S4.1 in detail. All of the investigated input parameters play an important role in the modeling of NH_3 exchange. In order to determine the impact of these parameters on modeled NH_3 fluxes, we calculated NH_3 fluxes for the land-use class spruce forest with DEPAC-1D by replacing a specific input parameter by its measured entity while all other input data were from LOTOS-EUROS. Figure 4.5 illustrates the results of this comparison. Since modeled and measured values of global radiation agreed well, deposition of NH_3 is only marginally reduced if measured values were used. Using measured values of temperature as input parameter led to an increase in modeled NH_3 deposition by 0.82 kg N ha^{-1}, whereas measured relative humidity led to a decrease in modeled NH_3 deposition by 0.80 kg N ha^{-1}.We found significant differences in u_*, but considering measured values in the flux calculation leads only to a reduction by 1.3 kg N ha^{-1} As expected from the analysis of Fig. S4.6, NH_3 concentration had the largest impact on deposition. Using measured NH_3 concentration reduced the deposition substantially by 5.3 kg N ha^{-1} compared to using modeled concentrations. All reported differences refer to the entire campaign duration.

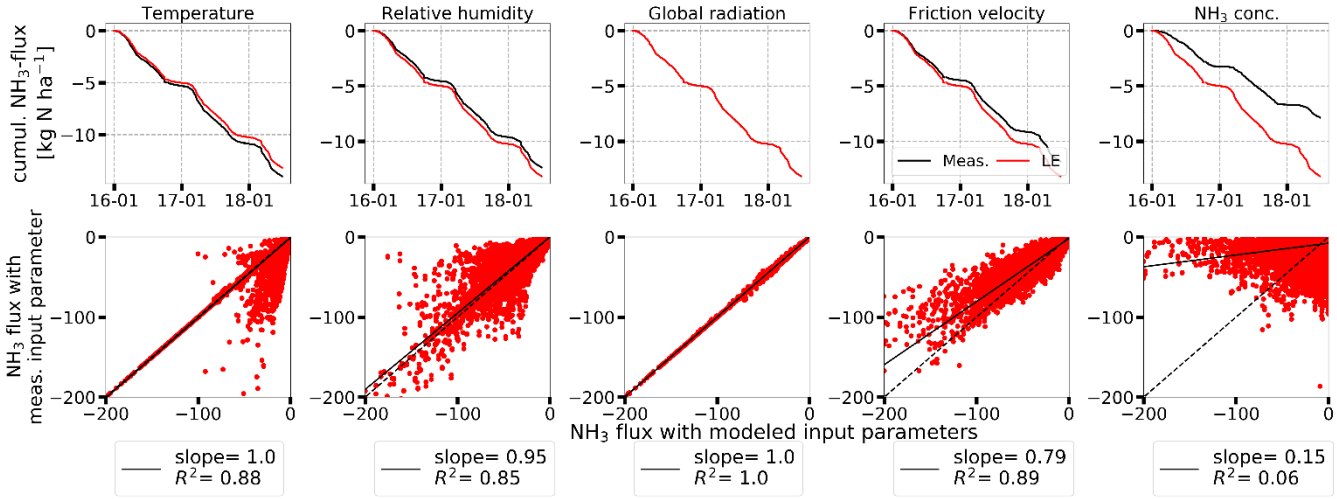

Figure 4.12: Comparison of NH_3 fluxes calculated with DEPAC-1D for the land-use class spruce forest based on measured (black) and modeled input data (red). The comparison was made for temperature, relative humidity, global radiation, friction velocity, and NH_3 concentrations. In the first row, NH_3 fluxes are shown as cumulative sums in kg N ha^{-1}. In the second row, scatter plots of NH_3 fluxes in ng N m^{-2} s^{-1} are given. Linear regressions are shown as black, solid lines, black, dashed lines represent 1:1 lines.

4.3.3.2 Comparison of modeled and measured ΣN_r deposition fluxes

The comparison of modeled ΣN_r fluxes with TRANC fluxes is presented in Fig. 4.6. Only periods during which high quality flux measurements were available were considered for the analysis. Models were basically able to capture the seasonal pattern of the ΣN_r fluxes well, but generally overestimated the measured flux amplitude. The ΣN_r exchange of DEPAC-1D is near zero during the entire winter, and thus the difference to measured deposition was nearly zero. During summer, a systematic overestimation of DEPAC-1D compared to measured fluxes was observed. Modeled deposition of LOTOS-EUROS was slightly lower than DEPAC-1D during summer and consequentially closer to measured fluxes. However, during autumn and spring predicted deposition of LOTOS-EUROS was significantly higher than deposition determined by DEPAC-1D and TRANC measurements due to the overestimated input NH_3 concentrations. Deposition was considerably high in LOTOS-EUROS during winter whereas median ΣN_r deposition of DEPAC-1D and TRANC was close to zero. Note that during February 2018 high aerosol concentrations were both modeled and observed. The TRANC flux data also show the impact of the aerosol deposition, but to a larger extend as LOTOS-EUROS. Median fluxes for each season and the entire campaign are given in Table S2.

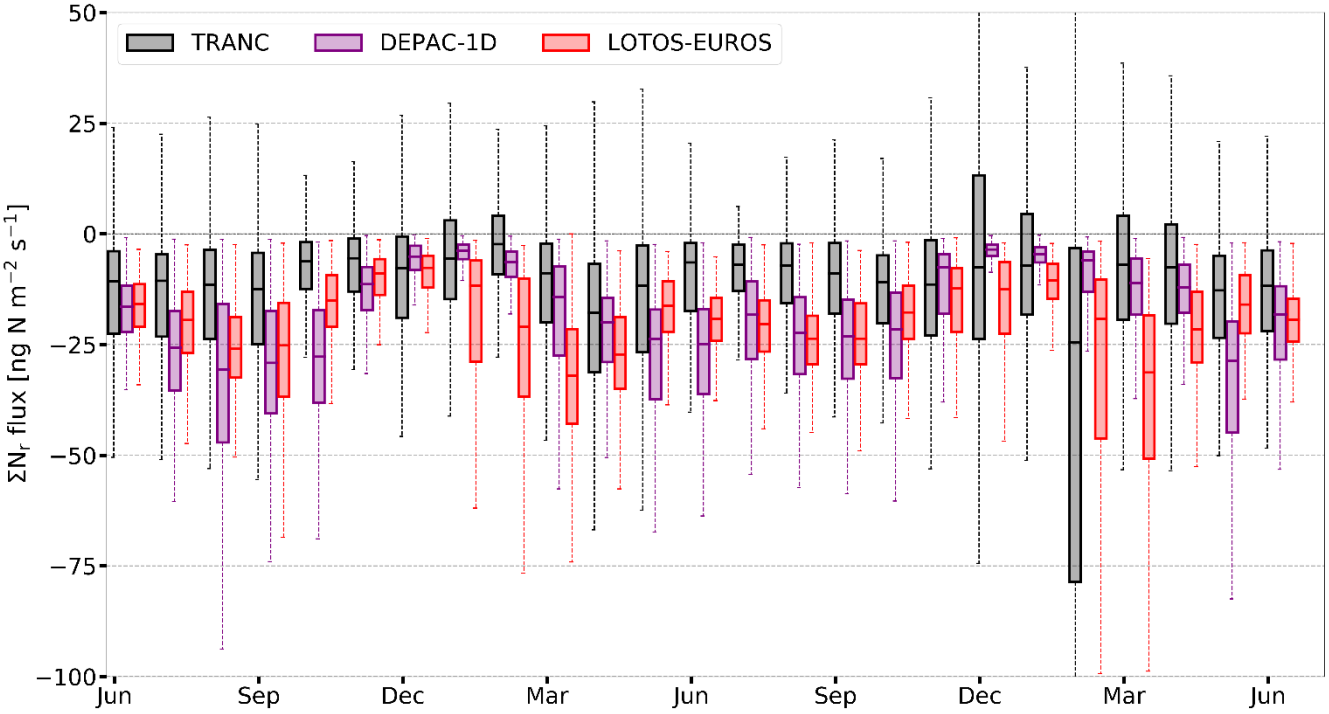

Figure 4.13: Fluxes of DEPAC-1D (purple), LOTOS-EUROS (red), and TRANC (black) from June 2016 to June 2018 shown as box-and-whisker plots. Whiskers of TRANC fluxes cover the range from -191 to 105 ng N m^{-2} s^{-1} in February 2018; the upper whisker of December 2017 reached 69 ng N m^{-2} s^{-1}.

Figure S4.8 shows exemplarily monthly diurnal cycles of ΣN_r based on TRANC, DEPAC-1D, and LOTOS-EUROS. As previously written, during winter LOTOS-EUROS overestimated deposition whereas measurements showed near-zero exchange with occasional emission phases. From May to September/October, DEPAC-1D exhibited a clear diurnal pattern with lowest deposition during the night and highest values around noon, which was in line with results from TRANC measurements. However, fluxes were systematically overestimated as indicated by Fig. 4.6 and Fig. S4.8 during those months. During the same period, ΣN_r deposition of LOTOS-EUROS was lower but still higher than TRANC fluxes except for September. During that month, LOTOS-EUROS was similar to DEPAC-1D. Generally, the diurnal deposition pattern of LOTOS-EUROS was considerably dampened, thereby not agreeing well with DEPAC-1D and TRANC.

4.3.4 Cumulative N exchange and method comparison

To derive annual deposition numbers the gap-filling procedures were applied to the time series of TRANC and DEPAC-1D (see Sect. 4.2.1). Figure 4.7 shows the cumulative ΣN_r dry deposition of each method from January 2016 to end of June 2018. The contributions of the individual components to the dry ΣN_r deposition of DEPAC-1D were: 67.9 % NH_3, 15.3 % HNO_3, 10.4 % NO_2, 5.2 % NH_4^+, 1.0 % NO_3^-, and 0.1 % NO showing that modeled deposition was clearly driven by NH_3. Since emission processes could only be treated for NH_3, the observed emission of ΣN_r, for example in December 2017 (Wintjen et al., 2022), could not be sufficiently modeled. Due to issues in the parameterization of stability in LOTOS-EUROS (see Sect. 4.4.2.2), particle deposition was enhanced in the LOTOS-EUROS results compared to DEPAC-1D (Fig. 4.7). Deposition of gases only was higher in DEPAC-1D due to the higher deposition velocities for NH_3, NO_2, and HNO_3 during summer compared to LOTOS-EUROS (Sect. 4.3.2.1). Comparing TRANC fluxes using MDV and DEPAC-1D in combination for gap-filling called TRANC(MDV+DEPAC-1D) to LOTOS-EUROS and DEPAC-1D, the differences in

total dry deposition estimates were 5.4 and 2.8 kg N ha^{-1} after 2.5 years, respectively.

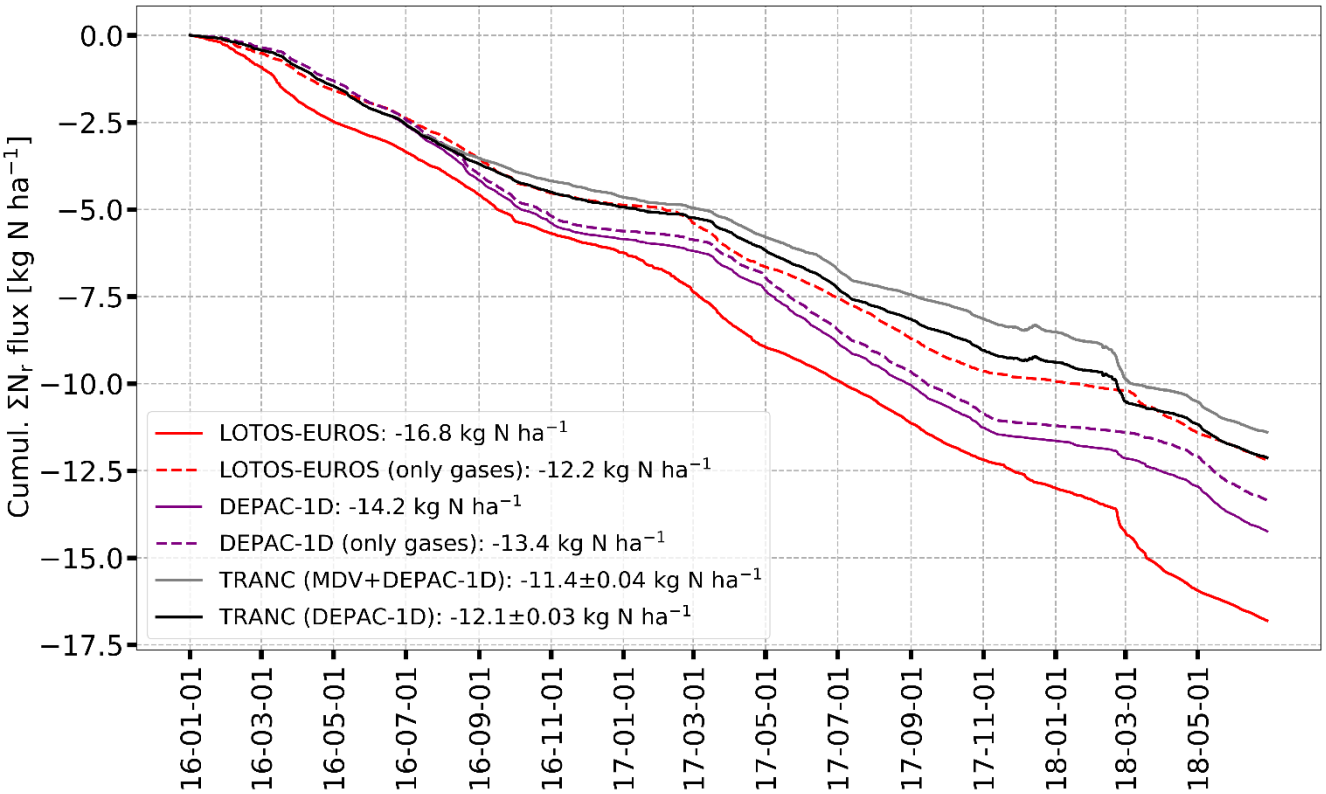

Figure 4.14: Comparison of measured and modeled cumulative ΣN_r dry deposition after gap-filling for the entire measurement campaign. Colors indicate different methods: TRANC+DEPAC-1D (black), TRANC+MDV+DEPAC-1D (grey), DEPAC-1D (purple), and LOTOS-EUROS (red). Dashed lines refer to cumulative dry deposition considering only gases. Number shown in the legend represent dry deposition and uncertainties after 2.5 years.

Since all cumulative curves exhibit generally the same shape, we conclude that the variability in fluxes is reproduced by DEPAC-1D and LOTOS-EUROS well, although the amplitude and duration of certain deposition events is different. Furthermore, both gap-filling strategies resulted in similar deposition estimates showing that the application of MDV as gap-filling tool is reasonable. Uncertainties related to gap-filling measured TRANC time series by MDV and DEPAC-1D by Eq. (4.1) were negligible. In Fig. 4.8, a comparison of the ΣN_r dry deposition separated by methods and measurement years is shown. Corresponding values of the dry deposition estimates are given in Table 4.2.

Table 4.4 ΣN_r dry deposition of TRANC, DEPAC-1D, LOTOS-EUROS, and CBT for the entire measurement campaign, i.e., January 2016 to June 2018. Results from CBT were weighted according to the measured land-use weighting. For a visualization of the annual dry deposition see Fig. 4.8.

Method	2016 [kg N ha^{-1} a^{-1}]	2017 [kg N ha^{-1} a^{-1}]	until June 2018 [kg N ha^{-1} a^{-1}]
TRANC (MDV+DEPAC-1D)	4.6	3.9	2.9
TRANC (DEPAC-1D)	4.9	4.5	2.7
DEPAC-1D	5.8	5.8	2.6
LOTOS-EUROS	6.2	6.8	3.8
CBT (lower estimate)	3.3	4.3	
CBT (upper estimate)	6.4	7.0	

In 2016, annual TRANC deposition was higher than in 2017. Using only DEPAC-1D as gap-filling technique, resulted in slightly higher dry deposition estimates. In 2018, the difference to TRANC estimates until June was caused by the deposition fluxes in February 2018, which had an influence on the MDV method leading to significantly larger gap-filled fluxes. Hence, DEPAC-1D estimate was lowest among all methods for the first half of 2018. In 2016 and 2017, deposition estimates of DEPAC-1D were nearly identical due to similarities in micrometeorological and concentration input values. As expected from Fig. 4.7, annual LOTOS-EUROS estimates were highest in comparison to DEPAC-1D and TRANC. All deposition estimates were within the range of long-term lower and upper estimates of the CBT approach estimated from 2010 to 2018, with TRANC measurements close to the lower average and LOTOS-EUROS predictions to the higher average.

Averaging of the annual sums of each method for 2016 and 2017 resulted in a TRANC dry deposition of 4.3±0.4 and 4.7±0.2 kg N ha^{-1} a^{-1} depending on the gap-filling approach. DEPAC-1D showed 5.8±0.1 kg N ha^{-1} a^{-1}, LOTOS-EUROS predicted 6.5±0.3 kg N ha^{-1} a^{-1}. We determined 6.7±0.3 kg N ha^{-1} a^{-1} with CBT as averaged upper estimate, and 3.8±0.5 kg N ha^{-1} a^{-1} as averaged lower estimate.

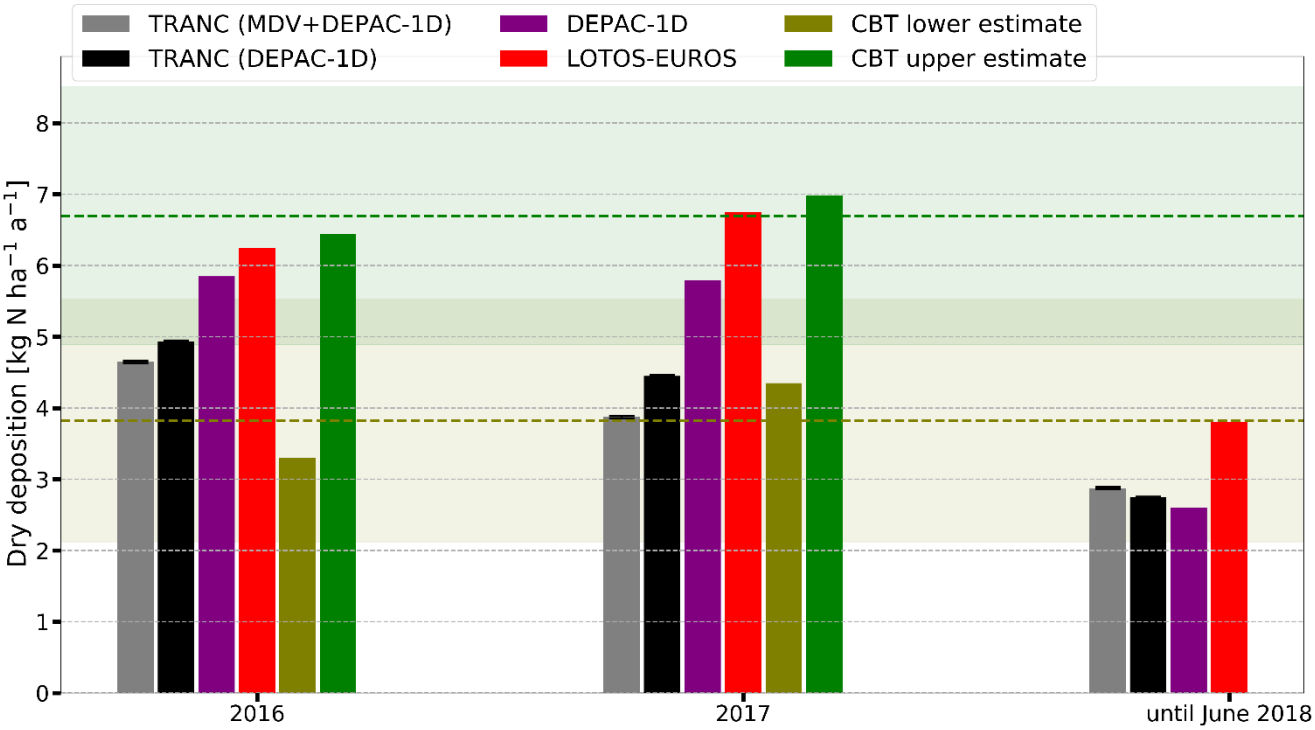

Figure 4.15: ΣN_r dry deposition for the years 2016 and 2017 and from January to June 2018 shown as bar chart. Colors indicate different methods: TRANC(DEPAC-1D) (black), TRANC(MDV+DEPAC-1D) (grey), DEPAC-1D (purple), LOTOS-EUROS (red), and canopy budget technique (olive and green). Data from TRANC, DEPAC-1D, and LOTOS-EUROS range from January 2016 to June 2018. CBTs' lower and upper estimates weighted according to the measured land use. The colored dashed lines indicate the averaged dry deposition of the lower and upper estimates (dashed, brown line and dashed, olive line, respectively) were from 2010 to 2018, the shaded areas represent their standard deviation.

4.4 Discussion

4.4.1 Comparison of concentrations, fluxes, and annual budgets

Differences in the concentration contribution of N_r species to ΣN_r

According to the LOTOS-EUROS simulations, NH_3 had a predominant role in the ΣN_r concentration pattern. This result was in contrast to concentration measurements of individual N_r species at the site

highlighting NO_x as the prevailing compound in the concentration pattern of ΣN_r (Wintjen et al., 2022). The predominant role of NH_3 in the modeled concentrations is caused by the emission inventory used in this study. The emission inventory spatially allocates NH_3 manure derived emissions through a procedure in which the animal numbers per region and agricultural land within a region are the two proxies used. Emissions from fertilizer application are allocated solely on land use. Hence, within a region all agricultural land is assumed to emit the same amount of NH_3, although the intensity of the agricultural practice and distribution of housing may vary substantially within such a region. Only south of the site, agricultural lands are located within 7 x 7 km^2 model resolution representing the site. This means that in the grid cell of the model, in which the station is located, there is an emission source contributing an increased NH_3 concentration even when the wind directions are not transporting air from this agricultural region towards the station.

In LOTOS-EUROS, particulate nitrogen also had a significant contribution to modeled ΣN_r, which could not be confirmed by measurements. However, the comparison of particulate nitrogen concentrations is difficult because of the aerosol cut-off size in DELTA measurements being at 4.5 µm (Tang et al., 2015). Aerosols available in fine mode like ammonium sulfate ($(NH_4)_2SO_4$) and ammonium nitrate (NH_4NO_3) are associated with aerodynamic diameter of less than 2.5 µm (Kundu et al., 2010; Putaud et al., 2010; Schwarz et al., 2016) and could be sufficiently sampled. Concentrations of coarse-mode aerosols with larger diameters than the cut-off size were partly underestimated. However, concentrations of sodium, magnesium, and calcium ions were negligible at the site (Wintjen et al., 2022) indicating that coarse-mode nitrate aerosols had no significant contribution to ΣN_r concentration. In addition, carbonate coated denuders used for collecting HNO_3 overestimate concentrations by approximately 45 % since nitrous acid also sticks to those prepared surfaces (Tang et al., 2021). Thus, disagreements could be related to emission inventory of $PM_{2.5}$ and PM_{10}, chemical process modeling, or to DELTA measurements.

NO_x concentrations agreed in their seasonal dynamics, thus processes responsible for modeling temporal dynamics of NO_x emissions are implemented reasonably in LOTOS-EUROS. However, the systematic underestimation of NO_x concentration by LOTOS-EUROS shows that NO_x sources within this grid cell, most likely emissions from road transport and private households due to the absence of large industrial areas or power plants in the surroundings of the station, are presumably not tracked sufficiently by the emission inventory.

Generally, the low measured concentrations of N_r compounds show that the site was mostly outside the transport range of nitrogen enriched air masses. Improvements in the close-range transport in LOTOS-EUROS regarding atmospheric lifetime of N_r species or in the definition of atmospheric layers are likely needed. A reduction in grid cell size could lead to a more accurate localization of potential nitrogen emission sources and a better description of close-range transport and dilution effects. The impact of an increase in model resolution is elaborated in Sect. 4.4.2.2.

Differences in measured and modeled ΣN_r fluxes

Overall, measured and modeled ΣN_r deposition were comparable in the order of magnitude and partly agreed in temporal dynamics but still exhibited disagreements in flux amplitude, which were related to differences in concentration, micrometeorology, and the integration of exchange pathways in DEPAC. Currently, a compensation point is only implemented for NH_3, and thus only deposition fluxes could be modeled for other compounds. Since the total compensation point of NH_3 was negligible in DEPAC, emission fluxes of NH_3 observed for a deciduous forest by Hansen et al. (2015) probably due to a decay of fallen leaves (Hansen et al., 2013) could not be reproduced. The soil compensation point, which is integrated in the calculation of the NH_3 compensation point but currently set to zero, may reduce the observed differences to TRANC fluxes.

The observed temporal pattern in v_d of NO_2 is related to the stomatal uptake, which is close to zero in winter and highest in summer. The slight difference in deposition velocities of NO_2 were caused by

higher measured concentrations of NO_x (see Fig. S4.2). In addition, no compensation point is implemented for NO_2, and deposition on leaves is hardly allowed. Both assumptions are in disagreement with findings by Horii et al. (2004), who identified non-stomatal deposition as strongest contributor to the flux, and by Thoene et al. (1996), who proposed the existence of a compensation point for NO_2. However, nitrogen concentrations in leaf samples taken in surroundings of the site showed no unusually high enrichment of nitrogen in leaves and needles (Beudert and Breit, 2014). Thus, neglecting the emission pathway of oxidized nitrogen compounds like NO_2 seems reasonable for the measurement site.

To reduce the difference between measured and modeled fluxes, considering nitrogen emissions from soil may lead to a closer agreement with flux measurements. As written above, soil compensation point has no influence on deposition of N_r species in DEPAC yet, and soil resistance implementation is kept simple: A constant value is assumed depending on the soil wetness (dry, wet, or frozen). Improvements in the description of the exchange with the soil surface may allow to describe the observed TRANC emission fluxes in December 2017 reported by Wintjen et al. (2022). Changes made to the soil exchange path may lower the flux contribution of NH_3 as outlined before but increase the contribution NO since the latter is generally observed as emission from soil if it is produced through (de)nitrification processes (Butterbach-Bahl et al., 1997; Rosenkranz et al., 2006). At the reference height, contribution of NO may be still low due to fast conversion processes to NO_2 in the presence of ozone (O_3) within the forest canopy, especially close to the ground (Rummel et al., 2002; Geddes and Murphy, 2014). Increased NO_2 concentrations within the forest canopy may alter concentrations of various N_r species, e.g., resulting in the formation of HNO_3, which may contribute substantially to the deposition flux (Munger et al., 1996; Horii et al., 2006). Consequently, a soil compensation point may be also relevant for the exchange of other N_r species next to NH_3.

The observed large deposition fluxes in February 2018 were reproduced in the model simulations although the modeled flux amplitude was smaller. During that time, modeled concentrations and fluxes of particulate N_r were the largest contributor to total ΣN_r, leading to the assumption of particle driven ΣN_r deposition. DELTA measurements suggested that particulate NH_4^+ was most likely responsible for the measured ΣN_r deposition (Wintjen et al., 2022, Fig. 10). Modeled and measured NH_4^+ concentrations differed only by 0.75 µg N m^{-3} whereas a significant disagreement was found between NH_3 measurements and LOTOS-EUROS (approx. 2.7 µg N m^{-3}). According to DELTA measurements, the NH_3 concentration was approximately 0.17 µg N m^{-3}. The averaged SO_2 concentration obtained from LOTOS-EUROS and DELTA were comparable during the exposure period of the samplers (1.5 and 2.0 µg m^{-3}, respectively). According to the LOTOS-EUROS simulations, an excess of pNH_4^+ over pNO_3^- was modeled suggesting that particle deposition was most likely caused by pNH_4^+, which is in agreement with DELTA measurements. In conclusion, the high deposition fluxes seem to be driven by particulate NH_4^+ compounds, ammonium sulfate and ammonium nitrate. During February 2018, DELTA measurements revealed a slightly lower concentration of the SO_4^{2-} than the NO_3^- aerosol, 1.28 and 1.63 µg m^{-3}, respectively, suggesting that NH_4NO_3 was most responsible for the observed ΣN_r deposition fluxes. Still, the dominant aerosol is not fully known due to missing high-resolution measurements of nitrogen aerosols. Apart from February 2018, winter fluxes of LOTOS-EUROS were large compared to DEPAC-1D although the same size-resolved model for determining aerosol deposition velocities was used. By comparing dry deposition caused by gases+particles and gases only of DEPAC-1D and LOTOS-EUROS (Fig. 4.7), a substantial disagreement in aerosol deposition was found. The large particulate nitrogen fluxes of LOTOS-EUROS are caused by uncertainties in the stability parameterization (Sect. 4.4.2.2). Issues in the description of turbulence-controlled deposition had also an effect on HNO_3 since its R_c is set to a relatively low constant value. Thus, LOTOS-EUROS deposition fluxes of HNO_3 were substantially higher in winter than deposition fluxes of DEPAC-1D. During summer, differences in deposition velocities were related to higher measured concentrations of HNO_3 (see Fig. S4.2).

Analysis of ΣN_r deposition estimates

The ΣN_r dry deposition estimates of TRANC, DEPAC-1D, and LOTOS-EUROS were in the same range after 2.5 years but differences in seasonal flux patterns were found. In addition, both gap-filling methods applied to flux measurements led to similar dry deposition estimates indicating that the MDV approach is suitable for gap-filling of short-term gaps in TRANC flux timeseries. During summer, we found differences in the gap-filled fluxes due to systematic overestimation of DEPAC-1D, which was related to the different response of DEPAC-1D to micrometeorological conditions compared to TRANC (Fig. 4.4). It should be kept in mind that monthly integrated pNO_3^-, pNH_4^+, and HNO_3 concentration estimates may not be able to fully capture local events. Moreover, the aerosol cut-off size of DELTA was probably lower than of the TRANC measurements as supposed by Wintjen et al. (2022). Saylor et al. (2019) also noted that v_d of particles for forest are highly uncertain. Thus, differences to measurements and predictions of LOTOS-EUROS in particle deposition could be expected. Besides missing emission fluxes in DEPAC-1D, the agreement of the dry deposition estimates was reasonable indicating that an inferential model like DEPAC-1D can be a valuable alternative to purely statistical gap-filling tool at sites or seasons with predominant N deposition.

Annual dry deposition estimates from TRANC, LOTOS-EUROS, and DEPAC-1D were found to be within the range of the lower and upper estimates of the CBT approach. Adding the wet-only deposition results reported in Wintjen et al. (2022) to the determined dry depositions, we calculated annual total depositions ranging between 11.5 and 14.8 kg N ha^{-1} a^{-1} noted in Table 3 for each year.

Table 4.5: Annual ΣN_r deposition of TRANC, DEPAC-1D, LOTOS-EUROS, and CBT for 2016, 2017, and from January to June 2018 in kg N ha^{-1} a^{-1}. Wet-only depositions of NO_3^-, NH_4^+, and DON were adapted from Wintjen et al. (2022).

Method	2016 [kg N ha^{-1} a^{-1}]	2017 [kg N ha^{-1} a^{-1}]	Until June 2018 [kg N ha^{-1} a^{-1}]
TRANC (MDV+DEPAC-1D)	12.9	11.7	6.3
TRANC (DEPAC-1D)	13.1	12.3	6.2
DEPAC-1D	14.1	13.6	6.1
LOTOS-EUROS	14.4	14.6	7.3
CBT (upper estimate)	11.5	12.2	
CBT (lower estimate)	14.6	14.8	

Comparing the results obtained from the measurement site to results obtained for other forest ecosystems using a similar validation procedure is rather difficult due to a large temporal and spatial variability in N_r compounds contributing to ΣN_r. Additionally, micrometeorological measurements as carried out in this study require substantial effort in maintenance and processing of the acquired data. Thus, most currently available EC measurements are limited to time periods covering a few weeks or months and are only available for certain locations.

Recently, Ahrends et al. (2020) compared deposition estimates of a CBT approach, an inferential method, and LOTOS-EUROS for several forest ecosystems. However, their CBT was based on the variant suggested by Ulrich (1994), which is different to the version used in this study, and their inferential method (IFM) was only applied to NO_2 and NH_3 due to the limited availability of ambient concentration measurements for other N_r compounds. In addition, deposition velocities for NO_2 and NH_3 were calculated based on literature research for different forest types accompanied by various correction

factors. They reported similar annual dry deposition estimates for CBT and IFM, which were found to be 12.6 and 12.9 kg N ha^{-1} a^{-1}, respectively. Minimum dry deposition was 3.8 kg N ha^{-1} a^{-1} for CBT and 1.0 kg N ha^{-1} a^{-1} for IFM. The lowest average dry deposition was 9.3 kg N ha^{-1} a^{-1} given by LOTOS-EUROS but its minimum dry deposition was highest (approx. 6.3 kg N ha^{-1} a^{-1}). Since we measured N deposition in a low-polluted environment, the agreement to the minimum dry deposition estimates of Ahrends et al. (2020) seems reasonable.

In the consideration of critical loads, total nitrogen deposition is within the proposed limits. Critical loads ranging from 10 to 15 kg N ha^{-1} a^{-1} and 10 to 20 kg N ha^{-1} a^{-1} were defined by Bobbink and Hettelingh (2011) for *Picea abies* and *Fagus sylvatica*, respectively. Since *Picea abies* was the prevailing tree species in the flux footprint (approx. 80%), the critical load of the investigated forest ecosystem is probably closer to the limits of *Picea abies*. The state of tree physiological parameters suggested that the critical load concept, which indicated that the exposure of the forest to N deposition is still below critical limits, is a valuable tool to evaluate the functionality of an ecosystem. Long-term observations of nitrogen input to this ecosystem showed nitrogen concentrations in trees and water reservoirs, but ecosystem functionality was not impaired. According to leaf examinations done by Beudert and Breit (2014) at the site, balanced ratios of nitrogen to other nutrient concentrations in tree foliage were found, and usual tree growths were reported. Jung et al. (2021) found low nitrate concentrations in soil water, aquifers, and streams at the site showing an intact nitrogen retention and storage system. Moreover, green algae coatings on spruce needles usually indicating higher NH_x dry deposition (Grandin, 2011) were not found at the site.

4.4.2 Modeling uncertainties

Influence of micrometeorological parameters

In both DEPAC-1D and LOTOS-EUROS, wet leaf surfaces and high relative humidity were identified as conditions enhancing ΣN_r deposition from May to September. In case of temperature, dry leaf surfaces, and low relative humidity, diurnal cycles of v_d showed a different behavior: For DEPAC-1D, lower temperatures were found to increase v_d, whereas the opposite observation was made for LOTOS-EUROS and their shapes were different. These disagreements were probably related to the stomatal uptake of NH_3 prevailing in the ΣN_r deposition flux of LOTOS-EUROS. Only for wet leaf surfaces and high relative humidity, which generally hold an important role in the deposition of NH_3 (Wentworth et al., 2016), diurnal shapes of DEPAC-1D and LOTOS-EUROS were similar suggesting that cuticular deposition of NH_3 seemed to be most responsible for the modeled ΣN_r dry deposition at the measurement site. Similar observations were made by Wyers and Erisman (1998), who identified the cuticular pathway as a larger sink for NH_3 than the stomatal pathway.

However, the results from TRANC measurements highlighted higher temperatures, lower relative humidity, and dry leaf surfaces as important factors enhancing ΣN_r deposition, and diurnal cycles of the TRANC were different in shape from those of LOTOS-EUROS. The differences night-time deposition are probably related to low aerodynamic resistances in the model applications indicating high u_* values, which could not be verified by EC measurements. However, measuring night-time exchange with the EC method and micrometeorological methods in general is challenging. Common detection algorithms for a u_* threshold (Reichstein et al., 2005; Barr et al., 2013) are not applicable to N_r species yet since they are optimized for CO_2. The contradiction in wet and dry conditions lead to the assumption that the current implementation of the NH_3 exchange pathways in DEPAC was not fully suited for predicting NH_3 deposition correctly and needs further investigation. It should be kept in mind that we measured ΣN_r exchange at a low-polluted, mixed forest site. Sites with different micrometeorology, vegetation, and pollution climate may exhibit other parameters like surface wetness, canopy temperature, and ambient concentration responsible for the ΣN_r exchange as found by Milford et al. (2001). Further

comparisons to flux measurements of ΣN_r and NH_3 are needed to investigate the role of stomatal and cuticular deposition.

Influence of soil resistance and soil compensation point

In DEPAC, soil resistance is set to a constant value depending on soil status, i.e. frozen (R_{soil} =1000 s m^{-1}), dry (R_{soil} =100 s m^{-1}), or wet (R_{soil} =10 s m^{-1}). In addition, the in-canopy resistance (as part of the effective soil resistance) is dependent on the inverse of u_*, surface area index (LAI+ area index of stems and branches (van Zanten et al., 2010)) and may lower the exchange with the soil. A soil compensation point is currently set to zero for NH_3 and not implemented for other N_r species since an appropriate parameterization or value is not known so far as argued by van Zanten et al. (2010). Consequently, deposition through the soil pathway is close to zero for most half-hourly records according to the current parameterization. Including a soil compensation point in DEPAC and improvements in the soil resistance parameterization, may lead to a better agreement with flux measurements. However, modifications related to soil exchange are probably challenging since they may affect the contribution of various N_r species to the ΣN_r flux, and a parameterization of soil resistance, e.g., depending on soil moisture and temperature, is probably required instead of assuming a constant value.

At the site, no measurements of soil conductance, soil moisture, and soil temperature were made. Thus, we cannot evaluate the representativeness of the current soil parameterization. Moreover, those measurements would have been challenging at the site due to the large spatial variability in the wide flux foot print area. For further measurement campaigns of similar nature, measurements of soil specific parameters are highly recommended.

Cuticular compensation point of NH_3

Schrader et al. (2016) discovered problems in the calculation of the cuticular NH_3 compensation point under high ambient NH_3 concentrations and high temperatures, for instance during summer. The current implementation of Wichink Kruit et al. (2010) in DEPAC likely underestimates the cuticular compensation point at high temperatures. This issue is not solved yet and could not be verified for our measurement site due to generally low NH_3 concentrations and the implementation of monthly averaged NH_3 concentration instead of half-hourly values in the concentration time series of NH_3 to some extent. Moreover, the cuticular emission potential was estimated from monthly averaged concentrations in LOTOS-EUROS and DEPAC-1D, instead of instantaneous values as in the original parameterization of Wichink Kruit et al. (2010), likely somewhat alleviating the issue discussed in Schrader et al. (2016). Thus, this issue could not be the main reason for the difference to flux measurements at our site.

Influence of emission fluxes on ΣN_r

With the TRANC system, the contribution of ΣN_r emission fluxes above the limit of detection was estimated to 16 % (Wintjen et al., 2022). Unfortunately, robust QCL-based NH_3 flux measurements using the EC method were not possible at the measurement site (Wintjen et al., 2022). Thus, contribution of individual N_r species – at least the NH_3 and hence the reduced N contribution - to the measured ΣN_r flux is not known. However, the presence of emission fluxes shows that an implementation of a compensation point for soil and/or mechanisms describing emissions of oxidized N_r species like NO_2 and HNO_3 should be considered. As described above, fully integrating the soil compensation point in the exchange of NH_3 may explain emissions fluxes of ΣN_r. For HNO_3, emission fluxes were reported in recent publications (Tarnay et al., 2002; Farmer and Cohen, 2006, 2008). The latter conducted flux measurements of HNO_3 above a pine forest and found a significant contribution of emission fluxes during summer. Those emission could also be induced by the evaporation of NH_4NO_3 from leaf surfaces

occurring at higher temperatures (Wyers and Duyzer, 1997; Van Oss et al., 1998), or particles deposited or formed on leaf surfaces as discussed by Nemitz et al. (2004). Emission fluxes of NO and NO_2 were reported in several publications, e.g., Farmer and Cohen (2006), Horii et al. (2004), and Min et al. (2014) leading to the assumption of the existence of a compensation point (Thoene et al., 1996), whereas other authors still critically discuss such a compensation point for NO and NO_2 (Chaparro-Suarez et al., 2011; Breuninger, et al. 2013; Delaria, et al., 2018, 2020). Since no significant N concentrations in leaves were found at the site (Beudert and Breit, 2014), an integration of a compensation point for NO_2 is probably less useful for the measurement site. Still, further flux comparisons of oxidized nitrogen compounds to their modeled entities are needed which would possibly lead to improvements in the representation and accurate apportionment of exchange pathways in (bi)directional resistance models.

4.4.2.1 Uncertainties in DEPAC-1D

Leaf area index and displacement height

Besides the current implementation of the exchange pathways in DEPAC, deposition estimates could be more accurate if concentration measurements at a higher time resolution and measurements of the LAI would have been available. We did not take measurements of the LAI or other vegetation properties at the measurement site. Still, the interpretation of differences to flux measurements would be challenging since the vegetation inside the flux footprint was not uniform. Inside the footprint, we identified dead wood in southern direction and a mix of rather young and matured trees in easterly direction. Differences in tree age were related to a dieback by bark beetle in the mid-1990s and 2000s (Beudert and Breit, 2014) from which the forest stand is still recovering. Shifting z_0 or d by ±50 %, caused a change of +5.0 %/-3.2 % and +5.6 %/-9.1 %, respectively, in the nitrogen dry deposition after 2.5 years. An incorrect assessment of the modeled LAI by ±50 % had a significant influence on the dry deposition. It led to a change of +18.9 %/-27.2 %. It shows that in further field applications of DEPAC-1D measurements the LAI should be considered, but an incorrect assessment of the LAI would not solely explain the overestimation of DEPAC-1D to TRANC measurements.

Using long-term concentration averages

The main uncertainty of DEPAC-1D fluxes was most likely the usage of monthly integrated DELTA concentrations for the N_r compounds. Thus, the large variability in the timeseries of these compounds happening on timescales of a few seconds were not accounted for in deposition modeling. Even with high-resolution measurements of the QCL, the short-term variability in NH_3 concentrations was not detectable (Wintjen et al., 2022). As stated in Sect. 4.2.2.3, we did not superimpose monthly concentrations values with synthetic diurnal patterns. Concentrations of N_r compounds are highly variable during the day and depend on various parameters such as turbulence, temperature, relative humidity, precipitation, and emission sources. Thus, it is not possible to capture the short-term variability of N_r species, which is induced by those parameters, with long-term averages. We found that the NH_3 concentration was generally low during winter and assigned with a low variability as found by measurements. During those times, using monthly integrated averages is reasonable (Schrader et al., 2018). However, we probably overestimated modeled fluxes due to the use of monthly averaged concentrations. In order to get at least an impression which N_r compounds' fluxes may be biased by this approach, we compared monthly averaged fluxes of LOTOS-EUROS (A1) with fluxes calculated by multiplying monthly averaged v_d with their monthly concentration averages (A2) and subsequently corrected them by applying Eq. (9) and (10) of Schrader et al. (2018). Generally, we found that all N_r compounds' fluxes were overestimated by A2 whereas the difference to A1 depends on the investigated N_r compound and season. All N_r compounds had in common that the difference between both approaches was negligible during seasons with small deposition fluxes, for example in winter. Within seasons of large deposition fluxes, significant discrepancies were found, in particular for NH_3. Overall,

mean absolute deviations to A1 were 35.0, 0.27, 0.18, 0.92, 2.5, and 2.4 ng N m^{-2} s^{-1} for NH_3, NO_2, NO, HNO_3, NH_4^+, and NO_3^-, respectively.

It should be considered that we used LOTOS-EUROS data for this comparison. Especially for NH_3, NH_4^+, and NO_3^-, their modeled seasonality and concentrations exhibited significant disagreements to DELTA measurements. Thus, the flux overestimations should be seen as highest guess. Measured high resolution concentrations would have led to lower values. Still, the comparison highlights the necessity for high-resolution measurements of N_r compounds. Those measurements should be made for N_r compounds, which probably prevail the exchange dynamics of ΣN_r at a certain site and thereby at least cover time periods with large temporal variations in their concentrations. This procedure was performed for NH_3 and NO_2 at the measurement site and should be considered for further measurement campaigns.

4.4.2.2 Uncertainties in LOTOS-EUROS

The larger nitrogen deposition values for the measurement site as modeled by LOTOS-EUROS are mostly related to the overestimation of modeled input NH_3 concentrations. As visualized by Fig. S4.1, LOTOS-EUROS clearly exceed observed NH_3 concentrations in spring and autumn. Such an overestimation of NH_3 and NH_4^+ in precipitation at forest monitoring sites was identified before for stations in Baden-Württemberg and Bavaria (Schaap et al., 2017). A similar systematic overestimation by the model in southern Germany has also been identified in comparison to novel NH_3 satellite data (Ge et al., 2020). This leads us to believe that the overestimation is for a large part due to shortcomings in the emission information (Sect. 4.4.1), potentially in combination with the model resolution.

A reduction in grid cell size could lead to a more precise localization of potential nitrogen emission sources and a better description of close-range transport and dilution effects. For a simulation covering 2015, we were able to calculate concentrations and fluxes at a higher grid cell resolution (2 x 2 km^2) and compared the results to the standard spatial resolution (7 x 7 km^2). In case of the high grid cell resolution, concentrations were lower but only by 2 to 10 % depending on the compound compared to the standard spatial resolution. For the higher grid cell resolution, the annual N budget was higher than the budget of the standard spatial resolution case study, but only by 4.3 % probably due to differences in the relative fractions of land-use classes. The contribution of forest land-use classes was likely higher in case of the high spatial resolution. The higher grid cell resolution probably led to improvements in modeling atmospheric turbulence resulting in higher deposition velocities. This example shows that the grid cell resolution of 7 x 7 km^2 is not mainly responsible for the overestimation of concentrations and fluxes by LOTOS-EUROS.

Nevertheless, the seasonal cycle also indicates that the information, which LOTOS-EUROS extracts from the emission inventory, does not agree well with agricultural management practiced in the surrounding of the Bavarian Forest. The agricultural fields close to the Bavarian Forest are predominantly extensively managed grass lands. Manure application to grass lands is known to occur much more evenly distributed across the year in comparison to the application for crop production, which mainly occurs before or during the growing season. Hence, in reality the emission variability maybe prone more to summer conditions. Currently, the detailing of crop dependent emissions made within LOTOS-EUROS, i.e. the use of variable emission fractions within German regions in combination with the recent timing module of Ge et al. (2020), is under investigation to elucidate if these factors are contributing to the measurement-model mismatches observed for the measurement site.

Additional features may also contribute to the observed differences. Within LOTOS-EUROS, modeled concentrations were written out for a reference height of 2.5 m above z_0, which was lower than the measurement height of the flux tower. Slight differences between measured and modeled micrometeorological input data were found, for example the difference in relative humidity in the first half of 2016. Differences for that time period were related to the usage of local meteorological data taken at 50 m, which was higher than the model layer height associated with air temperature and relative

humidity. The deviations in u_* as illustrated in Fig. S4.6 and Fig. 4.5 were related to differences in measurement heights at which wind speeds and roughness lengths were calculated. The model grid cell consists of various vegetation types each with a unique surface roughness length. We showed that the weighting of the land use classes within the grid cell was not in agreement with the vegetation of the flux foot print affecting micrometeorological variables, e.g. u_*, L, and thereby the calculation of R_a and R_b.

The large contribution of aerosols to the total deposition (Fig. 4.7) modeled by LOTOS-EUROS was accompanied by unusually high deposition velocities of pNH_4^+, pNO_3^-, and HNO_3 from November 2017 to February 2018. LOTOS-EUROS did an integration over a fixed, i.e., neglecting influence of humidity, size distribution using a lognormal size distribution which needs a mass mean diameter, a geometric standard deviation, and a size-cut range to calculate v_d for particles. Deposition of HNO_3 and particulate nitrogen is mostly driven by the aerodynamic resistance and quasi-laminar resistance, R_a and R_b. Since v_d of those compounds was relatively high compared to measurements during that time, R_a and R_b were probably low or even close to zero. R_a and R_b depend on various parameters like u_*, the integrated stability corrections functions after Webb (1970) and Paulson (1970), surface roughness, and leaf area index. L determines the integrated stability functions and depends on wind speed close to the surface, cloud cover, and solar zenith angle (Manders-Groot et al., 2016). Snow cover is not considered in the parameterization of L yet. Including snow cover in the parameterization affect the albedo of the surface and thus the prevailing stratification of the boundary layer, which probably leads to more occurrences of stable stratification. An implementation of snow cover in the parameterization of L may reduce the deviations of simulated vs. measured stability and u_*.

An incorrect setting of the LAI and z_0 can have a significant influence on modeled ΣN_r deposition as shown in Sect. 4.4.2.1. The relative changes in modeled ΣN_r deposition caused by LAI and z_0 were comparable to values presented recently by van der Graaf et al. (2020), who used satellite-derived LAI and z_0 data from Moderate Resolution Imaging Spectroradiometer (MODIS) to calculate ΣN_r deposition with LOTOS-EUROS for a grid cell size of 7x7 km^2. Overall, they observed changes in ΣN_r dry deposition ranging from -20 % to +30 %. However, there was almost no change in ΣN_r dry deposition and in NH_3 concentration observable for the Bavarian Forest measurement site if LAI and z_0 from MODIS were used. The attempts of van der Graaf et al. (2020) and Ge et al. (2020) did not provide a solution for the general overestimation of the NH_3 deposition above southern Germany. We assume that the spatially and temporally imprecise allocation of emission data is most responsible for the disagreement to flux measurements. Further investigations on these issues are needed.

4.5 Conclusions

The annual total reactive nitrogen (ΣN_r) dry deposition estimates of all methods were in the same range considering uncertainties of measured fluxes and model applications. Annual estimates from the Total Reactive Atmospheric Nitrogen Converter (TRANC) were lower than the results from an in-situ inferential modeling approach using the bidirectional flux model DEPAC (Deposition of Acidifying Compounds) (here called DEPAC-1D) and the chemical transport model LOTOS-EUROS (Long Term Ozone Simulation – EURopean Operational Smog) v2.0. Annual dry deposition estimates of TRANC, DEPAC-1D, and LOTOS-EUROS were within the minimum and maximum dry deposition estimates of the canopy budget technique (CBT) showing ecological and micrometeorological measurements provide reasonable estimates. According to the critical load concept, annual nitrogen deposition was below critical values. Findings were supported by local vegetation samplings showing no indications for nitrogen exceedances leading to the conclusion that the critical load concept is a useful tool to describe the health status of an ecosystem.

Differences between DEPAC-1D and TRANC measurements could be related to uncertainties in parameterizing the exchange pathways of reactive gases, the usage of low-resolution input data, or the

missing exchange pathway with soil. Modeled ΣN_r deposition velocities of DEPAC-1D were enhanced with regard to wet conditions, which was in contrast to TRANC measurements leading to systematically larger deposition fluxes. To a smaller extent, the same observation was made for LOTOS-EUROS, and additionally deposition velocities of DEPAC-1D and LOTOS-EUROS did not agree well in their diurnal pattern. Thus, a further investigation of stomatal vs. non-stomatal deposition pathways needs to be conducted as these are likely the main factors for discrepancies in modeled vs. measured results. Besides possible uncertainty sources in DEPAC-1D, measured dry deposition estimates using DEPAC-1D for gap-filling were similar showing that DEPAC-1D (and by extension, inferential modeling in general) is a valuable gap-filling tool at sites with prevailing N deposition. The difference to dry deposition estimates of LOTOS-EUROS was mainly related to an overestimation of NH_3 concentrations by a factor of two to three compared to measured concentrations. Consequently, NH_3 contributed most to the ΣN_r concentration pattern in LOTOS-EUROS whereas NO_x was identified as predominant compound by measurements. The imprecise allocation of emission data may be responsible for the discrepancies to measured NH_3 concentrations since the general overestimation of NH_3 concentrations by LOTOS-EUROS has still not been solved by attempts of model developers (van der Graaf et al., 2020; Ge et al., 2020).

Further comparisons of flux measurements and model applications are needed to investigate exchange characteristics of ΣN_r and its individual compounds, if possible, simultaneously and at different ecosystems. Measuring several N_r compounds and ΣN_r at a high time resolution is probably not affordable due to operating and maintenance costs, high technical requirements, and time-consuming processing of the acquired data. A solution could be continuous monitoring of N_r compounds by low-cost samplers complemented by high-frequency measurements of ΣN_r and selected compounds like NH_3 for a limited time, which will result in a better understanding of exchange processes and thus in an improvement of deposition models (cf. Schrader et al., 2020).

Code and data availability. All data are available upon request from the first author of this study (pascal.wintjen@thuenen.de). Concentration, flux, and micrometeorological data from measurements and ecological information about the site are included in the following repository: https://zenodo.org/record/5841074 (Brümmer et al., 2022a). Also, Python 3.7 code for flux data analysis can be requested from the first author.

Author contributions. PW, FS, MS, and CB conceived the study. PW wrote the manuscript, carried out the measurements at the forest site, and the comparison of measured and modeled flux data and interpretation. FS evaluated meteorological measurements and set up DEPAC-1D. MS and RK provided insights in interpreting LOTOS-EUROS results. BB conducted canopy throughfall and wet deposition measurements. CB installed the instruments at the site. The results were thoroughly discussed with all authors, and FS, MS, BB, RK, and CB contributed to the manuscript.

Competing interests. The authors declare that they have no conflict of interest.

Acknowledgements. We thank Undine Zöll for scientific and logistical help to the measurements, Jeremy Rüffer and Jean-Pierre Delorme for excellent technical support, Ute Tambor, Andrea Niemeyer, and Dr. Daniel Ziehe for conducting laboratory analyses of denuder and filter samples, and the Bavarian Forest Nationalpark (NPBW) Administration, namely Wilhelm Breit and Ludwig Höcker for technical and logistical support at the measurement site.

Financial support. This work has been funded by the German Environment Agency (UBA) (project FORESTFLUX, support code FKZ 3715512110) and by the German Federal Ministry of Education and Research (BMBF) within the framework of the Junior Research Group NITROSPHERE (support code FKZ 01LN1308A).

References

Ahrends, B., Schmitz, A., Prescher, A.-K., Wehberg, J., Geupel, M., Henning, A., and Meesenburg, H.: Comparison of Methods for the Estimation of Total Inorganic Nitrogen Deposition to Forests in Germany, Frontiers in Forests and Global Change, 3, 1-22, doi:10.3389/ffgc.2020.00103, 2020.

Ammann, C., Wolff, V., Marx, O., Brümmer, C., and Neftel, A.: Measuring the biosphere-atmosphere exchange of total reactive nitrogen by eddy covariance, Biogeosciences, 9, 4247–4261, doi:10.5194/bg-9-4247-2012, 2012.

Ammann, C., Jocher M., and Voglmeier, K.: Eddy Covariance Flux Measurements of NH_3 and NO_y with a Dual-Channel Thermal Converter," *IEEE International Workshop on Metrology for Agriculture and Forestry (MetroAgriFor)*, pp. 46-51, doi: 10.1109/MetroAgriFor.2019.8909278, 2019.

Barr, A., Richardson, A., Hollinger, D., Papale, D., Arain, M., Black, T., Bohrer, G., Dragoni, D., Fischer, M., Gu, L., Law, B., Margolis, H., McCaughey, J., Munger, J., Oechel, W., and Schaeffer, K.: Use of change-point detection for friction–velocity threshold evaluation in eddy covariance studies, Agricultural and Forest Meteorology, 171–172, 31–45, doi: 10.1016/j.agrformet.2012.11.023, 2013.

Beudert, B. and Breit, W.: Kronenraumbilanzen zur Abschätzung der Stickstoffgesamtdeposition in Waldökosysteme des Nationalparks Bayerischer Wald, techreport, Umweltbundesamt, Dessau-Roßlau, Germany, available at: https://www.umweltbundesamt.de/sites/default/files/medien/370/dokumente/kronenraumbilanzen_stickstoffgesamtdeposition_nationalpark_bayerisches_wald_-_berichtsjahr_2013_im_forellenbach.pdf (last access: 14 March 2022), 2014.

Bobbink, R., Hornung, M. and Roelofs, J. G. M.: The effects of air-borne nitrogen pollutants on species diversity in natural and semi-natural European vegetation, Journal of Ecology, 86, 717–738, doi:10.1046/j.1365-2745.1998.8650717.x, 1998.

Bobbink, R. and Hettelingh, J.-P.: Review and revision of empirical critical loads and dose-response relationships. National Institute for Public Health and the Environment (RIVM), RIVM Report, https://www.rivm.nl/bibliotheek/rapporten/680359002.pdf (last access: 14 March 2022), 2011.

Breuninger, C., Meixner, F. X., and Kesselmeier, J.: Field investigations of nitrogen dioxide (NO_2) exchange between plants and the atmosphere, Atmospheric Chemistry and Physics, 13, 773–790, doi:10.5194/acp-13-773-2013, 2013.

Brümmer, C., Marx, O., Kutsch, W., Ammann, C., Wolff, V., Flechard, C. R., and Freibauer, A.: Fluxes of total reactive atmospheric nitrogen (ΣN_r) using eddy covariance above arable land, Tellus B: Chemical and Physical Meteorology, 65, 19770, doi:10.3402/tellusb.v65i0.19770, 2013.

Brümmer, C., Rüffer, J. J., Delorme, J.-P., Wintjen, P., Schrader, F., Beudert, B., Schaap, M., and Ammann, C.: Reactive nitrogen fluxes over peatland and forest ecosystems using micrometeorological measurement techniques, Earth System Science Data, 14, 743-761, doi:10.5194/essd-14-743-2022, 2022.

Brümmer, C., Rüffer, J. J., Delorme, J.-P., Wintjen, P., Schrader, F., Beudert, B., Schaap, M., and Ammann, C.: Reactive nitrogen fluxes over peatland (Bourtanger Moor) and forest (Bavarian Forest National Park) using micrometeorological measurement techniques (1.1) [Data set]. Zenodo. doi:10.5281/zenodo.5841074, 2022a.

Butterbach-Bahl, K., Gasche, R., Breuer, L., and Papen, H.: Fluxes of NO and N_2O from temperate forest soils: impact of forest type, N deposition and of liming on the NO and N_2O emissions, Nutrient Cycling in Agroecosystems, 48, 79–90, doi:10.1023/a:1009785521107, 1997.

Chaparro-Suarez, I., Meixner, F., and Kesselmeier, J.: Nitrogen dioxide (NO_2) uptake by vegetation controlled by atmospheric concentrations and plant stomatal aperture, Atmospheric Environment, 45, 5742–5750, doi:10.1016/j.atmosenv.2011.07.021, 2011

Damgaard, C., Jensen, L., Frohn, L. M., Borchsenius, F., Nielsen, K. E., Ejrnæs, R. and Stevens, C. J.: The effect of nitrogen deposition on the species richness of acid grasslands in Denmark: A comparison with a study performed on a European scale, Environmental Pollution, 159, 1778-1782, doi:10.1016/j.envpol.2011.04.003, 2011.

Delaria, E. R., Vieira, M., Cremieux, J., and Cohen, R. C.: Measurements of NO and NO_2 exchange between the atmosphere and Quercus agrifolia, Atmospheric Chemistry and Physics, 18, 14 161–14 173, doi:10.5194/acp-18-14161-2018, 2018.

Delaria, E. R., Place, B. K., Liu, A. X., and Cohen, R. C.: Laboratory measurements of stomatal NO_2 deposition to native California trees and the role of forests in the NO_x cycle, Atmospheric Chemistry and Physics, 20, 14 023–14 041, doi:10.5194/acp-20-14023-2020, 2020.

de Vries, W., Reinds, G. J., and Vel, E.: Intensive monitoring of forest ecosystems in Europe: 2: Atmospheric deposition and its impacts on soil solution chemistry, Forest Ecology and Management, 174, 97–115, doi:10.1016/S0378-1127(02)00030-0, 2003.

Dirnböck, T., Grandin, U., Bernhardt-Römermann, M., Beudert, B., Canullo, R., Forsius, M., Grabner, M.-T., Holmberg, M., Kleemola, S., Lundin, L., Mirtl, M. Neumann, M., Pompei, E., Salemaa, M., Starlinger, F., Staszewski, T., and Uziębło, A. K.: Forest floor vegetation response to nitrogen deposition in Europe, Global Change Biology, 20, 429-440, doi: 10.1111/gcb.12440 , 2014.

Dirnböck, T., Pröll, G., Austnes, K., Beloica, J., Beudert, B., Canullo, R., De Marco, A., Fornasier, M. F., Futter, M., Goergen, K., Grandin, U., Holmberg, M., Lindroos, A.-J., Mirtl, M., Neirynck, J., Pecka, T., Nieminen, T. M., Nordbakken, J.-F., Posch, M., Reinds, G.-J., Rowe, E. C., Salemaa, M., Scheuschner, T., Starlinger, F., Uziębło, A. K., Valinia, S., Weldon, J., Wamelink, W. G. W., and Forsius, M.: Currently legislated decreases in nitrogen deposition will yield only limited plant species recovery in European forests, Environmental research letters, 13, 125010, doi: 10.1088/1748-9326/aaf26b, 2018.

Draaijers, G. P. J. and Erisman, J. W.: A canopy budget model to assess atmospheric deposition from throughfall measurements, Water, Air, Soil Pollution, 85, 2253–2258, doi: 10.1007/BF01186169, 1995.

Emberson, L.D., Ashmore, M. R., Simpson, D., Tuovinen, J.-P. and Cambridge, H. M.: Towards a model of ozone deposition and stomatal uptake over Europe, EMEP/MSC-W 6/2000, Norwegian Meteorological Institute, Oslo, 2000a.

Emberson, L. D., Ashmore, M. R., Cambridge, H. M., Simpson, D., and Tuovinen, J. P.: Modelling stomatal ozone flux across Europe, Environmental Pollution, 109, 403–13, doi:10.1016/S0269-7491(00)00043-9, 2000b.

Erisman, J. W., Van Pul, A., and Wyers, P.: Parametrization of surface resistance for the quantification of atmospheric deposition of acidifying pollutants and ozone, Atmospheric Environment, 28, 2595–2607, doi:10.1016/1352-2310(94)90433-2, 1994.

Erisman, J. W., Galloway, J., Seitzinger, S., Bleeker, A. and Butterbach-Bahl, K.: Reactive nitrogen in the environment and its effect on climate change, Current Opinion in Environmental Sustainability, 3, 281-290, doi: 10.1016/j.cosust.2011.08.012., 2011.

Erisman, J. W., Galloway, J. N., Seitzinger, S., Bleeker, A., Dise, N. B., Petrescu, A. M., Leach, A. M. and de Vries, W.: Consequences of human modification of the global nitrogen cycle, Philosophical Transactions of the Royal Society London B: Biological Sciences, 368, 201301116, doi: 10.1098/rstb.2013.0116, 2013.

Falge, E., Baldocchi, D., Olson, R., Anthoni, P., Aubinet, M., Bernhofer, C., Burba, G., Ceulemans, R., Clement, R., Dolman, H., Granier, A., Gross, P., Grünwald, T., Hollinger, D., Jensen, N.-O., Katul, G., Keronen, P., Kowalski, A., Lai, C. T., Law, B. E., Meyers, T., Moncrieff, J., Moors, E., Munger, J., Pilegaard, K., Üllar Rannik, Rebmann, C., Suyker, A., Tenhunen, J., Tu, K., Verma, S., Vesala, T., Wilson, K., and Wofsy, S.: Gap filling strategies for defensible annual sums of net ecosystem exchange, Agricultural and Forest Meteorology, 107, 43–69, doi:10.1016/S0168-1923(00)00225-2, 2001.

Farmer, D. K., Wooldridge, P. J., and Cohen, R. C.: Application of thermal-dissociation laser induced fluorescence (TD-LIF) to measurement of HNO_3, Σalkyl nitrates, Σperoxy nitrates, and NO_2 fluxes using eddy covariance, Atmospheric Chemistry and Physics, 6, 3471–3486, doi:10.5194/acp-6-3471-2006, 2006.

Farmer, D. K. and Cohen, R. C.: Observations of HNO_3, ΣAN, ΣPN and NO_2 fluxes: evidence for rapid HO_x chemistry within a pine forest canopy, Atmospheric Chemistry and Physics, 8, 3899–3917, doi:10.5194/acp-8-3899-2008, 2008.

Ferm, M.: A Sensitive Diffusional Sampler, Report L91-172, Swedish Environmental Research Institute, Gothenburg, 1991.

Ferrara, R. M., Loubet, B., Di Tommassi, P., Bertolini, T., Magliulo, V., Cellier, P., Eugster, W., and Rana, G.: Eddy covarinance measurement of ammonia fluxes: Comparison of high frequency correction methodologies, Agricultural and Forest Meteorology, 158-159, 30-42, doi:10.1016/j.agrformet.2012.02.001, 2012.

Ferrara, R. M., Di Tommassi, P., Farmulari, D., and Rana G.: Limitations of an Eddy-Covariance System in Measuring Low Ammonia Fluxes, Boundary-Layer Meteorology, 180, 173-186, doi:10.1007/s10546-021-00612-6, 2021.

Finkelstein, P. L. and Sims, P. F.: Sampling error in eddy correlation flux measurements, Journal of Geophysical Research: Atmospheres, 106, 3503–3509, doi: 10.1029/2000JD900731, 2001.

Flechard, C. R., Nemitz, E., Smith, R. I., Fowler, D., Vermeulen, A. T., Bleeker, A., Erisman, J. W., Simpson, D., Zhang, L., Tang, Y. S., and Sutton, M. A.: Dry deposition of reactive nitrogen to European ecosystems: a comparison of inferential models across the NitroEurope network, Atmos. Chem. Phys., 11, 2703‑2728, doi:10.5194/acp-11-2703-2011, 2011.

Flechard, C. R., Ibrom, A., Skiba, U. M., de Vries, W., van Oijen, M., Cameron, D. R., Dise, N. B., Korhonen, J. F. J., Buchmann, N., Legout, A., Simpson, D., Sanz, M. J., Aubinet, M., Loustau, D., Montagnani, L., Neirynck, J., Janssens, I. A., Pihlatie, M., Kiese, R., Siemens, J., Francez, A.-J., Augustin, J., Varlagin, A., Olejnik, J., Juszczak, R., Aurela, M., Berveiller, D., Chojnicki, B. H., Dammgen, U., Delpierre, N., Djuricic, V., Drewer, J., Dufrene, E., Eugster, W., Fauvel, Y., Fowler, D., Frumau, A., Granier, A., Gross, P., Hamon, Y., Helfter, C., Hensen, A., Horvath, L., Kitzler, B., Kruijt, B., Kutsch, W. L., Lobo-do Vale, R., Lohila, A., Longdoz, B., Marek, M. V., Matteucci, G., Mitosinkova, M., Moreaux, V., Neftel, A., Ourcival, J.-M., Pilegaard, K., Pita, G., Sanz, F., Schjoerring, J. K., Sebastia, M.-T., Tang, Y. S., Uggerud, H., Urbaniak, M., van Dijk, N., Vesala, T., Vidic, S., Vincke, C., Weidinger, T., Zechmeister-Boltenstern, S., Butterbach-Bahl, K., Nemitz, E., and Sutton, M. A.: Carbon–nitrogen interactions in European forests and semi-natural vegetation – Part 1: Fluxes and budgets of carbon, nitrogen and greenhouse gases from ecosystem monitoring and modelling, Biogeosciences, 17, 1583–1620, doi:10.5194/bg-17-1583-2020, 2020.

Fowler, D., Coyle, M., Skiba, U., Sutton, M. A., Cape, J. N., Reis, S., Sheppard, L. J., Jenkins, A., Grizzetti, B., Galloway, J. N., Vitousek, P., Leach, A., Bouwman, A. F., Butterbach-Bahl, K., Dentener, F., Stevenson, D., Amann, M. and Voss, M.: The global nitrogen cycle in the twenty-first century, Philosophical Transactions of the Royal Society B: Biological Sciences, 368, 20130164, doi: 10.1098/rstb.2013.0164, 2013.

Galloway, J. N., Aber, J. D., Erisman, J. W., Seitzinger, S. P., Howarth, R. W., Cowling, E. B. and Cosby, B. J.: The Nitrogen Cascade, BioScience, 53, 341-356, doi: 10.1641/0006-3568(2003)053[0341:TNC]2.0.CO;2, 2003.

Garland, J. A.: The Dry Deposition of Sulphur Dioxide to Land and Water Surfaces, Proceedings of the Royal Society A: Mathematical, Physical and Engineering Sciences, 354, 245–268, doi:10.1098/rspa.1977.0066, 1977.

Ge, X., Schaap, M., Kranenburg, R., Segers, A., Reinds, G. J., Kros, H., and de Vries, W.: Modeling atmospheric ammonia using agricultural emissions with improved spatial variability and temporal dynamics, Atmos. Chem. Phys., 20, 16055–16087, doi:10.5194/acp-20-16055-2020, 2020.

Geddes, J. A. and Murphy, J. G.: Observations of reactive nitrogen oxide fluxes by eddy covariance above two midlatitude North American mixed hardwood forests, Atmospheric Chemistry and Physics, 14, 2939–2957, doi:10.5194/acp-14-2939-2014, 2014.

Grandin, U.: Epiphytic algae and lichen cover in boreal forests - a long-term study along a N and S deposition gradient in Sweden, Ambio, 40, 8, 857-866, doi: 10.1007/s13280-011-0205-x, 2011.

Hansen, K., Sørensen, L. L., Hertel, O., Geels, C., Skjøth, C. A., Jensen, B., and Boegh, E.: Ammonia emissions from deciduous forest after leaf fall, Biogeosciences, 10, 4577–4589, doi:10.5194/bg-10-4577-2013, 2013.

Hansen, K., Pryor, S. C., Boegh, E., Hornsby, K. E., Jensen, B., and Sørensen, L. L.: Background concentrations and fluxes of atmospheric ammonia over a deciduous forest, Agricultural and Forest Meteorology, 214-215, 380–392, doi: 10.1016/j.agrformet.2015.09.004, 2015.

Hettelingh, J.-P., Posch, M., De Smet, P. A. M. and Downing, R. J.: The use of critical loads in emission reduction agreements in Europe, Water, Air, and Soil Pollution., 85, 2381-2385, doi:10.1007/BF01186190, 1995.

Hettelingh, J.-P., Posch, M., Velders, G. J. M., Ruyssenaars, P., Adams, M., de Leeuw, F., Lükewille, A., Maas, R., Sliggers, J. and Slootweg, J.: Assessing interim objectives for acidification, eutrophication and ground-level ozone of the EU National Emission Ceilings Directive with 2001 and 2012 knowledge, Atmospheric Environment, 75, 129-140, doi:10.1016/j.atmosenv.2013.03.060, 2013.

Horii, C. V., Munger, J. W., Wofsy, S. C., Zahniser, M., Nelson, D., and McManus, J. B.: Fluxes of nitrogen oxides over a temperate deciduous forest, Journal of Geophysical Research: Atmospheres, 109, doi:10.1029/2003JD004326, 2004.

Horii, C. V., Munger, J. W., Wofsy, S. C., Zahniser, M., Nelson, D., and McManus, J. B.: Atmospheric reactive nitrogen concentration and flux budgets at a Northeastern US forest site, Agricultural and Forest Meteorology, 136, 159–174, doi:10.1016/j.agrformet.2006.03.005, 2006.

Jarvis, P. G.: The Interpretation of the Variations in Leaf Water Potential and Stomatal Conductance Found in Canopies in the Field, Philos. T. R. Soc. B, 273, 593‑610, doi:10.1098/rstb.1976.0035, 1976.

Jensen, N. and Hummelshøj, P.: Derivation of canopy resistance for water vapor fluxes over a spruce forest, using a new technique for the viscous sublayer resistance (correction to vol. 73, p. 339, 1995), Agricultural and Forest Meteorology, 85, 289, doi:10.1016/S0168-1923(97)00024-5, 1997.

Jensen, N. O. and Hummelshøj, P.: Derivation of canopy resistance for water-vapor fluxes over a spruce forest, using a new technique for the viscous sublayer resistance, Agricultural and Forest Meteorology, 73, 339–352, doi:10.1016/0168-1923(94)05083-I, 1995.

Jung, H., Senf, C., Beudert, B., and Krueger, T.: Bayesian hierarchical modeling of nitrate concentration in a forest stream affected by large-scale forest dieback, Water Resources Research, 57, 2, e2020WR027264, doi: 10.1029/2020WR027264 2021.

Krupa, S. V.: Effects of atmospheric ammonia (NH_3) on terrestrial vegetation: a review, Environmental Pollution, 124, 179-211, doi: 10.1016/S0269-7491(02)00434-7, 2003.

Kuenen, J., Dellaert, S., Visschedijk, A., Jalkanen, J.-P., Super, I., and Denier van der Gon, H.: CAMS-REG-v4: a state-of-the-art high-resolution European emission inventory for air quality modelling, Earth System Science Data, 14, 491–515, doi: 10.5194/essd-14-491-2022, 2022.

Kundu, S., Kawamura, K., and Lee, M.: Seasonal variation of the concentrations of nitrogenous species and their nitrogen isotopic ratios in aerosols at Gosan, Jeju Island: Implications for atmospheric processing and source changes of aerosols, Journal of Geophysical Research: Atmospheres., 115, D20305, doi: 10.1029/2009JD013323, 2010.

Li, Y., Schichtel, B. A., Walker, J. T., Schwede, D. B., Chen, X., Lehman, C. M. B., Puchalski, M. A., Gay, D. A., and Collett, J. L.; Increasing importance of deposition of reduced nitrogen in the United States, Proceedings of the National Academy of Sciences, 113, 5874-5879, doi: 10.1073/pnas.1525736113, 2016.

Marx, O., Brümmer, C., Ammann, C., Wolff, V., and Freibauer, A.: TRANC – a novel fast-response converter to measure total reactive atmospheric nitrogen, Atmospheric Measurement Techniques, 5, 1045–1057, doi:10.5194/amt-5-1045-2012, 2012.

Manders-Groot, A. M. M., Segers, A. J., and Jonkers, S.: LOTOS-EUROS v2.0 Reference Guide, TNO report TNO2016 R10898, TNO, Utrecht, The Netherlands, https://lotos-euros.tno.nl/media/10360/reference_guide_v2-0_r10898.pdf (last access: 14 March 2022), 2016.

Manders, A. M. M., Builtjes, P. J. H., Curier, L., Denier van der Gon, H. A. C., Hendriks, C., Jonkers, S., Kranenburg, R., Kuenen, J. J. P.,Segers, A. J., Timmermans, R. M. A., Visschedijk, A. J. H., Wichink Kruit, R. J., van Pul, W. A. J., Sauter, F. J., van der Swaluw, E., Swart, D. P. J., Douros, J., Eskes, H., van Meijgaard, E., van Ulft, B., van Velthoven, P., Banzhaf, S., Mues, A. C., Stern, R., Fu, G., Lu,S., Heemink, A., van Velzen, N., and Schaap, M.: Curriculum vitae of the LOTOS–EUROS (v2.0) chemistry transport model, Geoscientific Model Development, 10, 4145–4173, doi:10.5194/gmd-10-4145-2017, 2017.

Milford, C., Hargreaves, K. J., Sutton, M. A., Loubet, B., and Cellier, P.: Fluxes of NH_3 and CO_2 over upland moorland in the vicinity of agricultural land, Journal of Geophysical Research: Atmospheres, 106, 24 169–24 181, doi:10.1029/2001jd900082, 2001.

Min, K.-E., Pusede, S. E., Browne, E. C., LaFranchi, B. W., Wooldridge, P. J., and Cohen, R. C.: Eddy covariance fluxes and vertical concentration gradient measurements of NO and NO_2 over a ponderosa pine ecosystem: observational evidence for within canopy chemical removal of NO_x, Atmospheric Chemistry and Physics, 14, 5495–5512, doi:10.5194/acp-14-5495-2014, 2014.

Moravek, A., Singh, S., Pattey, E., Pelletier, L., and Murphy, J. G.: Measurements and quality control of ammonia eddy covariance fluxes: A new strategy for high frequency attenuation correction, Atmospheric Measurement Techniques, 12, 6059–6078, doi:10.5194/amt-12-6059-2019, 2019.

Munger, J. W., Wofsy, S. C., Bakwin, P. S., Fan, S. M., Goulden, M. L., Daube, B. C., Goldstein, A. H., Moore, K. E., and Fitzjarrald, D. R.: Atmospheric deposition of reactive nitrogen oxides and ozone in a temperate deciduous forest and a subarctic woodland: 1. Measurements and mechanisms, Journal of Geophysical Research-Atmospheres, 101, 12 639–12 657, doi:10.1029/96JD00230, 1996.

Nemitz, E., Sutton, M. A., Wyers, G. P., and Jongejan, P. A. C.: Gas-particle interactions above a Dutch heathland: I. Surface exchange fluxes of NH_3, SO_2, HNO_3 and HCl, Atmospheric Chemistry and Physics, 4, 989–1005, doi:10.5194/acp-4-989-2004, 2004.

Paulissen, M.P.C.P., Bobbink, R., Robat, S.A., and Verhoeven, J. T. A.: Effects of Reduced and Oxidised Nitrogen on Rich-Fen Mosses: a 4-Year Field Experiment., Water, Air, & Soil Pollution, 227, 18, doi:10.1007/s11270-015-2713-y, 2016.

Paulson, C. A.: The Mathematical Representation of Wind Speed and Temperature Profiles in the Unstable Atmospheric Surface Layer, Journal of Applied Meteorology, 9, 857–861, doi:10.1175/1520-0450(1970)009<0857:Tmrows>2.0.Co;2, 1970.

Reichstein, M., Falge, E., Baldocchi, D., Papale, D., Aubinet, M., Berbigier, P., Bernhofer, C., Buchmann, N., Gilmanov, T., Granier, A., Grünwald, T., Havránková, K., Ilvesniemi, H., Janous, D., Knohl, A., Laurila, T., Lohila, A., Loustau, D., Matteucci, G., Meyers, T., Miglietta, F., Ourcival, J.-M., Pumpanen, J., Rambal, S., Rotenberg, E., Sanz, M., Tenhunen, J., Seufert, G., Vaccari, F., Vesala, T., Yakir, D., and Valentini, R.: On the separation of net ecosystem exchange into assimilation and ecosystem respiration: review and improved algorithm, Global Change Biology, 11, 1424–1439, doi:10.1111/j.1365-2486.2005.001002.x, 2005.

Putaud, J.-P., Van Dingenen, R., Alastuey, A., Bauer, H., Birmili, W., Cyrys, J., Flentje, H., Fuzzi, S., Gehrig, R., Hansson, H., Harrison, R., Herrmann, H., Hitzenberger, R., Hüglin, C., Jones, A., Kasper-Giebl, A., Kiss, G., Kousa, A., Kuhlbusch, T., Löschau, G., Maenhaut, W., Molnar, A., Moreno, T., Pekkanen, J., Perrino, C., Pitz, M., Puxbaum, H., Querol, X., Rodriguez, S., Salma, I., Schwarz, J., Smolik, J., Schneider, J., Spindler, G., ten Brink, H., Tursic, J., Viana, M., Wiedensohler, A., and Raes, F.: A European aerosol phenomenology – 3: Physical and chemical characteristics of particulate matter from 60 rural, urban, and kerbside sites across Europe, Atmospheric Environment, 44, 1308–1320, doi: 10.1016/j.atmosenv.2009.12.011, 2010.

Rosenkranz, P., Brüggemann, N., Papen, H., Xu, Z., Seufert, G., and Butterbach-Bahl, K.: N2O, NO and CH4 exchange, and microbial N turnover over a Mediterranean pine forest soil, Biogeosciences, 3, 121–133, doi:10.5194/bg-3-121-2006, 2006.

Roth, M., Müller-Meißner, A., Michiels, H.-G., and Hauck, M.: Vegetation changes in the understory of nitrogen-sensitive temperate forests over the past 70 years, Forest Ecology and Management, 503, 119754, doi:10.1016/j.foreco.2021.119754 2022.

Rummel, U., Ammann, C., Gut, A., Meixner, F. X., and Andreae, M. O.: Eddy covariance measurements of nitric oxide flux within an Amazonian rain forest, Journal of Geophysical Research-Atmospheres, 107, LBA 17–1–LBA 17–9, doi:10.1029/2001JD000520, 2002.

Sauter, F., Sterk, M., van der Swaluw, E., Wichink Kruit, R., de Vries, W., and van Pul, A.: The OPS-model: Description of OPS 5.0.0.0, RIVM, Bilthoven, https://www.rivm.nl/media/ops/OPS-model.pdf (last access: 14 March 2022), 2020.

Saylor, R. D., Baker, B. D., Lee, P., Tong, D., Pan, L., and Hicks, B. B.: The particle dry deposition component of total deposition from air quality models: right, wrong or uncertain?, Tellus B: Chemical and Physical Meteorology, 71, 1550324, doi: 10.1080/16000889.2018.1550324, 2019.

Schaap, M., Wichink Kruit, R., Hendriks, C., Kranenburg, R., Segers, A., Builtjes, P., and Banzhaf, S.: Modelling and assessment of acidifying and eutrophying atmospheric deposition to terrestrial ecosystems (PINETI-2): Part I: Atmospheric deposition to German natural and semi-natural ecosystems during 2009, 2010 and 2011, techinal report, Umweltbundesamt, Dessau-Roßlau, Germany, https://www.umweltbundesamt.de/sites/default/files/medien/1410/publikationen/2017-08-15_texte_62-2017_pineti2-teil1.pdf (last access: 14 March 2022), 2017.

Schaap. M., Hendriks, C., Kranenburg, R., Kuenen, J., Segers, A., Schlutow, A., Nagel, H.-D., Ritter, A., and Banzhaf, S.: PINETI-3: Modellierung atmosphärischer Stoffeinträge von 2000 bis 2015 zur Bewertung der ökosystem-spezifischen Gefährdung von Biodiversität durch Luftschadstoffe in Deutschland, technical report, Umweltbundesamt, Dessau-Roßlau, Germany, https://www.umweltbundesamt.de/sites/default/files/medien/1410/publikationen/2018-10-17_texte_79-2018_pineti3.pdf (last access: 14 March 2022), 2018.

Schneider, C., Pelzer, M., Toenges-Schuller, N., Nacken, M., & Niederau, A.: ArcGIS basierte Lösung zur detaillierten, deutschlandweiten Verteilung (Gridding) nationaler Emissionsjahreswerte auf Basis des Inventars zur Emissionsberichterstattung - Kurzfassung ; UBA TEXTE 71/2016. Für Mensch & Umwelt, https://www.umweltbundesamt.de/publikationen/arcgis-basierte-loesung-zur-detaillierten (last access: 9 June 2022), 2016.

Schrader, F. and Brümmer, C.: Land Use Specific Ammonia Deposition Velocities: a Review of Recent Studies (2004–2013), Water, Air, and Soil Pollution, 225, 2114, doi:10.1007/s11270-014-2114-7, 2014.

Schrader, F., Brümmer, C., Flechard, C. R., Wichink Kruit, R. J., van Zanten, M. C., Zöll, U., Hensen, A., and Erisman, J. W.: Non-stomatal exchange in ammonia dry deposition models: comparison of two state-of-the-art approaches, Atmospheric Chemistry and Physics, 16, 13417–13430, doi:10.5194/acp-16-13417-2016, 2016.

Schrader, F., Schaap, M., Zöll, U., Kranenburg, R., and Brümmer, C.: The hidden cost of using low-resolution concentration data in the estimation of NH_3 dry deposition fluxes, Scientific Reports, 8, 969, doi:10.1038/s41598-017-18021-6, 2018.

Schrader, F, Erisman, J. W., and Brümmer, C: Towards a coupled paradigm of NH_3-CO_2 biosphere–atmosphere exchange modelling. Global Change Biology, 26, 4654–4663, doi: 10.1111/gcb.15184, 2020.

Schwarz, J., Cusack, M., Karban, J., Chalupníčková, E., Havránek, V., Smolík, J., and Ždímal, V.: $PM_{2.5}$ chemical composition at a rural background site in Central Europe, including correlation and air mass back trajectory analysis, Atmospheric Research, 176–177, 108–120, doi: 10.1016/j.atmosres.2016.02.017, 2016.

Schwede, D., Zhang, L., Vet, R., and Lear, G.: An intercomparison of the deposition models used in the CASTNET and CAPMoN networks, Atmospheric Environment, 45, 1337–1346, doi: 10.1016/j.atmosenv.2010.11.050, 2011.

Staelens, J., Houle, D.and De Schrijver, A., Neirynck, J., and Verheyen, K.: Calculating Dry Deposition and Canopy Exchange with the Canopy Budget Model: Review of Assumptions and Application to Two Deciduous Forests,Water, Air, and Soil Pollution, 191, 149–169, doi:10.1007/s11270-008-9614-2, 2008.

Sutton, M. A. and Fowler, D.: A Model for Inferring Bi-directional Fluxes of Ammonia Over Plant Canopies, in: Proceedings of the WMO conference on the measurement and modelling of atmospheric composition changes including pollutant transport, pp. 179–182, WMO/GAW(Gobal Atmosphere Watch)-91, Geneva, Switzerland, 1993.

Sutton, M. A., Tang, Y. S., Miners, B., and Fowler, D.: A New Diffusion Denuder System for Long-Term, Regional Monitoring of Atmospheric Ammonia and Ammonium, Water, Air and Soil Pollution: Focus, 1, 145–156, doi:10.1023/a:1013138601753, 2001.

Sutton, M. A., Howard, C. M., Erisman, J. W., Billen, G., Bleeker, A., Grennfelt, P., van Grinsven, H. and Grizzetti, B.: The European Nitrogen Assessment: sources, effects and policy perspectives, Cambridge University Press, Cambridge, UK, 2011.

Sutton, M. A., Reis, S., Riddick, S. N., Dragosits, U., Nemitz, E., Theobald, M. R., Tang, Y. S., Braban, C. F. , Vieno, M., Dore, A. J., Mitchell, R. F., Wanless, S., Daunt, F., Fowler, D., Blackall, T. D., Milford, C., Flechard, C. R., Loubet, B., Massad, R., Cellier, P., Personne, E., Coheur, P. F., Clarisse, L. Van Damme, M., Ngadi, Y., Clerbaux, C., Skjoth, C. A., Geels, C., Hertel, O., Wichink Kruit, R. J., Pinder, R. W., Bash, J. O., Walker, J. T., Simpson, D., Horvath, L., Misselbrook, T. H., Bleeker, A., Dentener, F. and de Vries, W.: Towards a climate-dependent paradigm of ammonia emission and deposition, Philosophical Transactions of the Royal Society of London. Series B.: Biological Sciences, 368, 20130166, doi: 10.1098/rstb.2013.0166, 2013.

Tang, Y. S., Simmons, I., van Dijk, N., Di Marco, C., Nemitz, E., Dämmgen, U., Gilke, K., Djuricic, V., Vidic, S., Gliha, Z., Borovecki, D., Mitosinkova, M., Hanssen, J. E., Uggerud, T. H., Sanz,M. J., Sanz, P., Chorda, J. V., Flechard, C. R., Fauvel, Y., Ferm, M., Perrino, C., and Sutton, M. A.: European scale application of atmospheric reactive nitrogen measurements in a low-cost approach to infer dry deposition fluxes, Agriculture, Ecosystems and Environment, 133, 183–195, doi:10.1016/j.agee.2009.04.027, 2009.

Tang, Y. S., Cape, J. N., Braban, C. F., Twigg, M. M., Poskitt, J., Jones, M. R., Rowland, P., Bentley, P., Hockenhull, K., Woods, C., Leaver, D., Simmons, I., van Dijk, N., Nemitz, E., and Sutton, M. A.: Development of a new model DELTA sampler and assessment of potential sampling artefacts in the UKEAP AGANet DELTA system: summary and technical report, Tech. rep., London, available at: https://uk-air.defra.gov.uk/library/reports?report_id=861 (last access: 22 July 2022), 2015.

Tang, Y. S., Flechard, C. R., Dämmgen, U., Vidic, S., Djuricic, V., Mitosinkova, M., Uggerud, H. T., Sanz, M. J., Simmons, I., Dragosits, U., Nemitz, E., Twigg, M., van Dijk, N., Fauvel, Y., Sanz, F., Ferm, M., Perrino, C., Catrambone, M., Leaver, D., Braban, C. F., Cape, J. N., Heal, M. R., and Sutton, M. A.: Pan-European rural monitoring network shows dominance of NH_3 gas and NH_4NO_3 aerosol in inorganic atmospheric pollution load, Atmospheric Chemistry and Physics, 1, 875–914, doi: 10.5194/acp-21-875-2021, 2021.

Tarnay, L. W., Gertler, A., and Taylor, G. E.: The use of inferential models for estimating nitric acid vapor deposition to semi-arid conifer-ous forests, Atmospheric Environment, 36, 3277–3287, doi:10.1016/S1352-2310(02)00303-5, 2002.

Thoene, B., Rennenberg, H., and Weber, P.: Absorption of atmospheric NO_2 by spruce (Picea abies) trees, New Phytologist, 134, 257–266, doi:10.1111/j.1469-8137.1996.tb04630.x, 1996.

Ulrich, B.: Nutrient and acid-base budget of central european forest ecosystems, in: Effects of Acid Rain on Forest Processes, edited by: Godbold, D., and Hüttermann, A., John Wiley & Sons, New York, USA, 1–50, 1994.

Van der Graaf, S. C., Kranenburg, R., Segers, A. J., Schaap, M., and Erisman, J. W.: Satellite-derived leaf area index and roughness length information for surface–atmosphere exchange modelling: a case study for reactive nitrogen deposition in north-western Europe using LOTOS-EUROS v2.0, Geoscientific Model Development, 13, 2451–2474, doi:10.5194/gmd-13-2451-2020, 2020.

Van Jaarsveld, J. A.: The Operational Priority Substances model. Description and validation of OPS-Pro 4.1., RIVM, Bilthoven, report 500045001, https://www.pbl.nl/sites/default/files/downloads/500045001.pdf (last access: 14 March 2022), 2004.

Van Oss, R., Duyzer, J., and Wyers, P.: The influence of gas-to-particle conversion on measurements of ammonia exchange over forest,Atmospheric Environment, 32, 465 – 471, doi:10.1016/S1352-2310(97)00280-X, 1998.

Van Pul, W. A. J. and Jacobs, A. F. G.: The conductance of a maize crop and the underlying soil to ozone under various environmental conditions, Boundary-Layer Meteorology, 69, 83–99, doi:10.1007/BF00713296, 1994.

Van Zanten, M. C., Sauter, F. J., Wichink Kruit, R. J., van Jaarsveld, J. A., and van Pul, W. A. J.: Description of the DEPAC module; Dry deposition modeling with DEPAC_GCN2010, Tech. rep., RIVM, Bilthoven, NL, 2010.

VDI: VDI-Guideline 3782 Part 5: Environmental meteorology – Atmospheric dispersion models – Deposition parameters, Tech. rep., Verein Deutscher Ingenieure, Düsseldorf, DE, 2006.

Webb, E. K.: Profile relationships: The log-linear range, and extension to strong stability, Quarterly Journal of the Royal Meteorological Society, 96, 67–90, doi:10.1002/qj.49709640708, 1970.

Wentworth, G. R., Murphy, J. G., Benedict, K. B., Bangs, E. J., and Collett Jr, J. L.: The role of dew as a nighttime reservoir and morning source for atmospheric ammonia, Atmospheric Chemistry and Physics Discussions, 16, 1–36, doi:10.5194/acp-2016-169, 2016.

Whitehead, J. D., Twigg, M., Famulari, D., Nemitz, E., Sutton, M. A., Gallagher, M. W., and Fowler, D.: Evaluation of laser absorption spectroscopic techniques for eddy covariance flux measurements of ammonia, Environ Sci Technol, 42, 2041–6, doi:10.1021/es071596u, 2008.

Wichink Kruit, R. J., van Pul,W. A. J., Sauter, F. J., van den Broek,M., Nemitz, E., Sutton,M. A., Krol,M., and Holtslag, A. A.M.:Modeling the surface–atmosphere exchange of ammonia, Atmospheric Environment, 44, 945–957, doi:10.1016/j.atmosenv.2009.11.049, 2010.

Wichink Kruit, R. J., Schaap, M., Sauter, F. J., van Zanten, M. C., and van Pul,W. A. J.: Modeling the distribution of ammonia across Europe including bi-directional surface–atmosphere exchange, Biogeosciences, 9, 5261–5277, doi:10.5194/bg-9-5261-2012, 2012.

Wichink Kruit, R. J., Aben, J., de Vries, W., Sauter, 1180 F., van der Swaluw, E., van Zanten, M. C., and van Pul, W. A. J.: Modelling trends in ammonia in the Netherlands over the period 1990–2014, Atmospheric Environment, 154, 20–30, doi: 10.1016/j.atmosenv.2017.01.031, 2017.

Wintjen, P., Ammann, C., Schrader, F., and Brümmer, C.: Correcting high-frequency losses of reactive nitrogen flux measurements, Atmospheric Measurement Techniques, 13, 2923–2948, doi:10.5194/amt-13-2923-2020, 2020.

Wintjen, P., Schrader, F., Schaap, M., Beudert, B., and Brümmer, C.: Forest–atmosphere exchange of reactive nitrogen in a remote region – Part I: Measuring temporal dynamics, Biogeosciences, 19, 389–413, doi:10.5194/bg-19-389-2022, 2022.

Wyers, G. and Duyzer, J.: Micrometeorological measurement of the dry deposition flux of sulphate and nitrate aerosols to coniferous forest, Atmospheric Environment, 31, 333 – 343, doi:10.1016/S1352-2310(96)00188-4, 1997.

Wyers, G. P. and Erisman, J. W.: Ammonia exchange over coniferous forest, Atmospheric Environment, 32, 441–451, doi:10.1016/S1352-2310(97)00275-6, 1998.

Zhang, L., Gong, S., Padro, J., and Barrie, L.: A size-segregated particle dry deposition scheme for an atmospheric aerosol module, Atmospheric Environment, 35, 549-560, doi:10.1016/S1352-2310(00)00326-5, 2001.

Zöll, U., Brümmer, C., Schrader, F., Ammann, C., Ibrom, A., Flechard, C. R., Nelson, D. D., Zahniser, M., and Kutsch, W. L.: Surface–atmosphere exchange of ammonia over peatland using QCL-based eddy-covariance measurements and inferential modeling, Atmospheric Chemistry and Physics, 16, 11 283–11 299, doi:10.5194/acp-16-11283-2016, 2016.

Zöll, U., Lucas-Moffat, A. M., Wintjen, P., Schrader, F., Beudert, B., and Brümmer, C.: Is the biosphere-atmosphere exchange of total reactive nitrogen above forest driven by the same factors as carbon dioxide? An analysis using artificial neural networks, Atmospheric Environment, 206, 108–118, doi: 10.1016/j.atmosenv.2019.02.042, 2019.

5. Summary of the key findings

In this thesis, I analyzed eddy-covariance (EC) flux measurements of total reactive nitrogen (ΣN_r) carried out with novel measurement techniques, the Total Reactive Atmospheric Nitrogen Converter (TRANC) coupled to a fast-response chemiluminescence detector (CLD). Before any reliable discussion on the measured fluxes could be made, I investigated the impact of different high-frequency flux correction methods, a mandatory flux adjustment step before interpretation. With this knowledge, an evaluation of long-term ΣN_r flux measurements was possible focusing on the temporal exchange dynamics and an estimation of dry deposition sums. Finally, modeled flux patterns and dry deposition fluxes were reviewed in comparison to measured values. These research topics were elaborated in detail in the previous chapters. Within this chapter, the highlights of the respective chapters are summarized.

5.1 High-frequency spectral flux correction

In this chapter, the performance of different high-frequency flux loss correction methods on the ΣN_r flux measurements was investigated for two different ecosystems, a semi-natural peatland and a remote mixed forest. We used the theoretical method by Moncrieff et al. (1997) (THEO) using modeled cospectra, a method based on measured power spectra of temperature and concentration (Ibrom et al., 2007) (IPS), and two methods based on measured ogives (IOG) and cospectra (ICO) of sensible heat and gas fluxes. The semi-empirical approach (sICO) uses measured and modeled cospectra. The performance analysis showed that the ICO approach performed best. The other empirical methods, IOG and sICO, showed generally trustworthy results with a tendency of lower damping values but underestimated the damping if it extended towards lower frequencies of the cospectrum. For the different ecosystems, a flux loss of 38 % was estimated for the peatland site and 22 % for the forest site using the ICO method. IPS results were biased because white noise prevailed in the power spectra of ΣN_r concentration making reliable calculations of flux correction factors impossible. No spectral similarity between the reference spectrum of temperature and the concentration spectrum can be guaranteed anymore. Power spectra of greenhouse gases like H_2O and CO_2 did not exhibit distinct noise structures due to their large autocorrelation. However, more power spectra of H_2O and CO_2 showed disturbances to white noise at the peatland site than at the forest site due to higher levels of humidity at the peatland site. To avoid the impact of humidity, an enclosed-path instrument with a heated intake tube should be used instead of an open-path sensor. Generally, methods based on power spectra are probably more suitable for compounds, which exhibit a large variability in concentrations, a high autocorrelation, and are likely inert.

Cospectra did not exhibit noise structures since noise of vertical wind and concentration are not correlated with each other. With the theoretical method, strong damping processes of chemical or physical nature occurring inside of the TRANC or at its inlet like adsorption processes could not be captured. In addition, the contribution of the different compounds to ΣN_r is not known, and it is not possible to describe the distribution and strength of sources and sinks by theoretical (co)spectra. Dependencies of flux damping factors on stability and wind speed, which are prerequisites for describing damping processes with THEO, could not be fully verified by flux damping factors estimated with ICO and IOG. Thus, it is assumed that damping effects of wind speed and stability were superimposed by damping effects of TRANC/CLD system, the contribution of N_r compounds to ΣN_r, and the vegetation. Thus, methods making use of theoretical (co)spectra are not suitable for the analysis of ΣN_r fluxes measured with the TRANC/CLD system. By using an empirical method based on ogives or cospectra, such damping effects are taken into account.

A general objective in EC flux measurements is to keep the flow regime inside sampling tubes turbulent. Therefore, the Reynolds number (Re) (Aubinet al., 2012) has to be at 2300 or even larger. Calculations of Re for the TRANC/CLD EC setup yielded values below 2300 indicating a laminar flow. Since we

had no possibility to measure the pressure gradient after the critical orifice, no reasonable explanation to that low number can be made (Sect. 3.2.2). However, with the applied empirical flux correction method an accurate estimation of the damping is possible even under strong laminar conditions and a limited amount of high-quality cospectra.

5.2 Temporal dynamics in the exchange of ΣN_r

After a successful development of a method correcting high-frequency flux losses, an analysis of the measured concentrations, fluxes, and deposition velocities of ΣN_r was made in chapter 4. Therefore, flux measurements of ΣN_r using the TRANC coupled to a CLD were made above a temperate mixed forest in southeast Germany located in a remote area, the Bavarian Forest National Park. These measurements lasted 2.5 years from January 2016 until July 2018, and this dataset represents one of the first long-term flux measurements of ΣN_r providing the opportunity to estimate N dry deposition and to give insights in the temporal flux and concentration pattern of N_r species. Since the TRANC converts common N_r compounds efficiently (Marx et al., 2012), only one instrument is needed for determining the total N dry deposition instead of installing several instruments - each of them designed for a single compound. The setup was complemented by micrometeorological instruments, a DELTA system, passive samplers, and a fast-response QCL for measuring NH_3 concentrations.

Furthermore, measured fluxes, concentrations, and micrometeorological data were used in various publications leading to insights in drivers of the ΣN_r exchange using artificial neural networks (Zöll et al., 2019), a new approach in the uncertainty estimation of gap-filled fluxes (Lucas-Moffat et al., 2022), and new strategies using low-resolution NH_3 sampling methods for estimating fluxes using bidirectional fluxes models (Schrader et al., 2018). This year, flux measurements and additional data of the campaign were published making the data available for the scientific community (Brümmer et al., 2022).

A key message of the campaign was the reasonable agreement of averaged TRANC concentrations and DELTA plus NO_x concentrations showing that the TRANC can adequately convert most of the important N_r compounds. This was not proven on a long-term time scale before. Indeed, Brümmer et al. (2013) made a comparison of TRANC to DELTA concentrations but NO_x was not measured at their site. However, a comprehensive comparison needs concentration measurements at the same resolution preferably half-hourly. However, a setup measuring different N_r species in an AGM setup or even installing fast-response analyzers for different N_r compounds in combination with the TRANC leads to high acquisition cost and maintenance effort. It may be only feasible for a short intercomparison campaign.

The temporal concentration pattern of ΣN_r showed largest concentrations in spring and winter. Seasonal changes in the contribution of NO_x and NH_3 were most responsible for the variability in the total concentration pattern. On average, both gases contributed with 71.0 % to the observed ΣN_r concentration. For the entire campaign duration, we determined concentrations of 1.0, 1.4, and 3.1 µg N m^{-3} for NH_3, NO_x, and ΣN_r, respectively, showing the absence of air pollutants.

After applying common flux quality selection criteria, approx. 80 % of half-hourly fluxes were deposition fluxes. Median deposition fluxes were between -15 and -5 ng N m^{-2} s^{-1} with largest median depositions in spring and summer. Values are comparable to fluxes of Brümmer et al. (2013) and Ammann et al. (2012) for agricultural field sites apart from management periods. Diurnals are likely comparable to publications on individual N_r compounds above forest, but up to now no flux measurements of ΣN_r based on micrometeorological methods have been made above forests. Thus, comparison possibilities are very scarce. Corresponding deposition velocities of ΣN_r ranged between 0.2 and 0.5 cm s^{-1}. An analysis of the seasonal dynamics of v_d revealed that changes in the concentrations of N_r compounds and micrometeorological controls like global radiation and linked parameters like friction velocity, temperature, and relative humidity had probably a strong influence on v_d. Furthermore,

dry conditions, namely high temperatures, low relative humidity, and dry leaf surfaces, were found to be responsible for enhancements in v_d. ΣN_r concentration emerged not as a controlling variable probably due to minor interseasonal concentration differences.

Such an analysis on parameters enhancing ΣN_r deposition velocities has not been done before and may be useful for comparisons to deposition velocities of bidirectional flux models. However, the findings are only representative for this measurement site. At other (forest) sites, the mixture of compounds contributing to concentrations and fluxes is different. Unfortunately, NH_3 flux measurements were not possible at the measurement site. A comparison to TRANC measurements would have revealed the non-NH_3 flux, which corresponds to the flux of oxidized nitrogen compounds (NO_y) assuming that pNH_4^+ exchange is negligible. The large uncertainty in the covariances of the NH_3 flux likely caused by a non-detectable short-term variability in the NH_3 raw concentrations made time lag detection impossible.

Nitrogen dry deposition at the Bavarian Forest site was determined for two years of flux measurements: 3.8 kg N ha a^{-1} was estimated from June 2016 to May 2017, 4.0 kg N ha^{-1} a^{-1} from June 2017 until May 2018 based purely statistical gap-filling methods, the mean-diurnal-variation approach and monthly averages of half-hourly values. To prove the performance of this gap-filling procedure, a comparison to methods based on inferential modeling or artificial neural networks is recommended. By adding wet deposition measurements, obtained total nitrogen depositions were 12.2 and 10.9 kg N ha^{-1} a^{-1} in the first and second measurement year, respectively. These estimates were found to be at upper end of the critical load range suggesting that the ecosystem is close to the limit of receiving too much nitrogen through atmospheric deposition.

5.3 Comparison of modeled and measured reactive nitrogen fluxes

In a final step, TRANC flux measurements were compared to nitrogen deposition models, LOTOS-EUROS and DEPAC-1D. Both used DEPAC as bidirectional flux model with the difference that DEPAC-1D utilizes site-based measurements of concentrations and micrometeorology as input data, whereas LOTOS-EUROS requires modeled concentrations and meteorological data from the (ECMWF) to predict deposition for a grid cell of 7x7 km^2, in which the measurement site was located. Fluxes of DEPAC-1D and LOTOS-EUROS were weighted according to the distribution of coniferous and deciduous forest measured within the flux footprint. Furthermore, modeled and measured dry deposition were compared to dry deposition estimates based on the canopy budget technique (CBT) (Draaijers and Erisman, 1995; de Vries et al., 2003; Beudert and Breit, 2014). For the years 2016 and 2017, the following averaged annual N dry deposition estimates were calculated:

- From TRANC measurements, 4.7±0.2 and 4.3±0.4 kg N ha^{-1} a^{-1} depending on the gap-filling approach were estimated.
- Applying the inferential model DEPAC-1D led to 5.8±0.1 kg N ha^{-1} a^{-1}.
- LOTOS-EUROS predicted 6.5±0.3 kg N ha^{-1} a^{-1}.
- Following the CBT approach, its minimum and maximum estimates were 3.8±0.5 and 6.7±0.3 kg N ha^{-1} a^{-1}, respectively.

Adding complementary wet deposition measurements to dry deposition estimates, total N deposition ranged between 11.5 and 14.8 kg N ha^{-1} a^{-1}. Annual dry deposition estimates were within the range of minimum and maximum estimates of the CBT approach showing that ecological, micrometeorological, and model applications provided reasonable estimates. According to the critical load concept, total N deposition is below critical values proposed by Bobbink and Hettelingh (2011). The examination of tree physiological parameters and showed no indications of critical load exceedances.

Overall, LOTOS-EUROS and DEPAC-1D were able to capture the seasonality of the ΣN_r flux pattern but exhibited significant biases to flux measurements during certain seasons of the year. During summer,

a systematic overestimation of ΣN_r deposition by DEPAC-1D was found. In winter, deposition fluxes of DEPAC-1D and TRANC were both near zero. LOTOS-EUROS predicted slightly lower ΣN_r deposition in summer and therewith was closer to TRANC measurements. However, LOTOS-EUROS showed large differences to measured ΣN_r deposition in spring and autumn. Furthermore, LOTOS-EUROS deposition was considerably high in winter, which could not be verified by measurements and DEPAC-1D.

The overestimation of ΣN_r deposition fluxes by DEPAC-1D during summer was caused by the different response to micrometeorological conditions compared to TRANC measurements ΣN_r deposition velocities of DEPAC-1D were enhanced in the presence of wet leaf surfaces and high relative humidity. Similar observations were made for LOTOS-EUROS, but the models exhibited a different response to temperature. Lower temperatures favored v_d of DEPAC-1D, whereas the opposite observation was made for LOTOS-EUROS, and additionally deposition velocities showed disagreements in their diurnal pattern. This comparison indicates that a further investigation of stomatal vs. non-stomatal uptake is necessary, which may reduce the difference to measured fluxes.

In DEPAC, no soil compensation point has been included yet. In addition, the current implementation of the soil resistance is kept simple, i.e., assuming constant values for different soil wetness states, since an in-depth analysis on the response of N_r flux measurements in dependence of soil parameters has not been made so far. Most campaigns of N_r flux measurements focused on the N_r exchange of vegetated surfaces (e.g., see Table 1 of Walker et al. (2020)). Thus, an appropriate soil parameterization has not been implemented in DEPAC yet (van Zanten et al., 2010).

For determining N dry deposition with DEPAC-1D, monthly integrated concentration averages from DELTA and passive samplers were used. Due to the nature of these measurement, the short-term variability could not be considered in dry deposition fluxes of HNO_3 and nitrogen aerosols. In case of NH_3, high resolution concentration measurements of the QCL were available. The combination of both measurement techniques appears to be the most suitable approach since a setup consisting of high-resolution instruments for each N_r compound is not affordable. At least for certain seasons, high-resolution flux measurements could be made at sites equipped with low-resolution samplers for a limited time, which may lead to improvements in the description of exchange pathways and a better agreement to flux measurements (Schrader et al., 2020).

Apart from possible uncertainties in DEPAC-1D, TRANC dry deposition estimates using DEPAC-1D for gap-filling provided similar results suggesting that inferential modeling is a suitable gap-filling tool at sites with prevailing N deposition.

High ΣN_r deposition fluxes of LOTOS-EUROS in spring and autumn were related to modeled NH_3 concentrations. Comparisons to measured NH_3 concentrations of DELTA measurements, passive samplers, and QCL measurements revealed overestimations of LOTOS-EUROS in modeled NH_3 concentrations by a factor two to three compared to measured concentrations. Shortcomings in the allocation of emission data like the agricultural practice and distribution of animal housings were probably responsible for the discrepancies in concentrations. The general overestimation of NH_3 concentrations by LOTOS-EUROS was subject of recent studies (e.g., van der Graaf et al., 2020; Ge et al., 2020) and has not been solved yet. The discrepancy of LOTOS-EUROS to TRANC and DEPAC-1D in dry deposition fluxes during winter was related to large particulate nitrogen fluxes (pNH_4^+, pNO_3^-). Parameterization of the stability is done in LOTOS-EUROS without including the influence of snow cover. Including snow cover may change the prevailing stratification of the boundary layer, and consequentially lead to a reduction in aerosol deposition due to higher values of R_a and R_b.

This is the first time a comparison of micrometeorological and ecological measurements techniques with modeled nitrogen deposition estimates using a bidirectional flux model has been made. The comparison of annual dry deposition estimates showed a reasonable agreement. With further improvements in the measurement system, in steps of flux analysis like the high-frequency flux loss correction and gap-

filling, and in model process descriptions, a better in agreement in N dry deposition estimates will be achieved. An improvement of the measurement system, the TRANC/CLD setup, is presented in the last chapter.

6. Recommendations and outlook

At last, I would like to provide a few recommendations based on my works and made experciences in the field of micrometeorological flux measurements and a future perspective of the TRANC flux measurements.

As I started my research in micrometeorological flux measurements, I greatly acknowledged that open-source flux processing softwares like EddyPro were available, which provide the user several options for flux calculation making them usable for different compounds. In principle, it is possible to use them for reactive species but with limitations, e.g., the high-frequency flux loss correction. I found that high-frequency flux loss correction methods based on theoretical assumptions or power spectra were not suitable for ΣN_r flux measurements since white noise prevailed in power spectra and theoretical turbulence cospectra did not agree well with gas flux and even sensible heat cospectra. Swart et al. (2022) made a comparison of the ICO method and the theoretical flux loss correction method by Moncrieff et al. (1997) for an open-path NH_3 and a CO_2/H_2O infrared gas analyzer. For both analyzers, the theoretical flux damping factors were by ca. 10 % larger. Possibly, mismatches in theoretical and measured cospectra were most responsible for the difference in flux damping. It shows that methods based on measured (co)spectra are a valuable option for determining high-frequency flux losses and should be preferably used. A comparison of measured and theoretical spectra is highly recommended to identify the exact contributions of small and large-scale eddies to the flux. Nowadays, computers are more powerful compared to times when the theoretical damping calculation was originally published making FFT calculations and solving minimization problems much faster.

Before I started writing stand-alone high-frequency flux loss correction scripts, I wrote scripts visualizing the flux estimation according to Eq. (1.5). Plots of cross-covariance functions, which are not supported by EddyPro, are a valuable tool showing if the theoretical time lag based on sensor separation, tube length, tube diameter, and flow velocity exists and give an impression on the random uncertainty of the flux. Having scripts for basic flux calculation and high-frequency flux loss correction, I started developing an independent flux processing script.

This script was used for calculating fluxes of a novel converter-CLD system outlined below and successfully adapted by other colleagues for analyzing NH_3 fluxes carried out with a QCL. Personally, I highly recommend to write scripts providing cross-covariance functions and choose options related to flux calculation and post-processing wisely. Suggestions to the high-frequency flux loss correction procedure were discussed in detail in Sect. 2.4.3.

In the sense of flux post-processing, we found that inferential modeling is a valuable tool for gap-filling of ΣN_r deposition fluxes. With further modifications in the exchange path with soil like the implementation of a soil compensation point and improvements in the parameterization of micrometeorological flux dependencies, the agreement may get better. High-resolution measurements of the input data are definitely preferred but not a must-have. At least, they should be made for N_r compounds, which contribute presumably most to the flux pattern of ΣN_r. Seasonal dynamics should also be taken into account. For example, high-resolution measurements of NH_3 during winter are less useful due to low daily flux dynamics. During that time, instruments maintenance can be done. A combination of TRANC with DELTA and passive sampler measurements may be a suitable choice as done in this thesis.

Statistical methods like the MDV approach or linear interpolation techniques can be applied but limited to gaps spanning a few days since the assumed autocorrelation is mostly not valid for N_r compounds. Recently, Lucas-Moffat et al. (2022) suggested to use a framework of different gap-filling techniques instead of a single approach to minimize uncertainties making budget estimates more robust. The general performance of an artificial neural network approach as a gap-filling tool was highest for NH_3 and ΣN_r. In case of NH_3, an inferential modeling approach was found to be less useful. It shows that valuable process has been made in the field of gap-filling of non-CO_2 compounds. Recent publications of

Mahabbati et al. (2021) and Zhu et al. (2022) suggested random forest approaches for gap-filling of CO_2 fluxes, sensible, and latent heat. Applying these novel gap-filling approaches to N_r species and different high-frequency flux loss correction methods is worthwhile for a reanalysis nitrogen budgets and further measurement campaigns.

Besides the successful quantification of the nitrogen dry deposition, the investigation of the non-NH_3 flux was not possible at the forest site due to the non-detectable variability in the high-resolution NH_3 concentrations. Our findings are supported by Ferrara et al. (2021), who found large flux uncertainties at low NH_3 fluxes. It seems that the current QCL model is not able to resolve the NH_3 concentrations dynamics sufficiently. In addition, a simultaneous operation of a NH_3 QCL and the TRANC/CLD system requires regular maintenance, high power consumption, a temperature-controlled environment, and significant space for setting up the instruments making measurements above forest canopies for example challenging. Generally, the entire setup has high acquisition costs, which are probably not fundable by every institute.

Using TRANC measurements alone, it is not possible to split the total nitrogen deposition into the reduced nitrogen compounds ($NH_x = NH_3 + NH_4^+$) and the oxidized nitrogen compounds ($NO_y = NO + NO_2 + HNO_3 + NO_3^- + PAN + N_2O_5$ etc.). The main benefit of the TRANC is the determination of the total nitrogen deposition with a single instrument (Cowan et al., 2022).

A proper solution is the combination of a NO_y converter consisting of a heated gold tube coupled to a CLD using CO or gaseous hydrogen (H_2) as reducing gas (Munger et al., 1996; Marx, 2004; Horii et al., 2006) and the TRANC. In both converters, NO_y and ΣN_r are converted NO. Coupled to a dual-channel CLD, this measurement system allows the determination of the NH_x concentration in ambient air by subtracting NO_y from ΣN_r concentrations. Depending on the contribution of NH_4^+ aerosol to NH_x, this measurement system enables the determination of NH_3 concentrations and fluxes using the EC method if the dual-channel analyzer is fast enough. Apart from Ammann et al. (2019) who proposed a dual-channel converter for NO_y and ΣN_r in EC field applications, this novel converter, henceforth called NO_y-TRANC, has not been used in any other field studies.

Together with my supervisor, Dr. Christian Brümmer, and our technicians, we designed the concept of the NO_y-TRANC and installed the converter at an intensively managed grassland site on organic soil in northern Germany. The setup was complemented with passive sampler measurements of NH_3 and a DELTA system. Meteorological and soil data were taken from ongoing measurements at the field site. The focus of this measurement campaign was to investigate the N_r response of the ecosystem to field management. The basic scheme of the converter is shown in Fig. 6.1.

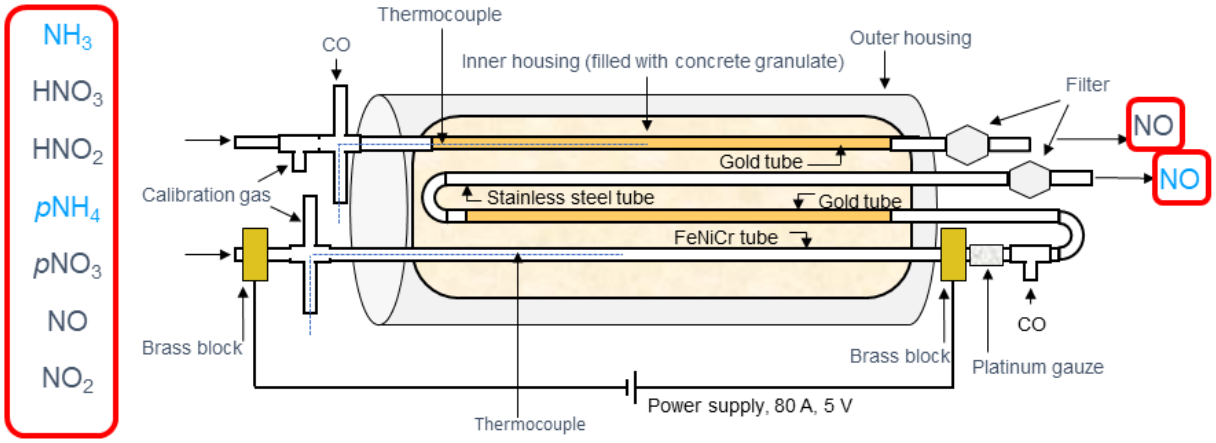

Figure 6.1: Schematic sketch of the NO_y-TRANC.

In principle, we added a second gold tube to our custom-built TRANC and inserted a thermocouple into the NO_y converter tube for observing the inner temperature. Keeping the design of the TRANC and the temperature of the FeNiCr at 870°C, ensured temperatures above 300°C in both gold tubes allowing the conversion of NO_2 to NO using CO as reducing agent. The dual-channel CLD (nCLD 899 SL, EcoPhysics, Dürnten, Switzerland) had an *e*-folding time of approx. 1 sec. Hence, the novel measurement system fulfills the requirements for EC flux measurements. NO_y-TRANC and sonic anemometer (GILL-R3, Gill Instruments, Lymington, UK) were installed 2.5 m above the surface, and the nCLD was placed in an air-conditioned box. However, the integrated pump of the nCLD had a very low pump flow (less than 0.5 L min^{-1}). To increase the airmass flow in the sampling line and to reduce the residence time in the system, we integrated membrane pumps ahead of the nCLD, one for each sample line. Still, the overall flow regime is likely laminar and significant high-frequency flux losses were found according to the empirical flux correction methods ICO and IOG. We found flux losses of 30 % and 40 % for NO_y and ΣN_r, respectively. Flux calculation was made with an independent processing script including the following pre-processing steps in that order: outlier filters similar to Vickers and Mahrt (1997), angle of attack correction (Nakai et al., 2006), double rotation (Wilczak et al., 2001), and linear detrending (Gash and Culf, 1996). Low-frequency flux losses were considered following the correction by Moncrieff et al. (2004).

The measurement campaign started mid of December 2019 and proceeded until mid of October 2021 covering two fertilization seasons. Apart from a regular maintenance period in winter 2021, no substantial data loss occurred. O_2 consumption of the nCLD was very low compared to the one-channel version. O_2 tanks of the nCLD were exchanged every two to three months, whereas the replacement was done in two-week intervals for the CLD 780 TR. Due to the stable instrument performance, no substantial flux data gaps occurred during the fertilization season.

Figure 6.2 shows fluxes of NO_y, NH_x, and ΣN_r after quality filtering as box-whisker plots. For quality filtering, I removed fluxes measured during low turbulence ($u_* < 0.1$ m s^{-1}) and discarded outliers and fluxes with QC = 2 (Mauder and Foken, 2006).

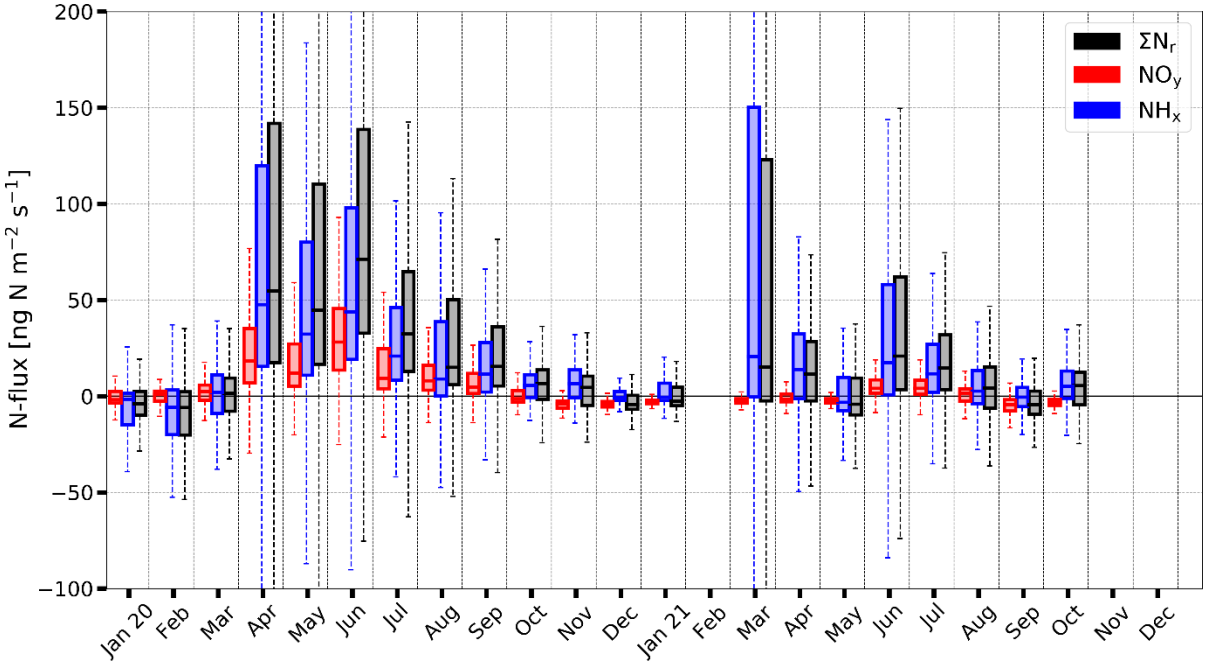

Figure 6.2: Half-hourly ΣN_r, NO_y, and NH_x fluxes represented by box-and-whisker plots in ng N m^{-2} s^{-1} (box frame = 25 % to 75 % interquartile ranges (IQR), bold line = median, whisker = 1.5 · IQR) colored in black, red, and blue, respectively.

This flux pattern is highly in contrast to the observations made for the forest site. Emission fluxes dominated the flux pattern and reached extremely high values due to fertilization. Deposition played a

minor role in the flux pattern and occurred during autumn, winter, and after fertilization events in case of 2021. In 2020, especially from May to September, emission fluxes prevailed. Furthermore, the NO_y contribution was clearly different between the years. Meteorological and soil measurements showed prolonged dry periods in spring and summer 2020, whereas precipitation happened more frequently in 2021 leading to a higher soil water content. The difference in soil water content may be a reason for the large discrepancy in the annual NO_y budget.

The investigations on the response of N_r emissions to meteorological, soil, and agricultural parameters are not completed yet. Nevertheless, it highlights the potential of the NO_y-TRANC-nCLD system to determine reduced and oxidized N_r fluxes with a single instrument while keeping the benefit of the TRANC to measure the ΣN_r exchange using the EC method. If NH_4^+ aerosol concentrations are relatively low compared to NH_3 concentrations, which was likely the case at the measurement site (ca. 21 % on average according to DELTA measurements), the findings for NH_x can be directly inferred to NH_3 making obtained flux data relevant for the nitrogen modeling community. The separation of N_r compounds into NO_y and NH_x provides the opportunity to draw conclusions about the origin of N_r in case of deposition fluxes. NO_y compounds emerge from emission sources of industry and traffic, and NH_x compounds originate mainly from agriculture. A subsequent step would be the partitioning of the net N_r EC fluxes into gross emission and gross deposition fluxes. A corresponding partitioning method for N_r compounds has not been developed yet. The complex bidirectional exchange behavior of N_r compounds makes the implementation of a partitioning tool challenging. However, it will lead to a better understanding of the N_r exchange.

In conclusion, the NO_y-TRANC is a valuable tool for further comparison campaigns to nitrogen dry deposition models as done in this thesis and can be further considered as an option for determining atmospheric NH_3 emission factors, which are essential for defining nitrogen mitigation strategies.

To further improve the development NO_y-TRANC, comparison measurements are needed. At the field site, we had no possibility to compare the high-resolution flux data of the NO_y-TRANC to EC flux measurements of the NH_3 QCL. The outcome of a comparison campaign of the NO_y-TRANC to different NH_3 measurement techniques is planned for spring next year and will be a step forward in the development of the NO_y-TRANC. At the grassland site, only a comparison to low-resolution DELTA and passive samplers was made. From those measurements, we found that long-period concentration averages of NH_x agreed well. Since we combined two converter types, which showed reasonable conversion efficiencies for the most relevant N_r compounds (Marx, 2004; Marx et al. 2012), we assume that the conversion efficiency of the NO_y-TRANC was likely similar. Further comparison campaigns and conversion efficiency tests will help to investigate the assumption.

Still, the nCLD and NO_y-TRANC come up with high costs regarding maintenance, power consumption, materials, etc. The experience with the TRANC was a great benefit while constructing and maintaining the improved version. Other research groups, which intend to rebuild this system, cannot make use of this advantage. Therefore, we write publications about our research, participate at workshops and conferences, and share our experiences. To tackle the cost factor, the solution may be the installation of a measuring network consisting of low-cost devices like passive samplers and DELTA systems. High resolution measurements of ΣN_r and its subcomponents could be done for a few weeks or months and afterwards moving the setup to another field site. Schrader et al. (2018) suggested taking these parallel measurements for a limited time is sufficient for an improvement in deposition velocities. These measurements should be preferentially carried out at field sites which are already integrated in research networks like ICOS (Heiskanen et al., 2022) and equipped with EC related instrumentation. Schrader et al. (2020) showed that stomatal conductances determined from CO_2 flux measurements are a potential alternative in the derivation of NH_3 deposition velocities compared common empirical models. Both findings are valuable for improving dry deposition estimates of N_r compounds obtained by inferential models or large-scale CTMs resulting in an improvement of nitrogen deposition maps. Even with local

measurements of turbulence, which offer comparison possibilities to modeled micrometeorology, an improvement in deposition estimates may be achieved.

At the forest site, the comparison to in-situ modeled aerosol deposition revealed that aerosol deposition of LOTOS-EUROS was unrealistically high due to an issue in the CTMs' stability parameterization. Thus, I recommend to develop and validate the dry deposition schemes in conjunction with the novel measurement studies to further reduce modeling uncertainties.

The reduction in N_r emission as well as the anthropogenic greenhouse gas effect will be the major environmental challenges of mankind. We as scientists have high responsibility to measure and model data precisely and provide our messages understandable for policymakers. I hope that the scientific community can benefit from my moderate work to the field of reactive nitrogen flux measurements.

Appendix

A.1 Supplementary materials to chapter 3: Forest-atmosphere exchange of reactive nitrogen in a remote region – Part I: Measuring temporal dynamics

Description of wet deposition measurements

Wet-only and bulk deposition were collected by four samplers, one wet-only and three bulk samplers, at an open site. The measurements took place in southwest direction of the tower (approx. 1.3 km). Bulk samplers had a funnel opening of 321 cm^2 at 1.25m above ground. The automatic wet-only sampler (NSA 181K – cooled, Eigenbrodt, Königsmoor, Germany) had a funnel opening of 500 cm^2 at 2 m above ground. During the weekly sampling intervals, precipitation samples were kept dark and cool (< 4 °C). After sampling they were filtered (< 0.45 µm, Whatman) and cooled at 2 to 4 °C without chemical preservation/treatment until analysis. No biocides were used during sampling because denitrification was unlikely due to the short exposure time and permanent cooling. In fact, we found very low carbon concentrations and no nitrite as an intermediate product of denitrification in the precipitation samples. NH_4^+ and NO_3^- were analyzed following DIN EN ISO 10304-1. Determination of total wet N was done according to DIN 38409-27 and EN 12260. Dissolved organic nitrogen is calculated by subtracting NH_4^+-N and NO_3^--N from total wet N.

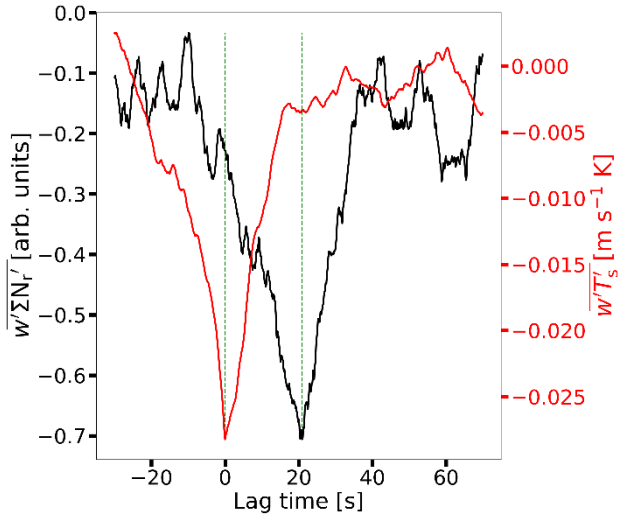

Figure S3.1: Covariance function of vertical wind and temperature (red) and covariance function of vertical wind and ΣN_r concentration (black). Green, dashed lines indicate the maximum covariance, which is around 20 s for the TRANC-CLD. Data were recorded at the April 2017 from 05:00 to 05:30 LT.

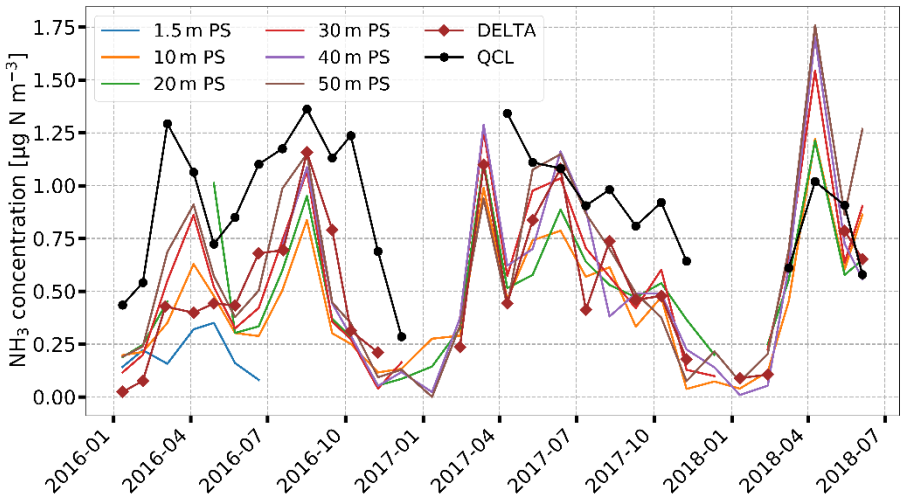

Figure S3.2: Concentrations of NH_3 measured by the DELTA and passive samplers, and the QCL in µg N m^{-3}. NH_3 of the QCL was averaged to the exposition period of the long-term samplers. Colors of the passive samplers indicate different measurement heights.

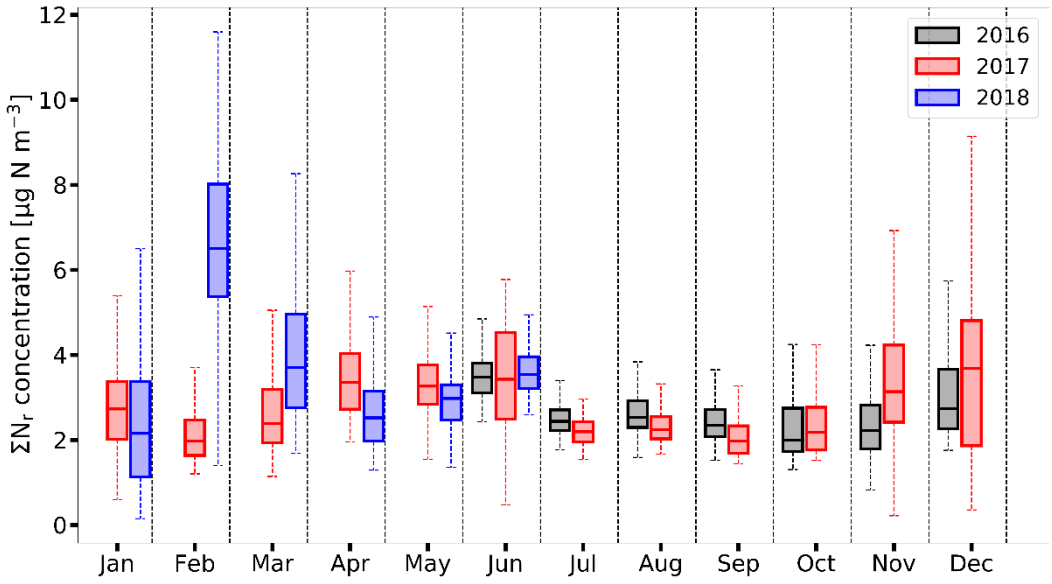

Figure S3.3: Time series of measured ΣN_r concentrations shown as box-and-whisker plots on monthly basis (box frame = 25% to 75% interquartile ranges (IQR), bold line = median, whisker = 1.5· IQR) in µg N m^{-3}. Colors indicate different years.

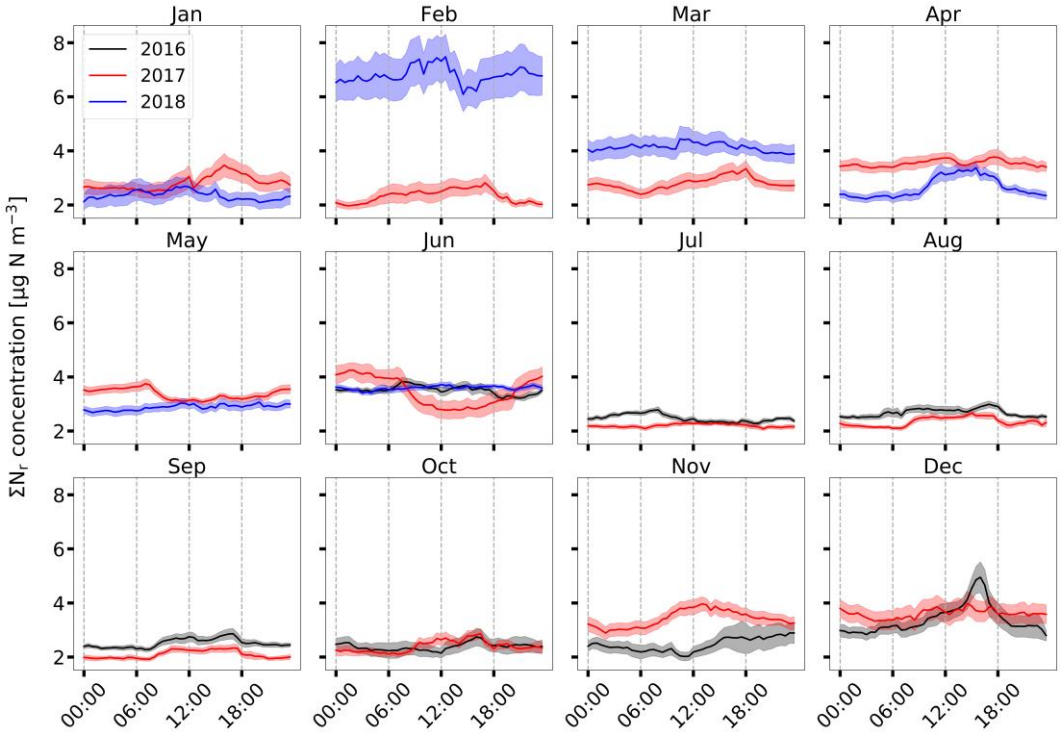

Figure S3.4: Mean diurnal cycle of ΣN_r concentrations (µg N m^{-3}) based on half-hourly measurements for every month from June 2016 to June 2018. The shaded area represents the standard error of the mean. Colors indicate different years.

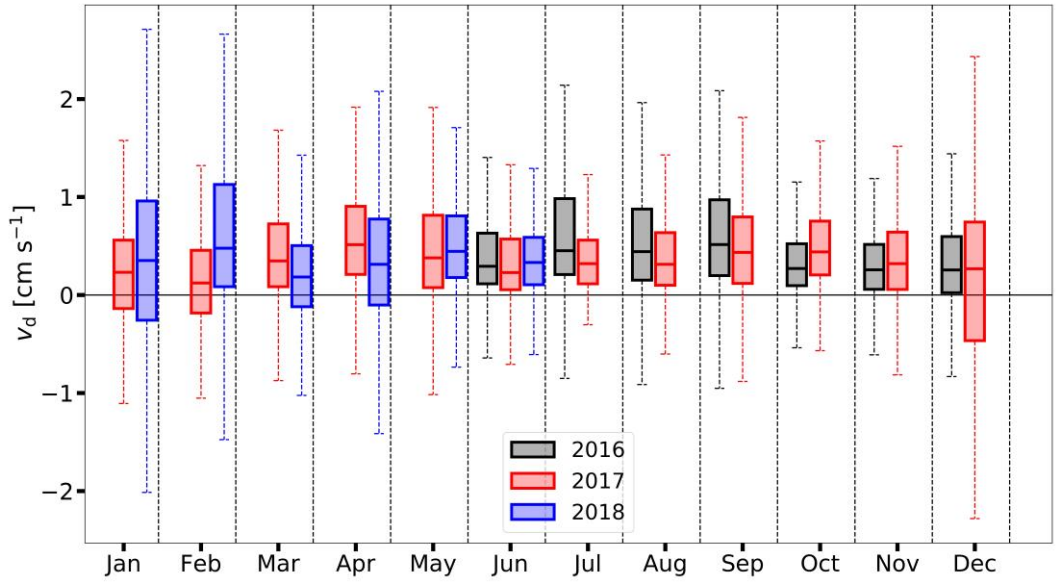

Figure S3.5: Time series of measured $v_d(\Sigma N_r)$ presented by box-and-whisker plots on monthly basis (box frame = 25% to 75% interquartile ranges (IQR), bold line = median, whisker = 1.5· IQR) in cm s^{-1}. Colors indicate different years.

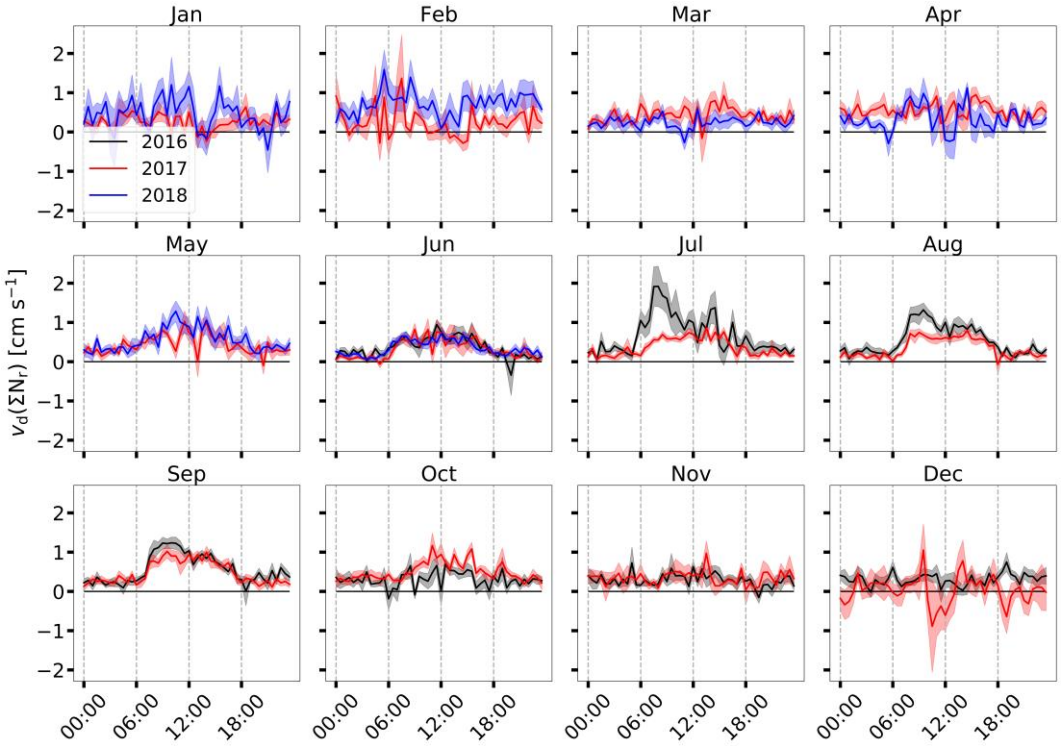

Figure S3.6: Mean diurnal cycle of $v_d(\Sigma N_r)$ (cm s^{-1}) based on half-hourly measurements for every month from June 2016 to June 2018. The shaded area represents the standard error of the mean. Colors indicate different years.

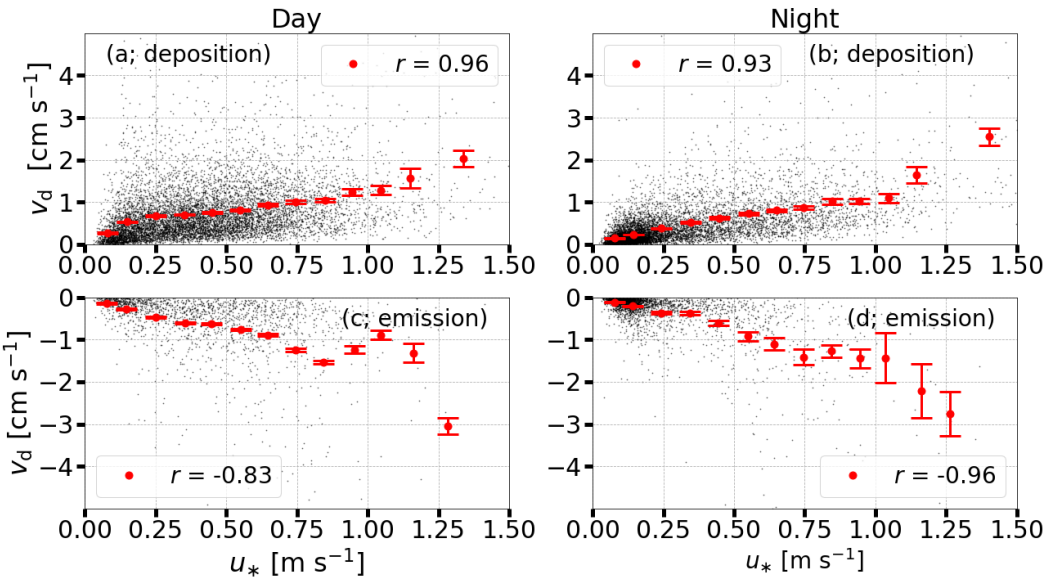

Figure S3.7: Relationships between measured u_* and corresponding ΣN_r v_d separated in emission and deposition during day ((a) and (c)) and night ((b) and (d)). Half-hourly data is displayed in black, red dots represents averages binned in increments of 0.1 m s^{-1}. Error bars indicate the standard error of the averages. The threshold for identifying day and nighttime v_d was set to 10 W m^{-2}. r represents the measure of correlation evaluated for the binned data.

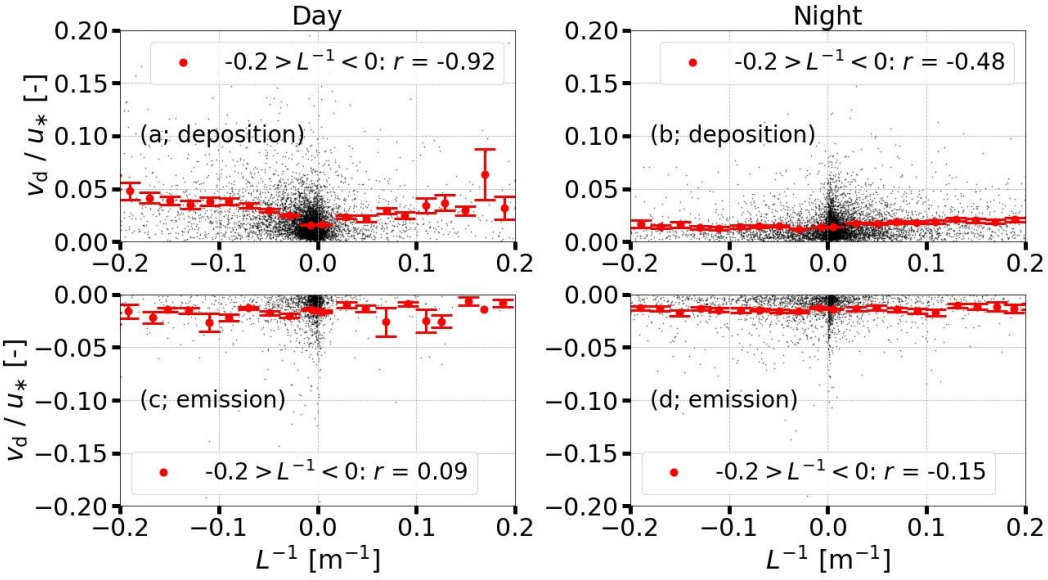

Figure S3.8: Relationships between L^{-1} and corresponding ratios v_d/u_* separated in emission and deposition during day ((a) and (c)) and night ((b) and (d)). Half-hourly data is displayed in black, red dots represents averages binned in increments of 0.02 m^{-1}. Error bars indicate the standard error of the averages. The threshold for identifying day and nighttime v_d was set to 10 W m^{-2}. r represents the measure of correlation evaluated for the binned data.

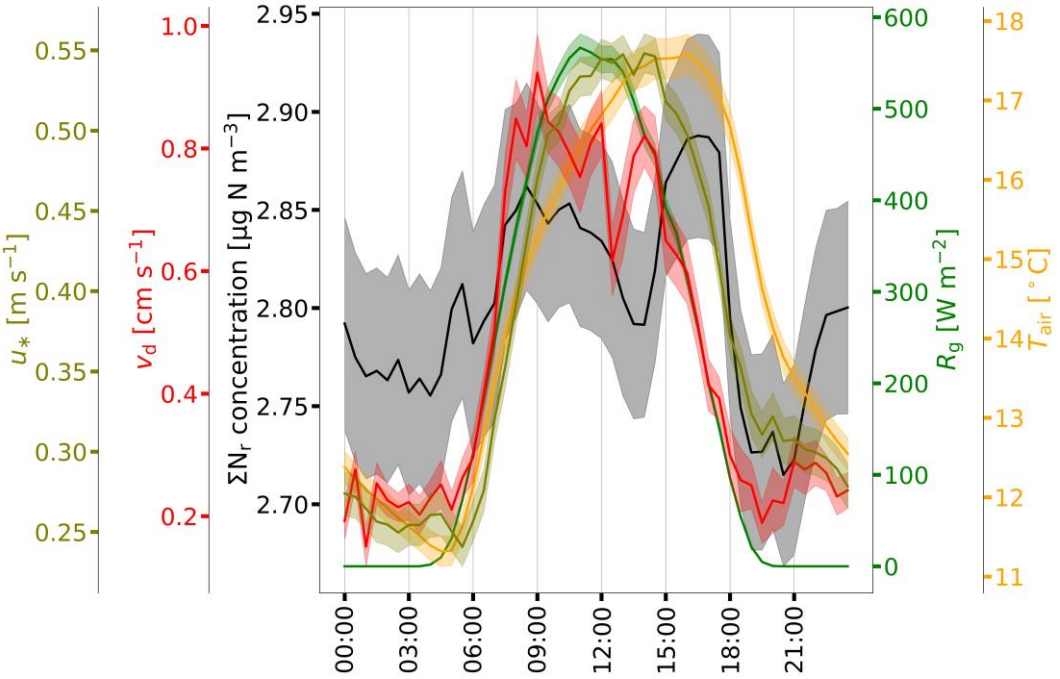

Figure S3.9: Diurnal cycles of ΣN_r (black) concentration, R_g (green), u_* (olive), air temperature T_{air} (orange), and v_d (red) for the period from May to September. Shaded areas represent the standard error of the mean.

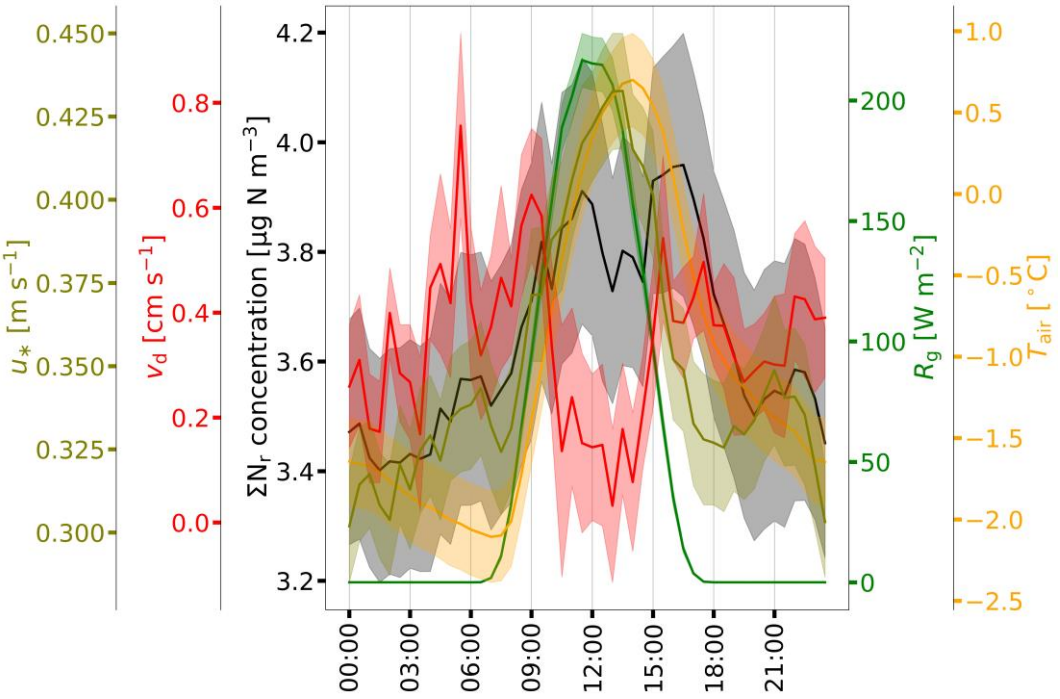

Figure S3.10: Diurnal cycles of ΣN_r (black) concentration, R_g (green), u_* (olive), air temperature T_{air} (orange), and v_d (red) for the period from December to February. Shaded areas represent the standard error of the mean.

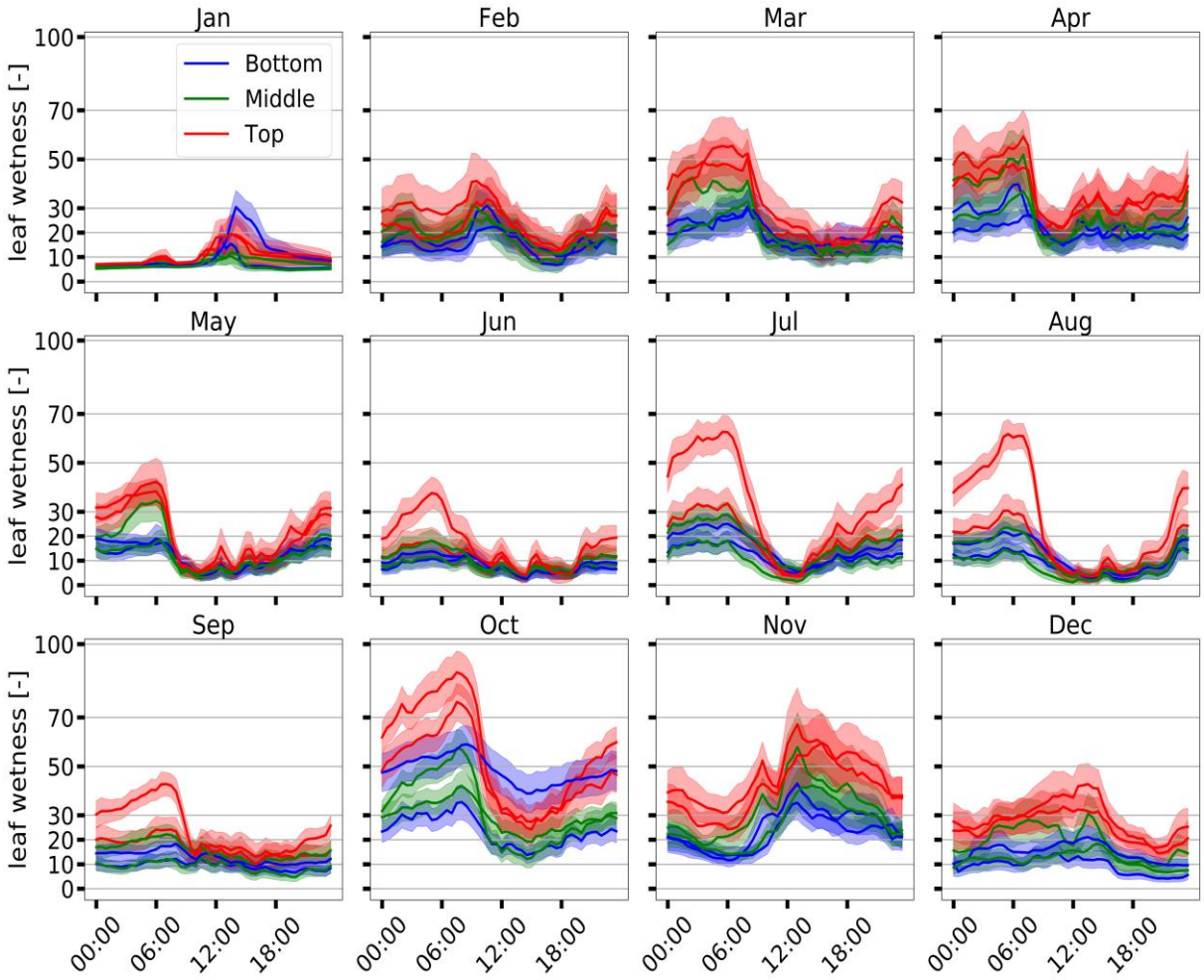

Figure S3.11: Diurnal cycles of the leaf wetness for 2017. Colors indicate installation heights of the sensors (red=top, green=middle, blue=bottom). Shaded areas represent the standard error of the mean.

Figure S3.11 shows diurnal cycles of the leaf wetness for all sensors on monthly basis for 2017. On monthly basis, the diurnal patterns of the sensors were almost the same for a season. From April, the start of the growing season, to September highest values were measured during dawn and lowest values during the day. During daylight, only slight differences in measurement height were visible. Considering the standard error, the differences in measurement heights diminished, especially between the lowest and middle sensor. Also, sensors from the mid and the top were within their uncertainty ranges. In conclusion, sensors at the lowest height seem to remain "wet" later during the morning, but effect is within the standard error range. Using only the top sensors for deriving the leaf wetness value, seems not to be appropriate with regard to the uncertainty ranges. Thus, we used all sensors for deriving a wetness boolean, which also lowered its uncertainty.

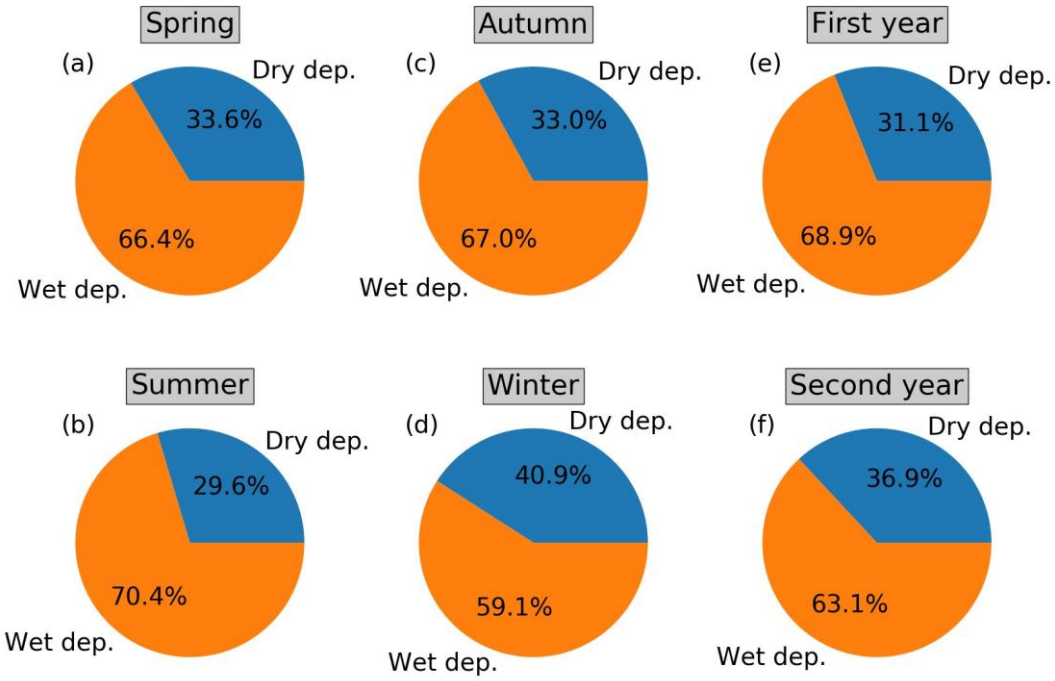

Figure S3.12: Contribution of dry and wet deposition to total deposition for each season and both measurement years labeled from (a) to (f).

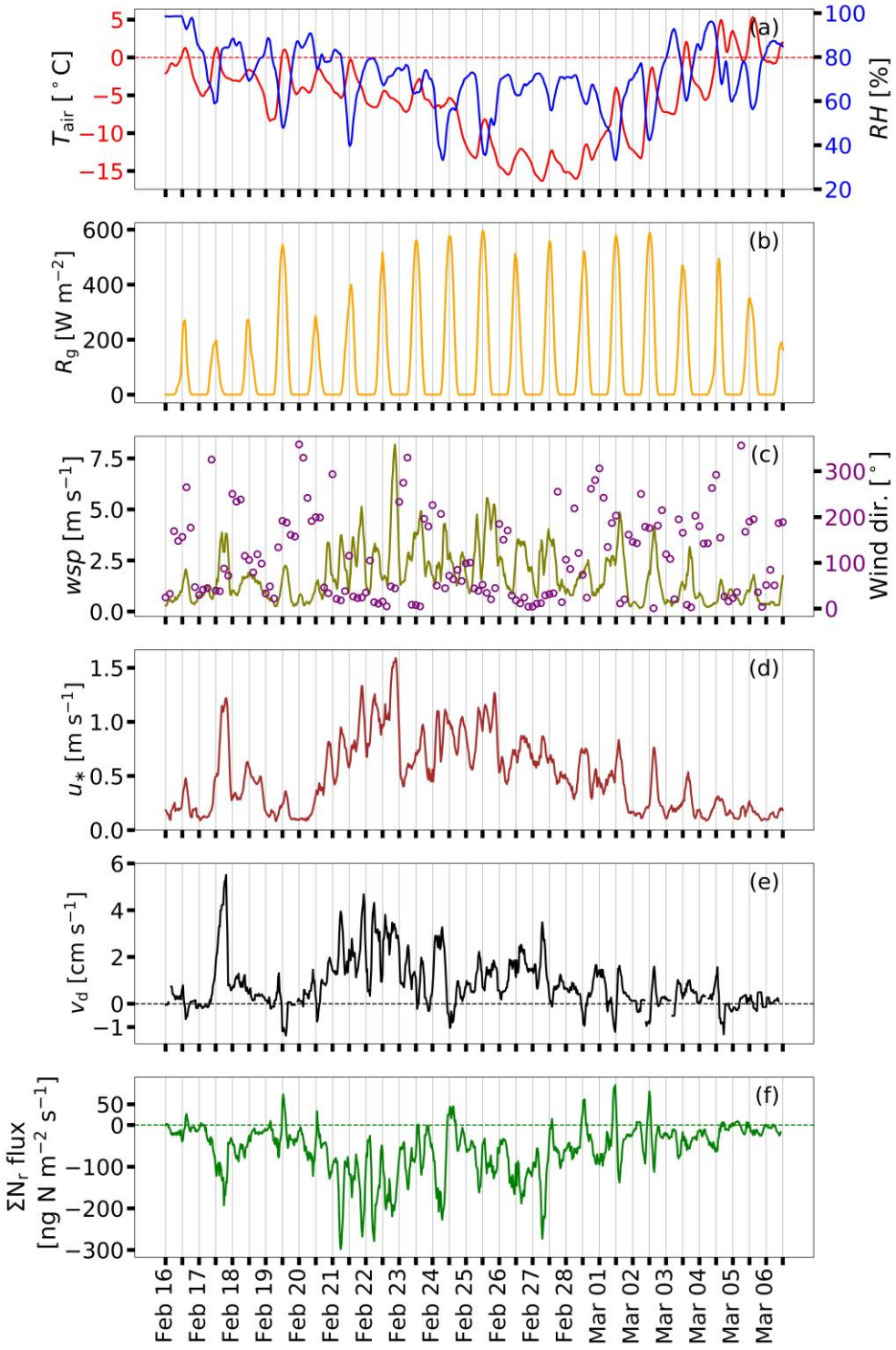

Figure S3.13: Recorded air temperature (T_{air}), relative humidity (*RH*), global radiation (R_g), wind speed (*wsp*), friction velocity (u_*), v_d, and ΣN_r flux as 3-h running mean from 16 February to 6 March 2018. Wind direction corresponds to values measured in three-hourly intervals.

A.2 Supplementary materials to chapter 4: Forest-atmosphere exchange of reactive nitrogen in a remote region – Part II: Modeling annual budgets

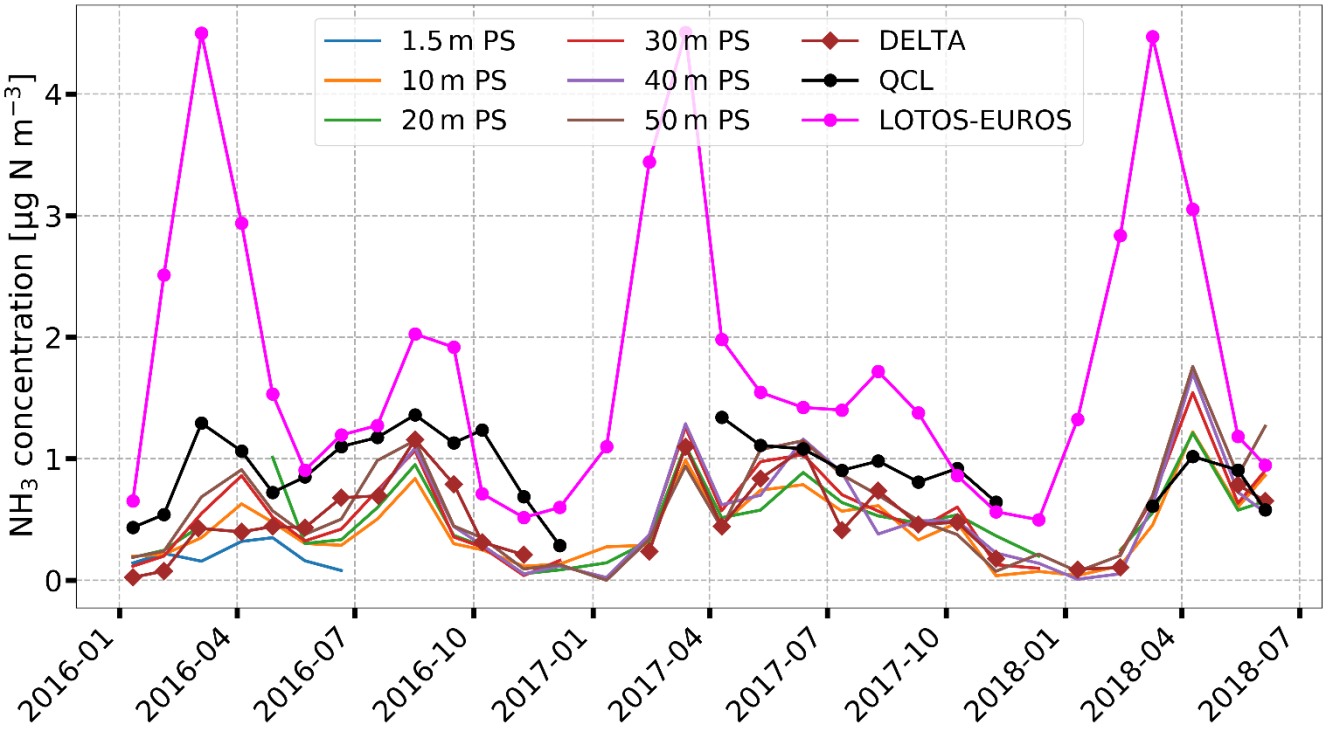

Figure S4.16: Concentrations of NH_3 obtained from DELTA and passive samplers, LOTOS-EUROS, and the QCL in µg N m^{-3}. NH_3 of the QCL and LOTOS-EUROS was averaged to the exposition period of the long-term sampling methods. Colors of the passive samplers indicate different exposition heights.

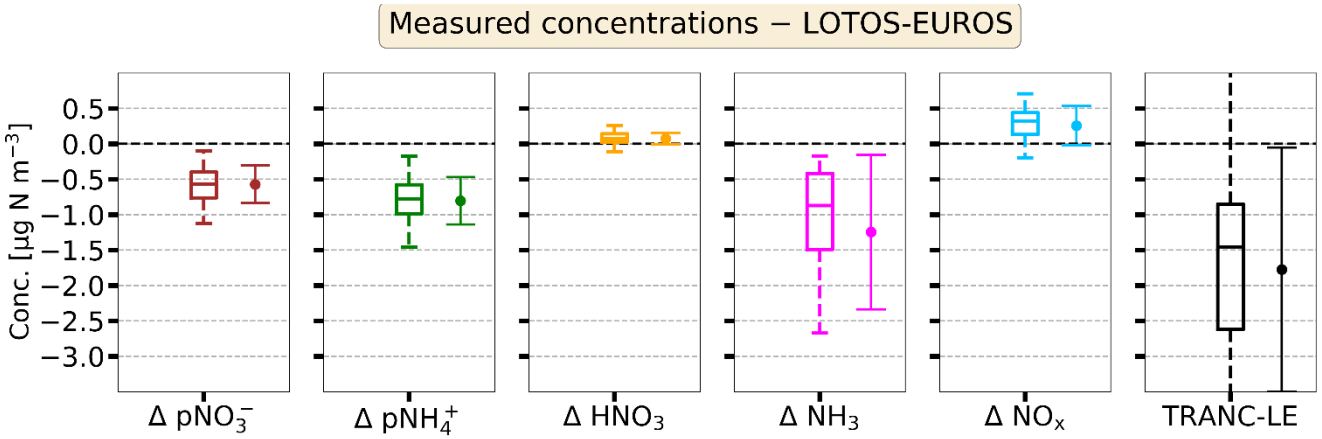

Figure S4.17: Differences in concentration between DELTA and LOTOS-EUROS for NO_x, NH_3, HNO_3, pNH_4^+, and pNO_3^- and in µg N m^{-3} depicted as boxplots (box frame = 25 % to 75 % interquartile range (IQR), bold line = median, whisker = 1.5*IQR)). In case of ΣN_r, the difference between TRANC and LOTOS averages for exposure periods of DELTA samplers is visualized. Colors indicate different N_r compounds. Negative difference indicates overestimation by LOTOS-EUROS, positive difference underestimation.

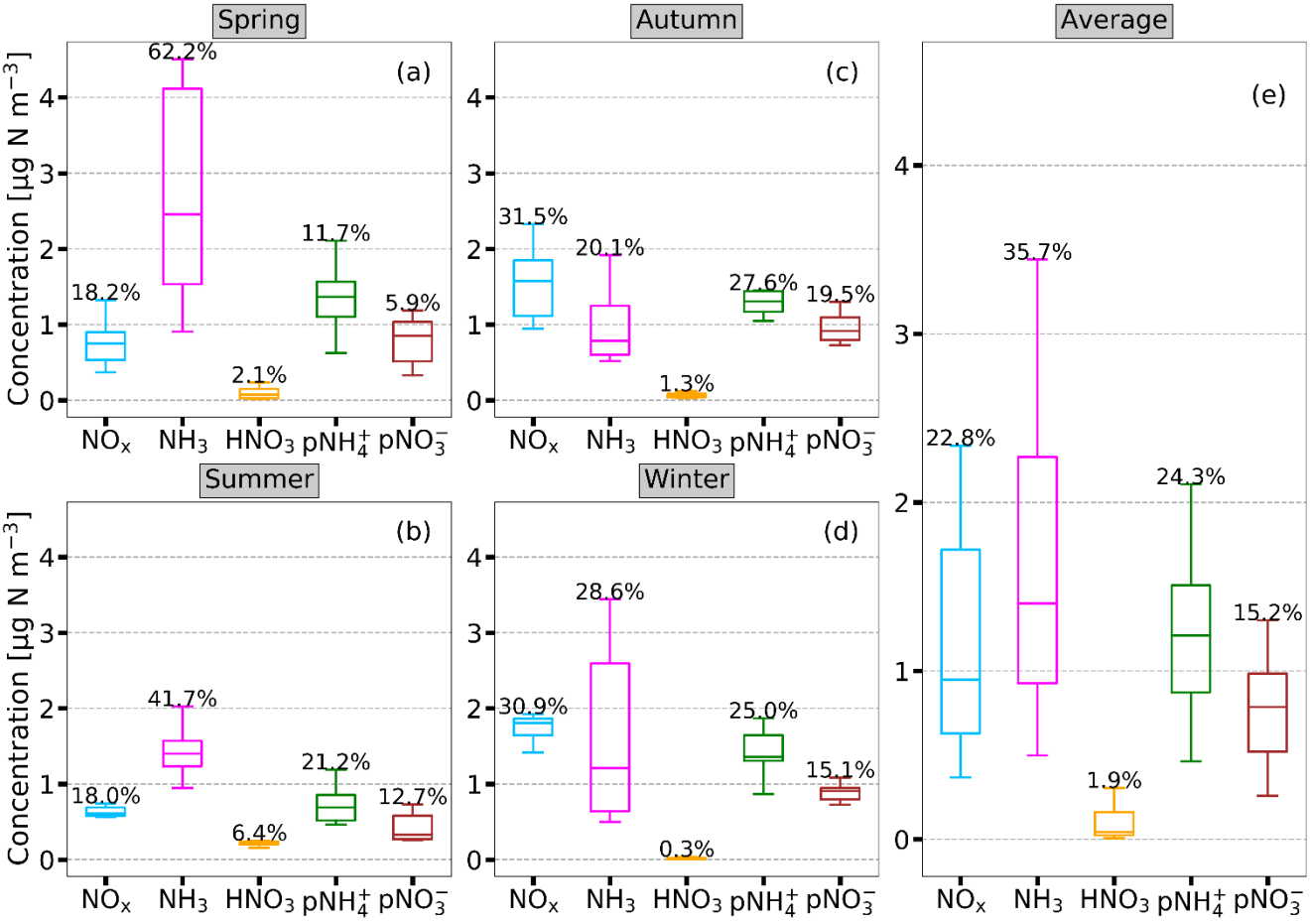

Figure S4.18: LOTOS-EUROS concentrations of NO_x, NH_3, HNO_3, pNH_4^+, and pNO_3^- in µg N m^{-3} for each season ((a), (b), (c), (d)) and the entire period (e) depicted as boxplots (box frame = 25 % to 75 % interquartile range (IQR), bold line = median, whisker = 1.5*IQR)). Colors indicate different N_r compounds. Numbers above whiskers show the relative contributions of each compound to ΣN_r for the respective period. Values based on the average concentrations.

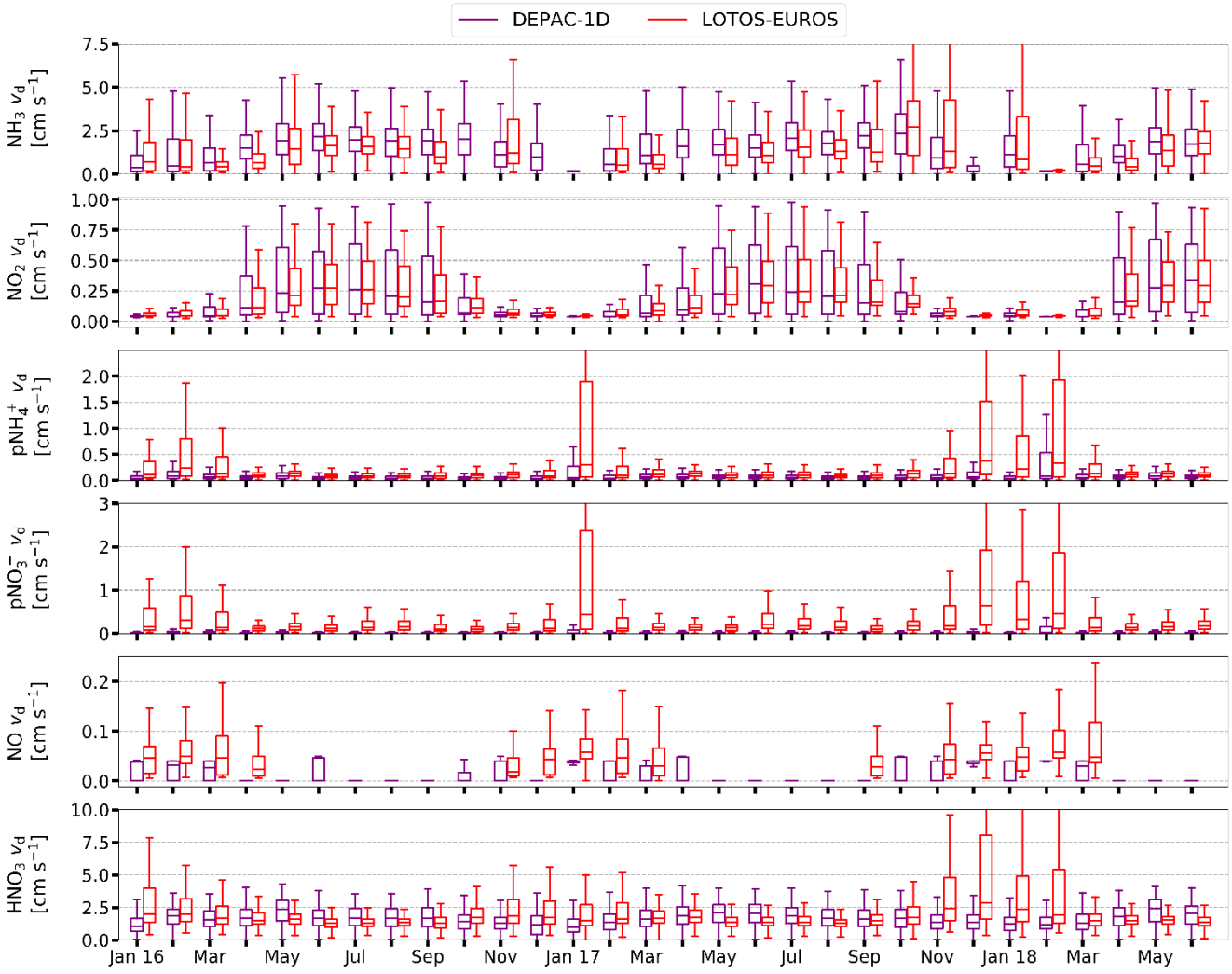

Figure S4.19: Deposition velocities of DEPAC-1D (purple) and LOTOS-EUROS (red) for NH_3, NO_2, pNH_4^+, pNO_3^-, NO, and HNO_3 in cm s^{-1} as monthly boxplots (box frame = 25 % to 75 % interquartile range (IQR), bold line = median, whisker = 1.5*IQR)).

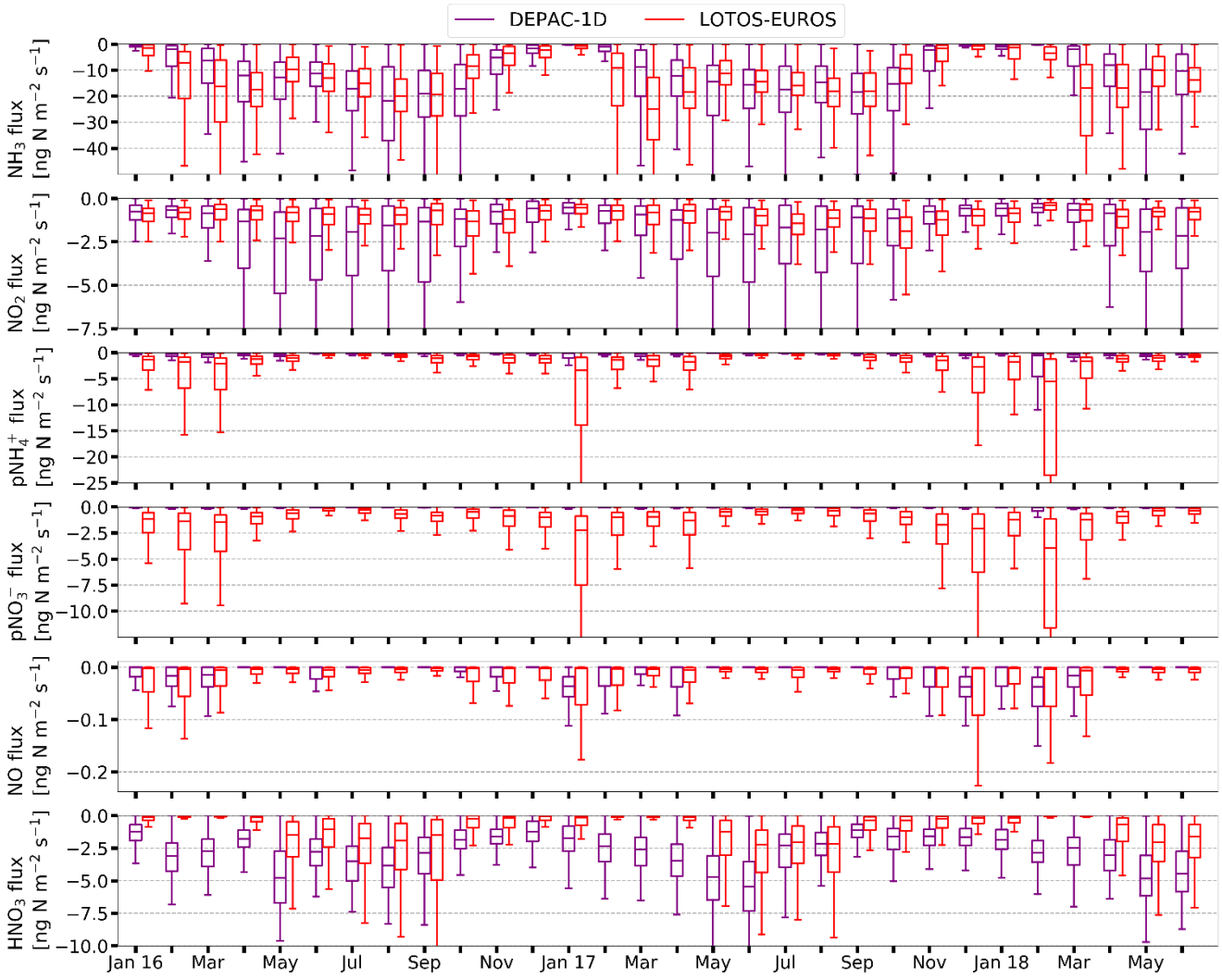

Figure S4.20: Fluxes of DEPAC-1D (purple) and LOTOS-EUROS (red) for NH_3, NO_2, pNH_4^+, pNO_3^-, NO, and HNO_3 in ng N m^{-2} s^{-1} as monthly boxplots (box frame = 25 % to 75 % interquartile range (IQR), bold line = median, whisker = 1.5*IQR)).

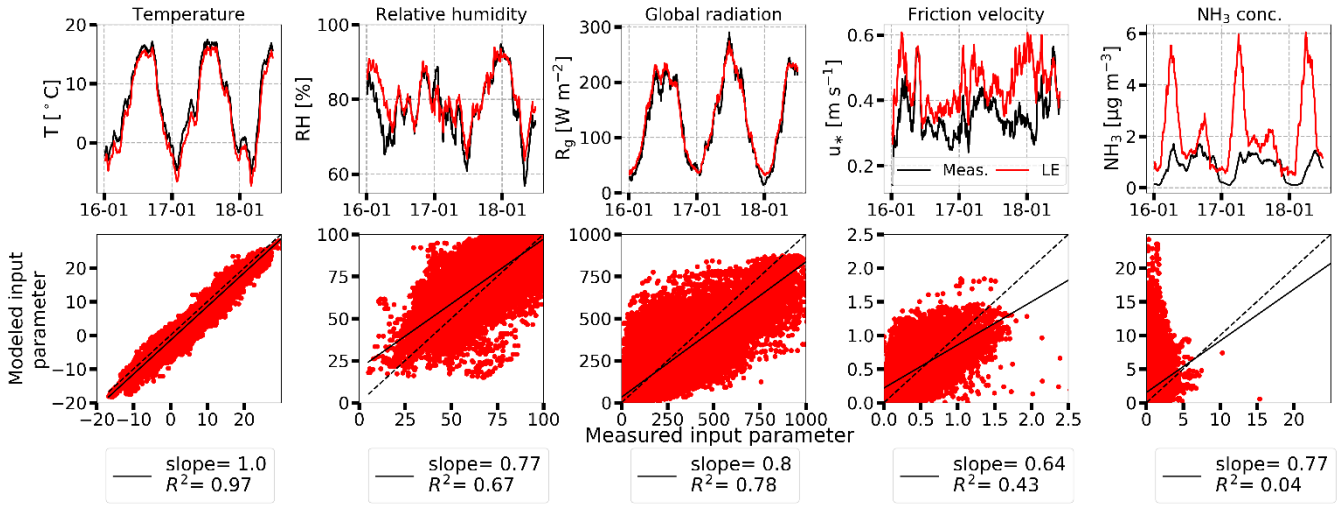

Figure S4.21: Comparison of LOTOS-EUROS (red) and measured (black) input data smoothed with a 30-day running average is applied to the input data for better visibility. The latter is applied to time series shown in the first row. In the second row, scatter plots of input data on half-hourly basis are shown for each input variable. Linear regressions are shown as black, solid lines, black, dashed lines represent 1:1 lines.

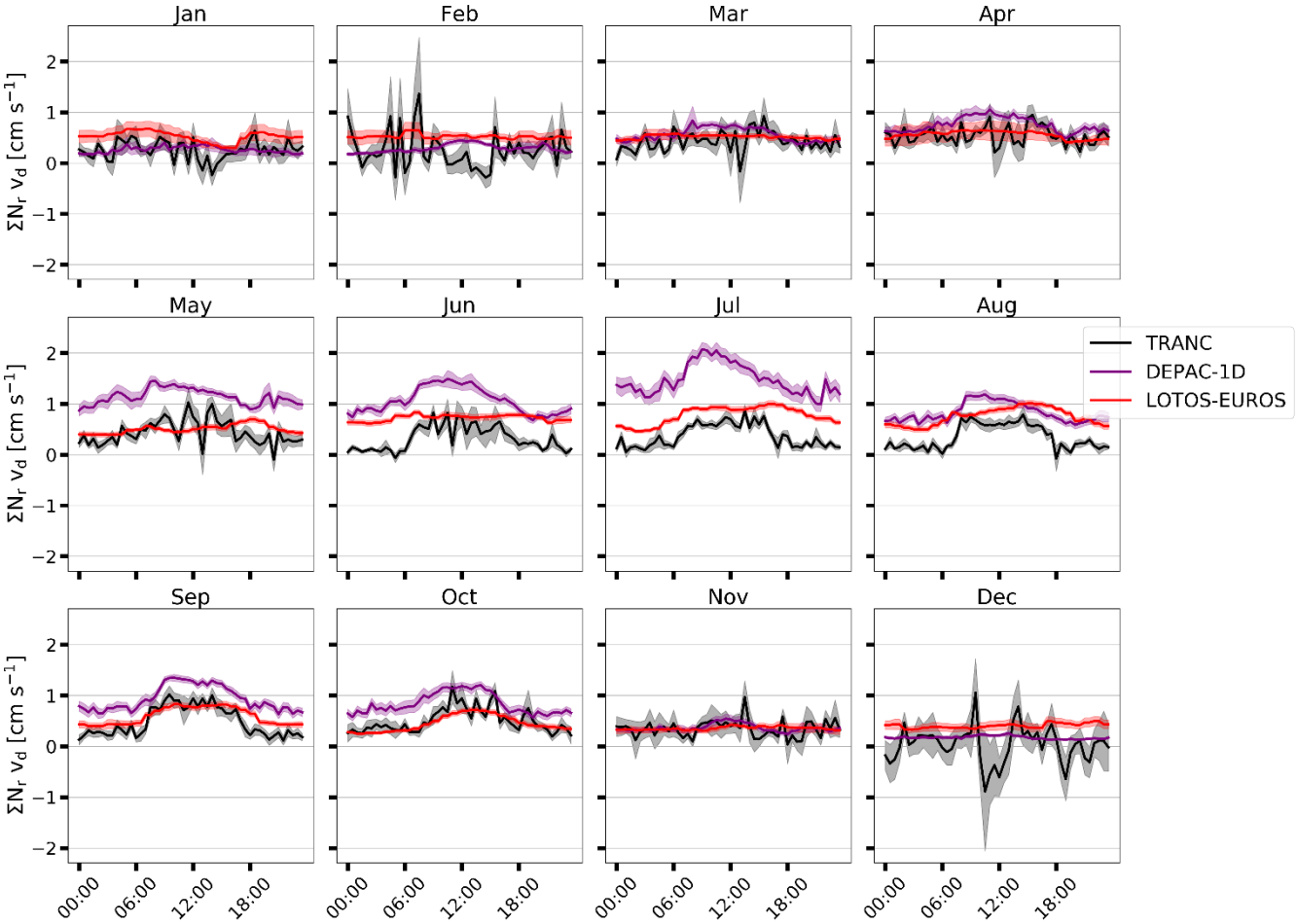

Figure S4.22: Mean diurnal cycles of ΣN_r deposition velocties for DEPAC-1D (purple), LOTOS-EUROS (red), and TRANC (black) in cm s^{-1} exemplarily shown for the year 2017. Shaded areas represent the standard error of the mean.

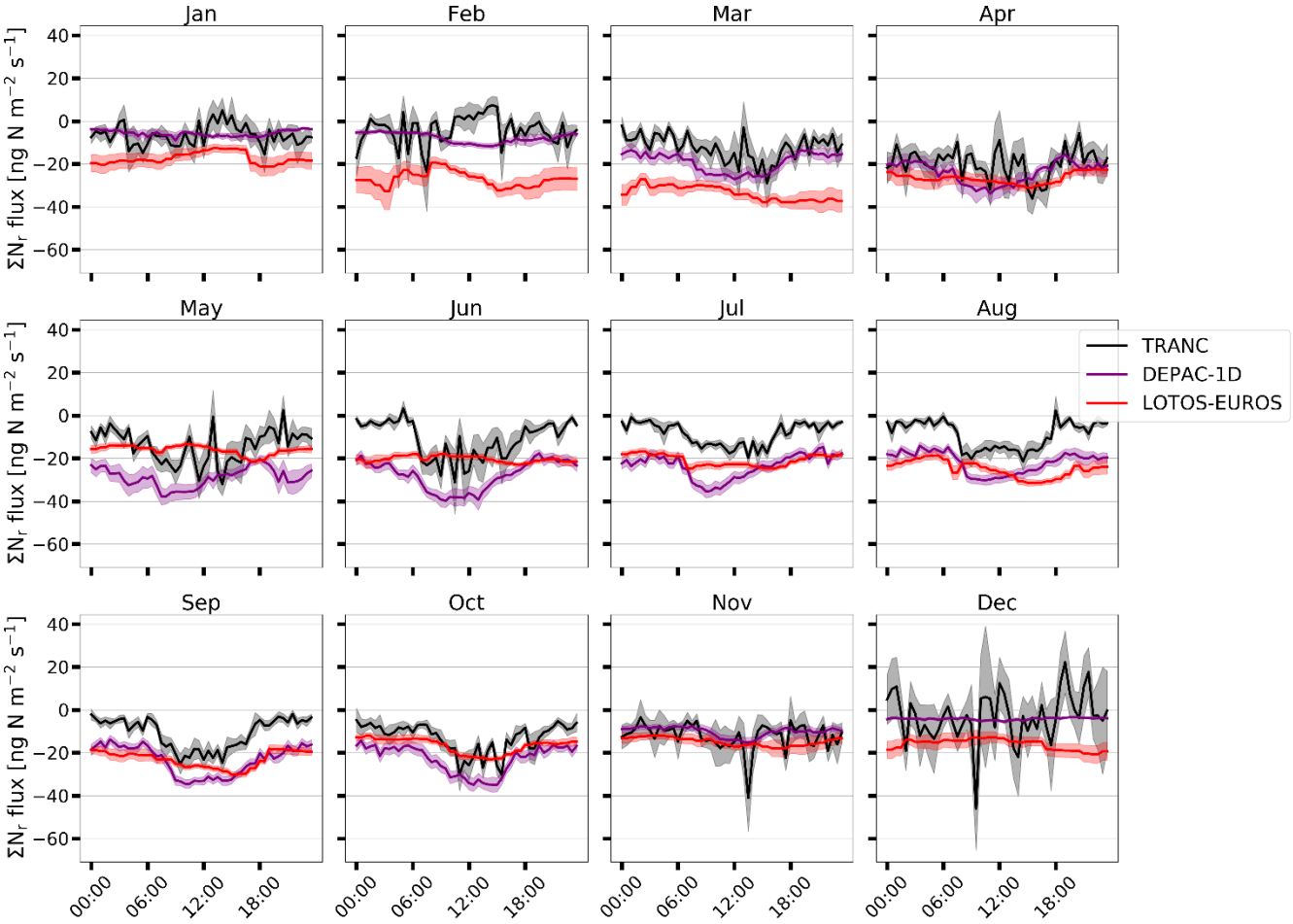

Figure S4.23: Mean diurnal cycles of ΣN_r fluxes for DEPAC-1D (purple), LOTOS-EUROS (red), and TRANC (black) in ng N m^{-3} s^{-1} exemplarily shown for the year 2017. Shaded areas represent the standard error of the mean.

Table S4.6: Medians and lower and upper quartile (LQ and UQ) of measured and modeled deposition velocities for each N_r compound. Values refer to the entire campaign duration.

Method		Deposition velocities [cm s^{-1}]						
		NH_3	NO_2	NO	HNO_3	pNO_3^-	pNH_4^+	ΣN_r
TRANC	UQ							0.73
	Median							**0.34**
	LQ							0.08
DEPAC-1D	UQ	2.4	0.27	0.04	2.3	0.03	0.10	1.0
	Median	**1.3**	**0.06**	**0.0**	**1.6**	**0.01**	**0.05**	**0.52**
	LQ	0.4	0.04	0.0	1.0	0.01	0.03	0.18
LOTOS-EUROS	UQ	2.1	0.24	0.07	2.2	0.32	0.19	0.71
	Median	**1.0**	**0.12**	**0.04**	**1.6**	**0.15**	**0.11**	**0.42**
	LQ	0.4	0.05	0.01	1.2	0.08	0.05	0.22

Table S4.7: Median fluxes of TRANC, DEPAC-1D and LOTOS-EUROS ng N m^{-2} s^{-1} in for different periods

Time	TRANC [ng N m^{-2} s^{-1}]	DEPAC-1D [ng N m^{-2} s^{-1}]	LOTOS-EUROS [ng N m^{-2} s^{-1}]
Winter	7.5	4.7	12.5
Spring	10.8	18.3	22.5
Summer	9.3	21.9	21.1
Autumn	9.5	20.3	17.5
Entire campaign	9.3	15.4	19.2

References

Aerts, R. and de Caluwe, H.: Nitrogen deposition effects on carbon dioxide and methane emissions from temperate peatland soils, Oikos, 84, 44–54, https://doi.org/10.2307/3546865, 1999.

Ammann, C.: On the applicability of relaxed eddy accumulation and common methods for measuring trace gas fluxes, PhD thesis, ETH Zurich, https://doi.org/10.3929/ethz-a-002031554, 1999.

Ammann, C., Brunner, A., Spirig, C., and Neftel, A.: Technical note: Water vapour concentration and flux measurements with PTR-MS, Atmospheric Chemistry and Physics, 6, 4643–4651, https://doi.org/10.5194/acp- 6-4643-2006, 2006.

Ammann, C., Wolff, V., Marx, O., Brümmer, C., and Neftel, A.: Measuring the biosphere-atmosphere exchange of total reactive nitrogen by eddy covariance, Biogeosciences, 9, 4247–4261, https://doi.org/10.5194/bg-9-4247-2012, 2012.

Ammann, C., Jocher M., and Voglmeier, K.: Eddy Covariance Flux Measurements of NH_3 and NO_y with a Dual-Channel Thermal Converter," *IEEE International Workshop on Metrology for Agriculture and Forestry (MetroAgriFor)*, pp. 46-51, https://doi.org/10.1109/MetroAgriFor.2019.8909278, 2019.

Aubinet, M., Grelle, A., Ibrom, A., Rannik, U., Moncrieff, J., Foken, T., Kowalski, A. S., Martin, P. H., Berbigier, P., Bernhofer, C., Clement, R., Elbers, J., Granier, A., Grünwald, T., Morgenstern, K., Pilegaard, K., Rebmann, C., Snijders, W., Valentini, R., and Vesala, T.: Estimates of the Annual Net Carbon and Water Exchange of Forests: The EUROFLUX Methodology, Adv. Ecol. Res., 30 113–175, https://doi.org/10.1016/S00652504(08)60018-5, 1999.

Aubinet, M., Feigenwinter, C., Heinisch, B., Bernhofer, C., Canepa, E., Lindroth, A., Montagnani, L., Rebmann, C., Sedlak, P., and Van Gorsel, A.: Direct advection measurements do not help to solve the nighttime CO_2 closure problem: Evidence from three different forests, Agricultural and Forest Meteorology, 150, 5, 655-664, https://doi.org/10.1016/j.agrformet.2010.01.016, 2010.

Aubinet, M., Vesala, T., and Papale, D. (Eds.): Eddy Covariance: A Practical Guide to Measurement and Data Analysis, Springer Science+Business Media B.V., Dordrecht, The Netherlands, 2012.

Avnery, S., Mauzerall, D. L., Liu, J., and Horowitz, L. W.: Global crop yield reductions due to surface ozone exposure: 2. Year 2030 potential crop production losses and economic damage under two scenarios of O_3 pollution, Atmospheric Environment, 45, 2297–2309, https://doi.org/10.1016/j.atmosenv.2011.01.002, 2011.

Baldocchi, D., Falge, E., Gu, L., Olson, R., Hollinger, D., Running, S., Anthoni, P., Bernhofer, C., Davis, K., Evans, R., Fuentes, J., Goldstein, A., Katul, G., Law, B., Lee, X., Malhi, Y., Meyers, T., Munger, W., Oechel, W., Paw, K. T., Pilegaard, K., Schmid, H. P., Valentini, R., Verma, S., Vesala, T., Wilson, K., and Wofsy, S.: FLUXNET: A New Tool to Study the Temporal and Spatial Variability of Ecosystem–Scale Carbon Dioxide, Water Vapor, and Energy Flux Densities, Bulletin of the American Meteorological Society, 82, 2415–2434, https://doi.org/10.1175/1520-0477(2001)082<2415:FANTTS>2.3.CO;2, 2001.

Baldocchi, D. D.: Assessing the eddy covariance technique for evaluating carbon dioxide exchange rates of ecosystems: past, present and future, Global Change Biology, 9, 479–492, https://doi.org/10.1046/j.1365-2486.2003.00629.x, 2003.

Behera, S. N., Sharma, M., Aneja, V. P., and Balasubramanian, R.: Ammonia in the atmosphere: a review on emission sources, atmospheric chemistry and deposition on terrestrial bodies, Environ. Sci. Pollut. Res. Int., 20, 8092–8131, https://doi.org/10.1007/s11356-013-2051-9, 2013.

Beudert, B. and Breit, W.: Integrated Monitoring Programm an der Meßstelle Forellenbach im Nationalpark Bayerischer Wald, Untersuchungen zum Stickstoffeintrag und zum wassergebundenen Stickstoffhaushalt des Forellenbachgebiets, Förderkennzeichen 351 01 012. Nationalparkverwaltung Bayerischer Wald, Sachgebiet IV, techinal report, Umweltbundesamt, Dessau-Roßlau, Germany, available at: http://www.umweltbundesamt.de/sites/default/files/medien/370/dokumente/ece_im_forellenbach_berichtsjahr_2009.pdf (last access: 2 November 2022), 2010.

Beudert, B. and Breit, W.: Kronenraumbilanzen zur Abschätzung der Stickstoffgesamtdeposition in Waldökosysteme des Nationalparks Bayerischer Wald, techreport, Umweltbundesamt, Dessau-Roßlau, Germany, available at: https://www.umweltbundesamt.de/sites/default/files/medien/370/dokumente/kronenraumbilanzen_stickstoffgesamtdeposition_nationalpark_bayerisches_wald_-_berichtsjahr_2013_im_forellenbach.pdf (last access: 2 November 2022), 2014.

Beudert, B., and Gietl, G.: Long-term monitoring in the Große Ohe catchment, Bavarian Forest National Park, Silva Gabreta, 21, 5-27, https://www.npsumava.cz/wp-content/uploads/2019/06/sg_21_1_beudertgietl.pdf (last access: 2 November 2022), 2015.

Bobbink, R., Hicks, K., Galloway, J., Spranger, T., Alkemade, R., Ashmore, M., Bustamante, M., Cinderby, S., Davidson, E., and Dentener, F.: Global assessment of nitrogen deposition effects on terrestrial plant diversity: a synthesis, Ecological applications, 20, 30–59, https://doi.org/10.1890/08-1140.1, 2010.

Bobbink, R. and Hettelingh, J.-P.: Review and revision of empirical critical loads and dose-response relationships. National Institute for Public Health and the Environment (RIVM), RIVM Report, https://www.rivm.nl/bibliotheek/rapporten/680359002.pdf (last access: 2 November 2022), 2011.

Bodelier, P. L., and Steenbergh, A. K.: Interactions between methane and the nitrogen cycle in light of climate change, Current Opinion in Environmental Sustainability, 9, 26–36, https://doi.org/10.1016/j.cosust.2014.07.004, 2014.

Breuninger, C., Meixner, F. X., and Kesselmeier, J.: Field investigations of nitrogen dioxide (NO_2) exchange between plants and the atmosphere, Atmos. Chem. Phys., 13, 773–790, https://doi.org/10.5194/acp-13-773-2013, 2013.

Brümmer, C., Marx, O., Kutsch, W., Ammann, C., Wolff, V., Flechard, C. R., and Freibauer, A.: Fluxes of total reactive atmospheric nitrogen (ΣNr) using eddy covariance above arable land, Tellus B: Chemical and Physical Meteorology, 65, 19770, https://doi.org/10.3402/tellusb.v65i0.19770, 2013.

Brümmer, C., Rüffer, J. J., Delorme, J.-P., Wintjen, P., Schrader, F., Beudert, B., Schaap, M., and Ammann, C.: Reactive nitrogen fluxes over peatland and forest ecosystems using micrometeorological measurement techniques, Earth System Science Data, 14, 743–761, https://doi.org/10.5194/essd-14-743-2022, 2022.

Burba, G.: Eddy Covariance Method for Scientific, Industrial, Agricultural and Regulatory Applications: A Field Book on Measuring Ecosystem Gas Exchange and Areal Emission Rates, LICOR Biosciences, Lincoln, Nebraska, USA, 2013.

Businger, J. A., Wyngaard, J. C., Izumi, Y., and Bradley, E. F.: Flux-profile relationships in the atmospheric surface layer, Journal of Atmospheric Sciences, 28,181–189, https://doi.org/10.1175/1520-0469(1971)028<0181:FPRITA>2.0.CO;2, 1971.

Businger, J. A.: Evaluation of the accuracy with which dry deposition can be measured with current micrometeorological techniques, Journal of Applied Meteorology and Climatology, 25, 1100–1124, https://doi.org/10.1175/1520-0450(1986)025<1100:EOTAWW>2.0.CO;2, 1986.

Businger, J. A. and Oncley, S. P.: Flux measurements with conditional sampling, Journal of Atmospheric and Oceanic Technology, 7, 349-352, https://doi.org/10.1175/1520-0426(1990)007<0349:FMWCS>2.0.CO;2, 1990.

Butterbach-Bahl, K., Nemitz, E., Zaehle, S., Billen, G., Boeckx, P., Erisman, J. W., Garnier, J., Upstill-Goddard, R., Kreuzer, M., and Oenema, O.: Nitrogen as a threat to the European greenhouse gas balance, in: The European nitrogen assessment: sources, effects and policy perspectives, Cambridge University Press, 434–462, 2011.

Büttner, G., and Kosztra, B.: CLC2012, Addendum to CLC2006 Technical Guidelines, EEA/ETC SIA Working document. 2011.

Büttner, G., and Kosztra, B.: CLC2018 Technical Guidelines, (https://land.copernicus.eu/user-corner/technical-library/clc2018technicalguidelines_final.pdf, last access: 02 November 2022), 2017.

Carter, T. S., Clark, C. M., Fenn, M. E., Jovan, S., Perakis, S. S., Riddell, J., Schaberg, P. G., Greaver, T. L., and Hastings, M. G.: Mechanisms of nitrogen deposition effects on temperate forest lichens and trees, Ecosphere, 8, e01717, https://doi.org/10.1002/ecs2.1717, 2017.

Civerolo, K. L. and Dickerson, R. R.: Nitric oxide soil emissions from tilled and untilled cornfields, Agricultural and Forest Meteorology, 90, 307–311, https://doi.org/10.1016/S0168-1923(98)00056-2, 1998.

Chaparro-Suarez, I., Meixner, F., and Kesselmeier, J.: Nitrogen dioxide (NO_2) uptake by vegetation controlled by atmospheric concentrations and plant stomatal aperture, Atmospheric Environment, 45, 5742–5750, https://doi.org/10.1016/j.atmosenv.2011.07.021, 2011

Cowan, N., Nemitz, E., Walker, J. T., Fowler, D., Finnigan, J. J., Webster, H. N., Levy, P., Twigg, M., Tang, S. Y., Bachiller-Jareno, N., Trembath, P., Kinnersley, R. P., and Braban, C. F.: Review of methods for assessing deposition ofreactive nitrogen pollutants across complex terrain with focus on the UK, Environmental Science: Atmospheres, 2, 829-851, https://doi.org/10.1039/D2EA00012A, 2022.

Dammers, E., McLinden, C. A., Griffin, D., Shephard, M. W., Van Der Graaf, S., Lutsch, E., Schaap, M., Gainairu-Matz, Y., Fioletov, V., Van Damme, M., Whitburn, S., Clarisse, L., Cady-Pereira, K., Clerbaux, C., Coheur, P. F., and Erisman, J. W.: NH_3 emissions from large point sources derived from CrIS and IASI satellite observations, Atmos. Chem. Phys., 19, 12261–12293, https://doi.org/10.5194/acp-19-12261-2019, 2019.

Dämmgen, U., Thöni, L., Lumpp, R., Gilke, K., Seitler, E., and Bullinger, M.: Feldexperiment zum Methodenvergleich von Ammoniak- und Ammonium-Konzentrationsmessungen in der Umgebungsluft, 2005 bis 2008 in Braunschweig, vol. 337 of Landbauforschung: Sonderheft, Johann Heinrich von Thünen-Institut, Braunschweig, jahresberichtskategorie: 10-M4;10-3, available at: https://www.openagrar.de/receive/timport_mods_00006160 (last access: 2 November 2022), 2010.

Dabberdt, W. F., Lenschow, D. H., Horst, T. W., Zimmerman, P. R., Oncley, S. P., and Delany, A. C.: Atmosphere-surface exchange measurements, Science, 260, 1472–1481, https://doi.org/10.1126/science.260.5113.1472, 1993.

Damgaard, C., Jensen, L., Frohn, L. M., Borchsenius, F., Nielsen, K. E., Ejrnæs, R. and Stevens, C. J.: The effect of nitrogen deposition on the species richness of acid grasslands in Denmark: A comparison with a study performed on a European scale, Environmental Pollution, 159, 1778–1782, https://doi.org/10.1016/j.envpol.2011.04.003, 2011.

Davidson, E.: The contribution of manure and fertilizer nitrogen to atmospheric nitrous oxide since 1860, Nature Geoscience, 2, 659–662, https://doi.org/10.1038/ngeo608, 2009.

de Vries, W., Reinds, G. J., and Vel, E.: Intensive monitoring of forest ecosystems in Europe: 2: Atmospheric deposition and its impacts on soil solution chemistry, Forest Ecology and Management, 174, 97–115, https://doi.org/10.1016/S0378-1127(02)00030-0, 2003.

de Vries, W., Du, E., and Butterbach-Bahl, K.: Short and long-term impacts of nitrogen deposition on carbon sequestration by forest ecosystems, Current Opinion in Environmental Sustainability, 9, 90–104, https://doi.org/10.1016/j.cosust.2014.09.001, 2014.

de Vries, W.: Impacts of nitrogen emissions on ecosystems and human health: A mini review. Current Opinion in Environmental Science and Health, 21, [100249], https://doi.org/10.1016/j.coesh.2021.100249, 2021

Delany, A. C., Fitzjarrald, D. R., Lenschow, D. H., Pearson, R., Wendel, G. J., and Woodrufl, B.: Direct measurements of nitrogen oxides and ozone fluxes over grassland, Journal of Atmospheric Chemistry, 4, 429–444, https://doi.org/10.1007/BF00053844, 1986.

Desjardins, R. L.: A Study of Carbon Dioxide and Sensible Heat Fluxes Using the Eddy Correlation Technique, PhD thesis, Cornell University, 1972

Desjardins, R. l.: Technique to measure CO_2 exchange under field conditions, International Journal of Biometeorology, 18, 76–83, https://doi.org/10.1007/BF01450667, 1974.

Dise, N. B., Ashmore, M., Belyazid, S., Bleeker, A., Bobbink, R., de Vries, W., Erisman, J. W., van den Berg, L., Spranger, T., and Stevens, C.: Nitrogen as a threat to European terrestrial biodiversity - Chapter 20, in: *The European Nitrogen Assessment* (Eds. Sutton, M.A., Howard, C. M., Erisman, J. W., Billen, G., Bleeker, A., Grennfelt, P., van Grinsven, H. and Grizzetti, B.), 463–494, Cambridge University Press, 2011.

Draaijers, G. P. J. and Erisman, J. W.: A canopy budget model to assess atmospheric deposition from throughfall measurements, Water, Air, Soil Pollution, 85, 2253–2258, https://doi.org/10.1007/BF01186169, 1995.

Driscoll, C. T., Whitall, D., Aber, J., Boyer, E., Castro, M., Cronan, C., Goodale, C. L., Groffman, P., Hopkinson, C., Lambert, K., Lawrence, G., and Ollinger, S.: Nitrogen Pollution in the Northeastern United States: Sources, Effects, and Management Options, BioScience, 53, 357–374, https://doi.org/10.1641/0006-3568(2003)053[0357:NPITNU]2.0.CO;2, 2003.

Dyer, A. J. and Hicks, B. B.: Flux-gradient relationships in the constant flux layer, Quarterly Journal of the Royal Meteorological Society, 96, 715–721, https://doi.org/10.1002/qj.49709641012, 1970.

Edwards, G. C., Rasmussen, P. E., Schroeder, W. H., Wallace, D. M., Halfpenny-Mitchell, L., Dias, G. M., Kemp, R. J., and Ausma, S.: Development and evaluation of a sampling system to determine gaseous Mercury fluxes using an aerodynamic micrometeorological gradient method, Journal of Geophysical Research, 110, D10306, https://doi.org/10.1029/2004JD005187, 2005.

Ellis, R. A., Murphy, J. G., Pattey, E., van Haarlem, R., O'Brien, J. M., and Herndon, S. C.: Characterizing a Quantum Cascade Tunable Infrared Laser Differential Absorption Spectrometer (QCTILDAS) for measurements of atmospheric ammonia, Atmos. Meas. Tech., 3, 397–406, https://doi.org/10.5194/amt-3-397-2010, 2010.

Emberson, L.D., Ashmore, M. R., Simpson, D., Tuovinen, J.-P. and Cambridge, H. M.: Towards a model of ozone deposition and stomatal uptake over Europe, EMEP/MSC-W 6/2000, Norwegian Meteorological Institute, Oslo, 2000a.

Emberson, L. D., Ashmore, M. R., Cambridge, H. M., Simpson, D., and Tuovinen, J. P.: Modelling stomatal ozone flux across Europe, Environmental Pollution, 109, 403–13, https://doi.org/10.1016/S0269-7491(00)00043-9, 2000b.

Erisman, J. W. and Wyers, G. P.: Continuous measurements of surface exchange of SO_2 and NH_3; Implications for their possible interaction in the deposition process, Atmos. Environ. A-Gen., 27, 1937–1949, https://doi.org/10.1016/0960-1686(93)90266-2, 1993.

Erisman, J. W., Van Pul, A., and Wyers, P.: Parametrization of surface resistance for the quantification of atmospheric deposition of acidifying pollutants and ozone, Atmospheric Environment, 28, 2595–2607, https://doi.org/10.1016/1352-2310(94)90433-2, 1994.

Erisman, J. W. and Draaijers, G. P. J.: Atmospheric deposition in relation to acidification and eutrophication, Elsevier, (Studies in environmental science 63), 1995.

Erisman, J., and Schaap, M.: The need for ammonia abatement with respect to secondary PM reductions in Europe, Environmental Pollution, 129, 159–163, https://doi.org/10.1016/j.envpol.2003.08.042, 2004.

Erisman, J. W., Sutton, M. A., Galloway, J., Klimont, Z., and Winiwarter, W.: How a century of ammonia synthesis changed the world, Nat. Geosci., 1, 636–639, https://doi.org/10.1038/ngeo325, 2008.

Erisman, J. W., Galloway, J. N., Seitzinger, S., Bleeker, A., and Butterbach-Bahl, K.: Reactive nitrogen in the environment and its effect on climate change. Current Opinion in Environmental Sustainability, 3, 281–290. https://doi.org/10.1016/j.cosust.2011.08.012, 2011.

Erisman, J. W., Galloway, J. N., Seitzinger, S., Bleeker, A., Dise, N. B., Petrescu, A. M., Leach, A. M. and de Vries, W.: Consequences of human modification of the global nitrogen cycle, Philosophical Transactions of the Royal Society London B: Biological Sciences, 368, 201301116, https://doi.org/10.1098/rstb.2013.0116, 2013.

Erisman, J. W., Galloway, J., Dice, N. B., Sutton, M., Bleeker, A., Grizzetti, B., Leach, A., and de Vries, W.: Nitrogen: too much of a vital resource, Science Brief, WWF Netherlands, Zeist, The Netherlands, 2015.

Eugster, W. and Hesterberg, R.: Transfer resistances of NO_2 determined from eddy correlation flux measurements over a litter meadow at a rural site on the swiss plateau, Atmospheric Environment, 30, 307–311, https://doi.org/10.1016/1352-2310(95)00418-1, 1996.

Falge, E., Baldocchi, D., Olson, R., Anthoni, P., Aubinet, M., Bernhofer, C., Burba, G., Ceulemans, R., Clement, R., Dolman, H., Granier, A., Gross, P., Grünwald, T., Hollinger, D., Jensen, N.-O., Katul, G., Keronen, P., Kowalski, A., Lai, C. T., Law, B. E., Meyers, T., Moncrieff, J., Moors, E., Munger, J., Pilegaard, K., Üllar Rannik, Rebmann, C., Suyker, A., Tenhunen, J., Tu, K., Verma, S., Vesala, T., Wilson, K., and Wofsy, S.: Gap filling strategies for defensible annual sums of net ecosystem exchange, Agricultural and Forest Meteorology, 107, 43–69, https://doi.org/10.1016/S0168-1923(00)00225-2, 2001.

Farmer, D. K., Wooldridge, P. J., and Cohen, R. C.: Application of thermal-dissociation laser induced fluorescence (TD-LIF) to measurement of HNO_3, Σalkyl nitrates, Σperoxy nitrates, and NO_2 fluxes using eddy covariance, Atmospheric Chemistry and Physics, 6, 3471–3486, https://doi.org/10.5194/acp-6-3471-2006, 2006.

Farquhar, G. D., Firth, P. M., Wetselaar, R., and Weir, B: On the Gaseous Exchange of Ammonia between Leaves and the Environment: Determination of the Ammonia Compensation Point, Plant Physiol., 66, 710–714, https://doi.org/10.1104/pp.66.4.710, 1980.

Flechard, C. R., Nemitz, E., Smith, R. I., Fowler, D., Vermeulen, A. T., Bleeker, A., Erisman, J. W., Simpson, D., Zhang, L., Tang, Y. S., and Sutton, M. A.: Dry deposition of reactive nitrogen to European ecosystems: a comparison of inferential models across the NitroEurope network, Atmospheric Chemistry and Physics., 11, 2703–2728, https://doi.org/10.5194/acp-11-2703-2011, 2011.

Flechard, C. R., Massad, R.-S., Loubet, B., Personne, E., Simpson, D., Bash, J. O., Cooter, E. J., Nemitz, E., and Sutton, M. A.: Advances in understanding, models and parameterizations of biosphere-atmosphere ammonia exchange, Biogeosciences, 10, 5183–5225, https://doi.org/10.5194/bg-10-5183-2013, 2013.

Flechard, C. R., Ibrom, A., Skiba, U. M., de Vries, W., van Oijen, M., Cameron, D. R., Dise, N. B., Korhonen, J. F. J., Buchmann, N., Legout, A., Simpson, D., Sanz, M. J., Aubinet, M., Loustau, D., Montagnani, L., Neirynck, J., Janssens, I. A., Pihlatie, M., Kiese, R., Siemens, J., Francez, A.-J., Augustin, J., Varlagin, A., Olejnik, J., Juszczak, R., Aurela, M., Berveiller, D., Chojnicki, B. H., Dämmgen, U., Delpierre, N., Djuricic, V., Drewer, J., Dufrêne, E., Eugster, W., Fauvel, Y., Fowler, D., Frumau, A., Granier, A., Gross, P., Hamon, Y., Helfter, C., Hensen, A., Horváth, L., Kitzler, B., Kruijt, B., Kutsch, W. L., Lobo-do-Vale, R., Lohila, A., Longdoz, B., Marek, M. V., Matteucci, G., Mitosinkova, M., Moreaux, V., Neftel, A., Ourcival, J.-M., Pilegaard, K., Pita, G., Sanz, F., Schjoerring, J. K., Sebastià, M.-T., Tang, Y. S., Uggerud, H., Urbaniak, M., van Dijk, N., Vesala, T., Vidic, S., Vincke, C., Weidinger, T., Zechmeister-Boltenstern, S., Butterbach-Bahl, K., Nemitz, E., and Sutton, M. A.: Carbon–nitrogen interactions in European forests and semi-natural vegetation – Part 1: Fluxes and budgets of carbon, nitrogen and greenhouse gases from ecosystem monitoring and modelling, Biogeosciences, 17, 1583–1620, https://doi.org/10.5194/bg-17-1583-2020, 2020.

Foken, T.: 50 Years of the Monin–Obukhov Similarity Theory, Boundary-Layer Meteorology, 119, 431–447, https://doi.org/10.1007/s10546-006-9048-6, 2006.

Foken, T.; Angewandte Mikrometeorologie, Mikrometeorologische Methoden, Springer-Verlag Berlin, Heidelberg, Germany, 2016.

Fowler, D., Cape, J., and Unsworth, M.: Deposition of atmospheric pollutants on forests, Philosophical Transactions of the Royal Society of London. B, Biological Sciences, 324, 247-265, http://www.jstor.org/stable/2990182, 1989.

Fowler, D., Duyzer, J., and Baldocchi, D.: Inputs of trace gases, particles and cloud droplets to terrestrial surfaces, Proceedings of the Royal Society of Edinburgh, Section B: Biological Sciences, 97, 35–59, https://doi.org/10.1017/S0269727000005285, 1990.

Ferm, M.: A Sensitive Diffusional Sampler, Report L91-172, Swedish Environmental Research Institute, Gothenburg, 1991.

Ferrara, R. M., Loubet, B., Di Tommasi, P., Bertolini, T., Magliulo, V., Cellier, P., Eugster, W., and Rana, G.: Eddy covariance measurement of ammonia fluxes: Comparison of high frequency correction methodologies, Agr. Forest Meteorol., 158–159, 30– 42, https://doi.org/10.1016/j.agrformet.2012.02.001, 2012.

Ferrara, R. M., Di Tommasi, P., Famulari, D., and Rana, G.: Limitations of an Eddy-Covariance System in Measuring Low Ammonia Fluxes, Bound.-Lay. Meteorol., 180, 173–186, https://doi.org/10.1007/s10546-021-00612-6, 2021.

Fowler, D., Coyle, M., Skiba, U., Sutton, M. A., Cape, J.N., Reis, S., Sheppard, L .J., Jenkins, A., Grizzetti, B., Galloway, J. N., Vitousek, P., Leach, A., Bouwman, A. F., Butterbach-Bahl, K., Dentener, F., Stevenson, D., Amann, M., and Voss, M.: The global nitrogen cycle in the twenty-first century, Philos. Trans. R. Soc. B Biol. Sci., 368, 20130164, https://doi.org/10.1098/rstb.2013, 2013.

Galloway, J. N., Aber, J. D., Erisman, J. W., Seitzinger, S. P., Howarth, R. W., Cowling, E. B., and Cosby, B. J.: The nitrogen cascade, Bioscience, 53, 341–356, https://doi.org/10.1641/0006-3568(2003)053[0341:Tnc]2.0.Co;2, 2003.

Garland, J. A.: The Dry Deposition of Sulphur Dioxide to Land and Water Surfaces, P. Roy. Soc. A-Math. Phy., 354, 245–268, https://doi.org/10.1098/rspa.1977.0066, 1977.

Gash, J. H. C. and Culf, A. D.: Applying linear de-trend to eddy correlation data in real time. Boundary-Layer Meteorology, 79, 301-306, https://doi.org/10.1007/BF00119443, 1996.

Ge, X., Schaap, M., Kranenburg, R., Segers, A., Reinds, G. J., Kros, H., and de Vries, W.: Modeling atmospheric ammonia using agricultural emissions with improved spatial variability and temporal dynamics, Atmos. Chem. Phys., 20, 16055–16087, https://doi.org/10.5194/acp-20-16055-2020, 2020.

Geddes, J. A. and Murphy, J. G.: Observations of reactive nitrogen oxide fluxes by eddy covariance above two midlatitude North American mixed hardwood forests, Atmos. Chem. Phys., 14, 2939–2957, https://doi.org/10.5194/acp-14-2939-2014, 2014.

Geupel, M., Heldstab, J., Schäppi, B., Reutimann, J., Bach, M., Häußermann, U., Knoll, L., Klement, L., and Breuer, L. A: National Nitrogen Target for Germany, Sustainability, 13, 1121, https://doi.org/10.3390/su13031121, 2021.

Giannakis, E., Kushta, J., Bruggeman, A., and Lelieveld, J.: Costs and benefits of agricultural ammonia emission abatement options for compliance with European air quality regulations, Environmental Sciences Europe, 31, 93, https://doi.org/10.1186/s12302-019-0275-0, 2019.

Granier, C., Bessagnet, B., Bond, T., D'Angiola, A., Denier van der Gon, H., Frost, G. J., Heil, A., Kaiser, J. W., Kinne, S., Klimont, Z., Kloster, S., Lamarque, J.-F., Liousse, C., Masui, T., Meleux, F., Mieville, A., Ohara, T., Raut, J.-C., Riahi, K., Schultz, M.G., Smith, S. J., Thompson, A., van Aardenne, J., van der Werf, G. R., and van Vuuren, D. P.: Evolution of anthropogenic and biomass burning emissions of air pollutants at global and regional scales during the 1980-2010 period. Clim. Change 109, 163–190, https://doi.org/10.1007/s10584-011-01, 2011.

Grünhage, L. and Haenel, H.D.: Platin (plant-atmosphere interaction) I: a model of plant-atmosphere interaction for estimating absorbed doses of gaseous air pollutants, Environmental Pollution, 98, 37–50, https://doi.org/10.1016/s0269-7491(97)00114-0 1997.

Grünhage, L., Haenel, H.D., 2008. Detailed documentation of the PLATIN (PLant-ATmosphere INteraction) model. Landbauforschung Völkenrode 319, 1–85, available at: http://www.uni-giessen.de/cms/ukl-en/PLATIN, 2008.

Haber, F.: Verfahren zur synthetischen Darstellung von Ammoniak aus den Elementen. DE235421. Badische Anilin- & Soda-Fabrik in Ludwigshafen, 1908.

Hansen, K., Sørensen, L. L., Hertel, O., Geels, C., Skjøth, C. A., Jensen, B., and Boegh, E.: Ammonia emissions from deciduous forest after leaf fall, Biogeosciences, 10, 4577–4589, https://doi.org/10.5194/bg-10-4577-2013, 2013.

Hansen, K., Pryor, S. C., Boegh, E., Hornsby, K. E., Jensen, B., and Sørensen, L. L.: Background concentrations and fluxes of atmospheric ammonia over a deciduous forest, Agricultural and Forest Meteorology, 214-215, 380–392, , https://doi.org/10.1016/j.agrformet.2015.09.004, 2015.

Heiskanen, J., Brümmer, C., Buchmann, N., Calfapietra, C., Chen, H., Gielen, B., Gkritzalis, T., Hammer, S., Hartman, S., Herbst, M., Janssens, I., Jordan, A., Juurola, E., Karstens, U., Kasurinen, V., Kruijt, B., Lankreijer, H., Levin, I., Linderson, M.-L., Loustau, D., Merbold, L., Lund Myhre, C., Papale, D., Pavelka, M., Pilegaard, K., Ramonet, M., Rebmann, C., Rinne, J., Rivier, L., Saltikoff, E., Sanders, R., Steinbacher, M., Steinhoff, T., Watson, A., Vermeulen, A., Vesala, T., Vítková, G., and Kutsch, W.: The Integrated Carbon Observation System in Europe, B. Am. Meteorol. Soc., 103, E855-E872, https://doi.org/10.1175/BAMS-D-19-0364.1, 2022.

Hensen, A., Nemitz, E., Flynn, M. J., Blatter, A., Jones, S. K., Sørensen, L. L., Hensen, B., Pryor, S. C., Jensen, B., Otjes, R. P., Cobussen, J., Loubet, B., Erisman, J. W., Gallagher, M. W., Neftel, A., and Sutton, M. A.: Inter-comparison of ammonia fluxes obtained using the Relaxed Eddy Accumulation technique, Biogeosciences, 6, 2575–2588, https://doi.org/10.5194/bg-6-2575-2009, 2009.

Hertel, O., Reis, S., Skjøth, C. A., Bleeker, A., Harrison, R. M., Cape, J. N., Fowler, D., Skiba, U., Simpson, D., Jickells, T., Baker, A. R., Kulmala, M., Gyldenkærne, S., Sørensen, L. L., and Erisman, J. W.: Nitrogen Processes in the Atmosphere, in: The European Nitrogen Assessment – Sources, Effects and Policy Perspectives, edited by: Sutton, M. A., Howard, C. M., Erisman, J. W., Billen, G., Bleeker, A., Grennfelt, P., van Grinsven, H., and Grizzetti, B., Cambridge University Press, Cambridge, 177–207, 2011.

Hertel, O., Skjøth, C. A., Reis, S., Bleeker, A., Harrison, R. M., Cape, J. N., Fowler, D., Skiba, U., Simpson, D., Jickells, T., Kulmala, M., Gyldenkærne, S., Sørensen, L. L., Erisman, J. W., and Sutton, M. A.: Governing processes for reactive nitrogen compounds in the European atmosphere, Biogeosciences, 9, 4921–4954, https://doi.org/10.5194/bg-9-4921-2012, 2012.

Hicks, B. B., & McMillen, R. T.: A Simulation of the Eddy Accumulation Method for Measuring Pollutant Fluxes, Journal of Applied Meteorology and Climatology, 23, 637–643, https://doi.org/10.1175/1520-0450(1984)023<0637:ASOTEA>2.0.CO;2., 1984.

Horii, C. V., Munger, J. W., Wofsy, S. C., Zahniser, M., Nelson, D., and McManus, J. B.: Fluxes of nitrogen oxides over a temperate deciduous forest, Journal of Geophysical Research: Atmospheres, 109, D08305, https://doi.org/10.1029/2003JD004326, 2004.

Horii, C. V., Munger, J. W., Wofsy, S. C., Zahniser, M., Nelson, D., and McManus, J. B.: Atmospheric reactive nitrogen concentration and flux budgets at a Northeastern US forest site, Agricultural and Forest Meteorology, 136, 159–174, https://doi.org/10.1016/j.agrformet.2006.03.005, 2006.

Högberg, P.: Nitrogen impacts on forest carbon, Nature, 447, 781–782, https://doi.org/10.1038/447781a, 2007.

Hurkuck, M., Brümmer, C., Mohr, K., Grünhage, L., Flessa, H., and Kutsch, W. L.: Determination of atmospheric nitrogen deposition to a semi-natural peat bog site in an intensively managed agricultural landscape, Atmospheric Environment, 97, 296–309, https://doi.org/10.1016/j.atmosenv.2014.08.034, 2014.

Hurkuck, M., Brümmer, C., and Kutsch, W. L.: Near-neutral carbon dioxide balance at a seminatural, temperate bog ecosystem, Journal of Geophysical Research: Biogeosciences, 121, 370–384, https://doi.org/10.1002/2015jg003195, 2016.

Ibrom, A., Dellwick, E., Flyvbjerg, H., Jensen, N. O., and Pilegaard, K.: Strong low-pass filtering effects on water vapour flux measurements with closed-path eddy correlation systems, Agricultural and Forest Meteorology, 147, 140–156, https://doi.org/10.1016/j.agrformet.2007.07.007, 2007.

IPCC: Climate Change 2013: The Physical Science Basis. Contribution of Working Group I to the Fifth Assessment Report of the Intergovernmental Panel on Climate Change [Stocker, T.F., D. Qin, G.-K. Plattner, M. Tignor, S.K. Allen, J. Boschung, A. Nauels, Y. Xia, V. Bex and P.M. Midgley (eds.)]. Cambridge University Press, Cambridge, United Kingdom and New York, NY, USA, 1535 pp., 2013.

Kaimal, J. C., Wyngaard, J. C., Izumi, Y., and Coté, O. R.: Spectral characteristics of surface-layer turbulence, Q. J. Roy. Meteor. Soc., 98, 563–589, https://doi.org/10.1002/qj.49709841707, 1972.

Jacob, D. J.: Introduction to Atmospheric Chemistry, Princeton University Press, Princeton, New Jersey, USA, 1999.

Jensen, N. O. and Hummelshøj, P.: Derivation of canopy resistance for water-vapor fluxes over a spruce forest, using a new technique for the viscous sublayer resistance, Agricultural and Forest Meteorology, 73, 339–352, https://doi.org/10.1016/0168-1923(94)05083-I, 1995.

Jensen, N. O. and Hummelshøj, P.: Derivation of canopy resistance for water vapor fluxes over a spruce forest, using a new technique for the viscous sublayer resistance (correction to vol. 73, p. 339, 1995), Agricultural and Forest Meteorology, 85, 289, https://doi.org/10.1016/S0168-1923(97)00024-5, 1997.

Kamp, J. N., Häni, C., Nyord, T., Feilberg, A., and Sørensen, L. L.: The Aerodynamic Gradient Method: Implications of Non-Simultaneous Measurements at Alternating Heights, Atmosphere, 11, 1067, https://doi.org/10.3390/atmos11101067, 2020.

Kenagy, H. S., Sparks, T. L., Ebben, C. J., Wooldrige, P. J., Lopez-Hilfiker, F. D., Lee, B. H., Thornton, J. A., McDuffie, E. E., Fibiger, D. L., Brown, S. S., Montzka, D. D., Weinheimer, A. J., Schroder, J. C., Campuzano-Jost, P., Day, D. A., Jimenez, J. L., Dibb, J. E., Campos, T., Shah, V., Jaeglé, L., and Cohen, R. C.: NO_x lifetime and NO_y partitioning during WINTER. Journal of Geophysical Research: Atmospheres, 123, 9813–9827, https://doi.org/10.1029/2018JD028736, 2018.

Kljun, N., Calanca, P., Rotach, M. W., and Schmid, H. P.: A simple two-dimensional parameterisation for Flux Footprint Prediction (FFP), Geoscientific Model Development, 8, 3695–3713, https://doi.org/10.5194/gmd-8-3695-2015, 2015.

Kolle, O. and Rebmann, C.: EddySoft Documentation of a Software Package to Acquire and Process Eddy Covariance Data, techreport, MPI-BGC, available at: https://repository.publisso. de/resource/frl:4414276-1/data (last access: 2 November 2022), 2007.

Lelieveld, J., Evans, J. S., Fnais, M., Giannadaki, D., and Pozzer, A.: The contribution of outdoor air pollution sources to premature mortality on a global scale, Nature, 525, 367–371, https://doi.org/10.1038/nature15371, 2015.

Li, Y., Aneja, V. P., Arya, S. P., Rickman, J., Brittig, J., Roelle, P., and Kim, D. S.: Nitric oxide emission from intensively managed agricultural soil in North Carolina, Journal of Geophysical Research: Atmospheres, 104, 26115–26123, https://doi.org/10.1029/1999JD900336, 1997.

Li, Y., Schichtel, B. A., Walker, J. T., Schwede, D. B., Chen, X., Lehman, C. M. B., Puchalski, M. A., Gay, D. A., and Collett, J. L.; Increasing importance of deposition of reduced nitrogen in the United States, Proceedings of the National Academy of Sciences, 113, 5874–5879, https://doi.org/10.1073/pnas.1525736113, 2016.

Liakakou, E., Fourtziou, L., Paraskevopoulou, D., Speyer, O., Lianou, M., Grivas, G., Myriokefalitakis, S., and Mihalopoulos, N: High-Resolution Measurements of SO_2, HNO_3 and HCl at the Urban Environment of Athens, Greece: Levels, Variability and Gas to Particle Partitioning, Atmosphere, 13, 218. https://doi.org/10.3390/atmos13020218, 2022.

Loubet, B., Milford, C., Hensen, A., Daemmgen, U., Erisman, J.-W., Cellier, P., and Sutton, M. A.: Advection of NH_3 over a pasture field and its effect on gradient flux measurements, Biogeosciences, 6, 1295–1309, https://doi.org/10.5194/bg-6-1295-2009, 2009.

Lovett, G. M., Reiners, W. A., and Olson, R. K.: Cloud droplet deposition in subalpine balsam fir forests: Hydrological and chemical inputs, Science, 218, 1303–1304, https://doi.org/10.1126/science.218.4579.1303, 1982.

Luan, J., Wu, J., Liu, S., Rouglet, N., and Wang, M.:. Soil nitrogen determines greenhouse gas emissions from northern peatlands under concurrent warming and vegetation shifting, Communications Biology, 2, 132, https://doi.org/10.1038/s42003-019-0370-1, 2019.

Lucas-Moffat, A. M., Schrader, F., Herbst, M., and Brümmer, C.: Multiple gap-filling for eddy covariance datasets, Agricultural and Forest Meteorology, 325, 109114, https://doi.org/10.1016/j.agrformet.2022.109114, 2022.

Magnani, F., Mencuccini, M., Borghetti, M., Berbigier, P., Berninger, F., Delzon, S., Grelle, A., Hari, P., Jarvis, P. G., Kolari, P., Kowalski, A. S., Lankreijer, H., Law, B. E., Lindroth, A., Loustau, D., Manca, G., Moncrieff, J. B., Rayment, M., Tedeschi, V., Valentini, R., and Grace, J.: The human footprint in the carbon cycle of temperate and boreal forests, Nature, 447, 848–850, https://doi.org/10.1038/nature05847, 2007.

Mahabbati, A., Beringer, J., Leopold, M., McHugh, I., Cleverly, J., Isaac, P., and Izady, A.: A comparison of gap-filling algorithms for eddy covariance fluxes and their drivers, Geosci. Instrum. Method. Data Syst., 10, 123–140, https://doi.org/10.5194/gi-10-123-2021, 2021.

Manders, A. M. M., Builtjes, P. J. H., Curier, L., Denier van der Gon, H. A. C., Hendriks, C., Jonkers, S., Kranenburg, R., Kuenen, J. J. P.,Segers, A. J., Timmermans, R. M. A., Visschedijk, A. J. H., Wichink Kruit, R. J., van Pul, W. A. J., Sauter, F. J., van der Swaluw, E., Swart, D. P. J., Douros, J., Eskes, H., van Meijgaard, E., van Ulft, B., van Velthoven, P., Banzhaf, S., Mues, A. C., Stern, R., Fu, G., Lu,S., Heemink, A., van Velzen, N., and Schaap, M.: Curriculum vitae of the LOTOS–EUROS (v2.0) chemistry transport model, Geoscientific Model Development, 10, 4145–4173, https://doi.org/10.5194/gmd-10-4145-2017, 2017.

Marx, O.: Validierung eines NOy-Messverfahrens in Eddy-Kovarianz-Technik, Diploma thesis, Faculty of Chemical and Earth Sciences, Friedrich-Schiller University, Jena, 70 pp., 2004.

Marx, O., Brümmer, C., Ammann, C., Wolff, V., and Freibauer, A.: TRANC – a novel fast-response converter to measure total reactive atmospheric nitrogen, Atmospheric Measurement Techniques, 5, 1045–1057, https://doi.org/10.5194/amt-5-1045-2012, 2012.

Massman, W. J.: A review of the molecular diffusivities of H2O, CO2, CH4, CO, O3, SO2, NH3, N2O, NO, and NO2 in air, O2 and N2 near STP, Atmospheric Environment, 32, 1111–1127, https://doi.org/10.1016/S1352-2310(97)00391-9, 1998.

Massman, W. J. and Ibrom, A.: Attenuation of concentration fluctuations of water vapor and other trace gases in turbulent tube flow, Atmospheric Chemistry and Physics., 8, 6245–6259, https://doi.org/10.5194/acp-8-6245-2008, 2008.

Mauder, M. and Foken, T.: Impact of post-field data processing on eddy covariance flux estimates and energy balance closure, Meteorologische Zeitschrift, 15, 597–609, https://doi.org/10.1127/09412948/2006/0167, 2006.

Meyers, T.P., Finkelstein, P., Clarke, J., Ellestad, T.G., and Sims, P.F.: A multilayer model for inferring dry depositiousing standard meteorological measurements, Journal Geophysical Research: Atmospheres, 103, 22645–22661, , https://doi.org/10.1029/98JD01564, 1998.

McMillen, R. T: An eddy correlation technique with extended applicability to non-simple terrain. Boundary-Layer Meteorology, 43, 231–245, https://doi.org/10.1007/BF00128405, 1988.

Meixner, F. X.: Surface exchange of odd nitrogen oxides, Nova Acta Leopoldina NF, 70, 299–348, 1994.

Meng, C., Tian, D., Zeng, H., Li, Z., Yi, C., and Niu, S.: Global soil acidification impacts on belowground processes, Environ. Res. Lett. 14, 074003, https://doi.org/10.1088/1748-9326/ab239c, 2019.

Milford, C., Theobald, M. R., Nemitz, E., Hargreaves, K. J., Horvath, L., Raso, J., Dämmgen, U., Neftel, A., Jones, S. K., Hensen, A., Loubet, B., Cellier, P., and Sutton, M. A.: Ammonia fluxes in relation to cutting and fertilization of an intensively managed grassland derived from an inter-comparison of gradient measurements, Biogeosciences, 6, 819–834, https://doi.org/10.5194/bg-6-819-2009, 2009.

Milne, R., Beverland, I. J., Hargreaves, K., and Moncrieff, J. B.: Variation of the beta coefficient in the relaxed eddy accumulation method, Boundary-Layer Meteorology, 93, 211–225, 1999.

Moncrieff, J. B., Massheder, J. M., deBruin, H., Elbers, J., Friborg, T., Heusinkveld, B., Kabat, P., Scott, S., Soegaard, H., and Verhoef, A.: A system to measure surface fluxes of momentum, sensible heat, water vapour and carbon dioxide, J. Hydrol., 188, 589–611, https://doi.org/10.1016/S0022-1694(96)03194-0, 1997.

Moncrieff, J. B., Clement, R., Finnigan, J., and Meyers, T.: Averaging, Detrending, and Filtering of Eddy Covariance Time Series, Kluwer Academic, Dordrecht, 7–31, https://doi.org/10.1007/14020-2265-4_2, 2004.

Montagnani, L., Manca, G., Canepa, E., and Georgieva, E.: Assessing the method-specific differences in quantification of CO_2 advection at three forest sites during the ADVEX campaign, Agricultural and Forest Meteorology, 150, 702–711, https://doi.org/10.1016/j.agrformet.2010.01.013, 2010.

Montagnani, L., Grünwald, T., Kowalski, A., Mammarella, I., Merbold, L., Metzger, S., Sedlák, P., and Siebicke, L.: Estimating the storage term in eddy covariance measurements: the ICOS methodology, International Agrophysics, 32, 551–567, https://doi.org/10.1515/intag-2017-0037, 2018.

Moore, C. J.: Frequency response corrections for eddy correlation systems, Boundary-Layer Meteorology, 37, 17–35, https://doi.org/10.1007/BF00122754, 1986.

Moravek, A., Singh, S., Pattey, E., Pelletier, L., and Murphy, J. G.: Measurements and quality control of ammonia eddy covariance fluxes: a new strategy for high-frequency attenuation correction, Atmospheric Measurement Techniques, 12, 6059–6078, https://doi.org/10.5194/amt-12-6059-2019, 2019.

Mueller, H., Kramm, G., Meixner, F., Dollard, G. J., Fowler, D., and Possanzini, M.: Determination of nitric acid dry deposition by modified Bowen ratio and aerodynamic profile techniques, Tellus B: Chemical and Physical Meteorology, 45, 346–367, https://doi.org/10.3402/tellusb.v45i4.15735, 1993.

Muller, J. B. A., Coyle, M., Fowler, D., Gallagher, M. W., Nemitz, E. G., and Percival, C. J.: Comparison of ozone fluxes over grass-land by gradient and eddy covariance technique, Atmospheric Science Letters, 10, 164–169, https://doi.org/10.1002/asl.226, 2009.

Munger, J. W., Wofsy, S. C., Bakwin, P. S., Fan, S. M., Goulden, M. L., Daube, B. C., Goldstein, A. H., Moore, K. E., and Fitzjarrald, D. R.: Atmospheric deposition of reactive nitrogen oxides and ozone in a temperate deciduous forest and a subarctic woodland: 1. Measurements and mechanisms, Journal of Geophysical Research: Atmospheres, 101, 12639–12657, https://doi.org/10.1029/96JD00230, 1996.

Munger, J. W., Fan, S.-M., Bakwin, P. S., Goulden, M. L., Goldstein, A. H., Colman, A. S., and Wofsy, S. C.: Regional budgets for nitrogen oxides from continental sources: Variations of rates for oxidation and deposition with season and distance from source regions, Journal of Geophysical Research: Atmospheres, 103, 8355–8368, https://doi.org/10.1029/98JD00168, 1998.

Myles, L., Meyers, T.P., Robinson, L., 2007. Relaxed eddy accumulation measurements of ammonia, nitric acid, sulfur dioxide and particulate sulfate dry deposition near Tampa, FL, USA. Environ. Res. Lett. 2, 034004.

Myhre, G., Samset, B. H., Schulz, M., Balkanski, Y., Bauer, S., Berntsen, T. K., Bian, H., Bellouin, N., Chin, M., Diehl, T., Easter, R. C., Feichter, J., Ghan, S. J., Hauglustaine, D., Iversen, T., Kinne, S., Kirkevåg, A., Lamarque, J.-F., Lin, G., Liu X., Lund, M. T., Luo, G., Ma, X., van Noije, T., Penner, J. E., Rasch, P. J., Ruiz, A., Seland, Ø., Skeie, R. B., Stier, P., Takemura, T., Tsigaridis, K., Wang, P., Wang, Z., Xu, L., Yu, H., Yu, F., Yoon, J.-H., Zhang, K., Zhang, H., and Zhou, C.: Radiative forcing of the direct aerosol effect from AeroCom Phase II simulations, Atmospheric Chemistry and Physics, 13, 1853–1877, https://doi.org/10.5194/acp-13-1853-2013, 2013.

Nakai, T., van der Molen, M. K., Gash, J. H. C., and Kodama, Y.: Correction of sonic anemometer angle of attack errors, Agricultural and Forest Meteorology, 136, 19–30, https://doi.org/10.1016/j.agrformet.2006.01.006, 2006.

Neirynck, J. and Ceulemans, R.: Bidirectional ammonia exchange above a mixed coniferous forest, Environmental Pollution, 154, 424–438, https://doi.org/10.1016/j.envpol.2007.11.030, 2008.

Nemitz, E., Sutton, M. A., Schjoerring, J. K., Husted, S., and Wyers, G. P.: Resistance modelling of ammonia exchange over oilseed rape, Agricultural and Forest Meteorology, 105, 405–425, https://doi.org/10.1016/S0168-1923(00)00206-9, 2000.

Nemitz, E., Milford, C., and Sutton, M. A.: A two-layer canopy compensation point model for describing bi-directional biosphere-atmosphere exchange of ammonia, Q. J. Roy. Meteor. Soc., 127, 815–833, https://doi.org/10.1002/qj.49712757306, 2001.

Nemitz, E., Sutton, M. A., Wyers, G. P., and Jongejan, P. A. C.: Gas-particle interactions above a Dutch heathland: I. Surface exchange fluxes of NH_3, SO_2, HNO_3 and HCl, Atmospheric Chemistry and Physics, 4, 989–1005, https://doi.org/10.5194/acp-4-989-2004, 2004.

Oke, T. R: Boundary layer climates, Routledge, London and New York, 1987.

Pan, Y., Birdsey, R. A., Fang, J., Houghton, R., Kauppi, P. E., Kurz, W. A., Phillips, O. L., Shvidenko, A., Lewis, S. L., Canadell, J. G., Ciais, P., Jackson, R. B., Pacala, S. W., McGuire, A. D., Piao, S., Rautiainen, A., Sitch, S., and Hayes, D.: A large and persistent carbon sink in the world's forests. Science, 333, 988–993, https://doi.org/10.1126/science.1201609, 2011.

Panofksy, H. A. and Dutton, J. A.: Atmospheric turbulence, models and methods for engineering applications, John Wiley & Sons, New York, USA, 1984.

Pattey, E., Desjardins, R.L., and Rochette, P.: Accuracy of the relaxed eddy-accumulation technique, evaluated using CO_2 flux measurements, Boundary-Layer Meteorology, 66**,** 341–355, https://doi.org/10.1007/BF00712728, 1993.

Paulissen, M.P.C.P., Bobbink, R., Robat, S.A., and Verhoeven, J. T. A.: Effects of Reduced and Oxidised Nitrogen on Rich-Fen Mosses: a 4-Year Field Experiment, Water, Air, & Soil Pollution, 227, 18, https://doi.org/10.1007/s11270-015-2713-y, 2016.

Paulson, C. A.: The Mathematical Representation of Wind Speed and Temperature Profiles in the Unstable Atmospheric Surface Layer, Journal of Applied Meteorology, 9, 857–861, https://doi.org/10.1175/1520-0450(1970)009<0857:Tmrows>2.0.Co;2, 1970.

Peake, E. and Legge, A. H.: Evaluation of methods used to collect air quality data at remote and rural sites in Alberta, Canada, in: Proc. 1987 EPA/APCA Symposium on Measurements of Toxic and Related Air Pollutants, APCA, Research Triangle Park, North Carolina (NC), 3–6 May 1987, 174–182, 1987.

Peake, M.: A Preliminary Report on the Design and Testing of the KAPS (Kananaskis Atmospheric Pollutant Sampler) for the Collection of Acidic and Basic Gases and Fine Particles, Document 0012e/July 8/85, Typskript University Calgary, 1985.

Pilegaard, K.: Processes regulating nitric oxide emissions from soils, Phil. Trans. R. Soc. B, 368, 20130126, http://dx.doi.org/10.1098/rstb.2013.0126, 2013.

Pope III, C. A., Ezzati, M., and Dockery, D. W.: Fine-particulate air pollution and life expectancy in the United States, New England Journal of Medicine, 360, 376-386, https://doi.org/10.1056/NEJMsa0805646, 2009.

Poschenrieder, C., Gunsé, B., Corrales, I., and Barceló, J.: A glance into aluminum toxicity and resistance in plants, Science of The Total Environment, 400, 356–368, https://doi.org/10.1016/j.scitotenv.2008.06.003, 2008.

Pryor, S.C., Barthelmie, R.J., Jensen, B., Jensen, N.O., and Sørensen, L.L.: HNO3 fluxes to a deciduous forest derived using gradient and REA methods. Atmospheric Environmnent, 36, 5993–5999, https://doi.org/10.1016/S1352-2310(02)00765-3, 2002.

Pryor, S.C. and Klemm, O.: Experimentally derived estimates of nitric acid dry deposition velocity and viscous sub-layer resistance at a conifer forest. Atmospheric Environment, 38, 2769–2777, https://doi.org/10.1016/j.atmosenv.2004.02.038, 2004.

Pye, H.O.T., Liao, H., Wu, S., Mickley, L.J., Jacob, D.J., Henze, D.K., and Seinfeld, J. H.: Effect of changes in climate and emissions on future sulfate-nitrate-ammonium aerosol levels in the United States. Journal of Geophysical Research: Atmospheres, 114, D01205, https://doi.org/10.1029/2008jd010701, 2009.

Rannik, Ü. and Vesala, T.: Autoregressive filtering versus linear detrending in estimation of fluxes by the eddy covariance method, Boundary-Layer Meteorology, 91**,** 259–280, https://doi.org/10.1023/A:1001840416858, 1999.

Reichstein, M., Falge, E., Baldocchi, D., Papale, D., Aubinet, M., Berbigier, P., Bernhofer, C., Buchmann, N., Gilmanov, T., Granier, A., Grünwald, T., Havránková, K., Ilvesniemi, H., Janous, D., Knohl, A., Laurila, T., Lohila, A., Loustau, D., Matteucci, G., Meyers, T., Miglietta, F., Ourcival, J.-M., Pumpanen, J., Rambal, S., Rotenberg, E., Sanz, M., Tenhunen, J., Seufert, G., Vaccari, F., Vesala, T., Yakir, D., and Valentini, R.: On the separation of net ecosystem exchange into assimilation and ecosystem respiration: review and improved algorithm, Glob. Change Biol., 11, 1424–1439, https://doi.org/10.1111/j.1365-2486.2005.001002.x, 2005.

Reis, S., Pinder, R. W., Zhang, M., Lijie, G., and Sutton, M. A.: Reactive nitrogen in atmospheric emission inventories, Atmos. Chem. Phys., 9, 7657–7677, https://doi.org/10.5194/acp-9-7657-2009, 2009.

Rockström, J., Steffen, W., Noone, K., Persson, A., Chapin III, F. S., Lambin, E. F., Lenton, T. M., Scheffer, M., Folke, C., and Schellnhuber, H. J., Nykvist, B., de Wit, C. A., Hughes, T., van der Leeuw, S., Rodhe, H., Sörlin, S., Snyder, P. K., Costanza, R., Svedin, U., Falkenmark, M., Karlberg, L., Corell, R. W., Fabry, V. J., Hansen, J., Walker, B., Diana, L., Richardson, K., Crutzen, P., and Foley, J. A.: A safe operating space for humanity: identifying and quantifying planetary boundaries that must not be transgressed could help prevent human activities from causing unacceptable environmental change, argue Johan Rockstrom and colleagues, Nature, 461, 472-476, https://doi.org/10.1038/461472a, 2009.

Sala, O. E., Chapin III, F. S., Armesto, J. J., Berlow, E., Bloomfield, J., Dirzo, R., Huber-Sanwald, E., Huenneke, L.F., Jackson, R. B., Kinzig, A., Leemans, R., Lodge, D. M., Mooney, H. A., Oesterheld, M., Poff, N. L., Sykes M. T., Walker, B. H., Walker, M. and Wall, D. H.: Global biodiversity scenarios for the year 2100, Science, 287, 1770–1774, https://doi.org/10.1126/science.287.5459.1770, 2000.

Schaap. M., Hendriks, C., Kranenburg, R., Kuenen, J., Segers, A., Schlutow, A., Nagel, H.-D., Ritter, A., and Banzhaf, S.: PINETI-3: Modellierung atmosphärischer Stoffeinträge von 2000 bis 2015 zur Bewertung der ökosystem-spezifischen Gefährdung von Biodiversität durch Luftschadstoffe in Deutschland, technical report, Umweltbundesamt, Dessau-Roßlau, Germany, https://www.umweltbundesamt.de/sites/default/files/medien/1410/publikationen/2018-10-17_texte_79-2018_pineti3.pdf (last access: 2 November 2022), 2018.

Schrader, F., Brümmer, C., Flechard, C. R., Wichink Kruit, R. J., van Zanten, M. C., Zöll, U., Hensen, A., and Erisman, J. W.: Non-stomatal exchange in ammonia dry deposition models: comparison of two state-of-the-art approaches, Atmospheric Chemistry and Physics, 16, 13417–13430, https://doi.org/10.5194/acp-16-13417-2016, 2016.

Schrader, F., Schaap, M., Zöll, U., Kranenburg, R., and Brümmer, C.: The hidden cost of using low resolution concentration data in the estimation of NH_3 dry deposition fluxes, Scientific Reports, 8, 969, https://doi.org/10.1038/s41598-017-18021-6, 2018.

Schrader, F, Erisman, J.W. and Brümmer, C.: Towards a coupled paradigm of NH_3-CO_2 biosphere–atmosphere exchange modelling, Global Change Biology, 26, 4654–4663, https://doi.org/10.1111/gcb.15184, 2020.

Schwede, D., Zhang, L., Vet, R., and Lear, G.: An intercomparison of the deposition models used in the CASTNET and CAPMoN networks, Atmospheric Environment, 45, 1337–1346, https://doi.org/10.1016/j.atmosenv.2010.11.050, 2011.

Seinfeld, J. H. and Pandis, S. N.: Atmospheric Chemistry and Physics: From Air Pollution to Climate Change, 2nd ed., John Wiley & Sons, Inc.: New York, NY, USA, 2006.

Selman, M., Sugg, Z., and Greenhalgh, S.: Eutrophication and Hypoxia in Coastal Areas: A global assessment of the state of knowledge, WRI Policy Note,1–6, 2008.

Sheppard, L.J., Leith, I.D., Mizunuma, T., Neil Cape, J., Crossley, A., Leeson, S., Sutton, M.A., van Dijk, N. and Fowler, D.: Dry deposition of ammonia gas drives species change faster than wet deposition of ammonium ions: evidence from a long-term field manipulation. Global Change Biology, 17, 3589–3607, https://doi.org/10.1111/j.1365-2486.2011.02478.x, 2011.

Siebicke, L., Hunner, M., and Foken T.: Aspects of CO_2 advection measurements, Theoretical and Applied Climatology, 109, 109–131, https://doi.org/10.1007/s00704-011-0552-3 , 2012

Sievering, H., Kelly, T., McConville, G., Seibold, C., Turnipseed, A.: Nitric acid dry deposition to conifer forests: Niwot Ridge spruce-fir-pine study. Atmospheric Environment, 35, 3851–3859, https://doi.org/10.1016/S1352-2310(01)00156-X, 2001.

Smil, V.: Enriching the earth: Fritz Haber, Carl Bosch, and the transformation of world food production, MIT press, Cambridge, USA, 2001.

Smith, R. I., Fowler, D., Sutton, M. A., Flechard, C., and Coyle, M.: Regional estimation of pollutant gas deposition in the UK: model description, sensitivity analyses and outputs, Atmos. Environ., 34, 3757–3777, 2000.

Smith, V. H., and Schindler, D. W.: Eutrophication science: where do we go from here?, Trends in ecology & evolution, 24, 201–207, https://doi.org/10.1016/j.tree.2008.11.009, 2009.

Soares, A.R.; Silva, C. Review of Ground-Level Ozone Impact in Respiratory Health Deterioration for the Past Two Decades, Atmosphere, 13, 434, https://doi.org/10.3390/atmos13030434, 2022.

Staelens, J., De Schrijver, A., Van Avermaet, P., Genouw, G., and Verhoest, N.: A comparison of bulk and wet-only deposition at two adjacent sites in Melle (Belgium), Atmos. Environ., 39, 7–15, https://doi.org/10.1016/j.atmosenv.2004.09.055, 2005.

Stella, P., Loubet, B., Laville, P., Lamaud, E., Cazaunau, M., Laufs, S., Bernard, F., Grosselin, B., Mascher, N., Kurtenbach, R., Mellouki, A., Kleffmann, J., and Cellier, P.: Comparison of methods for the determination of NO-O_3-NO_2 fluxes and chemical interactions over a bare soil, Atmospheric Measurement Techniques, 5, 1241–1257, https://doi.org/10.5194/amt-5-1241-2012, 2012.

Sutton, M. A. and Fowler, D.: A Model for Inferring Bi-directional Fluxes of Ammonia Over Plant Canopies, in: Proceedings of the WMO conference on the measurement and modelling of atmospheric composition changes including pollutant transport, pp. 179–182, WMO/GAW(Gobal Atmosphere Watch)-91, Geneva, Switzerland, 1993.

Sutton, M. A., Fowler, D., and Moncrieff, J. B.: The exchange of atmospheric ammonia with vegetated surfaces. I: Unfertilized vegetation, Q. J. Roy. Meteor. Soc., 119, 1023–1045, 1993.

Sutton, M. A., Burkhardt, J. K., Guerin, D., Nemitz, E., and Fowler, D.: Development of resistance models to describe measurements of bi-directional ammonia surface–atmosphere exchange, Atmospheric Environment, 32, 473–480, doi:10.1016/S1352-2310(97)00164-7, 1998.

Sutton, M. A., Tang, Y. S., Miners, B., and Fowler, D.: A New Diffusion Denuder System for Long-Term, Regional Monitoring of Atmospheric Ammonia and Ammonium, Water, Air and Soil Pollution: Focus, 1, 145–156, https://doi.org/10.1023/a:1013138601753, 2001.

Sutton, M. A., Simpson, D., Levy, P. E., Smith, R. I., Reis, S., van Oijen, M., and de Vries, W.: Uncertainties in the relationship between atmospheric nitrogen deposition and forest carbon sequestration, Global Change Biology, 14, 2057–2063, https://doi.org/10.1111/j.1365-2486.2008.01636.x, 2008a.

Sutton, M. A., Erisman, J.W., Dentener, F., and Möller, D.: Ammonia in the environment: from ancient times to the present. Environmental Pollution, 156, 583–604, https://doi.org/10.1016/j.envpol.2008.03.013, 2008b.

Sutton, M. A., Howard, C. M., Erisman, J. W., Billen, G., Bleeker, A., Grennfelt, P., van Grinsven, H., and Grizzetti, B. (Eds.): The European Nitrogen Assessment: sources, effects and policy perspectives, Cambridge University Press, Cambridge, UK, 2011.

Sutton, M. A., Reis, S., Riddick, S. N., Dragosits, U., Nemitz, E., Theobald, M. R., Tang, Y. S., Braban, C. F., Vieno, M., Dore, A. J., Mitchell, R. F., Wanless, S., Daunt, F., Fowler, D., Blackall, T. D., Milford, C., Flechard, C. R., Loubet, B., Massad, R., Cellier, P., Personne, E., Coheur, P. F., Clarisse, L., Van Damme, M., Ngadi, Y., Clerbaux, C., Skjoth, C. A., Geels, C., Hertel, O., Wichink Kruit, R. J., Pinder, R. W., Bash, J. O., Walker, J. T., Simpson, D., Horvath, L., Misselbrook, T. H., Bleeker, A., Dentener, F., and de Vries, W.: Towards a climate-dependent paradigm of ammonia emission and deposition, Philos. T. Soc. B, 368, 20130166, https://doi.org/10.1098/rstb.2013.0166, 2013.

Swart, D., Zhang, J., van der Graaf, S., Rutledge-Jonker, S., Hensen, A., Berkhout, S., Wintjen, P., van der Hoff, R., Haaima, M., Frumau, A., van den Bulk, P., Schulte, R., and van Goethem, T.: Measuring dry deposition of ammonia using flux-gradient and eddy covariance methods with two novel open-path instruments, Atmos. Meas. Tech. Discuss. [preprint], https://doi.org/10.5194/amt-2022-171, in review, 2022.

Tang, Y. S., Simmons, I., van Dijk, N., Di Marco, C., Nemitz, E., Dämmgen, U., Gilke, K., Djuricic, V., Vidic, S., Gliha, Z., Borovecki, D., Mitosinkova, M., Hanssen, J. E., Uggerud, T. H., Sanz,M. J., Sanz, P., Chorda, J. V., Flechard, C. R., Fauvel, Y., Ferm, M., Perrino, C., and Sutton, M. A.: European scale application of atmospheric reactive nitrogen measurements in a low-cost approach to infer dry deposition fluxes, Agriculture, Ecosystems and Environment, 133, 183–195, doi:10.1016/j.agee.2009.04.027, 2009.

Taylor, G. I.: The spectrum of turbulence, Philosophical Transactions of the Royal Society London A, 164, 476–490, 1938.

Theobald, M. R., Vivanco, M. G., Aas, W., Andersson, C., Ciarelli, G., Couvidat, F., Cuvelier, K., Manders, A., Mircea, M., Pay, M.-T., Tsyro, S., Adani, M., Bergström, R., Bessagnet, B., Briganti, G., Cappelletti, A., D'Isidoro, M., Fagerli, H., Mar, K., Otero, N., Raffort, V., Roustan, Y., Schaap, M., Wind, P., and Colette, A.: An evaluation of European nitrogen and sulfur wet deposition and their trends estimated by six chemistry transport models for the period 1990–2010, Atmospheric Chemistry and Physics, 19, 379–405, https://doi.org/10.5194/acp-19-379-2019, 2019.

Trebs, I., Ammann, C., and Junk, J.: Immission and dry deposition, in: Springer Handbook of Atmospheric Measurements, edited by: Foken, T., Springer Handbooks, Springer, Cham., https://doi.org/10.1007/978-3-030-52171-4_54, 2021.

United States Environmental Protection Agency (EPA): Nitrogen Oxides (NO_x), Why and How They Are Controlled, Technical Bulletin, EPA 456/F-99-006R, Office of Air Quality Planning and Standards, Research Triangle Park. https://www3.epa.gov/ttn/catc/dir1/fnoxdoc.pdf, 1999.

Van der Graaf, S. C., Kranenburg, R., Segers, A. J., Schaap, M., and Erisman, J. W.: Satellite-derived leaf area index and roughness length information for surface–atmosphere exchange modelling: a case study for reactive nitrogen deposition in north-western Europe using LOTOS-EUROS v2.0, Geoscientific Model Development, 13, 2451–2474, https://doi.org/10.5194/gmd-13-2451-2020, 2020.

Van Dingenen, R., Dentener, F. J., Raes, F., Krol, M. C., Emberson, L., and Cofala, J.: The global impact of ozone on agricultural crop yields under current and future air quality legislation, Atmospheric Environment, 43, 604–618, https://doi.org/10.1016/j.atmosenv.2008.10.033, 2009.

Van Grinsven, H. J., Rabl, A., and de Kok, T. M.: Estimation of incidence and social cost of colon cancer due to nitrate in drinking water in the EU: a tentative cost-benefit assessment, Environmental health, 9, 1–12, https://doi.org/10.1186/1476-069X-9-58, 2010.

Van Oss, R., Duyzer, J., and Wyers, P.: The influence of gas-to-particle conversion on measurements of ammonia exchange over forest, Atmospheric Environment, 32, 465–471, https://doi.org/10.1016/S1352-2310(97)00280-X, 1998.

Van Pul, W. A. J. and Jacobs, A. F. G.: The conductance of a maize crop and the underlying soil to ozone under various environmental conditions, Boundary-Layer Meteorology, 69, 83–99, https://doi.org/10.1007/BF00713296, 1994.

Van Zanten, M. C., Sauter, F. J., Wichink Kruit, R. J., van Jaarsveld, J. A., and van Pul, W. A. J.: Description of the DEPAC module; Dry deposition modeling with DEPAC_GCN2010, Tech. rep., RIVM, Bilthoven, NL, 2010.

Vestreng, V., Ntziachristos, L., Semb, A., Reis, S., Isaksen, I. S. A., and Tarrasón, L.: Evolution of NO_x emissions in Europe with focus on road transport control measures, Atmospheric Chemistry and Physics, 9, 1503–1520, https://doi.org/10.5194/acp-9-1503-2009, 2009.

Vickers, D. and Mahrt, L.: Quality Control and Flux Sampling Problems for Tower and Aircraft Data, J. Atmos. Ocean. Tech., 14, 512–526, https://doi.org/10.1175/15200426(1997)014<0512:QCAFSP>2.0.CO;2, 1997.

Vitousek, P. M., Cassman, K., Cleveland, C., Crews, T., Field, C. B., Grimm, N. B., Howarth, R. W., Marino, R., Martinelli, L., and Rastetter, E. B.: Towards an ecological understanding of biological nitrogen fixation, in: The nitrogen cycle at regional to global scales, Springer, 1–45, https://doi.org/10.1007/978-94-017-3405-9_1, 2002.

von Bobrutzki, K., Braban, C. F., Famulari, D., Jones, S. K., Blackall, T., Smith, T. E. L., Blom, M., Coe, H., Gallagher, M., Ghalaieny, M., McGillen, M. R., Percival, C. J., Whitehead, J. D., Ellis, R., Murphy, J., Mohacsi, A., Pogany, A., Junninen, H., Rantanen, S., Sutton, M. A., and Nemitz, E.: Field inter-comparison of eleven atmospheric ammonia measurement techniques, Atmos. Meas. Tech., 3, 9–112, https://doi.org/10.5194/amt-3-91-2010, 2010.

Walker, T., Beachley, G., Zhang, L., Benedict, K. B., Sive, C. B., Schwede, D. B.: A review of measurements of air-surface exchange of reactive nitrogen in natural ecosystems across North America, Science of The Total Environment, 698, 133975, https://doi.org/10.1016/j.scitotenv.2019.133975, 2020.

WallisDeVries, M. F.: Linking species assemblages to environmental change: Moving beyond the specialist-generalist dichotomy, Basic and Applied Ecology, 15, 279–287, https://doi.org/10.1016/j.baae.2014.05.001, 2014.

Watt, S. A., Wagner-Riddle, C., Edwards, G., and Vet, R. J.: Evaluating a flux-gradient approach for flux and deposition velocity of nitrogen dioxide over short-grass surfaces, Atmospheric Environment, 38, 2619–2626

Wang, K., Kang, P., Lu, Y., Zheng, X., Liu, M., Lin, T.-J., Butterbach-Bahl, K., and Wang, Y.: An open-path ammonia analyzer for eddy covariance flux measurement, Agricultural and Forest Meteorology, 308–309, 108570, https://doi.org/10.1016/j.agrformet.2021.108570, 2021.

Wang, K., Wang, J., Qu, Z., Xu, W., Wang, K., Zhang, H., Shen, J., Kang, P., Zhen, X., Wang, Y., Zheng, X., and Liu, X.: A significant diurnal pattern of ammonia dry deposition to a cropland is detected by an open-path quantum cascade laser-based eddy covariance instrument, Atmospheric Environment, 278, 119070, https://doi.org/10.1016/j.atmosenv.2022.119070, 2022.

Webb, E. K.: Profile relationships: The log-linear range, and extension to strong stability, Quarterly Journal of the Royal Meteorological Society, 96, 67–90, https://doi.org/10.1002/qj.49709640708, 1970.

Wesely, M. L.: Parameterization of Surface Resistances to Gaseous Dry Deposition in Regional-Scale Numerical-Models, Atmospheric Environment, 23, 1293–1304, https://doi.org/10.1016/0004-6981(89)90153-4, 1989.

Wichink Kruit, R. J., van Pul,W. A. J., Sauter, F. J., van den Broek,M., Nemitz, E., Sutton,M. A., Krol,M., and Holtslag, A. A.M.:Modeling the surface–atmosphere exchange of ammonia, Atmospheric Environment, 44, 945–957, https://doi.org/10.1016/j.atmosenv.2009.11.049, 2010.

Wichink Kruit, R. J., Schaap, M., Sauter, F. J., van Zanten, M. C., and van Pul,W. A. J.: Modeling the distribution of ammonia across Europe including bi-directional surface–atmosphere exchange, Biogeosciences, 9, 5261–5277, https://doi.org/10.5194/bg-9-5261-2012, 2012.

Wichink Kruit, R. J., Aben, J., de Vries, W., Sauter, 1180 F., van der Swaluw, E., van Zanten, M. C., and van Pul, W. A. J.: Modelling trends in ammonia in the Netherlands over the period 1990–2014, Atmospheric Environment, 154, 20–30, https://doi.org/10.1016/j.atmosenv.2017.01.031, 2017.

Wilczak, J. M., Oncley, S. P., and Stage, S. A.: Sonic Anemometer Tilt Correction Algorithms, Bound.-Lay. Meteorol., 99, 127–150, https://doi.org/10.1023/A:1018966204465, 2001.

Wolff, V., Trebs, I., Foken, T., and Meixner, F. X.: Exchange of reactive nitrogen compounds: concentrations and fluxes of total ammonium and total nitrate above a spruce canopy, Biogeosciences, 7, 1729–1744, https://doi.org/10.5194/bg-7-1729–2010, 2010a.

Wolff, V., Trebs, I., Ammann, C., and Meixner, F. X.: Aerodynamic gradient measurements of the NH_3-HNO_3-NH_4NO_3 triad using a wet chemical instrument: an analysis of precision requirements and flux errors, Atmospheric Measurement Techniques, 3, 187–208, https://doi.org/10.5194/amt-3-187-2010, 2010b.

Wu, Y., Gu, B., Erisman, J. W., Reis, S., Fang, Y., Lu, X., and Zhang, X.: $PM_{2.5}$ pollution is substantially affected by ammonia emissions in China, Environmental Pollution, 218, 86–94, https://doi.org/10.1016/j.envpol.2016.08.027, 2016.

Wyers, G. and Duyzer, J.: Micrometeorological measurement of the dry deposition flux of sulphate and nitrate aerosols to coniferous forest, Atmospheric Environment, 31, 333–343, https://doi.org/10.1016/S1352-2310(96)00188-4, 1997.

Wyers, G. P. and Erisman, J. W.: Ammonia exchange over coniferous forest, Atmospheric Environment, 32, 441–451, https://doi.org/10.1016/S1352-2310(97)00275-6, 1998.

Yuvaraj, S., Fan-Yuan, L., Tsong-Huei, C., and Chuin-Tih, Y.: Thermal Decomposition of Metal Nitrates in Air and Hydrogen Environments, The Journal of Physical Chemistry B, 107, 1044–1047, https://doi.org/10.1021/jp026961c, 2003.

Zeller, K. F., Massman, W. J., Stocker, D. W., Fox, D. A., and Stedman, D. H.: Initial results from the Pawnee Eddy Correlation system for dry acid-deposition research, United States Department of Agriculture, Forest Service, Rocky Mountain Forest and Range Experiment Station Fort Collins, CO, Forest Service research paper, Report No., RM-282, 30 pp., 1988.

Zemmelink, H. J., Gieskes, W. W. C., Klaassen, W., Beukema, W. J., de Groot, H. W., de Baar, H. J. W., Hintsa, E. J., McGillis, W. R., and Dacey, J. W. H.: Relaxed eddy accumulation measurements of the sea-to-air transfer of dimethylsulfide over the northeastern Pacific, Journal of Geophysical Research, 109, C01025, https://doi.org/10.1029/2002JC001616, 2004.

Zhang, L., Wright, L. P., and Asman, W. A. H.: Bi-directional air-surface exchange of atmospheric ammonia: A review of measurements and a development of a big-leaf model for applications in regional-scale air-quality models, Journal Geophysical Research: Atmospheres, 115, D20310, https://doi.org/10.1029/2009JD013589, 2010

Zhu, S., Clement, R., McCalmont, J., Davies, C. A., and Hill, T.: Stable gap-filling for longer eddy covariance data gaps: A globally validated machine-learning approach for carbon dioxide, water, and energy fluxes, Agricultural and Forest Meteorology, 314, 108777, https://doi.org/10.1016/j.agrformet.2021.108777, 2022.

Zöll, U., Brümmer, C., Schrader, F., Ammann, C., Ibrom, A., Flechard, C. R., Nelson, D. D., Zahniser, M., and Kutsch, W. L.: Surface–atmosphere exchange of ammonia over peatland using QCL-based eddy-covariance measurements and inferential modeling, Atmos. Chem. Phys., 16, 11283–11299, https://doi.org/10.5194/acp-16-11283-2016, 2016.

Zöll, U., Lucas-Moffat, A. M., Wintjen, P., Schrader, F., Beudert, B., and Brümmer, C.: Is the biosphere-atmosphere exchange of total reactive nitrogen above forest driven by the same factors as carbon dioxide? An analysis using artificial neural networks, Atmospheric Environment, 206, 108–118, https://doi.org/10.1016/j.atmosenv.2019.02.042, 2019.

Danksagung

Abschließend möchte ich mich bei all denjenigen bedanken, die ich während meiner Promotionsjahre kennenlernen durfte, mich durch Höhen und Tiefen begleitet haben und zur Fertigstellung der vorliegenden Promotionsarbeit beigetragen haben. Mein besonderer Dank gilt meinen Betreuern Christian und Martijn. Beide unterstützten mich tatkräftig bei der Datenanalyse, dem Verfassen der Publikationen, ermöglichten die Zusammenarbeit Kollegen aus der Schweiz und den Niederlanden und hatten immer ein offenes Ohr – auch für Themen neben dem Arbeitsplatz.

Auch möchte ich den derzeitigen und ehemaligen Kollegen der AG-Stoffflüsse danken. Dazu zählt mein ehemaliger, geschätzter Bürokollege Frederik, bei dem ich mich für seinen uneingeschränkten Support bei dem Verfassen der Publikationen und der Einführung in die Modellierung des Stickstoffaustausches bedanken möchte. Ebenfalls ein herzliches Dankeschön an meine ehemalige Kollegin Undine für die Sammlung von Messdaten am Waldstandort. Ohne den technischen Support von Jeremy, Jean-Pierre und Jens-Kristian wäre diese Arbeit nicht möglich gewesen. Mein besonderer Dank gilt an dieser Stelle Jeremy, mit dem ich die meiste Zeit an den Messstandorten verbrachte.

Nicht unerwähnt bleiben soll die exzellente Analyse der Denuder- und Passivsammlermessungen, die vom Zentrallabors des Thünen-Instituts durchgeführt wurde und die Unterstützung der Kollegen der Nationalparkverwaltung Bayerischer Wald, die sofort bereitstanden, falls Hilfe am Messstandort nötig war. Ein großes Dankeschön auch an Liv und Dominik für die Unterstützung bei der Wartung der Messgeräte am Grünlandstandort. An dieser Stelle möchte ich Liv auch für die Auswertung der Ernte- und Düngedaten danken.

Ebenfalls soll die finanzielle Unterstützung des Bundesministeriums für Bildung und Forschung im Projekt NITROSPHERE und des Umweltbundesamtes im Project FORESTFLUX hervorgehoben werden. Ein großes Dankeschön an das Thünen-Institut, das mir tolles Arbeitsumfeld bot und dessen Engagement im Fördern neuer wissenschaftlicher Karrieren.

Mein größter Dank gilt jedoch meiner Familie, auf deren uneingeschränkte Unterstützung ich mich immer verlassen konnte.

Selbstständigkeitserklärung

Hiermit erkläre ich an Eides Statt, dass ich die vorliegende Arbeit selbstständig und ohne fremde Hilfe angefertigt, keine anderen als die angegeben Quellen und Hilfsmittel benutzt und die den benutzten Quellen wörtlich oder inhaltlich entnommenen Stellen als solche gekennzeichnet habe.

Diese Arbeit hat in gleicher oder ähnlicher Form noch keiner Prüfungsbehörde vorgelegen.

Pascal Wintjen,

Braunschweig, den 03.11.2022